Mohammad Hadi Bordbar

THEORETICAL ANALYSIS AND SIMULATIONS OF VERTICALLY VIBRATED GRANULAR MATERIALS

Thesis for the degree of Doctor of Science (Technology) to be presented with the due permission for public examination and criticism in the Auditorium 1382 at Lappeenranta University of Technology, Finland, on the 16th of December, 2005, at noon.

Acta Universitatis
Lappeenrantaensis
230

Supervisor Professor Piroz Zamankhan
Department of Energy and Environmental Technology
Lappeenranta University of Technology
Finland

Reviewers Professor Goodarz Ahmadi
Department of Mechanical and Aeronautical Engineering
Clarkson University
USA

Professor Kambiz Vafai
Department of Mechanical Engineering
University of California
USA

Opponents Professor Goodarz Ahmadi
Department of Mechanical and Aeronautical Engineering
Clarkson University
USA

Professor Kambiz Vafai
Department of Mechanical Engineering
University of California
USA

ISBN 952-214-161-5
ISBN 952-214-165-8 (PDF)
ISSN 1456-4491
Lappeenrannan teknillinen yliopisto
Digipaino 2005

ABSTRACT

M.Sc. Mohammad Hadi Bordbar
Theoretical Analysis and Simulations of Vertically Vibrated Granular Materials
Lappeenranta, 2005
129p.
Acta Universitatis Lappeenrantaensis 230
Diss. Lappeenranta University of Technology

ISBN 952-214-161-5, ISBN 952-214-165-8 (PDF), ISSN 1456-4491

The dynamical properties of shaken granular materials are important in many industrial applications where the shaking is used to mix, segregate and transport them. In this work a systematic, large scale simulation study has been performed to investigate the rheology of dense granular media, in the presence of gas, in a three dimensional vertical cylinder filled with glass balls. The base wall of the cylinder is subjected to sinusoidal oscillation in the vertical direction. The viscoelastic behavior of glass balls during a collision, have been studied experimentally using a modified Newton's Cradle device.
By analyzing the results of the measurements, using numerical model based on finite element method, the viscous damping coefficient was determined for the glass balls. To obtain detailed information about the interparticle interactions in a shaker, a simplified model for collision between particles of a granular material was proposed. In order to simulate the flow of surrounding gas, a formulation of the equations for fluid flow in a porous medium including particle forces was proposed. These equations are solved with Large Eddy Simulation (LES) technique using a subgrid-model originally proposed for compressible turbulent flows.

For a pentagonal prism-shaped container under vertical vibrations, the results show that oscillon type structures were formed. Oscillons are highly localized particle-like excitations of the granular layer. This self-sustaining state was named by analogy with its closest large-scale analogy, the soliton, which was first documented by J.S. Russell in 1834. The results which has been reported by Bordbar and Zamankhan(2005b)also show that slightly revised fluctuation-dissipation theorem might apply to shaken sand, which appears to be a system far from equilibrium and could exhibit strong spatial and temporal variations in quantities such as density and local particle velocity. In this light, hydrodynamic type continuum equations were presented for describing the deformation and flow of dense gas-particle mixtures. The constitutive equation used for the stress tensor provides an effective viscosity with a liquid-like character at low shear rates and a gaseous-like behavior at high shear rates.

The numerical solutions were obtained for the aforementioned hydrodynamic equations for predicting the flow dynamics of dense mixture of gas and particles in vertical cylindrical containers. For a heptagonal prism shaped container under vertical vibrations, the model results were found to predict bubbling behavior analogous to those observed experimentally. This bubbling behavior may be explained by the unusual gas pressure distribution found in the bed.

In addition, oscillon type structures were found to be formed using a vertically vibrated, pentagonal prism shaped container in agreement with computer simulation results. These observations suggest that the pressure distribution plays a key role in deformation and flow of dense mixtures of gas and particles under vertical vibrations. The present models provide greater insight toward the explanation of poorly understood hydrodynamic phenomena in the field of granular flows and dense gas-particle mixtures. The models can be generalized to investigate the granular material-container wall interactions which would be an issue of high interests in the industrial applications. By following this approach ideal processing conditions and powder transport can be created in industrial systems.

Keywords: Dense Granular flows, Oscillon, Gas-particle flow, Continuum approach, Computer simulation, Computational Fluid Dynamics, Viscoelasticity, and Vertically Vibration

UDC 534.1 : 519.62/.64 : 62-492

To my wife Marzieh,

The most precious gift I have received from God.

Acknowledgments

The work on this thesis has been an inspiring, often exciting, sometimes challenging, but always interesting experience. It has been made possible by many other people, who have supported me.

I am very grateful to my supervisor Professor Piroz Zamankhan who has given me the chance to participate in several interesting research projects. He has supported me with his encouragement and many fruitful discussions.

I am also indebted to Professor Goodarz Ahmadi and Professor Kambiz Vafai who are reviewers of this thesis and this work couldn't be completed without their fruitful suggestions and comments.

Special thanks also goes to the head of Department of Energy and Environmental Technology, Professor Esa Marttila, and Professor Timo Hyppanen who encouraged me during my research work.

I acknowledge the financial support by the Finland Graduate School in Computational Fluid Dynamics; especially Professor Timo Siikonen for his kind help. I am grateful to the members of the laboratory of computational fluid dynamics and their comradeship during my work in this lab.

I should wish all the best for my entire friends in Lappeenranta who always made me hopeful with their kindness and support.

Finally, I wish to thank my family and my wife's family for their continuous support and encouragement.

As I wrote previously, I dedicate this thesis to my kind wife Marzieh for all her patience and making the balance between work and life. In fact her contribution in doing this work isn't less than mine. I wish to be able to compensate her abnegations.

Mohammad Hadi Bordbar
Dec.2005
Lappeenranta, Finland

Table of Contents

Abstract…….3
Acknowledgment……..7
Table of Contents……..……... 9
List of Publications……..…...……11
Nomenclature…….…....…12

1. Introduction……...……..…… …….…17

2. Shaking and Vibration in Granular Media……..…..……...…..……20

2-1.Instability in Fluid Systems……...……...….20
2-1-1- Reyligh-Bernard Convection……...……...…...……21
2-2. Theory of Instability in Granular Media…….…...…...22
2-2-1.Stability Analysis in Dry Granular Systems……...…..…..22
2-2-1-1.Constitutive Equations……..…….……23
2-2-1-2. Boundary Conditions……..……...24
2-2-1-3. Base State Solution……..……..25
2-2-2. Stability Analysis in Gas-Particle Systems……..……..25
2-2-2-1.Stability Analysis in the Homogeneous Gas-Particle Systems…….....25
2-2-2-2-Stability Analysis in the Non-homogeneous Gas-Particle Systems….…….....26
2-3. Granular Materials under Effect of Vertically Vibration……..…26
2-3-1.Instability Introduced by Vertically Vibration in the Dry Solid Granular Systems…....27
2-3-1-1.Pattern Formations in Dry Granular Materials…… ……...….…….27
2-3-1-2.Oscillon Forming in the Absence of Air Effects……...……30
2-3-2. Instability in Fluid-Solid Granular Systems…….……..30
2-3-2-1.Gas-Solid Granular Systems……..……....30
2-3-2-2. Liquid-Solid Granular Systems……..……...32

3. Experimentation and Collision Modeling……...….33

3-1.Overview…….....……....……..…33
3-1-1. Review of other group works…….…….……33
3-2.Short Review of Dynamic of Binary Collision……..…35
3-2-1.Kinematic analysis of collision between a ball and a surface…….……..…...35
3-2-2.Kinematic analysis of collision between a moving sphere with an initially stationary sphere (Newton Cradle Device)…… ……..…....35
3-2-3.Kinematic Analysis of Oblique Collision……..……...36
3-3. Force Analysis in Binary Collision between Multisize Spherical Particles……..…37
3-3-1: Elastic Forces……..……37
3-3-2: Viscous Forces……..……...40
3-4. Models of Normal Collisions……....42
3-4-1.Linear Model…….……...42
3-4-2:Non-Linear Model…….……...42
3-4-3. Simplified Model for Collision of Multisize Viscoelastic Spheres…….……43
3-5.Review of Hertz Theory Formulation in Elastic Collision……46
3-6.Finite Elements Methods Approach in Modeling Multisize Collision……..…48
3-7.Our Experimental Device……...52

4. Analysis and Simulation of Vertical Vibration in Granular Media……..55

4-1. Wave Analysis in the Plates…….……56
4-1-1.Analytical Solution for 2D Vibrations of a Square Membrane…….…...…56

4-1-2.2D-Vibration of a Circular Memberane……..……59
4-1-3.2D-vibartion of plates with other shapes……..……..60
4-2.Collective Processes in Gas-Particle Flows……...67
4-2-1. Fluid Flow through a Stationary Irregular Array of Particles……..……67
4-2-1-1. Large Eddy Simulation (LES) ……..……68
4-2-1-2. Numerical Results……..……....71
4-2-2. Fluid Flow in the Presence of Moving Bodies…….……...72
4-2-2-1. Turbulence Enhencement ……..……....73
4-2-2-1-1. Shedding of Vortices…….……73
4-2-2-1-2. Enhancement of the Gas Velocity Gradient……....76
4-2-3. Simplified discrete model……..……..…78
4-2-3-1. Numerical models……...78
4-2-3-2. Simulation Procedure…….80
4-2-3-3. Results of Molecular Dynamics Simulations…….81
4-3.Continuum Approach in Simulating Vibrated Granular Bucket ……..….84
4-3-1.Different Regimes on Granular System under Shearing……..85
4-3-1-1. Rate-Independent Quasi-Static Regime……..……...86
4-3-1-2. Transition Regime……..……....88
4-3-1-3. Rapid Flow Regime……..……..88
4-3-2.Continuum Approach Analysis in Gas-Particle System……..……88
4-3-2-1.Constitutive Equations in Rate-Independent Quasi-Static Regime…….…89
4-3-2-2.Constitutive Equations in Transitional Regime……...90
4-3-2-3.Viscous-like behavior……..92
4-3-2-4.Fluctuation Energy……..95
4-3-2-5.Continuous Phase……96
4-4.Continuum Model for Vibro-Granular Medium Device……98
4-4-1.Results and Discussions in Continuum Model……...101

5. Concluding Remarks……....104

References……..……**106**

Appendix A-Coefficient Matrixes for polygonal plates and ellipse membrane……..……111
Appendix B
-Bordbar M.H, Zamankhan P.," Dynamical States of Bubbling in Vertically Vibrated Granular Materials,Part I: Collective Processes", Communications in Nonlinear Science and Numerical Simulations, Article in press(2005).
Appendix C
-Bordbar M.H, Zamankhan P.," Dynamical States of Bubbling in Vertically Vibrated Granular Materials,Part II: Theoretical Analysis and Simulations", Communications in Nonlinear Science and Numerical Simulations, Article in press(2005).
Appendix D
-Zamankhan P.,***Bordbar M.H,*** " Complex Flow Dynamics in Dense Granular Flows, Part I: Experimentation",Journal of Applied Mechanics, Accepted for publication(2005)
Appendix E
-Bordbar M.H, Zamankhan P. and Huang J.," Theoretical Analysis and Numerical Simulations of Vertical Vibrated Granular Materials", Journal of Applied Physics, Accepted with revision (2005).
Appendix F
-Bordbar M.H, Tanskanen V. and Zamankhan P.," Structural Ordering in a Bounded Dense Shear Flow of Visco-elastic Spherical Particles", Published in proceeding of International Conference of Numerical Analysis and Applied Mathematics, Greece,Sep.2005

-List of Publications:
This thesis is based on the papers listed below.

1-***Bordbar M.H***, Zamankhan P.," Dynamical States of Bubbling in Vertically Vibrated Granular Materials,Part I: Collective Processes", Communications in Nonlinear Science and Numerical Simulations, Article in press(2005).
2-***Bordbar M.H***, Zamankhan P.," Dynamical States of Bubbling in Vertically Vibrated Granular Materials,Part II: Theoretical Analysis and Simulations", Communications in Nonlinear Science and Numerical Simulations, Article in press(2005).
3-Zamankhan P., ***Bordbar M.H***," Complex Flow Dynamics in Dense Granular Flows, Part I: Experimentation", Journal of Applied Mechanics, Accepted for publicaton (2005).
4-***Bordbar M.H***, Zamankhan P.," Complex Flow Dynamics in Dense Granular Flows, Part II: Simulations", Journal of Applied Mechanics, Accepted with major revision (2005).
5-***Bordbar M.H***, Zamankhan P. and Huang J.," Theoretical Analysis and Numerical Simulations of Vertical Vibrated Granular Materials", Journal of Applied Physics, Accepted with revision (2005).
6-***Bordbar M.H***., Zamankhan P.," Dynamical States of Bubbling in Vertical Vibrated Granular Materials", Proceeding of ASME Fluids Engineering Summer Conference 2005, Texas, Jun 2005.
7-***Bordbar M.H***, Tanskanen V. and Zamankhan P.," Structural Ordering in a Bounded Dense Shear Flow of Visco-elastic Spherical Particles", Proceeding of International Conference of Numerical Analysis and Applied Mathematics, Greece,Sep.2005.

Nomenclature

A	The coefficient was considered to be fit parameter in equations (3-56, 57).
A	Amplitude of the displacement.
c	the coefficients characterizing viscoelastic behavior of the grains.
c_n	the normal damping coefficient,(eq.3-60).
C_0	A constant is defined in eq.(3-31).
Ce	The effective viscosity(eq.3-53).
C	Characterizes speed of wave(section4).
C_{ij}	The interaction between large and small scales(section4).
D_l^p	Total drag force acts on particle.
d	The layer thickness.
e_p	The coefficient of restitution for collisions between particles.
e_w	The coefficient of restitution for collisions between particles and the wall.
e^2	The ratio of kinetic energy (after) to kinetic energy (before) is evidently, in this situation.
e	The Coefficient of restitution.
E	The total energy per unit mass of the granular material(section2).
E	Young modulus (section4).
E_{MK}	The kinetic energy associated with local average velocity u, $(E_{MK} = \frac{1}{2}\lvert u\rvert^2)$.
E_{PT}	The 'pseudo-thermal' energy associated with deviations of the motion of individual particles from the local average.
E_h	The true thermal internal energy of the solid material.
f	The container oscillation frequency.
F_{el}	The total elastic force.
F_{dis}	The total dissipative force acting between the bodies, eq.(3-47).
g	The gravity acceleration.
g^n	The normal component of relative velocity of particles.
$G_{ik}(x,y,z)$	The corresponding Green function in eq.(3-14).
G_0	The instantaneous shear modulus.
G_∞	The long-time shear modulus.
I	The rate of dissipation due to the inelasticity of collisions between particles.
k	The thermal diffusivity(section2).
k	The coefficients characterizing the elastic behavior of the grains(section3,4).
K	The coefficient for define mode of oscillations in x direction(section4).
Ke	The effective stiffness (eq.3-53).
l	coefficient which characterizes the mode of oscillations in y direction.
L_{ij}	Interactions among the large scales.
m	The mass of single particle.
M_p	The mass holdup in linear stability analysis in vertically vibrated pure granular materials.
m_1	The mass of the first particle in binary collision.
m_2	The mass of the second particle in binary collision.
n	The unit normal to the wall(in eq.2-16 and 2-17.), pointing into the granular material.
N_j	Number of neighboring particles.
p	The tensor of thermodynamic pressure(section2).
$P_z(x,y)$	The normal pressure which acts between the compressed bodies in the plane $z=0$ (eq.3-20).
$\vec{P}(x,y)$	The pressure that acts on the surface of an elastic semi-space.

$p(r)$ The normal pressure (eq.3-66).

P_m The normal pressure is related to the normal force P ,eq.(3-67).

$P_z^{dis}(x,y)$ The dissipative pressure in the contact area, eq. (3-50).

$\bar{p}$ The filtered pressure (section4).

q The total energy flux vector.

q_h The true heat flux.

q_{PT} The flux of the pseudo-thermal energy.

Q_t The energy input in linear stability analysis in vertically vibrated pure granular materials.

R_{ij} Interaction between the subgrid scales.

R_a Rayleigh number ($R_a = \alpha\beta g d^4 / k\upsilon$).

R_{eff} The equivalent radius.

R_1, R_2 The principle radius of curvature of the first body at the point of the contact. (eq(3-17)).

R_1', R_2' The principle radius of curvature of the second body at the point of the contact. (eq(3-17)).

S The deviatoric part of the rate of deformation tensor.

S_{ij} resolved strain rate.

St Particle Stokes number ($St = 4mV_0 / 6\pi\mu\sigma^2$).

t The unit vector tangent to the wall, in the direction of the slip velocity (eqs.(2-16,17)).

t_c The duration of the collision.

T The granular temperature' defined by $T = \frac{1}{3}\overline{v^2}$, where $\overline{v^2}$ is the mean square of the velocity fluctuations about u .

u the velocity vector $u = u_j$ for $j = 1,2,3$.

u_{sl} The velocity of the granular material in contact with the wall(section2).

u_1 The velocity of first particle in binary collision before contact.

u_2 The velocity of second particle in binary collision before contact.

$\dot{u}_{ij}(\vec{r})$ Deformation rate.

u_{z1} , u_{z2} The z -components of the displacement in the material of the first and of the second bodies on the plane $z = 0$,respectively.(eq(3-16)).

$\bar{u}$ x-component of velocity.

u_i Velocity of gas at the particle position.

u_i^l rapidly fluctuating velocity of particles of kind l.

v_1 The velocity of first particle in binary collision after collision.

v_2 The velocity of second particle in binary collision before collision.

V_{imp} The relative velocity of the grains before impact.

V Particle velocity (rigid body motion).

$\bar{v}$ y- Components of velocity.

V_i The slowly varying mean velocity.

V_0 Sedimentation velocity of a single particle.

$\mathbf{V}_{tr}$ Particle terminal velocity.

V_{imp} Impact velocity.

x_i The Curvilinear coordinates.

(x, y, z)	Cartesian coordinates system.
y^+	Characterize distances.
Y	The Young modulus.

Greece

α	The coefficient of thermal expansion (section2).
β	The temperature gradient ($\beta = -dT / dz$) in Rayleigh-Bernard convection stability analysis (section2).
υ	The kinematics viscosity.
ρ	The density of the fluid.
ρ	The bulk density of the particulate material in eq.(2-8), given by $\rho = \rho_P \phi$.
ρ_p	The small disturbance of density in stability analysis in density dependence systems.
ϕ	The solid volume fraction.
ϕ'	A specularity factor (which measures the fraction of the momentum of an incident particle in the direction of slip which is transmitted, on average, to the wall in a collision).
σ	The total-stress tensor, defined in the compressive sense.
σ_c	The collisional-translational contributions to the total stress.
σ_f	The frictional contributions to the total stress.
Γ	The acceleration amplitude $\Gamma = 4\pi^2 f^2 A / g$.
$\sigma_{el}^{ij}(\vec{r})$	The stress tensor that describes the i -component of the force (eq.3-12).
υ	The Poisson ratio.
ζ	The sum of the compressions of both bodies in the center of the contact area (eq.3-16).
φ	The angle between the planes corresponding to the curvature radius R_1 and R_1' (eq(3-17)).
$\psi_1(t)$	The (dimensionless) functions that is the relaxation function for the distortion deformation.(eq.3-35).
$\psi_2(t)$	The (dimensionless) functions that is the relaxation function for the dilatation deformation.(eq.3-35).
$\tau_{vis,1/2}$	The characteristic relaxation times of the dissipative processes.
η_1, η_2	The viscous constants (eq.3-38).
σ_{el}^{zz}	The component of the elastic stress.
ρ	A constant that defined in (3-34).
ζ	The amount of overlap between two particles.
$\dot{\zeta}$	The relative velocity of the two spheres moving towards each other (eq.3-53).
β	The decay coefficient.
ρ^l	The apparent density of particles of kind l .
ρ_s	The particle material density.
ϕ_s	The average solid volume fraction of particles.
θ_f	The value of the angle of internal friction.
σ	The particle diameter.
λ	Mixing parameter.
σ_i	The principal stresses.
$\mathbf{\Pi}$	The resistance tensor.
ρ	Density.

γ Exponent in the expression for contact force.

τ Relaxation time.

(ξ, ζ, η) Parametric coordinates.

ν Poisson's ratio.

σ_p Particle diameter.

σ Stress vector whose transpose is given as $\sigma^t = \left(\sigma_{xx}, \sigma_{yy}, \sigma_{zz}, \sigma_{xy}, \sigma_{yz}, \sigma_{zx}\right)$.

δ Overlapping of a pair spherical particles with diameter σ_p at positions $\mathbf{r}_1$ and $\mathbf{r}_2$.

τ_{ij} The subgrid tensor.

$\bar{\Delta}$ The cutoff length, to the Navier-Stokes equation for an incompressible viscous Newtonian fluid in Cartesian coordinates.

$\breve{\tau}_{ij}$ Subgrid tensor.

ω_v Frequency of wave.

ω Vorticity Vector**.**

Superscripts

Double prime	post-collisional value of the relative velocity.
Overbar	mean values.
Prime	fluctuation quantities.
Dot	The derivative with respect to time.
l	particle of kind *l.*
k	particle of kind *k.*
p	particle.
g	gas.

1. Introduction

A granular material is a conglomeration of discrete solid, macroscopic particles characterized by a loss of energy whenever the particles interact (the most common example would be friction when grains collide). A granular flow is a mixture of grains and a fluid phase (e.g., gas, liquid). The grains are called the dispersed phase, while the fluid phase is the carrier phase supporting the grains. These materials are all around us, a few examples include food products such as rice, corn, breakfast cereal flakes, building materials such as sand, gravel and soil, and chemicals such as coal, plastics and pharmaceuticals. The constituents that compose granular material must be large enough such that they are not subject to thermal motion fluctuations. Thus, the lower size limit for grains in granular material is about 1 μm. On the upper size limit, the physics of granular materials may be applied to ice floes, where the individual grains are icebergs (Duran, 2000).

Granular materials are commercially important in applications as diverse as pharmaceutical industry, agriculture and energy production. Research into granular materials is thus directly applicable and goes back to at least Coulomb, whose law of friction was originally stated for granular materials. Some examples of granular flows are demonstrated in Fig. 1-1.

A good understanding of the physics of granular materials is desired in order to design efficient processing and handling systems. The significance of this is apparent when one considers the following statistic; in the chemical industry approximately one-half of the products and at least three-quarters of the raw materials are in granular form (Nedderman ,1992).

Some of the interesting points about the significance of granular flow are listed below

- Ennis *et al*. (1994) estimate that $61 billion in the chemical industry is linked to particle technology.
- Approximately 1.3% of the U.S. electrical power production goes toward grinding particles or ores (Ennis *et al*. , 1994).
- Landslides cause a minimum of $1.5 billion of property damage and at least 25 fatalities in the United States annually.
- Each year over 1,000 silos, bins and hoppers fail in North America (Knowlton et al., 1994).
- In Mexico, 5 million tons of corn is handled each year, 30% of which is lost due to poor handling systems (Mena, 1993).

Unfortunately there remains a poor understanding of how to model granular materials. Most of the particulate handling knowledge is empirical and no general approach to analyzing these flows exists. A recent study of 40 solids processing plants in the U.S. and Canada found that 80% of the facilities experienced solids handling problems, and most of the plants were slow coming on-line. Furthermore, once operational, handling problems continued resulting in the performance of only 40% to 50% that of design (Knowlton et al., 1994). In order to avoid such problems and properly design systems involving particulates, there needs to be a better understanding of the mechanics and dynamics of granular materials.

A distinguishing feature between flows of granular materials and other solid-fluid mixtures is that in granular flows, the direct interaction of particles plays an important role in the flow mechanics. A significant fraction of the energy dissipation and momentum transfer in granular flows occurs when particles are in contact with each other or with a boundary.

In some sense, granular materials do not constitute a single phase of matter but have flow characteristics that roughly resemble those of ordinary Newtonian fluids. However, granular materials dissipate energy quickly, so techniques of statistical mechanics that assume conservation of energy are of limited use. Depending on the average energy of the individual grains they may exhibit the properties of

solids, liquids, or gases. When the average energy of the individual grains is low and the grains are fairly stationary relative to each other, the granular material acts like a solid.

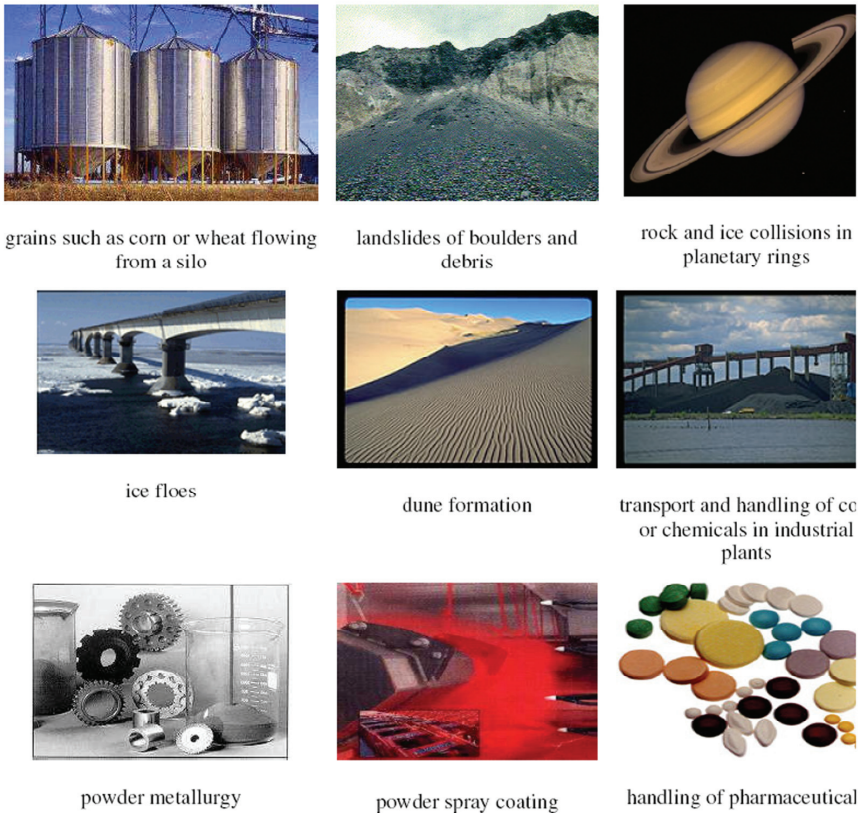

Fig. 1-1: *Some examples of granular material*

When the granular matter is driven and energy is fed into the system (such as by shaking) so that the grains are not in constant contact with each other, the granular material is said to fluidize and enter a liquid-like state. If the granular material is driven harder so that contacts between the grains become highly infrequent, the material enters a gaseous state. Correspondingly, one can define a granular temperature equal to the root mean square of grain velocity fluctuations, which is analogous to thermodynamic temperature. Bulk flow characteristics of granular materials do differ from those of homogeneous fluids in several important ways. Some of these differences are listed below

- Shearing or shaking a granular material may result in its becoming inhomogeneous in space and time (see Brazil nut effect)
- Granular materials tend to clog when forced through a constriction (as in a salt cellar)
- A compacted granular material must expand (or dilate) before it can deform
- Turbulence is almost impossible to achieve in granular materials
- Granular materials can support (small) shear stresses indefinitely
- Granular materials are often inhomogeneous and non isotropic
- Granular materials exhibit avalanches.

According to the definition we used (and explained) for granular flow in the first paragraph of section 1, the problem now is that we must deal with multi-phase flow theory. Hence, we must also deal with multi-phase flow turbulence. This leads to huge theoretical development, which is always difficult to

deal with. The advantage of this definition is that it is so powerful that we can basically describe anything we want. Indeed, the gas phase is always there, even in highly concentrated granular flows. Therefore, for granular flows found in nature, we must always have a continuum between highly concentrated flows (where the dispersed phase dominates) to highly diluted flow (where the gas phase dominates).

- If we consider the two end-members of granular flows, highly concentrated to highly diluted, it should be possible to define in meaningful ways the constitutive equations of such end-member flows, along with equations to connect those end-member rheology's. Knowing, understanding, and defining those equations are the necessary steps for carrying out super-computer modeling of granular flows.
- One, the main and most important aspect in those equations, is to understand the distribution of all the forces acting on the granular fluid … however, instead of analyzing those forces, we prefer to deal with forces acting on a surface of a fluid parcel. Force acting on a surface is called stress, for example, normal stress (e.g., pressure) and shear (tangential) stress. If we understand how stress is distributed within the granular flow, we make great progress in the job of modeling granular flows. In addition, understanding the distribution of stress within granular flows is a key aspect for understanding the fundamental differences between granular fluid and any other fluid (such as gas or water).

The transport, mixing and segregation of granular materials are important in the pharmaceutical, mining, agricultural, metal, food, and energy industries. Even in the chemical industry, the majority of the products are in granular rather than liquid form (Ennis et al., 1994), thus a large amount of engineering literature has been developed on "powders and particulates". However, a basic understanding of the physical mechanisms underlying the collective behavior of particles in a granular medium is lacking. Granular media can exhibit both solid and fluid properties (e.g., one can walk on a beach or pour the sand from a bucket), but granular media is not as well understood as those of solids and fluids. While fluids are processed in industry with high efficiency, the efficiency of handling (crushing, mixing and separation) of granular materials is estimated to be well below optimum (Ennis et al., 1994).
The scientific study of granular systems has a long history, including a discussion by Galileo in his Dialogues, and a study by Faraday of convective motion of grains in heaps, in vertically oscillated granular layers (Faraday and Philos ,1831). Bagnold started a systematic study of granular materials in 1930's. In recent years there has been a resurgence of interest in granular media amongst physicists(Cao et al.,1996), thanks to Pierre-Giles de Gennes, who recommended in the early 1980s, to young French scientists, that granular matter was an interesting subject worthy of study(Evesque and Rajhenbach,1989;De Gennes,1999). In the past two decades there has been an explosion of interest in granular systems. A search in INSPEC on the word" granular" followed by "system, medium, matter, flow, or gas" yields 20 papers in the two year period 1980-82, while a decade later the number of papers in a three year period jumped to 112, and in 2000-2002 there were 691 papers on the subject.

2. Shaking and Vibration in Granular Media

Granular materials, which can be either wet or dry and range from nanometer to centimeters in size, are widely encountered in both industries and nature. They can withstand deformation and form heaps when they are combined with a solid, with liquids they can flow, and with gas they can have compressibility. These features give rise to another state of matter, which is poorly understood. Their response to the many usual excitations are different from the response of other kinds of materials, for example, inserting energy into the systems consisted from granular materials caused some unusual behavior and instability in these systems. Shaking a column of these materials vertically is an interesting way of inserting energy into these systems.

The study of periodic vibrations on the granular flow of materials is of great importance, due to both theoretical and practical reasons, for scientists and engineers. For instance, for the mixing, separation and drying processes of particles in industries such as mining, agriculture, construction and chemical engineering shakers has been widely used. The existence of instabilities in this system has been shown with the occurrence of traveling waves (Pak and Behringer, 1993) and standing waves (Umbanhowar, 1997) on the free surface.

Granular materials have two different behaviors, they deform plastically like a solid under weak shear and they flow like a fluid under high shear. Hence, one way for simulating their behavior is to consider them as an ordinary fluid or solid, and to define the relative properties according to this assumption. Another aim is to create shaken vibration in the bottom of the column of these materials. By doing many experiments in this field (Umbanhowar et al., 1996; Pak and Behringer, 1993) the studying of the resulting phenomena is finding suitable correlation for fluid-like properties of the granular materials such as Cell Viscosity, Bulk Viscosity, Thermal Conductivity and Thermal Dissipation of Energy (Umbanhowar, 2003).

In this section, we want to review some previous works that have been done in the field of study of instability in different kinds of granular systems (i.e. dry granular system, gas-particle system and liquid-particle system). As stated earlier, many aspects of instability problems in a granular system are not well understood; but in a pure fluid system, instability problems are clearer than in a granular fluids field. Hence, at first we will explain more about the general concept of stability and instability in a pure fluid system, then we will look at one famous instability in a pure fluid system (Reyleigh-Bernard convection problem), and finally we will make a short review of previous research works carried out in the field of instability in a granular system, especially in the vertical vibration of granular systems.

The aim of studying pure fluid system instability is for making a good basis for the better understanding of the nature of similar instable phenomena in the granular system. For example, in Raleigh-Bernard a layer of fluid between two parallel plates is excited by heating the bottom, so energy enters the system by heat transfer to molecules near the bottom, which will cause some standing patterns in the interface of the fluids. In granular systems, inserting energy to one part of the grains may be caused by vibration of the boundary and the granular temperature of grains near the vibrated boundary will increase and cause instability in these systems. It this light, it appears that an analogy exists between these two aforementioned systems (one in the pure fluid system and the other one in a granular system).

2-1. Instability in Fluid Systems

The study of instability of fluid systems, when the systems are driven away from equilibrium, has been one of the most interesting fields between researchers (Liu and Roux 1992, Deng and Wang 2003, Melo et al. 1994, Wang et al. 1996, Wang et al. 1997). Driving systems away from equilibrium is often made by locally inserting energy or momentum into the systems. In fact, inserting energy may cause different internal energies or even chaos in different regions of fluids and may form some spatial structures in the system, for example, the patterns in a hydrodynamic system. Examples of inserting energy into systems are; thermal convection in pure fluids and binary mixtures, Tylor-Couette flow, parametric wave instabilities, as well as patterns in solidification fronts, nonlinear optics, oscillatory chemical reactions and

excitable biological media (Chandrasekhar, 1981). For theoretical study of this kind of problem, usually at first a set of deterministic equations of motion, typically in the form of nonlinear partial differential equations, has been written. These equations usually have some stochastic terms that represent thermal or instrumental noise. A goal of this theory is to describe solutions of deterministic equations that are likely to be reached starting from typical initial conditions and to persist at long times. One of the most famous phenomena in this kind of system is spatiotemporal pattern formation. In many previous works in this field, the linear instability of homogeneous state usually has been employed and leads to a classification of patterns including three different types of patterns in terms of the characteristic wave vector q_0 and the frequency ω_0 of the instability (Cross and Hohenberg, 1993). In the first type $\omega_0 = 0, q_0 \neq 0$ the systems are stationary in time and periodic in space. In the second type $\omega_0 \neq 0, q_0 = 0$, the systems are periodic in time and stationary in space and in the last type of systems $\omega_0 \neq 0, q_0 \neq 0$ are periodic in time and space. "Amplitude equations" may describe accurately the dynamics of the systems near a continuous (or supercritical) instability. A form of these equations is universal for each type of instability but the specifics of each system enter through the nonuniversal coefficients. "Phase equation" describes the state of the systems far from the instability threshold, but it is limited to slow distortions of an ideal pattern. The starting equations for many systems usually are either not known or are too complicated to analyze conveniently. One solution to this order is by introducing phenomenological order-parameter models, which may interpret the correct amplitude equation near the threshold and may be solved analytically or numerically in the nonlinear regimes away from the instability. The aforementioned methods are useful in analyzing "real pattern effects," for example, the influence of external boundaries or the formation and dynamics of defects in ideal structures (Cross and Hohenberg, 1993).

2-1-1. Reyligh-Bernard Convection

Generally in this problem a layer of fluid heated from below is considered. Clearly a result of heating from below is that the density on the bottom layer becomes lighter than that at the top. The system is thus bottom heavy but it is not completely enough for the systems to undergo convective motion, since viscosity and thermal diffusivity of the fluid try to prevent the convective motion. If the fluid is heated to a temperature higher than the temperature gradient across, then only the top heavy state becomes unstable and convective motion ensues. We will consider the suitable condition necessary for the onset of thermal instability.

Bernard in 1900 did intensive experiments in this field for the first time. He used a thin layer of fluid and he observed that when the instability in the form of convection developed, some hexagonal cells appearance. Rayleigh in 1916 found the condition for the instability with two free surfaces. He found that the instability will occur if the temperature gradient $\beta = -dT/dz$ was large enough so that the so-called Rayleigh number $R_a = \frac{\alpha\beta g d^4}{k\upsilon}$ exceeds a value, where g represents the gravity acceleration, α is the coefficient of thermal expansion, d is the layer thickness, and k and υ are the thermal diffusivity and kinematics viscosity respectively. The parameter R_a represents the ratio of destabilizing buoyancy force to the stabilizing viscous force. Experiments in the early stage were carried out with fluid being heated from the bottom and with the top surface open to the atmosphere. Thus the top surface is free to move and deform. It was later (around 1960) realized that this could lead to another instability mechanism (Benard-Marangoni convection) due to gradient in surface tension. This mechanism coexists with the Rayleigh's mechanism but dominates in the thin layer. Most of the findings reported by Benard were actually due to this second instability mechanism. The instabilities driven by surface tension decreases as the layer become thicker. Later experiments on thermal convection (with or without a free upper surface) have obtained convective cells of many forms such as rolls, squares and hexagons (Simanovskii and Nepomnyashchy, 1993).

2-2. Theory of Instability in Granular Media

2-2-1. Stability Analysis in Dry Granular Systems

Regarding the different behavior of granular materials from other fluids, various interesting phenomena have been observed and studied. Most scientists in different fields are eager to study and research about granular fluids. This field of research is interesting for scientists of physics, mechanical engineering and chemical engineering, each of which has focused on particular aspects of granular fluids behavior.

Assume that there is a granular system and it is in a stationary state according to the equations governing it, i.e. in a state in which none of the variables describing it is a function of time. Usually you can assume that there is a set of parameters that define the behavior of the system. These parameters may include; geometrical parameters such as the dimensions of the system, parameters characterizing the velocity field that may prevail in the system, and the magnitude of the forces that may be acting on the system such as vibration force, pressure gradients, temperature gradients and others.

In studying the stability of such a system with a given set of parameters, we seek to determine the response of the system to small disturbances. We can say that a system is stable with respect to the particular disturbance if when it is disturbed, the disturbance gradually dies down. It is unstable if when it is disturbed, the disturbance grows in amplitude in such a way that the system progressively departs from the initial state and never reverts to it. Clearly, it is enough to consider a system as unstable if there is just one special mode of disturbance in respect to which it is unstable. We cannot consider a system stable, unless it is stable with respect to every possible disturbance to which it can be subjected. In other words, stability must imply that there exists no mode of disturbance for which it is unstable.

Instability in a granular system introduces because of the some locally difference in internal energy, momentum of grains. As we will convey in the next section (section3) energy can be transferred in granular material by both the collision and convection process. One good scale for showing the amount of internal energy of a granular material is the granular temperature, which is defined according to the amount of velocity fluctuations, and has a key role in the energy equation of a granular system. In the study of this instability problem, assessment of the parameters that are governing on the behavior of the system is very important. For example, in the granular layers that have been under effect of the vertical vibration, in the previous research, some different parameters have been considered as the governing parameters on the instability of the system. For example, Deng and Wang (2003) considered the mass holdup (M_p) and energy input (Q_t) as a major parameter in linear analysis of stability. Figure 2-3 illustrates the schematic of the system that was used by Deng and Wang (2003). They considered Q_0 as the energy flux supplied from the bottom plate to the granular layer, and also they assume that the bed expands from its original height to H as a result of the vibration.

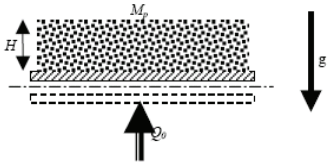

Fig. 2-3: *A schematic of a layer of granular material that was vibrated vertically and the effective parameters that governs the behavior of the system, which has been used for the study of instability in these kinds of systems by Deng and Wang (2003).*

Generally speaking, linear analysis of stability includes two major steps, firstly, the base state at various values of governing parameters should be calculated and secondly, small perturbations should be introduced to verify the stability of the base state by solving the resultant eigenvalue problem derived from the linearized governing equations and corresponding boundary conditions. In this light, precise governing equations and boundary conditions are required to obtain accurate assessment of the parameters that are governing the behavior of the system.

2-2-1-1.Constitutive Equations

For finding governing equations we can write the three following assumptions: First,

$$\sigma = \sigma_c + \sigma_{f,}, \tag{2-5}$$

Where σ represents the total-stress tensor, defined in the compressive sense, while σ_c is the collisional-translational contributions to the total stress and σ_f is the frictional contributions to the total stress.

Second,

$$E = E_{MK} + E_{PT} + E_h, \tag{2-6}$$

where E represents the total energy per unit mass of the granular material, which is the summation of three components: E_{MK} ,the kinetic energy associated with local average velocity u , $(E_{MK} = \frac{1}{2}|u|^2)$, E_{PT} , the 'pseudo-thermal' energy associated with deviations of the motion of individual particles from the local average, and E_h ,the true thermal internal energy of the solid material. E_{PT} may be replaced by a 'granular temperature' T defined by $E_{PT} = \frac{1}{2}\overline{v^2} = \frac{3}{2}T$, where $\overline{v^2}$ is the mean square of the velocity fluctuations about u . Third,

$$q = q_{PT} + q_h, \tag{2-7}$$

where q is the total energy flux vector, which is the summation of the true heat flux, q_h , and the flux q_{PT} of the pseudo-thermal energy. The former is related in the usual way to the gradient of thermodynamic temperature and the effective thermal conductivity of the assembly of solid particles, while the latter is similarly related to the gradient in granular temperature as discussed below.

The balance equation for the true thermal internal energy is taken to be of the form (Johnson and Jackson, 1987)

$$\rho \frac{DE_h}{Dt} = -\nabla.q_h - \sigma_f : \nabla u + I\,. \tag{2-8}$$

Where ρ represents the bulk density of the particulate material, given by $\rho = \rho_P \phi$ where ϕ is the solid volume fraction, and D/Dt denotes the material derivative. The term $-\sigma_f : \nabla u$ represents the rate of working of the frictional component of the stress, while I is the rate of dissipation due to the inelasticity of collisions between particles. Implicit in eq. (2-8) is the assumption that work done by the frictional component of stress is translated directly into thermal internal energy, and does not contribute to the pseudo-thermal energy of the particles.

Using eq. (2-5) in the momentum equation, and then subtracting both eq. (2-8) and the mechanical-energy equation from the total-energy equation can lead to the following set of equations of change:

$$\text{Continuity:} \frac{\partial \rho}{\partial t} + \nabla.(\rho u) = 0 \tag{2-9}$$

$$\text{Momentum:} \rho \frac{Du}{Dt} = -\rho g - \nabla.(\sigma_c + \sigma_f), \tag{2-10}$$

$$\text{Energy:} \frac{3}{2}\rho \frac{DT}{Dt} = -\nabla.q_{PT} - \sigma_c : \nabla u - I \tag{2-11}$$

Where g is the specific-gravity force vector and again ρ represents the bulk density of the particulate material, given by $\rho = \rho_P \phi$ where ϕ is the solid volume fraction. The third of these equations represents the balance of pseudo-thermal energy, and we see that the rate of working of the collisional-translational component of stress is the source term, while the inelasticity of collisions provides a sink term. This reflects our earlier assumption about the form of the true thermal-energy balance. If the distribution of thermodynamic temperature is needed, the above equations must be supplemented by eq. (2-8).

Johnson and Jackson (1987) did some modification on the equation that was presented by Lun et al. (1984) and they suggested the following relationship for calculating collisional-translational contribution to stress:

$$\sigma_c = \left[\rho T(1+4\eta\phi g_0) - \eta\mu_b \nabla.u\right] I$$
$$-\left(\frac{2+\alpha}{3}\right)\left\{\frac{2\mu}{\eta(2-\eta)g_0}(1+\frac{8}{5}\eta\phi g_0)[1+\frac{8}{5}\eta(3\eta-2)\phi g_0]+\frac{6}{5}\mu_b\eta\right\}S \tag{2-12}$$

and

$$q_{PT} = \frac{-\lambda}{g_0}\left\{(1+\frac{12}{5}\eta\phi g_0)[1+\frac{12}{5}\eta^2(4\eta-3)\phi g_0]+\frac{64}{25\pi}(41-33\eta)(\eta\phi g_0)^2\right\}\nabla T$$
$$\times\frac{-\lambda}{g_0}(1+\frac{12}{5}\eta\phi g_0)\frac{12}{5}\eta(2\eta-1)(\eta-1)\frac{d}{d\upsilon}(\phi^2 g_0)\frac{T}{\phi}\nabla\phi \tag{2-13}$$

and

$$I = \frac{48}{\pi^{\frac{1}{2}}}\eta(1-\eta)\frac{\rho_p\phi^2}{d}g_0 T^{\frac{3}{2}} \tag{2-14}$$

are the desired relations. Here S is the deviatoric part of the rate of deformation tensor, and

$$\eta = \frac{1}{2}(1+e_p),\quad \mu = \frac{5m(T/\pi)^{\frac{1}{2}}}{16d^2},\quad \lambda = \frac{75m(T/\pi)^{\frac{1}{2}}}{8\eta(41-33\eta)d^2},\quad \mu_b = \frac{256\mu\phi^2 g_0}{5\pi}, \tag{2-15}$$

where m is the mass of a single particle and e_p represents the coefficient of restitution for collisions between particles.

2-2-1-2. Boundary Conditions

After the determination of the governing parameters on the stability of the system and also writing constitutive equations, in the third step we should carefully write suitable equations that represent the boundary conditions of our case. For example, in the case of Deng and Wang (2003), which has been shown in Fig. (2-3), boundary conditions at the bottom plate, which take account the momentum and energy transfer between the wall and the materials, are the same as those used by Johnson & Jackson (1987)

$$t.\sigma.n + \left(\frac{\pi\sqrt{3}}{6\phi_m}\right)\phi'\rho_P\phi g_0(\phi)T^{1/2}u_{sl} = 0 \tag{2-16}$$

$$n.q = \left(\frac{\pi\sqrt{3}}{6\phi_m}\right)\phi'\rho_P\phi g_0(\phi)T^{1/2}u_{sl}^2 + Q_0 - \left(\frac{\pi\sqrt{3}}{4\phi_m}\right)(1-e_w^2)\rho_P\phi g_0(\phi)T^{3/2} \tag{2-17}$$

In equations (2-16) and (2-17), n is the unit normal to the wall, pointing into the granular material, u_{sl} is the velocity of the granular material in contact with the wall, and t is a unit vector tangent to the wall, in the direction of the slip velocity. The nature of the plate is characterized by ϕ', a specularity factor (which measures the fraction of the momentum of an incident particle in the direction of the slip that is transmitted, on average, to the wall in a collision), and e_w, the coefficient of restitution for collisions between particles and the wall. Since the value of u_{sl} is zero for the base state, equation (2-8) is satisfied trivially.

One boundary condition at the free surface can be obtained by examining the force balance for particles at the top layer, that is, the supporting force from the materials should balance the gravity,

$$\rho dg = n.\sigma\,. \tag{2-18}$$

Where d represents the distance that free surface changed. Another boundary condition is obtained from the fact that there is no energy input at the free surface, thus

$$n.q = 0\,. \tag{2-19}$$

2-2-1-3. Base State Solution

After determination of the governing parameters on stability, the constitutive equations and the boundary conditions, we should consider an initial value for velocity variables, mass variable and energy variable and add a small distribution value to these initial values. By solving set of the obtained linear equations numerically, we will be able to forecast the stability situation of the system. Then, the stability of these steady solutions to small perturbations can be studied. By using the above mentioned method, the stable and unstable regions will be obtained according to the amount of Q_t and M_t.

In a shearing flow problem, Wang, Jackson and Sundaresan (1997) studied the stability condition of a fully developed flow of rapid granular material driven by body force, such as gravity, along a channel bounded by plane parallel walls. They considered the governing equations and boundary conditions as explained earlier. For given properties of the particles and the channel walls they found that the condition of critical stability is a relation between mean concentration of the particles and the width of the channel. They reported that the fastest growing modes are traveling waves propagating in the axial direction and these induce characteristic patterns of variation in particle concentration, as well as velocity, when the base state is unstable (Wang et al.1997). In the case of bounded shearing flows, they found that stability of the system strongly depends on the thickness of granular material. For small thickness the system is stable but when the thickness is increased it becomes unstable.

2-2-2. Stability Analysis in Gas-Particle Systems

A fluidized bed is a two-phase flow system in which particles are suspended by an imposed upward fluid flow. In principle, the fluid phase could be entirely described by the Navier-Stokes equation whereas Newton's second law could individually describe the particles. Anderson & Jackson (1967) proposed, however, a fluidized bed modeled with particles and fluid being considered as two interpenetrating continua. Note that there exists an analogy between the vertically shaken granular system and fluidized beds. The local variables describing the motion of the fluid and of the particles may be replaced by smoothed variables obtained by averaging over large regions compared with the particle spacing, but small compared with the complete system.

In the previous section we did a review about stability analysis in a dry granular system and explained the linear stability analysis method that has been used widely in stability analysis of granular systems. In the next section we will present some more details regarding stability analysis in gas-particle systems.

2-2-2-1.Stability Analysis in the Homogeneous Gas-Particle Systems

In some gas-fluidized beds it is possible to expand the bed homogeneously or uniformly for some flow rate interval beyond that corresponding to minimum fluidization (Geldart, 1986), and (Tsinontides and Jackson, 1993). Anderson & Jackson (1967) were the first to develop a linear stability analysis, which found that in the absence of the particle pressure, gas-particle systems (i.e. fluidized beds) are always unstable to any harmonic disturbance imposed to the system. In real systems, disturbances can be found in the distributor and lead to the formation of bubbles of fluid. Garg & Pritchett (1975) introduced a particle pressure term and found that gas-particle systems can be stable in some conditions. There are few correlations for describing effects of particle pressure and particle viscosity in these systems (Harris and Crighton, 1994; and Hernandez and Jimenez, 1991).

Recently, Sobral and Cunha (2002) used averaged continuum equations for describing behavior of gas and particles in a uniform and homogenous fluidized bed. The averaged equations were perturbed with small disturbances from the homogeneous fluidization state, and linearized with respect to the perturbations. They employed stability analysis for studying the stability condition of this kind of system. The aim of that study was to explore by means of a normal mode analysis the dynamical behavior of a uniform fluidized bed subjected to small amplitude disturbances like a plane wave, say: $\Omega = \Omega_0 e^{\xi t} e^{i(\omega t - kz)}$. Such disturbances, usually arise close to the distributor region of real fluidized beds, could be the origin of bubbles and clusters that appear in the upper region of the bed, changing completely the dynamics of the system (Anderson et al., 1995 and Homsy and El-Kaissy, 1980). The stable condition for this analysis is the uniform state of

fluidization, one of the simplest solutions of the governing equations may be found in Batchelor (1988). The results show that both gas-fluidized beds and liquid-fluidized beds suffer the same primary one-dimensional instabilities of a uniform fluidized bed.
This difference is in general agreement with experimental observations of fluidized beds in narrow pipes (Homsy and El-Kaissy, 1980). It may occur because in a gas-fluidized bed the disturbances increase until a full bubble develops, whereas there is no intensification of the disturbances in a liquid-fluidized bed and then, no bubbles appear. Actually, the slower growth rate of this primary instability in liquid fluidized beds is a direct consequence of the lower fluidization velocity required. The linear theory is, however, unable to predict the mechanism of secondary instability originated by the gravitational overturning caused by a dense heavy region of the bed finding itself a light region. This is experimentally observed in wider containers (Homsy and El-Kaissy, 1980).

The particle pressure effect has a stabilizing effect, since it reduces the region of instability for the beds. It happens because the particles within the bed are in active motion, frequently bouncing off one another. As the particles collide, there is an exchange of momentum and this is described by the particle pressure term. A region of enhanced concentration would then be at a higher pressure and this would drive a flow to even out the disturbance. Gas-fluidized beds require a stronger particle pressure effect in order to achieve stability. In addition, it appeared that liquid-fluidized beds are more stable than gas-fluidized bed. The growth rates of disturbances were much smaller for the case of liquid beds and much lower values of particle pressure were required to reach stability (Sobral and Cunha, 2002).

2-2-2-2.Stability Analysis in the Non-homogeneous Gas-Particle Systems

In a fluidized bed, it can be recognized that the uniformly fluidized bed has only one possible flow regime. In most gas-fluidized beds, voidage waves were observed to form and move through the bed. For low flow rate of gas, the voidage waves take on the form of single bubbles of gas that pass upwards through the bed. The bubbles of gas are easily observed as they have dimensions that are many orders of magnitude larger that the particles (Johri and Benjamin, 2002).

Johri and Glasser (2002) showed that a fluid of variable density acted upon by density dependent force exhibits the same primary and secondary instability as is seen in a gas-fluidized bed. They showed that under certain simplifying assumptions the solution of the equation of motion and continuity for the gas and particles in a fluidized bed could be related to the solution of equations for a fluid with variable density. They reported that the uniform state could lose stability in the form of plane waves. The waves emerge through a Hopf bifurcation of the base state, which occurs at a Mach number of one. The waves are sinusoidal in shape at low amplitudes, but become increasingly asymmetrical as their amplitude increases. Their stability analysis showed that these waves lose instability in the lateral direction much like the waves in a stratified fluid of variable density.

2-3. Granular Materials under Effect of Vertically Vibration

According to the definition of instability that we presented in section 2-2, granular systems should be categorized into two different categories. The first one is when we have a continuum between highly concentrated flows (where the dispersed phase dominates), and the second one is highly diluted flows (where the fluid phase dominates). According to this categorizing some instability phenomena occur when the dispersed phase dominates, and some others occur when the fluid phase dominates. For example, pattern formation is in the first category.

One of the most famous phenomena, from the first category, is the pattern formation in a shallow layer of granular material. The formation of two-dimensional patterns in biological, chemical and physical systems is often described by the nonlinear interaction of plane waves (Cross and Hohenberg, 1993). An alternative approach views patterns as ensembles of interacting localized objects, analogous to the assembly of crystals from atoms. For macroscopic pattern forming systems, one objection to the latter approach is that no ‘atoms’ exist; however spatially localized states are observed in many systems (for example, solitary waves in water and optical fibers) and can organize into simple patterns. But few examples of two-dimensional localized states are known, and these tend to be unstable and/or do not show simple pattern-forming interaction (Umbanhowar et al., 1996).

Another famous kind of instability in a granular system is oscillon formation. These phenomena might be occurring in the presence of gas or without it. We will explain more about them in the following sections.

The oscillon is found in granular materials highly dissipative media, composed of macroscopic grains that interact by means of contact forces. Despite substantial interest, granular materials remain poorly understood (Jeager et al., 1996). Experiments in which the energy is supplied by a vertically, vibrated plate show heap formation and convection (Evesque and Rajhenbach, 1989, Laroche et al., 1989), size segregation (Knight, 1993), bubbling (Behringer and Pak, 1994) and subharmonic standing waves (Fauve et al., 1989, Melo et al., PRE 72, 1994, Melo et al., PRE 75, 1994). All but the last of these phenomena are caused by surrounding gas and/or sidewall friction (Pak et al., 1995). Granular standing waves, however, arise solely from cooperative behavior resulting from collisions between particles. So we will try to obtain more about the mechanism of energy transfer in the collisions between solid particles in next section of this thesis.

2-3-1. Instability Introduced by Vertical Vibration in Dry Solid Granular Systems

As mentioned in the previous section, a granular system should be categorized into two different categories. The first one is when dispersed phase dominates and the second one is when the fluid phase play an important role. In this section we want to explain more about two of the instability phenomena of the first category.

2-3-1-1. Pattern Formations in Dry Granular Materials

When a system of granular fluid excites in finite condition, this excitation transfers energy to grains near the excited region by interaction between grains and walls, and energy will also transfer to other grains by interacting with grains near the excited wall. This transfer process is made by some collisions that are happening between grains. Hence, after a finite time, a special arrangement will happen to the shape of the particle system. This arrangement is called a pattern.

In an interesting article, Harry et al. (2004) was studying pattern formations in granular gases. They consider a layer of non-cohesive grains in a container oscillating, sinusoidally with frequency f and dimensionless acceleration amplitude $\Gamma = 4\pi^2 f^2 A / g$, where 2A is the peak-to-peak amplitude of the displacement of the container and g is the gravitational acceleration. They consider patterns that arise spontaneously, not from sidewall forcing or from interstitial gas, but from correlations induced by multiple collisions between the grains, and between the grains and the container bottom. To minimize sidewall effects, the horizontal dimensions of the container are made large compared to the layer depth.

They considered the effect of some parameters on the pattern's behavior, such as frequency and amplitude of oscillation, ratio of the depth of the layer at rest to the diameter of the particles, and also the shape of container. Patterns oscillate at $f/2$, where f is the container oscillation frequency (Harry et al., 2004).

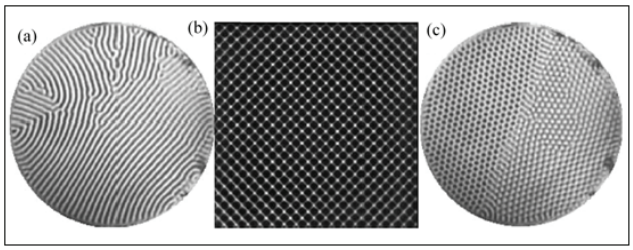

Fig. 2-11: *Patterns in oscillating granular layers (a) stripes, (b) squares, and (c) hexagons (with different phases on the left and right). The patterns oscillate at f/2, where f is the container oscillation frequency. Here* Γ, f *and* h/d *(ratio of the depth of the layer at rest to the diameter of the particles) are given by (a) 3.3, 67 Hz, 7, (b) 2.9, 25 Hz, 4, and (c) and (d) 4.0, 67 Hz, 7. In (a) and (c) the diameter of the container is* 770σ *and in (b) the container is square,* $1100\sigma \times 1100\sigma$*. The particles are bronze spheres of 0.165 mm diameter. (a) and (c) are from (Melo et al. PRL75, 1994) and (b) is from (Goldman et al., 2003).*

The phase diagram (Fig. 2-12), which is reported by Moon et al. (2002), shows the stability regions for different patterns as a function of Γ and dimensionless frequency f^*, where $f^* = f\sqrt{h/g}$ and h is the depth of the layer at rest. The transitions are well defined and are only weakly dependent on f^*. Except for the transition from a flat layer to squares, the hysteresis is small or perhaps zero. We know of no argument for the square to stripe transition as a function of frequency with Γ fixed, but we note that the transition has been found to occur at $f^* = 1/3$ (Umbanhowar and Swinney, 2000).

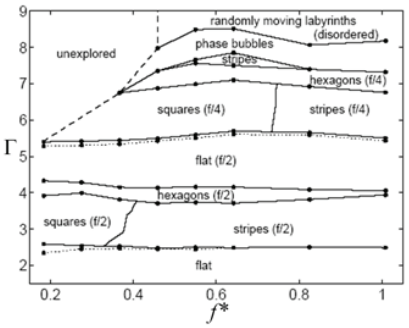

Fig. 2-12: *Phase diagram for granular patterns observed in a vertically oscillated container, as a function of the dimensionless acceleration Γ and dimensionless frequency* $f^* = f\sqrt{h/g}$. *The transitions from a flat layer to squares are hysteretic: solid lines denote the transition for increasing Γ while dotted lines denote decreasing Γ. (Bronze spheres, σ = 0.165 mm, layer depth, 5.0σ, container diameter, 770σ.) From (Moon et al., 2002).*

Some insight into the dynamics can be gained from consideration of the one-dimensional motion of a single, completely inelastic, ball on a vertically oscillating plate (Mehta and Luck, 1990). Such a model cannot of course describe the 2D spatial patterns that form in granular layers on an oscillating plate, but it does help in understanding the transitions in behavior as a function of Γ (Melo et al., 1994 and Moon et al., 2002). The inelastic ball motion, illustrated in Fig. 2-13, models the center of mass motion of a granular layer at small Γ, where the layer remains fairly compact and is highly dissipative as a consequence of multiple collisions. We will refer to the inelastic ball as "the layer", meaning the motion of the center of mass of the granular layer.

For Γ > 1, the layer leaves the plate at the point in each cycle when the plate acceleration exceeds $-g$. The layer continues in free flight until it later collides with the plate. In the regime with squares or stripes oscillating at $f/2$, the layer leaves and hits the plate every cycle, as Fig. 2-13(a) illustrates. At Γ ≈ 4.0, there is a bifurcation in the dynamics, illustrated by Fig. 2-13(b): successive trajectories now have different flight durations, with a short trajectory initiated by a collision of the layer with the plate whose acceleration is greater than g, followed by a long trajectory initiated by a collision of the layer with the plate whose acceleration is less than g. This bifurcation corresponds to a value of Γ close to that for the onset of hexagonal spatial patterns (Melo et al., 1994), pictured in Fig. 2-11(c).

While square or stripe patterns have the same appearance whether an image is obtained at time t or t + τ, hexagonal patterns at these two times are different. The two phases are both present and are separated by a phase discontinuity. In Fig. 2-11(c), the pattern on the right consists of a hexagonal array of dots, while the hexagonal pattern on the left is cellular; the two patterns will be switched one period, τ, later. Another bifurcation in the dynamics occurs for Γ > 4.5, where the layer flight duration exceeds τ, and the layer hit the container every other cycle. Now the velocity of the layer relative to the plate at the instant of collision goes to zero (at about Γ = 4.6), and the layer makes a soft landing; not enough momentum is transferred from the vertical to horizontal direction to form patterns. When Γ is increased above about 5.4, there is again a transition from a flat layer to a pattern, stripes at low frequencies and squares at high frequencies. However, now the pattern period is $f/4$ instead of $f/2$. Further increase in Γ leads to another bifurcation from trajectories with a single period to successive trajectories with different flight durations (Fig. 2-13(d)). Again this bifurcation in the dynamics of a ball corresponds to the bifurcation of the patterns from squares or stripes to hexagons.

At larger Γ, the layer becomes sufficiently dilated so that the inelastic, single ball model no longer provides a useful description of the dynamics. But even the $f/3$ and $f/6$ regimes of the single ball model (8 < Γ < 11) have been observed transiently in molecular dynamics simulations and laboratory experiments (Moon et al., 2002).

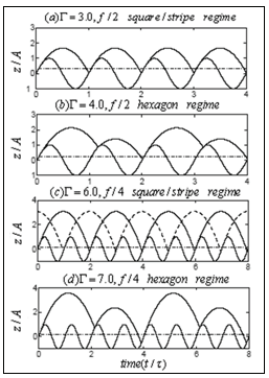

Fig. 2-13: *Trajectory of a completely inelastic ball on an oscillating plate. This is a model for the motion of the center of mass of a granular layer. The sinusoidal curve is the trajectory of the plate. The ball leaves the plate when the acceleration of the plate becomes -g, that is, when the dot-dashed line intersects the trajectory of the ball. If the ball collides with the plate above the dot-dashed line, as in (b) and (d), it leaves the plate immediately. From (Moon et al., 2002).*

There are three usual (famous) approaches for granular systems analysis: Experiments, Molecular Dynamics Simulation and Continuum system analysis. Despite the reservations regarding a continuum approach in granular media, observations of granular media have revealed many phenomena similar to those observed in continuum systems. For example, the stripe patterns shown in Fig. 2-14(a) look like those in vertically oscillated, liquid layers (Kudrolli and Gollub, 1996), (Fig. 2-14(b)) chemical reaction-diffusion systems (Ouyang and Swinney, 1991), Rayleigh-Benard convection in fluids (Behringer, 1985), and (Fig. 2-14(c)) liquid crystals (Dubois-Violette et al, 1978).

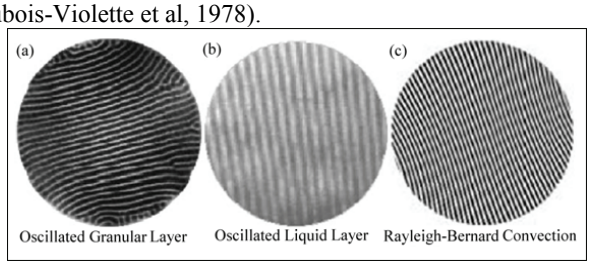

Fig. 2-14: *Forced granular materials produce qualitatively similar patterns as forced fluids: (a) stripe pattern formed by a vertically oscillated granular layer (Melo et al., PRL 75, 1994), (b) stripe pattern formed by a vertically oscillated layer of water (Kudrolli and Gollub, 1996), (c) stripe pattern formed in thermal convection of a fluid (CO2).*

Not only are the patterns similar for granular and continuum systems, but also some of the same pattern instabilities have been observed. For example, when the wavenumber of parallel convection rolls (stripes) in a Rayleigh-Benard convection becomes small, an instability leads to the formation of cross rolls with a larger wavenumber that are perpendicular to the original rolls (De Bruyn et al., 1998), (Cross and Hohenberg, 1993). The same instability has been observed for stripes in oscillated granular layers, as Fig.2-15 illustrates. The cross rolls invade the region of small wavenumber stripes such that, after sufficient time, the region contains a pattern of straight stripes perpendicular to the original pattern and with a larger wave number (Harry et al., 2004).

Granular stripe patterns also exhibit a skew varicose instability like that in convection roll patterns (Fig.2-15). When the local wavenumber becomes too large, an initially straight pattern of stripes will develop a distortion that evolves into a dislocation defect. The defect propagates away, destroying one of the stripes and decreasing the local wave number of the pattern. The stability of the stripe pattern in fluid convection is well described by amplitude equations derived from the Navier-Stokes equations for fluids (Cross and Hohenberg, 1993). That the granular pattern shows the same behavior strongly suggests a continuum description for the vibrated system is applicable (Harry et al., 2004).

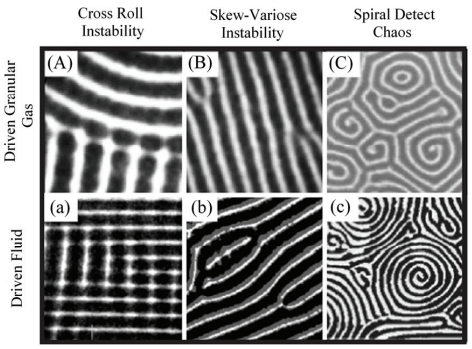

Fig. 2-15: *Instabilities of patterns found in oscillating granular layers and Rayleigh-Benard convection in a fluid. Cross roll instability in stripes: (A) Vibrated granular layer (De Bruyn et al., 1998) and (a) Rayleigh-Benard convection (Busse et al., 1971). Skew varicose instability in stripes: (B) Granular layer (De Bruyn et al., 1998) and (b) Rayleigh-Benard convection (Assenheimer and Steinberg, 1993). Spiral defect chaos in: (C) vibrated granular layer (De Bruyn et al., 2001) and (c) Rayleigh-Benard convection (Assenheimer and Steinberg, 1993).*

2-3-1-2.Oscillon Forming in the Absence of Air Effects

Granular materials deform plastically like a solid under weak shear and they flow like a fluid under high shear. These materials exhibit other unusual kinds of behavior, including pattern formation in the shaking of granular materials for which the onset characteristics of the various patterns are not well understood. Vertically shaken granular materials undergo a transition to a convective motion, which can result in the formation of bubbles.

Vibrating heaps of fine brass balls at critical amplitude, as illustrated in Fig.2-16, form themselves into fascinating patterns called oscillons (Umbanhowar et al., 1996). This self-sustaining state was named by analogy with its closest large-scale analogy, the soliton, which is a localized wave that maintains its integrity as it moves. Apparently, oscillons arise solely from cooperative behavior resulting from collisions between particles in an evacuated, vertically vibrated granular layer (Umbanhowar et al., 1996). The oscillon is likely to give insights into the dynamics of granular materials (Mukerjee, 1996).

Fig. 2-16: *The oscillon resembles a splash of water in a puddle. It moves back and forth between a state that resembles a crater and a state that resembles a peak (from the cover of Nature, 382, (1996))*

2-3-2. Instability in Fluid-Solid Granular Systems

In some industrial systems, granular material was considered in interaction with fluid. This means that space between grains was filled out by one continuous phase. This kind of system can be categorized according to the type of fluid. In some of the systems that were studied the fluid is liquid, and in some of the other systems gas interacts with the grains. In this section we will explain more about some of these kinds of systems.

2-3-2-1. Gas-Solid Granular Systems

Oscillon forming, which is explained in section 2-1-2, can be also occur in the presence of air. The situation appears somewhat similar when vibration is applied to thin layers of granular slurry with air above (Schleier-Smith and Stone, 2001). Note that interstitial fluid such as air or water is known to induce convection in a granular assembly as a vibrating plate accelerates downwards (Faraday, 1831).

In a closely related system, if a shallow bed of fine balls is shaken even at moderate amplitude with air filling the pore space, heaps develop (Pak et al.1995). In this case, the surrounding gas plays a key role in dynamics of vibrating particles at high amplitudes. It is likely that the gas trapped in the granular material is a source of the heaping. Pak et al. (1995) suggested that air heap formation in vibrating granular materials might be considered as criteria to determine when gas effects are relevant. Further understanding of the mechanism for heaping is of interest in creating ideal processing conditions and powder transport, which is of use in a number of industries, including the oil industries.

Recently, Goh and Jacobs (2002) introduced a semi-continuum model to investigate the dynamics of the formation of granular heaplets in tapped granular layers. The model was found to be able to reproduce qualitatively the heaplets characterized by an effective surface tension that depends on the magnitude of the tapping intensity. More recently, Eggers and Riecke (1993) have found that in vibrated sands the waves are excited non-resonantly, in contrast to the usual Faraday waves in liquids. They also reported that for strong hysteresis a localized oscillon solution could be found.

The shaking of granular material can be used to mix, segregate and transport the material. In an interesting article, Behringer and Pak (1994) showed, via some experiments, that such convective motion could involve bubbling the formation and upward motion of voids. The presence of gas between the grains is essential for bubbling to occur, and the instability shows characteristics of a Hopf bifurcation such as are seen at the onset of chaos. This bubbling behavior may be analogous to that observed in fluidized beds, and might be expected to occur when soils are fluidized during earthquakes.

The forming of oscillon that occurs when shaking the granular bed in the presence of air has been studied by some researchers (Umbanhowar et al, Nature 382, 1996) and study of this effect is one of our main goals in this thesis, which has been done by using the continuum approach.Fig. 2-18(b) shows one photo of an oscillon structure that formed during critical conditions of vibrations, and also you can observe the effect of air on the shape of the oscillon structure in comparing this figure with Fig. (2-16). We will study this effect in our simulations, in other sections of this thesis.

Fig. 2-17: *In material consisting of small diameter grains that are shaken at large amplitudes, bubbling of air pockets can occur after. Pak and Behringer (1994).*

Fig. 2-18: *(a) Photo of the usual device that has been used to do experiments in vibrations of a granular layer, we also used the same device for some of our observations. (b) Changing the form of oscillon in a sand-vibrating box under the presence of the air effect.*

A schematic of the device that has been used for experimental study of vibration in granular media is illustrated in Fig. 2-18(a). This device consists of one speaker with a frequency maker for creating oscillation in the bottom of a cylinder bucket. The boundary of the circle plate over the speaker is fixed and creates the same condition as we used in the continuum simulation, so the same device was made and used for some of the observations in this field (i.e. heap formation, convection motion and king formation).

2-3-2-2. Liquid-Solid Granular Systems

In some granular systems, grains have interactions with a liquid phase. Study of the instability in these kinds of systems was interesting for many researchers in recent years. Similar to what we wrote in section 2-1-1, in these systems some patterns were also observed.

The study of patterning in fluid and fluid-like systems under vertical vibration has led to an understanding of the Faraday surface instability in vibrated liquids (Faraday, 1831, Nedderman, 1992), and the recent illumination of the dynamics and properties of dry granular materials, which include a rich variety of spatiotemporal patterns (Melo et al., 1994;De Bruyn et al., 2001;Clement et al., 1996;Metcalf et al., 1997;Jaeger et al., 1996) and isolated soliton-like structures (Umbanhowar et al., 1996). Similar features were documented with clay suspensions (Lioubashevski et al., 1999), which illustrate one possible response of a fluid-particle system. Interstitial fluid (gas or liquid) is known to lead to convection in granular systems by a mechanism first postulated by Faraday, in which the surrounding fluid is drawn towards the center of the convicting domain, dragging particles along with it, as a vibrating plate accelerates downwards (Faraday, 1831;Tomas and Squires, 1998;Kozlov et al., 1998;Kumar et al., 1999;Schleier-Smith and Stone,2001) did some experiments in this field and studied the pattern formation in one liquid-solid particle layer. Their measurements were carried out in the layer that consisted of bronze micro-particle and water. They excited the bottom of this layer by an electromagnetic shaker that supplies vertical vibrations, driving the periodic motion $z(t) = A\sin(\omega t)$. The motion is parameterized by the frequency $f = \omega/2\pi$ and the dimensionless acceleration $\Gamma = A\omega^2 / g$, where g is the gravitational acceleration. They explored frequencies f from $10-150Hz$ and accelerations Γ from 0-10.

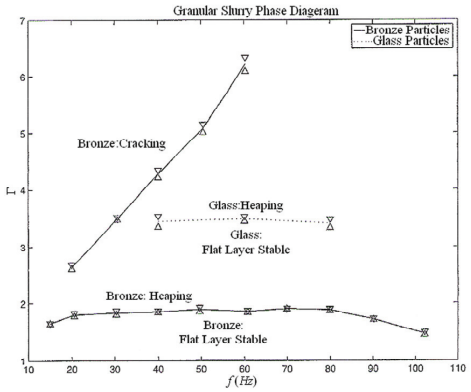

Fig. 2-19: *Composite phase portrait in acceleration versus frequency reported in (Schleier-Smith et al., 2001), for a layer of bronze or glass particles, 0.5 cm thick of 150 μm spheres. Further experiments, with a 0.75 cm thick layer, produce similar results. Shifting the cracking transition, but without a measurable effect on the transition to heaping, $\phi = 0.44$. For acceleration below $\Gamma_c = 1.9$, no motion is observed except at the highest frequencies, where the heaping response is somewhat ambiguous, forming only one pile. This is the best characterization of the high-frequency limit our experimental apparatus was able to provide (Schleier-Smith and Stone, 2001)*

In Schleier-Smith and Stone's experiments with thin layers of wet granular material, surface tension at the air-water interface precludes some aspects of this mechanism. They reported Fig.2-19 to construct the phase portrait for bronze particles. As shown in Fig.2-19, the onset of heaping occurs at nearly constant critical acceleration, $\Gamma_c = 1.9$ for bronze particles, across the range of frequencies where the response can be identified readily. They also reported that the cracking transition appears non-hysteretic, while the heaping transition exhibits hysteresis, when decreasing the forcing amplitude below Γ_c, convection stops and the surface relief cannot relax to the flat state. This latter observation is a consequence of the nonlinear constitutive response of the wet granular medium, which is a material with a yield stress. Further experiments demonstrate that varying layer thickness affect the amplitude of the cracking transition, but not its heaping instability. They reported that experiments with $150\mu m$ and $1\,mm$ glass beads reproduce all of the observed phenomena, despite the significantly different size and density of the particles.

3. Experimentation and Collision Modeling

3-1.Overview

Recall that granular standing waves arise solely from cooperative behavior resulting from collisions between particles (Umbanhowar et al., 1996). This observation highlight the important of insightful investigations of particle collision dynamics such as that presented in this section. In addition, energy and momentum transfer in granular systems is one of the most important aspects in this field of research; which is not that well understood. Granular materials transfer momentum and energy within themselves by two mechanisms, they transfer momentum by convection of lump grains and also by collision between particles. So study of the collision process and a sound understanding of these mechanisms are very important in the understanding of behavior in granular systems. An excellent understanding of energy losses, and the amount of energy dissipation when two particles collide into each other, is one of the eminent targets of this section.

Some of the experimental results that we have acquired will be presented and after a short review of other research works in this field, we will explain two of the most famous numerical solutions in modeling binary collision between two visco-elastic particles.

1) Numerical solution for solving constitutive partial differential equations of a linear and nonlinear model has been suggested for modeling binary collision.

2) Finite Elements Method.

3-1-1. Review of Other Group Works

In granular flow studies, the linear visco-elastic contact model considering Mohr friction law is applied most widely (Cundall and Strack, 1979; Babic and Shen, 1990; Zhang and Rauenzahn, 2000; Campbell, 2002). In this linear model, the normal and tangential contact forces are a linear function of the displacement and relative velocity, and the Mohr friction law controls the maximum tangential force. This linear contact model simplifies the computational procedure. Many granular flow behaviors have been studied using this simple contact force model.
In fact, for most granular material, the contact force has a nonlinear relationship with relative displacement and velocity, which has been proved by experimental data and analytical solutions (Zhang D and Whiten, 1996;Kuo et al., 2002;Mishra and Murty, 2001;Elata and Berryman, 1996).

More than one century ago, the famous Hertzain law for a non-linear, normal contact model of elastic sphere was established (Hertz, 1882). The original non-linear, tangential contact model was studied by Mindlin (1949). Both of them constructed the basic Hertzain-Mindlin contact theory for elastic granular materials. This theory has been applied widely. Walton et al. (1986) adopted a simple plastic model to handle collision dissipation. This model was applied in several other subsequent studies (Walton et al., 1986), (Thornton and Ning, 1998). Based on the Hertzain-Mindlin theory, but considering also the plastic behavior, a finite element method was used to investigate the details of a sphere colliding with a plane (Vu-Quoc and Zhang, 1999;Vu-Quoc et al., 2001;Sellgren et al., 2003).

Gugan et al. (2000) reported that in viscoelastic collision between two spheres, they lost about 40% of their kinetic energy over the range of their speeds studied. They also do some study about area of contact and duration of contact and their result was consistent with Hertz theory.

Gugan et al. (2000) reported that in the viscoelastic collision between two spheres, they lost about 40% of their kinetic energy over the range of speeds studied. They also did some studying in the area of contact and duration of contact; their results were consistent with Hertz theory.

There are many more experimental works in the field of collision. Bridges et al. (1984) did some experiments for measuring the coefficient of restitution for an ice particle as a granular particle. They attached an ice ball to an oscillator and let it strike a stationary block of ice. A sufficiently low impact velocity and reasonably large oscillator amplitude can be achieved with a compound pendulum, with the axis of rotation very close to the center of mass. For their measuring device, the angular frequency is $(Mgd / I)^{1/2}$ where M and I are the mass and moment of inertia of the system. They constructed such a

system using a disk mounted on an aluminum rod. Small weights at the top and bottom of the disk allow them to adjust the distance between the center of mass and suspension (that is rotation) axis, d. An ice ball is attached to one edge of the disk and a counter weight on the other edge in a manner such that their center of mass is at the center of the disk. Knife blades resting on polished agate plates suspend the entire system. With this system, they have achieved periods as long as 60 s with the Q-value equal to 4.For shorter oscillation periods, T<30s, 10<Q<30.

The main limitation of the above system is that collisions are not entirely free. The coupling between the ice particles and the pendulum body will cause a slight elastic deformation in the pendulum during a collision.

They made some different ambient conditions for their experiments and set the temperature of system 150-175K. In Fig. 3-1 it shows the computer simulation schematic of the collision between one rigid wall and one soft particle during the time period. This figure makes an imaginable picture of what was done by Bridge et al. As shown in the Fig. 3-2, they achieved results for the coefficient of restitution behavior by impact velocity and temperatures.

In other experimental research, Foerster et al. (1994) developed some experiments to measure the properties of the collisions between two small spheres, or between a small sphere and a semi-infinite flat wall. Their experimental apparatus is sketched in Fig. 3-3. It consists of two mechanisms that release the small spheres in a free fall. Through stroboscopic illumination, a photographic camera records successive positions of the spheres before and after the collision.

The relationship between the restitution coefficient and the impact velocity is also recognized by many researchers(Brilliantov et al,PRE , 1996 ; Gorham and Kharaz ,2000 ; Labous et al.,1997;Rosa et al.,1999).

This relationship can only be simulated with nonlinear contact model (Rosa et al.,1999;Schager and Poschel,1998). While most studies focused on normal impacts, the tangential restitution coefficient is found to be affected by the initial impact angle (Brilliantov et al, PRE,1996 ;Gorham and Kharaz,2000).

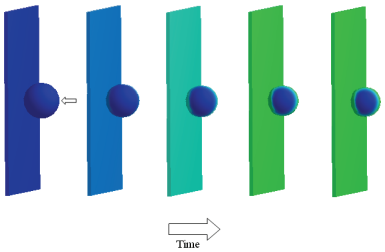

Fig. 3-1: *Schematic of the process of collision between a solid wall and one single particle during the time period. This figure shows the process of Bridge et al. experiments.*

From these studies, it is speculated that granular flow properties may depend on the details of the contact force model.

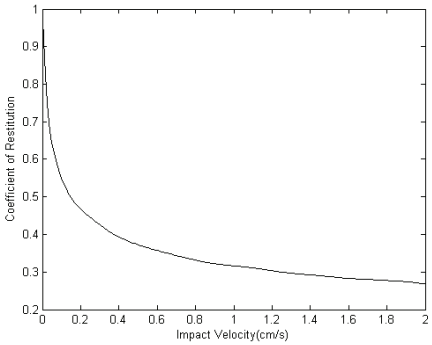

Fig. 3-2: *A schematic figure of Bridge et al. experiments and their results for coefficient of restitution verse impact velocity. They did this experiment for one single ice particle in contact of an ice wall at several different temperatures over the range 158-173K (Bridges et al., 1984).*

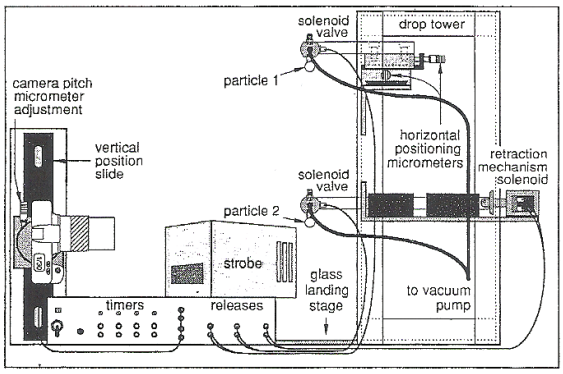

Fig. 3-3: *Side perspective of the experimental apparatus. The particles are drawn to an exaggerated scale.*

3-2. Short Review of Dynamic of Binary Collision

An elastic collision is one in which there is no loss of translational kinetic energy. That is, not only must no translational kinetic energy be degraded into heat, but also none of it may be converted to vibrational or rotational kinetic energy. It is well known, for example, that if a ball makes a glancing (i.e. not head-on) elastic collision with another ball of the same mass, initially stationary, then after collision the two balls will move off at right angles to reach other. But this is so only if the balls are smooth. If they are rough, after colliding the balls will spin, so this result (and any other results that assume no loss of translational kinetic energy) will not be valid. To help clarify the difference between the available states of collision we would like to exhibit the following example:
When a ball is dropped to the ground, one of four things may happen:
1. It may rebound with exactly the same speed as the speed at which it hit the ground. This is an elastic collision.
2. It may come to a complete rest, for example if it were a ball of soft putty. I shall call this a completely inelastic collision.
3. It may bounce back, but with a reduced speed. For want of a better term I shall refer to this as a somewhat inelastic collision.
4. If there happens to be a little heap of gunpowder lying on the table where the ball hits it, it may bounce back with a faster speed than it had immediately before collision. This would be a superelastic collision.
The ratio $\frac{Speed\ \ after\ \ collision}{Speed\ \ before\ \ collision}$ is called the coefficient of restitution, for which I shall use the symbol e.
The coefficient is 1 for an elastic collision, less than 1 for an inelastic collision, zero for a completely inelastic collision, and greater than 1 for a superelastic collision. The ratio of kinetic energy (after) to kinetic energy (before) is evidently, in this situation, e^2.

3-2-1. Kinematic Analysis of Collision between a Ball and a Surface

If a ball falls onto a table from a height h_0, it will take a time of $t_0 = \sqrt{2h_0 / g}$ to fall. If the collision is somewhat inelastic it will then rise to a height of $h_1 = e^2 h_0$ and it will take a time of et to reach a height of h_1. Then it will fall again, and bounce again, this time to a lesser height. And, if the coefficient of restitution remains the same, it will continue to do this for an infinite number of bounces. After a billion bounces, there are still an infinite number of bounces yet to come. The total distance traveled is $h = h_0 + 2h_0(1 + e^2 + e^4 + e^6 + ...)$ and the time taken is $t = t_0 + 2t_0(1 + e + e^2 + e^3 + ...)$. These are geometric series, and their sums are $h = h_0\left(\frac{1+e^2}{1-e^2}\right)$ which is independent of g (i.e. of the planet on which this experiment is performed), and $t = t_0\left(\frac{1+e}{1-e}\right)$.

3-2-2. Kinematic Analysis of Collision between a Moving Sphere with an Initially Stationary Sphere (Newton Cradle Device)

Multi-impact problems pose many difficulties and unanswered questions (Marghitu and Hurmuzlu, 1995). The simplest of these problems is the linear chain and the "Newton's Cradle" represents the most basic problem of this type. This classical problem involves a collision problem where one ball strikes one end of a linear chain of stationary balls that are in contact with one another. The system represents the simplest of the multi-body impact problems that one may consider. We have used this device as an experimental device for the multisized collision tests that will be explain in the following sections. Fig. 3-4 shows a schematic of this device.
Here, the positions of the balls before, at and after a collision were shown.
The coefficient of restitution is:

$$e = -\frac{\text{relative velocity of particles after collision}}{\text{relative velocity of particles before collision}} \tag{3-1}$$

We can consider the states shown in fig 3-5 for the velocity before and after the collision.

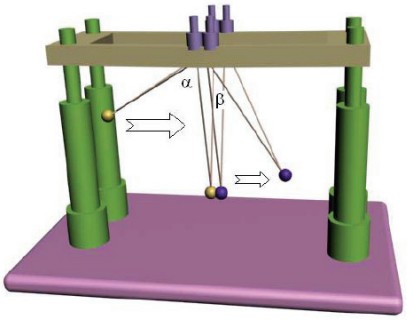

Fig. 3-4: *Schematic of apparatus used for the Newton's Cradle experiments. The balls used were nearly identical spherical glass particles suspended from very thin threads.*

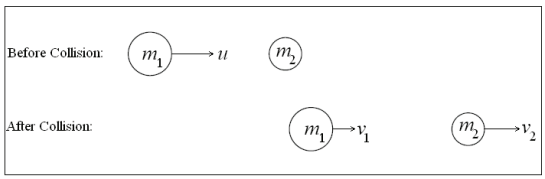

Fig. 3-5: *Binary collision between a moving ball and a stationary one.*

By applying an energy conservation law for the first particle in the Newton cradle device, as shown in Fig.3-1, we can derive the following formula for velocity of the first ball before the collision:

$$u = 2\sqrt{gl}\,\sin(\alpha/2)\,. \tag{3-2}$$

In the same way we can derive the following equation for velocity of the second particle after the collision (v_2) in our experiment device:

$$v_2 = 2\sqrt{gl}\,\sin(\beta/2)\,. \tag{3-3}$$

Since there are no external forces on the system, the linear momentum of the system is conserved:

$$m_1 u = m_1 v_1 + m_2 v_2\,. \tag{3-4}$$

So the velocity of the first particle after the collision (v_1) is:

$$v_1 = \frac{m_1 u - m_2 v_2}{m_1}\,. \tag{3-5}$$

So we can rewrite equation 3-1 for finding an equation for the coefficient of restitution in a multisized binary collision:

$$e = \left(1 + \frac{m_2}{m_1}\right)\frac{\sin(\beta/2)}{\sin(\alpha/2)} - 1\,. \tag{3-6}$$

3-2-3. Kinematic Analysis of Oblique Collision

In Fig.3-6 I show two balls just before a collision, and just after the collision. The horizontal line is the line joining the centers–for short, the "line of centers". We presume that we know the mass and velocity (speed and direction) of each ball before collision, and the goal is to find the coefficient of restitution for this multisized system. The direction of motion is to be described by the angle that the velocity vector makes with the line of centers. We want to find the velocities (speed and direction) of each ball after collision.

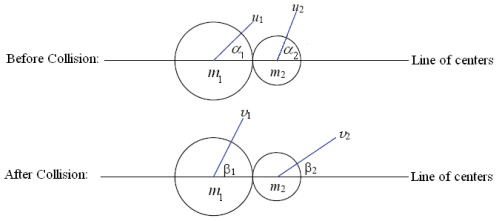

Fig. 3-6: A *schematic of an oblique collision between two multisized spherical particles.*

There are no external forces on the system along the line of centers. Therefore the component of momentum of the system along the line of centers is conserved:

$$m_1 v_1 \cos\beta_1 + m_2 v_2 \cos\beta_2 = m_1 u_1 \cos\alpha_1 + m_2 u_2 \cos\alpha_2 . \quad (3\text{-}7)$$

If we assume that the balls are smooth, i.e. that there are no forces perpendicular to the line of centers and the balls are not set into rotation, then the component of the momentum of each ball separately perpendicular to the line of centers is conserved:

$$v_1 \sin\beta_1 = u_1 \sin\alpha_1 \quad (3\text{-}8)$$

and $$v_2 \sin\beta_2 = u_2 \sin\alpha_2 . \quad (3\text{-}9)$$

Now, we can apply definition of coefficient of restitution for an oblique collision and we will have:

$$e = \frac{v_2 \cos\beta_2 - v_1 \cos\beta_1}{u_1 \cos\alpha_1 - u_2 \cos\alpha_2} . \quad (3\text{-}10)$$

3-3. Force Analysis in Binary Collision between Multisize Spherical Particles

In the collisions between granular particles, the force between particles consists of two main parts; one of them is the elastic force that causes elastic deformation in both particles, and vicious force that is made by viscosity properties in the bulk of the particles. In the following section some equations will be presented for calculating these two parts of force.

3-3-1. Elastic Forces

In the collision process, when particles deform one another due to a static (or quasistatic) contact they feel an elastic interaction force. Elastic deformation implies that after separation of the contacting particles, they recover their initial shape, i.e., there is no plastic deformation. The stress tensor $\sigma_{el}^{ij}(\vec{r})$ describes the i-component of the force, acting on a unit surface, which is normal to the direction $j (i, j = \{x, y, z\})$. In the elastic regime the stress is related to the material deformation

$$u_{ij}(\vec{r}) = \frac{1}{2}\left(\frac{\partial u_i}{\partial x_j} + \frac{\partial u_j}{\partial x_i} \right), \quad (3\text{-}11)$$

where $\vec{u}(\vec{r})$ is the displacement field at the point $\vec{r}$ in the deformed body, via the linear relation,

$$\sigma_{el}^{ij}(\vec{r}) = E_1 \left(u_{ij}(\vec{r}) - \frac{1}{3}\delta_{ij} u_{ll}(\vec{r}) \right) + E_2 \delta_{ij} u_{ll}(\vec{r}) . \quad (3\text{-}12)$$

Repeated indices are implicitly summed over (Einstein convention). The coefficients E_1 and E_2 read

$$E_1 = \frac{Y}{(1+\upsilon)}, \qquad E_2 = \frac{Y}{3(1-2\upsilon)}, \quad (3\text{-}13)$$

where Y is the Young modulus and υ is the Poisson ratio. Let the pressure $\vec{P}(x, y)$ act on the surface of an elastic semi-space, leading to a displacement field in the bulk of the semi-space (Landau and Lifsitz, 1965):

$$u_i = \iint G_{ik}(x - x', y - y', z) P_k(x', y') dx' dy' , \quad (3\text{-}14)$$

where $G_{ik}(x, y, z)$ is the corresponding Green function. For the contact problem addressed here we need only the z-component of the displacement on the surface $z = 0$, that is, we need only the component,

$$G_{zz}(x, y, z = 0) = \frac{(1-\upsilon^2)}{\pi Y} \frac{1}{\sqrt{x^2 + y^2}} = \frac{(1-\upsilon^2)}{\pi Y} \frac{1}{r}, \quad (3\text{-}15)$$

of the Green function (Landau and Lifsitz, 1965).

Consider a contact of two convex smooth bodies labeled as 1 and 2. We assume that only normal forces, with respect to the contact area, act between the particles. In the contact region their surfaces are flat. For the coordinate system centered in the middle of the contact region, where $x = y = z = 0$, the following relation holds true:

$$B_1 x^2 + B_2 y^2 + u_{z1}(x, y) + u_{z2}(x, y) = \zeta . \quad (3\text{-}16)$$

Where u_{z1} and u_{z2} are respectively the z-components of the displacement in the material of the first and of the second bodies on the plane $z=0$. The sum of the compressions of both bodies in the center of the contact area defines ζ. The constants B_1 and B_2 are related to the radius of curvature of the surfaces in contact (Landau and Lifsitz,1965).

$$2(B_1+B_2)=\frac{1}{R_1}+\frac{1}{R_2}+\frac{1}{R_1'}+\frac{1}{R_2'}$$
$$4(B_1-B_2)^2=\left(\frac{1}{R_1}-\frac{1}{R_2}\right)^2+\left(\frac{1}{R_1'}-\frac{1}{R_2'}\right)^2+2\cos(2\varphi)\left(\frac{1}{R_1}-\frac{1}{R_2}\right)\left(\frac{1}{R_1'}-\frac{1}{R_2'}\right) \tag{3-17}$$

Here R_1, R_2 and R_1', R_2' are respectively the principle radius of curvature of the first and the second body at the point of the contact and φ is the angle between the planes corresponding to the curvature radius R_1 and R_1'. The equations (3-16,17) describe the general case of contact between two smooth bodies (see (Landau and Lifsitz ,1965) for detail). The physical meaning of (3-16) is easy to see from the case of a contact of a soft sphere of a radius $R(R_1=R_2=R)$ with a hard, unreformed plane $(R_1'=R_2'=\infty)$. In this case, $B_1=B_2=\frac{1}{R}$ the compressions of the sphere and of the plane are respectively $u_{z1}(0,0)=\zeta$ and $u_{z2}=0$, and the surface of the sphere before the deformation is given by $z(x,y)=(x^2+y^2)/R.$ Then (3-16) reads in the flattened area, $u_{z1}(x,y)=\zeta-z(x,y)$, that is, it gives the condition for a point $z(x,y)$ on the body's surface to touch the plane $z=0$.

The displacements u_{z1} and u_{z2} may be expressed in terms of the normal pressure $P_z(x,y)$ which acts between the compressed bodies in the plane $z=0$. Using (3-14) and (3-15) we rewrite (3-16) as:

$$\frac{1}{\pi}\left(\frac{1-\upsilon_1^2}{Y_1}+\frac{1-\upsilon_2^2}{Y_2}\right)\iint\frac{P_z(x',y')}{r}dx'dy'=\zeta-B_1x^2-B_2y^2. \tag{3-18}$$

Where $r=\sqrt{(x-x')^2+(y-y')^2}$ and integration is performed over the contact area. Equation (3-18) is an integral equation for the unknown function $P_z(x,y)$. We compare this equation with the mathematical identity (Landau and Lifsitz, 1965),

$$\iint\frac{dx'dy'}{r}\sqrt{1-\frac{x'^2}{a^2}-\frac{y'^2}{b^2}}=\frac{\pi ab}{2}\int_0^\infty\left[1-\frac{x^2}{a^2+t}-\frac{y^2}{b^2+t}\right]\frac{dt}{\sqrt{(a^2+t)(b^2+t)t}}, \tag{3-19}$$

where integration is performed over the elliptical area $\frac{x'^2}{a^2}+\frac{y'^2}{a^2}=1$. The left-hand sides of both equations contain integrals of the same type, while the right-hand sides contain quadratic forms of the same type. Therefore, the contact area is an ellipse with the semi-axes a and b and the pressure is of the form $P_z(x,y)=cons.\sqrt{1-\frac{x^2}{a^2}-\frac{y^2}{a^2}}$. The constant may be found from the total elastic force F_{el} acting between the bodies. Integrating $P_z(x,y)$ over the contact area we obtain

$$P_z(x,y)=\frac{3F_{el}}{2\pi ab}\sqrt{1-\frac{x^2}{a^2}-\frac{y^2}{b^2}} \tag{3-20}$$

We substitute (3-20) into (3-18) and replace the double integration over the contact area by integration over the variable t, according to the identity (3-19). Thus, we obtain an equation containing terms proportional to x^2, y^2 and a constant. Equating the corresponding coefficients we obtain

$$\zeta=\frac{F_{el}D}{\pi}\int_0^\infty\frac{dt}{\sqrt{(a^2+t)(b^2+t)t}}=\frac{F_{el}D}{\pi}\frac{N(x)}{b} \tag{3-21}$$

$$B_1=\frac{F_{el}D}{\pi}\int_0^\infty\frac{dt}{(a^2+t)\sqrt{(a^2+t)(b^2+t)t}}=\frac{F_{el}D}{\pi}\frac{M(x)}{a^2b} \tag{3-22}$$

$$B_2 = \frac{F_{el}D}{\pi}\int_0^\infty \frac{dt}{(b^2+t)\sqrt{(a^2+t)(b^2+t)t}} = \frac{F_{el}D}{\pi}\frac{M(1/x)}{a^2 b}. \tag{3-23}$$

Where

$$D = \frac{3}{4}\left(\frac{1-\upsilon_1^2}{Y_1} + \frac{1-\upsilon_2^2}{Y_2}\right) \tag{3-24}$$

$x = a^2/b^2$ is the ratio of the ellipse semi-axes, and where we introduce the short-hand notation (the function $N(x)$ and $M(x)$ may be expressed as a combination of the jacobian elliptic functions $E(k)$ and $K(k)$ (Abramowitz and Stegun, 1965) :

$$N(x) = \int_0^\infty \frac{dt}{\sqrt{(1+xt)(1+t)t}} \tag{3-25}$$

$$M(x) = \int_0^\infty \frac{dt}{(1+t)\sqrt{(1+t)(1+xt)t}}. \tag{3-26}$$

From these relations follow the size of the contact area, $a, b,$ and the compression ζ as functions of the elastic force F_{el} and the geometrical coefficients B_1 and B_2.

The dependence of the force F_{el} on the compression ζ may be obtained from scaling arguments: If we rescale $a^2 \to \alpha a^2, b^2 \to \alpha b^2, \zeta \to \alpha\zeta$ and $F_{el} \to \alpha^{3/2} F_{el}$ with α constant, equations (3-21-3-23) remain unchanged. That is, when S changes by the factor, the semiaxis a and b change by the factor $\alpha^{1/2}$ and the force by the factor $\alpha^{3/2}$ i.e., $a \sim \zeta^{1/2}, b \sim \zeta^{1/2}$ and

$$F_{el} = const.\zeta^{3/2}. \tag{3-27}$$

The dependence (3-27) holds true for all smooth convex bodies in contact. To find the constant in (3-27) we divide (3-23) by (3-22) and obtain the transcendental equation:

$$\frac{B_2}{B_1} = \frac{\sqrt{x}M(1/x)}{M(x)} \tag{3-28}$$

For the ratio of semiaxes x. Let x_0 be the root of Eq. (3-28), then $a^2 = x_0 b^2$ and we obtain,

$$\zeta = \frac{F_{el}D}{\pi}\frac{N(x_0)}{b} \tag{3-29}$$

$$B_1 = \frac{F_{el}D}{\pi}\frac{M(x_0)}{x_0 b^3}. \tag{3-30}$$

Where $N(x_0)$ and $M(x_0)$ are pure numbers. Equations (3-29, 3-30) allow us to find the semiaxes b and the elastic force F_{el} as a function of the compression ζ. Hence we obtain for the force, i.e. we get the constant in (3-27):

$$F_{el} = \frac{\pi}{D}\left(\frac{M(x_0)}{B_1 x_0 N(x_0)}\right)^{1/2}\zeta^{3/2} = C_0\zeta^{3/2}. \tag{3-31}$$

For the special case of contacting spheres $(a = b)$:

$$B_1 = B_2 = \frac{1}{2}\left(\frac{1}{R_1} + \frac{1}{R_2}\right) = \frac{1}{2}\frac{1}{R_{eff}}. \tag{3-32}$$

In this case $x_0 = 1$, and $N(1) = \pi$, $M(1) = \pi/2$ and the solution of Eqs. (3-29, 30) yields,

$$a^2 = R_{eff}\zeta \tag{3-33}$$

$$F_{el} = \rho\zeta^{3/2}; \quad \rho = \frac{2Y}{3(1-\upsilon^2)}\sqrt{R_{eff}} \tag{3-34}$$

where we use the definition of the constant D, (3-34). This contact problem was solved by Heinrich Hertz in (1882). It describes the force between elastic particles. For inelastically deforming particles it describes the repulsive force in the static case.

3-3-2. Viscous Forces

When the contacting particles move with respect to each other, i.e. the deformation changes with time, an additional dissipative force arises, which acts in the opposite direction to the relative particle motion. The dissipative processes occurring in the bulk of the body cause a viscous contribution to the stress tensor. For small deformation the respective component of the stress tensor is proportional to the deformation rate $\dot{u}_{ij}(\vec{r})$ according to the general relation (Brilliantov et al.,1996a):

$$\sigma_{dis}^{ij}(\vec{r},t) = E_1 \int_0^t d\tau \psi_1(t-\tau)\left[\dot{u}_{ij}(\vec{r},\tau) - \frac{1}{3}\delta_{ij}\dot{u}_{ll}(\vec{r},\tau)\right] + E_2 \int_0^t d\tau \psi_1(t-\tau)\delta_{ij}\dot{u}_{ll}(\vec{r},\tau) \tag{3-35}$$

where the (dimensionless) functions $\psi_1(t)$ is the relaxation function for the distortion deformation and $\psi_2(t)$ for the dilatation deformation. In many important applications the viscous stress tensor may be simplified significantly if the relative velocity of the colliding bodies is much smaller than the speed of sound in the particle material, and if the characteristic relaxation times of the dissipative processes $\tau_{vis,1/2}$ are much smaller than the duration of the collision t_c,

$$\tau_{vis,1/2} = \int_0^\infty \psi_{1/2}(\tau)d\tau \ll t_c \,. \tag{3-36}$$

The viscous constants η_1 and η_2 may be used instead of the functions $\psi_1(t)$ and $\psi_2(t)$. Thus

$$\eta_{1/2} = E_{1/2}\tau_{vis,1/2} = E_{1/2}\int_0^\infty \psi_{1/2}(\tau)d\tau \tag{3-37}$$

and the dissipative stress tensor reads (Brilliantov et al., 1996)

$$\sigma_{dis}^{ij}(\vec{r},t) = \eta_1\left[\dot{u}_{ij}(\vec{r},\tau) - \frac{1}{3}\delta_{ij}\dot{u}_{ll}(\vec{r},\tau)\right] + \eta_2\delta_{ij}\dot{u}_{ll}(\vec{r},\tau)\,. \tag{3-38}$$

It may be also shown that the above conditions are equivalent to the assumption of quasistatic deformation (Brilliantov et al.,1996a), (Brilliantov et al., 1996b). When the material is deformed quasistatically, the displacement field $\vec{u}(\vec{r})$ in the particles coincides with that for the static case $\vec{u}_{el}(\vec{r})$, which is the solution of the elastic contact problem. The field $\vec{u}_{el}(\vec{r})$, in its turn, is completely determined by the compression ζ, which varies with time during the collision, i.e. $\vec{u}_{el} = \vec{u}_{el}(\vec{r},\zeta)$. Therefore, the corresponding displacement rate may be approximated as

$$\dot{\vec{u}}(\vec{r},t) \simeq \dot{\zeta}\frac{\partial}{\partial\zeta}\vec{u}_{el}(\vec{r},\zeta) \tag{3-39}$$

and the dissipative stress tensor reads, respectively

$$\sigma_{dis}^{ij} = \dot{\zeta}\frac{\partial}{\partial\zeta}\left[\eta_1\left(u_{ij}^{el} - \frac{1}{3}\delta_{ij}u_{ll}^{el}\right) + \eta_2\delta_{ij}u_{ll}^{el}\right]. \tag{3-40}$$

From (3-40) and (3-12) follows the relation between the elastic and dissipative stress tensors within the quasistatic approximation,

$$\sigma_{dis}^{ij} = \dot{\zeta}\frac{\partial}{\partial\zeta}\sigma_{el}^{ij}(E_1 \leftrightarrow \eta_1, E_2 \leftrightarrow \eta_2), \tag{3-41}$$

where we emphasize that the expression for the dissipative tensor may be obtained from the corresponding expression for the elastic tensor after substituting the elastic constants by the relative viscous constants and application of the operator $\dot{\zeta}\frac{\partial}{\partial\zeta}$.

The component σ_{el}^{zz} of the elastic stress is equal to the normal pressure P_z at the plane

$z = 0$ of the elastic problem, Eq. (3-20):

$$\sigma_{el}^{zz}(x,y,0) = E_1 \frac{\partial u_z}{\partial z} + \left(E_2 - \frac{E_1}{3}\right)\left(\frac{\partial u_x}{\partial x} + \frac{\partial u_y}{\partial y} + \frac{\partial u_z}{\partial z}\right) = \frac{3F_{el}}{2\pi ab}\sqrt{1 - \frac{x^2}{a^2} - \frac{y^2}{b^2}}\,. \tag{3-42}$$

Now we can compute the total dissipative force acting between the bodies. Instead of a direct computation of the dissipative stress tensor, we employ the method proposed in (Brilliantov et al., 1996a), (Brilliantov et al., 1996b). We transform the coordinate axes as

$$x = \alpha x', \qquad y = \alpha y', \qquad z = \alpha z' \tag{3-43}$$

with

$$\alpha = \left(\frac{\eta_2 - \frac{1}{3}\eta_1}{\eta_2 - \frac{2}{3}\eta_1}\right)\left(\frac{E_2 - \frac{2}{3}E_1}{E_2 - \frac{1}{3}E_1}\right) \qquad \beta = \frac{(\eta_2 - \frac{1}{3}\eta_1)}{\alpha(E_2 - \frac{1}{3}E_1)}. \tag{3-44}$$

$$a = \alpha a' \qquad b = \alpha b' \tag{3-45}$$

And perform the transformations:

$$\eta_1 \frac{\partial u_z}{\partial z} + \left(\eta_2 - \frac{\eta_1}{3}\right)\left(\frac{\partial u_x}{\partial x} + \frac{\partial u_y}{\partial y} + \frac{\partial u_z}{\partial z}\right) =$$

$$\beta\left[E_1 \frac{\partial u_z}{\partial z'} + \left(E_2 - \frac{E_1}{3}\right)\left(\frac{\partial u_x}{\partial x} + \frac{\partial u_y}{\partial y} + \frac{\partial u_z}{\partial z}\right)\right] = \tag{3-46}$$

$$\beta \frac{3F_{el}}{2\pi a'b'}\sqrt{1 - \frac{x'^2}{a'^2} - \frac{y'^2}{b'^2}} = \beta\alpha^2 \frac{3F_{el}}{2\pi ab}\sqrt{1 - \frac{x^2}{a^2} - \frac{y^2}{b^2}}$$

By applying the operator $\dot{\zeta}\,\partial/\partial\zeta$ to the last expression in the right-hand side we obtain the dissipative stress tensor. Subsequent integration over the contact area yields finally the total dissipative force acting between the bodies:

$$F_{dis} = A\dot{\zeta}\frac{\partial}{\partial\zeta}F_{el}(\zeta)\,, \tag{3-47}$$

where

$$A = \alpha^2\beta = \frac{1}{3}\frac{(3\eta_2 - \eta_1)^2}{(3\eta_2 + 2\eta_1)}\left[\frac{(1-\upsilon^2)(1-2\upsilon)}{Y\upsilon^2}\right]. \tag{3-48}$$

Using the scaling relations for the elastic force, Eq. (3-47), and for the semiaxes of the contact ellipse, we obtain

$$\frac{\partial F_{el}}{\partial\zeta} = \frac{2}{3}\frac{F_{el}}{\zeta}, \qquad \frac{\partial a}{\partial\zeta} = \frac{1}{2}\frac{a}{\zeta} \qquad \frac{\partial b}{\partial\zeta} = \frac{1}{2}\frac{b}{\zeta}\,. \tag{3-49}$$

Then from (3-46) and (3-31), the distribution of the dissipative pressure in the contact area may be found:

$$P_z^{dis}(x,y) = \frac{3A}{4\pi}\frac{AC_0}{ab}\dot{\zeta}\sqrt{\zeta}\left(1 - \frac{x^2}{a^2} - \frac{y^2}{b^2}\right)^{-1/2}\,, \tag{3-50}$$

where the constant C_0 is defined in (3-31).

We wish to stress, that to derive the above expressions, we only assumed that the surfaces of the two bodies in the vicinity of the contact point before the deformation, are described by quadratic the forms, $z_1 = k_{ij}^{(1)}x_i x_j$ and $z_2 = k_{ij}^{(2)}x_i x_j (i,j = x,y,z)$, where $k_{ij}^{(1/2)}$ are symmetric tensors (Landau L.D. and Lifsitz E.M., 1965). Therefore the obtained relations are valid for a contact of arbitrarily shaped convex bodies. For spherical particles of the identical material, (3-47) and (3-34) yield (Brilliantov et al.,1996a), (Brilliantov et al., 1996b),

$$F_{dis} = \frac{2}{3}A\rho\dot{\zeta}\sqrt{\zeta}\,, \tag{3-51}$$

with ρ as defined in (3-34). Hence, the total force acting between the viscoelastic spheres takes the simple form of (Brilliantov et al., 1996a), (Brilliantov et al., 1996b):

$$F = \rho\left(\zeta^{3/2} + \frac{3}{2} A\sqrt{\zeta}\dot{\zeta} \right). \tag{3-52}$$

The range of validity of (3-52) for the viscoelastic force is determined by the quasistatic approximation. The impact velocity must be significantly smaller than the speed of sound.

3-4. Models of Normal Collisions

In one of most usual fields in modeling collisions, the contact action between two particles can be described with an elastic spring, viscous dashpot and friction slider. If we only consider the normal force, generally, the mechanical model is shown as Fig. 3-7. In fact, the behavior of the materials is modeling with one simple Kelwin model. In this figure, Ke and Ce are the effective stiffness and viscosity respectively, m_1 and m_2 are the masses of the two colliding spheres.

In this contact model, the elastic force and viscous force can be written as

$$F_e = k_n \zeta^{\beta} \text{ and } F_V = C_n \zeta^{\alpha}\dot{\zeta}. \tag{3-53}$$

Where x represents the amount of overlap between the two particles, $\dot{x}$ is the relative velocity of the two spheres moving towards each other.

Based on the Newton's Second Law, the particle momentum equation is

$$m\ddot{\zeta} + c_n \zeta^{\alpha}\dot{\zeta} + k_n \zeta^{\beta} = 0 \tag{3-54}$$

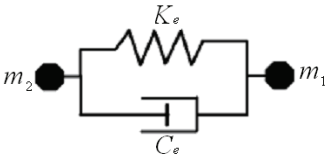

Fig. 3-7: *Particle contact model for normal force.*

Where m is the sphere mass, and α and β are the index for linear and non-linear contact models.

3-4-1. Linear Model

In the simple linear model, the elastic force and viscous force are the linear function of displacement and relative velocity respectively. We have $F_e = k_e\zeta$ and $F_V = c_n\dot{\zeta}$ when $\alpha = 0$ and $\beta = 1$.

Therefore, the momentum equation (Eq. 3-2) can be written as

$$m\ddot{\zeta} + c_n\dot{\zeta} + k_e\zeta = 0. \tag{3-55}$$

In the current granular flow simulations, this linear model is applied widely to study the basic physical process of complex granular systems (Babic and Shen, 1990;Zhang, Rauenzahn, 2000;Campbell, 2002; Zhang and Rauenzahn, 1997).

3-4-2. Non-Linear Model

When two spheres collide, in fact, the contact area increases with the increase of contact force. In this case a non- linear model can describe the interaction process of the two spheres more accurately. In the non- linear model, the elastic normal force was established by Hertz (1882). In his theory there is no damping and the elastic index in Eq. (3-2) is β=3/2. This model has been proven with physical experimentation and numerical solutions (Zhang and Whiten, 1996;Kuo et al., 2002;Falcon et al., 1998;Tsuji et al., 1992;Tsuji et al., 1993).

In previous research for calculating viscous force, several different values for α were determined based on experimental data and analytical solution. We found in the previous section that α=1/2 for sphere-to-sphere contact. Experiments by Falcon et al. (1998) showed that it was better to set α=1/4. Some analytical comparisons between a linear model and non-linear model with α=1/4 have been carried out (Zhang and Whiten, 1996;Tsuji et al., 1992). It was shown that the stress, displacement and relative velocity of the two colliding spheres were simulated more reasonably with the non-linear model. In earlier studies α=3/2 was also used to study the contact process (Mishra and Murty, 2001) and determined that α=4/5 and $\beta = 8/5$ fit to their experimental results.

Brilliantov et al. in 1996 (Brilliantov et al.,1996a) used the nonlinear model for modeling the collision and used the following equations (3-4). With the initial conditions $\dot{\xi}(0) = g^n, \xi(0) = 0$ (where g^n represent relative velocity of particles) for their model (Brilliantov et al.,1996a)

$$\ddot{\xi} + \frac{2Y\sqrt{R_{eff}}}{3m_{eff}(1-\nu^2)}(\xi^{3/2} + \frac{3}{2}A\sqrt{\xi}\dot{\xi}) = 0 \tag{3-56}$$

$$in \ \ the \ \ case \ \ A\dot{\xi} \ll \xi \ \ : \ddot{\xi} + \frac{2Y\sqrt{R_{eff}}}{3m_{eff}(1-\nu^2)}(\xi + A\dot{\xi})^{3/2} = 0. \tag{3-57}$$

Where ξ representing overlapping distance, Y is Young modulus and ν is the Poisson ratio for the material the particles consist of. The coefficient A was considered to be a fit parameter. Fig.3-9 shows their result and the experimental result of bridge et al.(1984)has been shown also in Fig,3-2 perviously.

3-4-3. Simplified Model for Collision of Multisize Viscoelastic Spheres

Collisions between particles, which have been studied since Newton's time, still pose many difficulties and unanswered questions. One of the simplest of these problems is the binary collision between two spherical grains, which involves repulsive, rigid elastic interactions as well as dissipative frictional contacts. A binary collision represents the simplest of the multi-body interactions in a dense granular flow. The frictional interaction represents the most fundamental difference between a granular system and a molecular system. Many diverse examples of granular flows exist, ranging from the flow of grains in a silo (Nedderman, 1992) to planetary rings (Bridges et al., 1984). Flow dynamics of granular materials are different from the other familiar forms of matter. As an example, in these systems solid-like and fluid-like qualities may exist side-by-side (Jaeger at al., 1996). This behavior could be due to a complex nonlinear elasticity exhibited collectively by an aggregate of grains that governs the flow properties of the system. In this light, developing realistic models for the granular collisions, by which slow collisions for rough as well as smooth grains can be described, would be invaluable in the understanding of the physics of deformation and flow of granular materials, especially in industrial systems.

Further examination of the impact problem studied in this section requires a quantitative description of the brittle behavior of particles. In the following section, a viscoelastic model will be presented characterized by a time dependent relation between stress and strain. Models for glass balls may be constructed by suitable combinations of springs and dashpots; where the dashpots introduce a viscous type resistance associated with internal friction in solids.

Note that the neither the Maxwell nor Kelvin model represents the behavior of most viscoelastic materials including the glass balls used in Newton's cradle device, illustrated in Fig. (3-4). For example, the Maxwell model (Findley et al., 1989) predicts that the stress asymptotically approaches zero when the strain is kept constant. On the other hand, the Kelvin model, does not describe a permanent strain after unloading. In this study, a second spring is placed in series with the Kelvin model used in (Brilliantov et al., 1996a), to develop a model of linear viscoelastic material equivalent to a Maxwell model with a spring in series. The schematic of the three-parameter model used in this study is shown in Fig. (3-8).

As we stated earlier in the nonlinear model section, a contact force model such as $F = k\xi^{\gamma} + c\xi^{\eta}\, d\xi/dt$ is often adopted to capture the key features of granular inelastic interactions when the impact velocity is much less than the speed of sound in the grain material (Kuwabara and Kono, 1987). Here, $\xi = (r_1 + r_2) - |\vec{r}_1 - \vec{r}_2|$ represents the overlapping of a pair of spherical particles with radiuses r_1 *and* r_2 at positions $\vec{r}_1$ *and* $\vec{r}_2$, k and c are the coefficients characterizing the elastic and viscoelastic behavior of the grains, respectively.

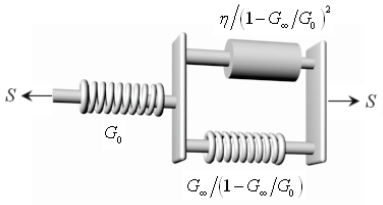

Fig. 3-8: *Model consists of auxiliary spring in series with Kelvin model.*

We have calculated the value of k, c, γ *and* n in section (3-3) according to classical calculation in continuum mechanics and Hertz theory, and rewrite them (Eqs. (3-52), (3-34)) as follows:

$$F = \rho\left(\zeta^{3/2} + \frac{3}{2}A\sqrt{\zeta}\dot{\zeta}\right)$$
$$k = \rho = \frac{2Y}{3(1-\upsilon^2)}\sqrt{R_{eff}}$$

So in fact, we calculated that $\gamma = 3/2, n = 1/2$ and $c = 3/2Ak$ when A represents a parameter for fitting behavior.

The $\zeta^{1/4}$ dependence of contact force on viscous dissipation observed in experiments (Falcon et al., 1998) appears to be at odds with the $\zeta^{1/2}$ scaling predicted by the Morgado and Oppenheim model (Morgado and Oppenheim, 1997). Moreover, Hunt and Crossley (1975) have suggested that by equating the energy loss derived from the momentum impulse approach, and that derived from hysteretic damping, an expression for the coefficient c in Eq. (3-58) may be found as $c = 3k\left(1-e^2\right)/4V_{imp}$, where e is the coefficient of restitution which is a measurable parameter relating the pre and post relative velocities in a collision, and V_{imp} is the relative velocity of the grains before impact. It is surprising that in Hunt and Crossley (1975) the $\zeta^{3/2}$ dependence of contact force on the viscous dissipation was assumed.

Schwager and Pöschel (1998) have suggested for colliding viscoelastic grains with radii R_1 and R_2, and masses m_1 and m_2 the coefficient c depends on the Young modulus, the viscous constants and the Poisson ratio of the material:

$$c = c_n \frac{E}{m_{eff}\left(1-\nu^2\right)}\left(R_{eff}\right)^{1/2}, \tag{3-60}$$

here c_n is the normal damping coefficient,

$$m_{eff} = m_1 m_2 / \left(m_1 + m_2\right) \tag{3-61}$$

and $R_{eff} = R_1 R_2 / \left(R_1 + R_2\right)$. (3-62)

The form of expression (3-60) was later revised by Morgado and Oppenheim (1997). They suggested that c has the same form as k, namely Eq. (3-59), with E and ν replaced by η_1 and η_2, respectively. Here η_1 and η_2 are the corresponding viscoelastic coefficients. These coefficients, however, are not easy to find in the literature (Schwager and Pöschel, 1998)

We tried to modify this equation for two particles that are different in material and define effective Young modulus as the following equation:

$$\frac{1}{E_{eff}} = \frac{(1-\nu_1^2)}{E_1} + \frac{(1-\nu_2^2)}{E_2}. \tag{3-63}$$

Brilliantov et al. (Brilliantov et al.,1996a) consider a Kelvin model the same as shown in Fig. 3-7 for modeling a monosized collision. They considered the Kelwin model for modeling the viscoelastic behavior of spherical particles. But we know that the real materials are not exactly Kelwin material, so as you see in Fig. (3-8) we have added one spring in seri of one Kelwin model for modeling viscoelastic behavior of the particles. So now we modify the previous equation for governing the multisized and multi-material state. So the following equation will be explaining the force between the two particles in this state:

$$F = \frac{4E_{eff}\sqrt{R_{eff}}}{3m_{eff}}\xi^{\frac{3}{2}} + 2A\frac{E_{eff}R_{eff}^{(1-n)}}{m_{eff}}\xi^n\dot{\xi}. \tag{3-64}$$

This force is acting on both particles in the opposite direction. So we can calculate acceleration of each particle from the following equation:

$$\left(\frac{d^2\xi}{dt^2}\right)_{particle\ i} = F \times \frac{m_{eff}}{m_i}. \tag{3-65}$$

We know that if we put n =1/2 in these equations (3-64) this model becomes the same as the model which was described previously in section (3-3) and also will be the same as the model that was used by Brilliantov et al. (Brilliantov et al., PRE, 1996) in 1996. We review that in equation (3-56, 3-57).

The initial conditions for Eq. (3-10) are $\xi(0)=0$ and $\dot{\xi}(0)=2\sqrt{gl}\sin\alpha/2$. The coefficient of n and A should be changed to obtain the best conformity with the experimental result.
From previous research, which was reviewed in section 3-4-2, the acceptable range for n is 0.4 to 1.5. So we tried to solve the model with several n's. For each n, we used constant A in the equation (3-64) as a fitting parameter for finding the best curve for which in our model obtains the greatest conformity with the experimental result reported by Bridge et al. in (1984). In this step we calculated the best value for A in a least squares sense for each n and after calculating the best value for A, we calculated the least square sense for each n according the calculated value for A, then we compared values of the lease square sense together for finding the best value for n.
At the end of this process we found that n = 0.65 had the greatest conformity with the experimental result. In Fig. (3-9) this conformity was shown. The property of material that was used for this Figure was the same property of an ice particle in low temperature (*Physical properties of rocks,* edited by Hellwege et al., 1982): Young modulus $E=10GPa$, Poisson ratio $\nu=0.3$, and particle size $D=2cm$, with density $\rho=1000kg/m^3$. By solving this model numerically the coefficient of restitution, which is defined as $e_n=-\dot{\xi}(t_c)/\dot{\xi}(0)$ will be calculated.
For impact velocity equal to $1cm/s$, we compared $\xi,\dot{\xi},\ddot{\xi}$ and Relative velocity in elastic collision and viscoelastic collision from our model. The result was shown in Fig. (3-10) to Fig. (3-13).

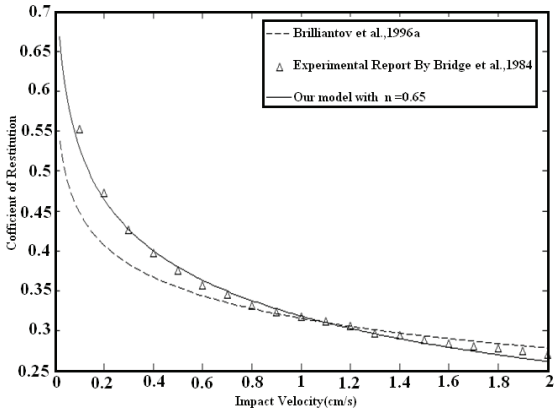

Fig. 3-9: *Coefficient for restitution in several different impact velocities measured in* (cm/s) *for a spherical ice particle in the diameter of* 1*cm for our model in comparing with the experimental result reported by Bridge et al (1984) and the model of Brilliantov et al. (Brilliantov et al., 1996a).*

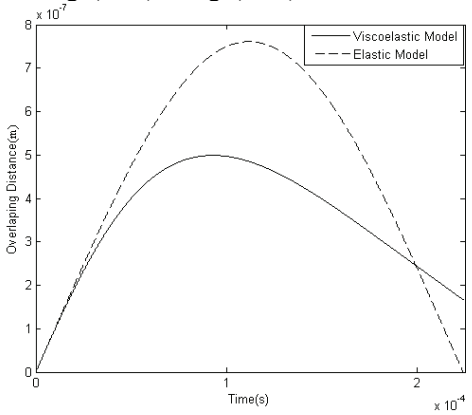

Fig. 3-10: *Overlapping distance in collision between two ice particles with diameter of 2 cm, and property of which is mentioned in the text, for Elastic state and Viscoelastic collision (our model n=0.65). One particle is stationary at the start of the collision and the other one has the velocity of 1cm/s.*

Fig. 3-11: *Rate of Overlapping distance change with time measured in (m/s) in the collision between two ice particles with a diameter of 2 cm, and property of which is mentioned in the text, for Elastic state and Viscoelastic collision (our model n=0.65). One particle is stationary at the start of the collision and the other one has the velocity of 1cm/s.*

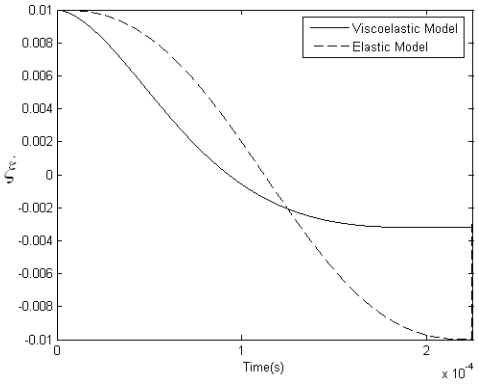

Fig. 3-12: *Acceleration $\ddot{\xi}$ measured in (m/s^2) in the collision between two ice particles with a diameter of 2 cm, and property of which is mentioned in the text, for Elastic state and Viscoelastic collision (our model n=0.65). One particle is stationary at the start of the collision and the other one has the velocity of 1cm/s.*

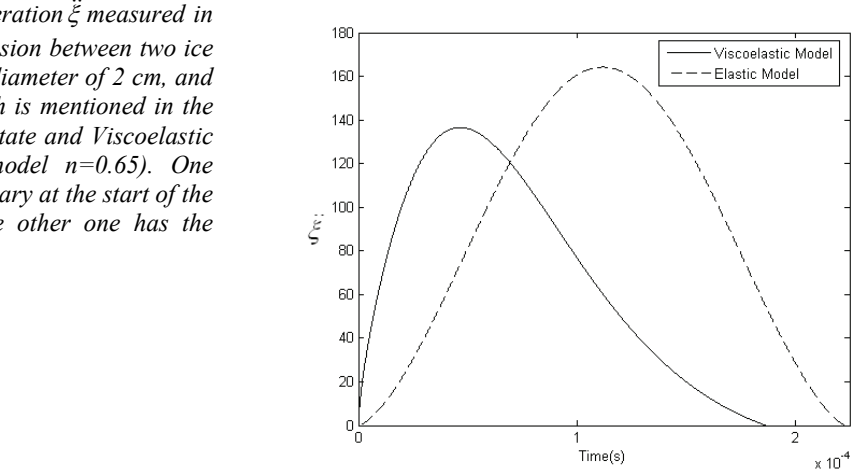

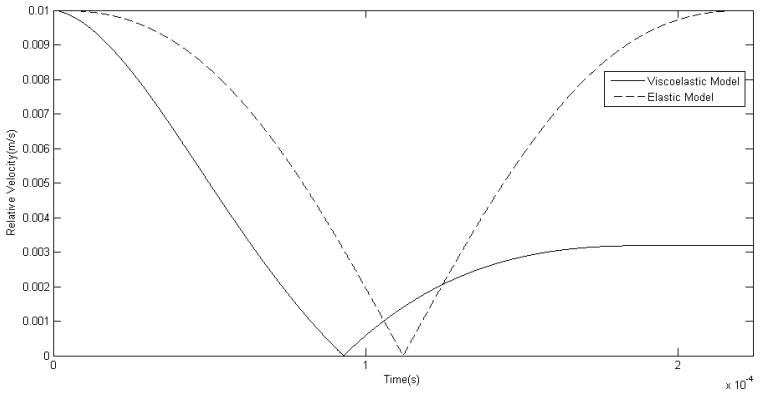

Fig. 3-13: *Relative velocity measured in (m/s) in the collision between two ice particles with a diameter of 2 cm, and property of which is mentioned in the text, for Elastic state and Viscoelastic collision (our model n=0.65). One particle is stationary at the start of collision and the other one has the velocity of 1cm/s.*

In the monosized case, when the impact velocity increases then the $\xi, \dot{\xi}, \ddot{\xi}$ will also increase. In Fig. (3-14) for spherical ice particles with a 2cm diameter, the effect of impact velocity on the $\xi, \dot{\xi}, \ddot{\xi}$ are shown.

3-5. Review of Hertz Theory Formulation in Elastic Collision

Hertz theory is the famous method in analysis of binary collisions in elastic materials. Many previous researchers have used this theory for confirming validation of their results. In this section we want to give a short review on this formulation for multisized collisions between two spherical balls.
Fig. (3-15) depicts the contact between two spheres subjected to normal load P. The equivalent elastic modulus E_{eff} and the equivalent contact curvature $1/R_{eff}$ are given in Eqs. (3-62) and (3-63).The contact area is a circle radius (Fig (3-15a)). On the contact surface, the distribution of the Hertz normal pressure p is axisymmetric and shaped as half of an ellipse. At a point A of a distance r from the center of the contact area, the normal pressure $p(r)$ can be expressed as

$$p(r) = P_m \left[1 - \left(\frac{r}{a} \right)^2 \right]^{1/2} \qquad (3\text{-}66)$$

The normal pressure is related to the normal force P by

$$P_m = \frac{3P}{2\pi a^2}. \qquad (3\text{-}67)$$

Fig. (3-16, b) depicts the elliptic profile of the Hertz normal pressure across the diameter of the contact area.

With the radius a of the contact area given by (Johnson , 1985):

$$a = \left(\frac{3PR_{eff}}{4E_{eff}} \right)^{1/3}. \qquad (3\text{-}68)$$

The approach of two distant points on the two spheres can be expressed as (Johnson KL.,1985):

$$\alpha_1 + \alpha_2 = \frac{a^2}{R_{eff}} = \left(\frac{9P^2}{16R_{eff}E_{eff}^2} \right)^{1/3}. \qquad (3\text{-}69)$$

By introducing Eq. (3-68) into Eq. (3-67), we obtain

$$P_m = \frac{3P}{2\pi a^2} = \left(\frac{6PE_{eff}^2}{\pi^3 R_{eff}^2} \right)^{1/3}. \qquad (3\text{-}70)$$

Hertz's theory assumes that the contact area is much smaller than the size of the spheres, i.e. $a \ll R_1 \text{ and } a \ll R_2$.

We calculated the elastic force in section 3-3-1 so we can write according to Eq. (3-34)

$$m\frac{d^2\delta}{dt^2} = -K\zeta^{3/2}. \qquad (3\text{-}71)$$

Integrating with respect to ζ gives

$$\frac{1}{2}\left\{ V^2 - \left(\frac{d\delta}{dt} \right)^2 \right\} = \frac{2}{5}\frac{K}{m}\zeta^{5/2}, \qquad (3\text{-}72)$$

where $V = (V_2 - V_1)_{t=0}$ is the velocity of approach. For $\zeta_{\max.}$, the maximum compression, which occurs when $d\zeta/dt = 0$, we can write

$$\zeta_{\max} = \left(\frac{5m_{eff}V^2}{4K} \right)^{2/5} = \left(\frac{15mV^2}{16R_{eff}^{1/2}E_{eff}} \right)^{2/5}. \qquad (3\text{-}73)$$

The compression time curve is found by a second integration, thus

$$t = \frac{\zeta_{\max}}{V} \int \frac{d(\zeta/\zeta_{\max.})}{\{1-(\zeta/\zeta_{\max})^{5/2}\}^{1/2}}. \qquad (3\text{-}74)$$

After the instant of maximum compression t^*, the spheres expand again. Since they are perfectly

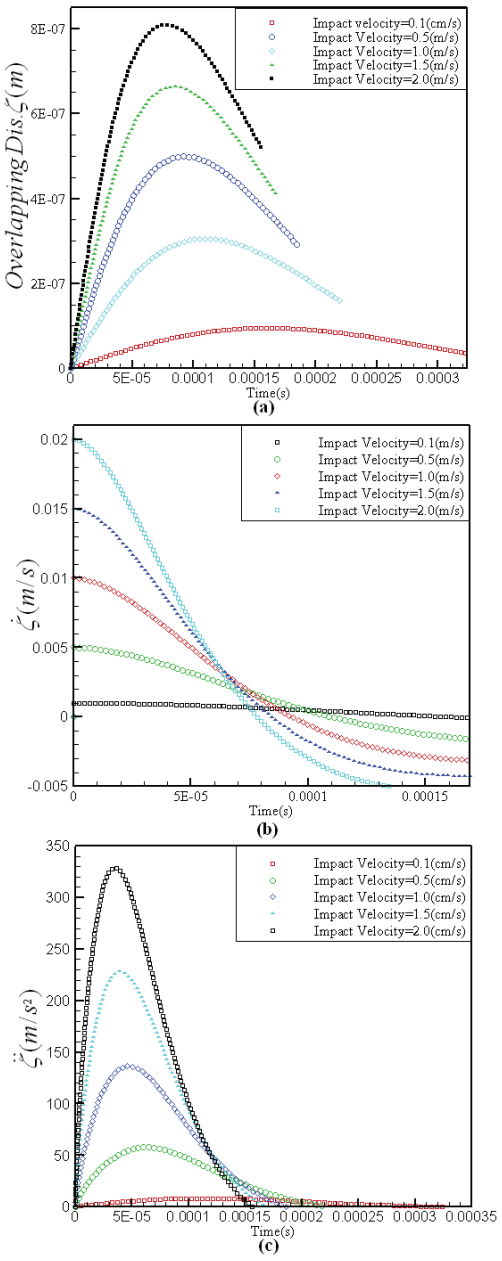

Fig. 3-14: *$\xi, \dot{\xi}, \ddot{\xi}$ measured in (m), (m/s), (m/s^2) in the collision between two ice particles with diameter of 2 cm, and property of which is mentioned in the text, for Elastic state and Viscoelastic collision (our model n=0.65). One particle is stationary at the start of the collision and the other one has several different velocities.*

elastic and frictionless,and the energy absorbed in wave motion is neglected, the deformation is perfectly reversible. The total time of impact T_c is, therefore, given by

$$T_c = 2t^* =$$
$$= \frac{2\zeta_{\max}}{V}\int_0^1 \frac{d(\zeta/\zeta_{\max})}{\{1-(\zeta/\zeta_{\max})^{5/2}\}^{1/2}} =$$
$$= 2.94\,\zeta_{\max}/V = 2.87(m_{eff}^2/R_{eff}E_{eff}^2V)^{1/5} \quad (3\text{-}75)$$

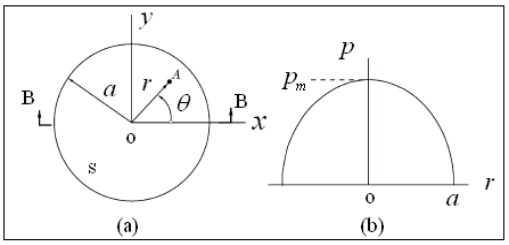

Fig. 3-15: *Contact area and Hertz normal pressure. (a) Circular contact area. (b) Hertz normal pressure p at section* $B-B$.

3-6. Finite Elements Methods Approach in Modeling Multisize Collision

The Finite Element method is a mathematical technique for analyzing stress, which breaks down a physical structure into substructures called "finite elements." The finite elements and their interrelationships are converted into equation form and solved mathematically. In our research cases, we want to solve stress distribution in the contact region of two multisized spherical particles and find more information about the loss of energy in a binary collision for visco-elastic materials.

Fig. (3-16) shows two identical spheres with a frictionless rigid planar surface, colliding with each other. The initial condition is this; the smaller particle is stationary at first and the second one moves at $t = 0$ with a certain velocity of $V_{imp.}$. In our nonlinear dynamic FEA, the size and the material properties of the spheres are chosen to be as follows; radius of the large sphere is 22.2mm and radius of the smaller one is 15.9mm. Young's modulus, Poisson's ratio and density are the same as listed in table (3-1).

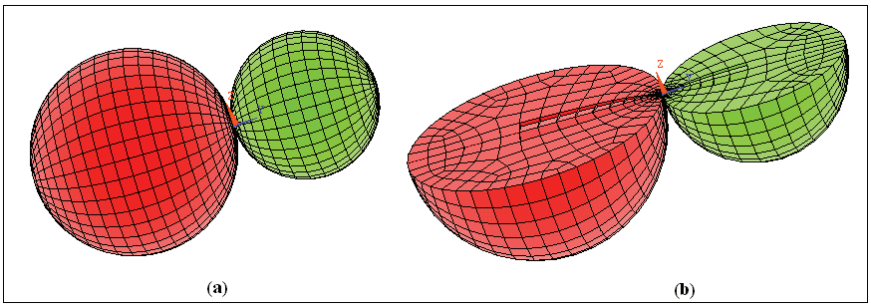

Fig. 3-16: *A schematic of the identical model that we modeled with FEA. According to axsymmetric property,we simple the 3D to 2D mesh model. And just analysis one half circle of two sphere that contact to each other in one single point (see Fig. 3-18).*

Since there is no rotation of the particle about itself in the collision that we studied, ax- symmetric FE models are employed to carry out the analyses. Fig. 3-17 shows one of the meshes employed in our FEA. In this FE model, the half sphere is discretized into 2354 square elements Fig. 3-17, a with a total of 6122 nodes, and with high levels of mesh refinement around the contact area Fig. 3-17, b. The nodes 1–6122 were numbered from top to bottom of the half circles shown in Fig. 3-18, a, with a more refined area around the contact point (Fig. 3-17b).

For low velocity impacts, the deformation of the sphere during a collision is concentrated in a small region around the contact area (see later results, such as the contours of stress in contact direction presented in Fig. (3-21, 22). In order to accurately represent the overall response, we refine the FE mesh in the small region close to the contact point (Fig. (3-17, b). For the FE model shown in Fig. (3-17), the size of the contact elements around the contact area is about $1.4\times10^{-5}m$, which is much less than the radius of the contact area. For example, the maximum radius of contact area is about $3.1\times10^{-4}m$ for the elastic collision

with an incoming velocity of $V_{imp.} = 0.5m/s$. Therefore, it can be concluded that the discretization of the sphere is fine enough to describe the collision behavior accurately.

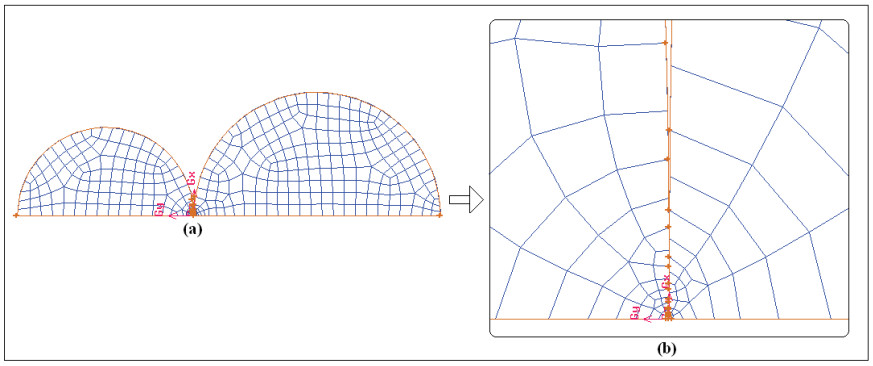

Fig.3-17: *An illustration of the meshing used in our 2D Finite Elements model. We used a square element with high refinement around the contact area.*

Fig. 3-18 shows that how velocities of particles change during the elastic collision in the case of $V_{imp} = 0.5(m/s), D_1 = 22.2mm, D_2 = 15.9mm$. We calculate the coefficient of restitution from this Figure as approximately 0.994, which is very near to one. This nearness confirms that our FM model has good validity for predicting the behavior of an elastic collision and that we can use this model for simulating a visco-elastic collision.

One of the important parameters that have been under focus by researchers is the time of the collision. Fig. (3-19) presents the collision time from the result of FEA for two identical spheres $D_1 = 22.2mm, D_2 = 15.9mm$ with comparison of the results with Hertz theory, which is described in section (3-5). From this Figure it is clear that collision time decreased with increasing velocity of impact, and the average of collision time for this range of size is about $8\times10^{-5}(s)$.

Behavior of stress in the contact area is the most important thing that we were eager to know more about. In Fig. (3-20) we presented the result of the stress in direction of contact σ_{yy} during the collision for several different impact velocities. In all velocities, we saw that for elastic collision there are two steps in collision; first is the compression part, then the second step is the separation part. In the compression step stress (pressure) increases to a maximum value in maximum deformation and after that decreases to zero, which occurs when the two particles completely separate from each other.

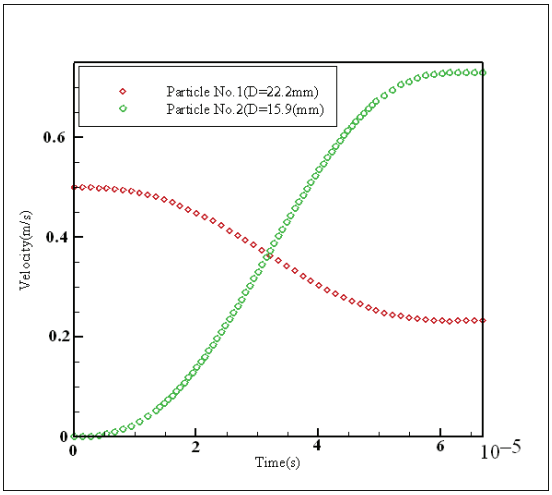

Fig 3-18: V*elocity behavior for two sphere particles during the elastic collision. For this case,* $V_{imp} = 0.5(m/s), D_1 = 22.2mm, D_2 = 15.9mm$ *and collision time is* 6.423×10^{-5} sec. *We calculated the coefficient of restitution for this case as equal to 0.994, which is very near to one and confirms the validity of the model for predicting the behavior of an elastic multisized collision.*

Also we can see from Fig. (3-20) that when impact velocity increases the absolute value of maximum stress (pressure) will increase and time of the collision will decrease. So for the higher velocities, a larger force is acting on the particles in a shorter period of time. So energy losses will be less than in the cases with a lower impact velocities. In fact, in collisions with lower impact velocities the larger amount of energy will be loosed in comparing with collision with larger impact velocity.

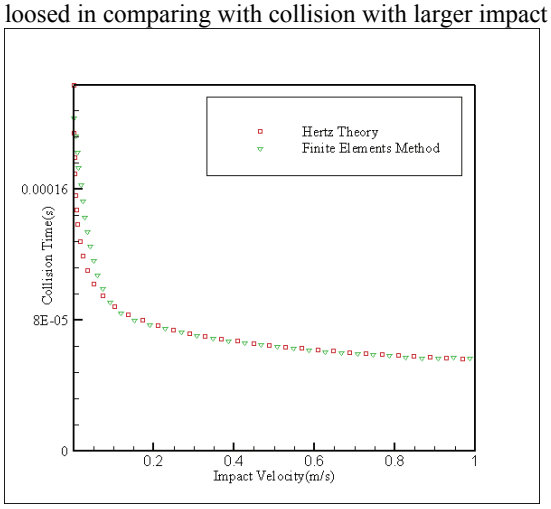

Fig. 3-19: *Collision time versus velocity of impact for two identical glass spheres. Their properties are listed in table (3-1). The sizes of the particles are* $D_1 = 22.2mm, D_2 = 15.9mm$. *It is clear that collision time decreases with the increasing of impact velocity, and collision time for this range of size is in order* 10^{-5} sec.

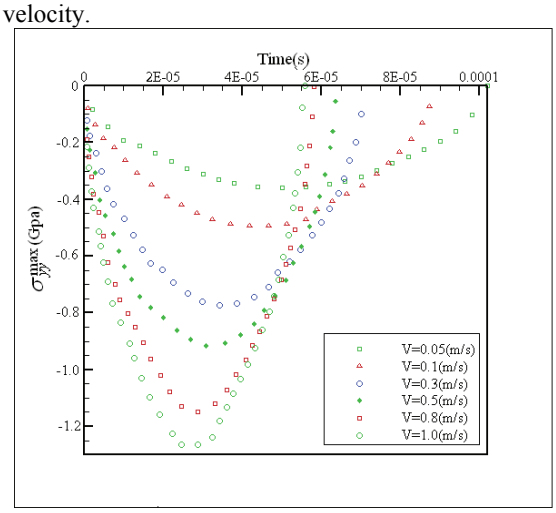

Fig. 3-20: *Stress behaviors in a multisized collision between two glass particles, their properties are listed in table (3-1). The sizes of the particles are* $D_1 = 22.2mm, D_2 = 15.9mm$. *The range of elastic stress in this case for range of impact velocities lower than 1 m/s is* $-1.3Gpa$. *And we can see in this Figure that the time of collision increases when impact velocity decreases, and maximum pressure will decrease with a decreasing of impact velocity.*

The distribution of stress in the contact area is one of most important things that we are interested to know more about. When we can make estimation about the area that is under the affect of the collision force, we can reach a suitable size of elements in the contact area for predicting behavior more accurately. Fig.3-21 shows the contours of stress in contact direction for different times during the collision; first point of contact Fig.3-21a, middle of compression period Fig.3-21b, maximum deformation Fig.3-21c, and middle of separation period Fig.3-21d. We can see that the shape of contour for the middle of the compression period Fig.3-21b and the middle of the separation period Fig.3-21d is the same. And the maximum affected area occurs during maximum deformation Fig.3-21c.

To demonstrate the usefulness of the finite elements method in the simulation of viscoelastic behavior of collision between two spherical particles of different size, we ran a case using the same mesh with the following material properties. The value of G_0 is found from the following equation:

$G_0 = E/2(1+\upsilon) = 2.53\times10^{10} kg/ms$.

The value of the long-time shear modulus G_∞ is set to zero. By using the above-mentioned properties and decay coefficient equal to $\beta = 2.708\times10^3 \frac{1}{s}$ we ran some cases with particles the sizes of $D_1 = 22.2mm, D_2 = 15.9mm$. Figure 3-24 shows the velocity changes of the two particles during the collision by using the finite element method and viscoelastic behavior. The result of these simulations conformed well to the experimental results that we will explain in next section. For example, from the result of this simulation we reached a coefficient of restitution equal to 0.9492 and in the case of impact velocity one equal to $0.5\,m/s$. For the size of the particles and velocity that are mentioned above, we measured the

coefficient of restitution equal to 0.9554 from the experiment. By comparing these two results, the capability of this method for modeling the viscoelastic behavior of a multisized collision between two glass particles has been shown.

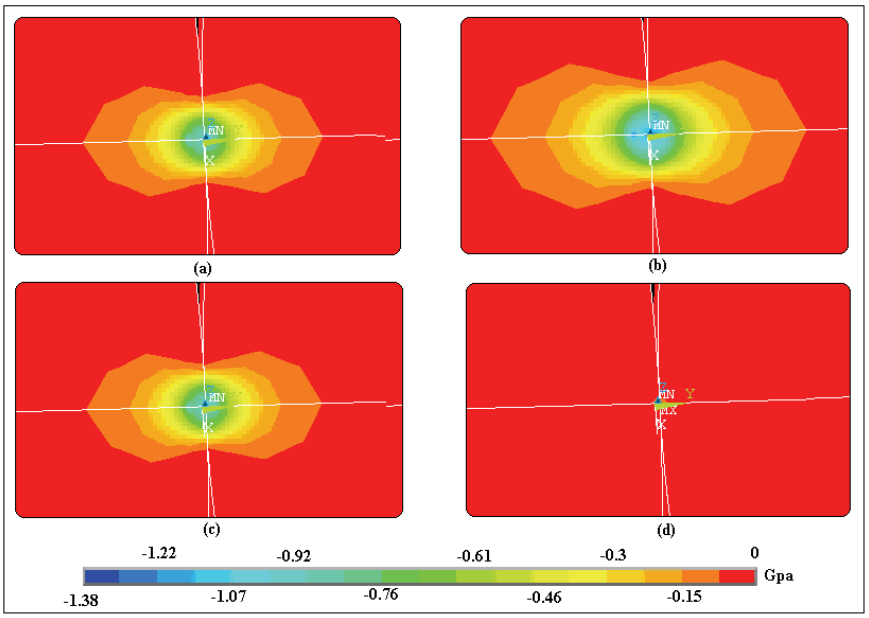

Fig. 3-21: *Contours of stress in contact direction σ_{yy} for a multisized elastic collision in the contact area for the four different steps of the collision. The particles size is $D_1 = 22.2mm, D_2 = 15.9mm$, their properties are listed in table (3-1) and velocity of impact is equal to 0.5 m/s. (a) The stress contours in middle of the compression period (b) The stress contours in maximum deformation (c) The stress contours in the middle of the separation period (d) The stress contours at the end of the collision.*

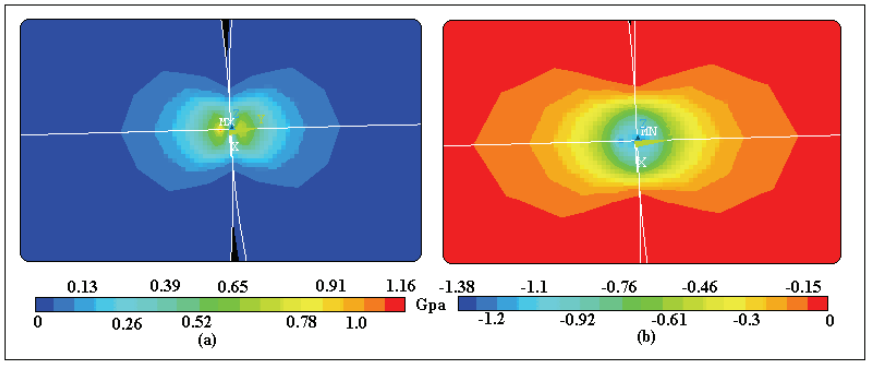

Fig 3-22: *Contours of stress in contact direction σ_{yy} and Von-Mises stress for an elastic collision between two multisized, identical spheres. The particle sizes are $D_1 = 22.2mm, D_2 = 15.9mm$, their properties are listed in table (3-1), and the velocity of impact is equal to 0.5 m/s.*

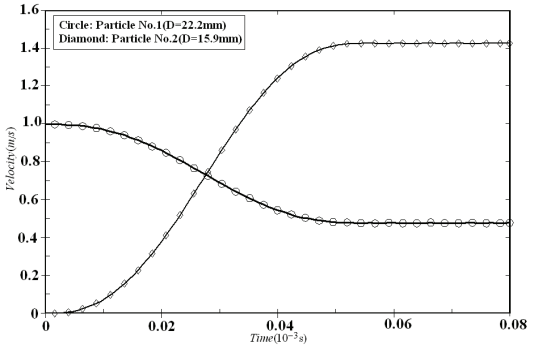

Fig. 3-23: *Velocity changes of two spherical particles during the viscoelastic collision. For this case* $V_{imp} = 0.5(m/s), D_1 = 22.2mm, D_2 = 15.9mm$. *We calculated the coefficient of restitution for this case equal to 0.9492, which is very near to the measured experimental value equal to 0.9554 and confirms the validity of the model for predicting the behavior of a viscoelastic multisized collision.*

3-7. Our Experimental Device

One aim of this study is to further investigate collisions between inelastic spherical particles. To this end the classical collision experiment known as Newton's Cradle was used, as shown previously in Fig. 3-4.

As illustrated in Fig.3-4, two nearly identical spherical particles with certain mass were arranged by suspending each particle from a frame using two very thin threads. In order to ensure the elimination of the rotation of the balls their centers of mass were aligned very carefully. For the mono-sized collision test two balls were chosen of the same material and size, but for the multi-sized collision test, the size and material of the two particles can be different.By releasing the first ball from an elevation an impact was generated which was captured using a digitalized, video camera (Sony DCR-HC17). Reflective tapes were used to mark the center of each ball. Note that it is important to have very bright, focused light sources closely aligned with the camera axis. Using the acquired video images, the dropping height and the corresponding inclination angle with respect to the equilibrium position of the first ball, α, and the maximum post impact height attained by the other ball as well as its corresponding inclination angle, β, were determined. To generate collisions at different impact velocities, the experiments were repeated using different elevations for the first ball.

In section (3-2-2), we described completely the kinematics of this experimental device, so we can use Eq. (3-2) and Eq. (3-6) for calculating the impact velocity and coefficient of restitution, respectively.

In the first set of experiments, the spheres have diameters of 22.2 *mm* and15.9 *mm*, the results of the experiment for coefficient of restitution are presented in Table (3-2) and its physical properties, as well as chemical compositions (provided by Sigmund Linder GmbH, Germany), are listed in Table (3-1). The diameter of the glass balls used in the second set of experiments was 22.2 *mm* and *10mm,* and the results are presented in Table (3-3). And for third set of experiments we used particles in diameter of15.9*mm*,10*mm* and the results are presented in Table (3-4). For comparison of the results of the multisized cases with those of the monosized, the results of the experiment for two same glass balls with the diameter of 22.2*mm* are also presented in Table (3-5). The sample results for the multisized collision test presented in Table 3-2, Table 3-3 and Table 3-4 represent the degree of plasticity of the collisions in terms of the impact velocity. Note that values of $e_n = 1$ and $e_n = 0$ denote the idealized cases of perfectly elastic and plastic impact, respectively. The present results suggest a nonlinear dependence of the coefficient of restitution on the impact velocity, consistent with the findings in previous attempts (Bridges et al., 1984), (Gugan, 2000).

Material	Properties	Symbol	Value
Glass	Elastic modulus	E	6.3×10^{10} Pa
	Density	ρ_p	2390 kg/m^3
	Poisson's ratio	ν	0.244
	Instantaneous shear modulus	G_0	$2.53\times10^{10}\ kg/ms$
	Long time shear modulus	G_∞	0
	The Relaxation Time	τ	1.676×10^{-4} sec
	The coefficient characterizing the viscous behavior of grains	K_n	100
	Chemical compositions	SiO_2 Na_2O CaO Al_2O_3 Bi_2O_3	66.0% 16.0% 7.0% 5.0% 3.0%
Air	Density	ρ_g	$1.225 kg/m^3$
	Kinematics Viscosity	ν_g	$1.7894\times10^{-5}\ kg/m.s$

Table 3-1: properties of glass particles and air has been used in the simulations of this section and next sections. All the properties have been mentioned in this table is for this condition. $T = 20^\circ C, P = 1Bar$

Table 3-2: *Measured values for the coefficient of restitution at different impact velocity for the glass balls in multisize test with diameters of* $22.2mm$ *and* $15.9\ mm$. *Properties of the samples are listed in Table (3-1).*

Impact Velocity(m/s)	Coefficient of Restitution
0.56	0.97
0.79	0.968
1.2914	0.938
1.39	0.92

Table 3-3: *Measured values for the coefficient of restitution at different impact velocity for the glass balls in multisize test with diameters of* $22.2mm$ *and* $10.0\ mm$. *Properties of the samples are listed in Table (3-1).*

Impact Velocity(m/s)	Coefficient of Restitution
0.56	0.947
0.863	0.93
1.103	0.924

Table 3-4: *Measured values for the coefficient of restitution at different impact velocity for the glass balls in multisize test with diameters of* $15.9mm$ *and* $10.0\ mm$. *Properties of the samples are listed in Table (3-1).*

Impact Velocity(m/s)	Coefficient of Restitution
0.52	0.965
0.7923	0.96
0.99	0.95
1.188	0.94

Also we observed in our experiments that when the size of the two multisized particles had become closer in size, and in fact moved closer towards a monosized state, the coefficient of restitution increases. In fact, when the differences between radiuses of curvature of the two particles increases, the coefficient of restitution will decrease and the amount of energy that is lost during the collision will increase. You can see this conclusion in the Fig. (3-24), which was made from the experimental results.

Table 3-5: *Measured values for the coefficient of restitution at different impact velocities for the glass balls in a monosize test with the diameter of* 22.2 *mm*. *Properties of the samples are listed in Table (3-1).*

Impact Velocity(m/s)	Coefficient of Restitution
0.524	0.986
0.6569	0.98
1.1719	0.954
1.3288	0.945
1.609	0.9131

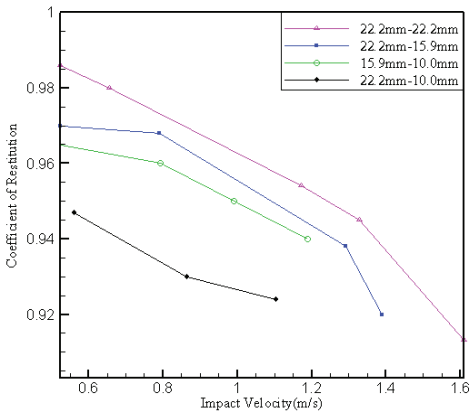

Fig. 3-24: *The variation of coefficient of restitution with impact velocity in some multisized collisions between glass balls. It seems that during one constant impact velocity, if the difference of radius of curvature between the two contact surfaces is smaller, the coefficient of restitution will be increased. In fact, we have more loss of energy in the multisized cases relative to the monosized cases.*

We also carried out some experiments for multisize collision for other sphere particles that have different materials and size, for example we do this kind of experiment for several arrangements of steel particles with three different sizes, and a steel ball that coated with plastic for study effect of surface of contact in coefficient of restitution. The details can be found in Halabia (2005).

4. Analysis and Simulation of Vertical Vibration in Granular Media

Vibrating heaps of fine brass balls at critical amplitude form themselves into fascinating patterns called oscillons (Umbanhowar et al, 1996). This self-sustaining state was named by analogy with its closest large-scale analogy, the soliton, which is a localized wave that maintains its integrity as it moves. The experimental observations suggested that oscillons might arise from cooperative behavior resulting from collisions between brass balls in an evacuated, vertically vibrated, granular layer (Umbanhowar et al., 1996). Similar behavior has been observed in many diverse nonlinear systems having little or no dissipation (Fineberg, 1996).

The situation appears somewhat similar when vibration is applied to thin layers of granular slurry with air above (Schleier-Smith and Stone, 2001). Note that interstitial fluid such as air or water is known to induce convection in a granular assembly as a vibrating plate accelerates downwards (Faraday, 1831).

In a closely related system, if a shallow bed of fine balls is shaken even at moderate amplitude with air filling the pore space, heaps develop (Pak et al.1995). In this case, the surrounding gas plays a key role in the dynamics of vibrating particles at high amplitudes. It is likely that the gas trapped in the granular material is a source of the heaping. Pak et al. (1995) suggested that air heap formation in vibrating granular materials might be considered as criteria to determine when gas effects are relevant. Further understanding of the mechanism for heaping is of interest in creating ideal processing conditions and powder transport, which is of use in a number of industries including oil industries.

Despite substantial industrial interests in processes such as food handling, mixing of building materials, and processing and handling of coal, the dynamics of both dry and wet granular systems remain poorly understood. In fact, the aforementioned discoveries are spurring theorists in their search for a comprehensive, hydrodynamic type description for granular materials.

The experiments detailed by Umbanhowar et al. (1996) triggered a number of theoretical works in which a wide range of approaches has been used (Aoki and Akiyama, 1996; Shinbrot, 1997; Rothman, 1998; Cerda et al., 1997; Tsimring and Aranson, 1997; Venkataramani, and Ott, 1998). Most notably, the molecular dynamics type simulations reported by Bizon et al. (1998) have reproduced the experimental results in great detail.

The objective of the current work is to develop a realistic model for a dense mixture of gas-particle typical of common industrial practices. The model is validated through its application to describe the influence of periodic vertical vibrations of the base of a vertical bucket on the dynamics of granular media for which interactions with the surrounding gas plays an important role in dynamical pattern deformation.

The organization of the section is as follows. In section (4-1), we will present the analysis of a wave in plates with several different shapes. In section (4-2), a detailed overview is presented of collective processes in gas-particle flows useful for developing a simplified model for molecular dynamic type simulations of dense gas-particle flows. The developed model is applied to the specific example of a dense gas-particle mixture under vertical vibrations in a pentagonal prism shaped. However, computations such as those presented in section (4-2) may not become feasible in the foreseeable future for producing detailed information for a system consists of large number particles. Hence, the use of continuum type models would be more obvious for granular flows. Note that in the granular flows at law shear rates, a quasi-static regime can be identified at which frictional forces between grains are predominating. At very high shear rates, the grains are moving very fast where friction between them may be neglected and short collisions between particles characterize the flow dynamics. Between the rapid and the slow flow regimes an intermediate regime exists where both collisional and frictional interactions between particles should be taken into account. In the present attempt, a modified version of the previously developed approximate theory of Zamankhan et al. (1997) is proposed for describing the motion of particles in dense mixtures of particles in a carrier gas. Whereas the previous model (Zamankhan et al., 1997) was limited to cases where the particle dynamics are collision-dominated, the present model may be applicable to cases in which the particle dynamics are characterized by both collisions as well as frictional contacts. Section (4-3) of this paper presents a set of continuum equations for dense gas-particle flows in the intermediate regime in which the particulate phase is to be considered as compressible. Note that some aspects of the model are speculative and borrowed from the results of the molecular dynamic type simulations discussed in Sec. (4-2). In Sec. (4-4), numerical solutions are presented of the integral form of the governing equations developed in Sec. (4-3) in order to assess the ability of the present model to predict dynamics of a dense mixture of gas particles in

prism shaped buckets with different cross sections whose base wall vibrates with a displacement defined as $z = A\sin(k_v x)\sin(l_v y)\cos(\omega_v t)$. The results appear to capture salient features of observation on vertically vibrated granular materials such as the formation of oscillon and bubbling. Finally, the concluding remarks are presented in Sec. (4-5), which may be of use in creating ideal processing conditions and powder transport in industrial systems.

4-1. Wave Analysis in the Plates

4-1-1. Analytical Solution for 2D Vibrations of a Square Membrane

Consider the vibrations of a square membrane inside the region $-a_0 \le x \le +a_0$ and $-b_0 \le y \le +b_0$. The wave equation is

$$\frac{\partial^2 z}{\partial t^2} = C^2\left(\frac{\partial^2 z}{\partial x^2} + \frac{\partial^2 z}{\partial y^2}\right) \tag{4-1}$$

describing the displacement, $z(x, y, t)$, of the membrane. Suppose the boundary conditions are taken as $z = 0$ on the main axis of the square $x = 0$, and $y = 0$. Try a solution of the form

$$z = X(x)Y(y)T(t) \tag{4-2}$$

so that the wave equation may be expressed in the separable form as

$$\frac{1}{C^2}\frac{1}{T}\frac{d^2T}{dt^2} = \frac{1}{X}\frac{d^2X}{dx^2} + \frac{1}{Y}\frac{d^2Y}{dy^2}. \tag{4-3}$$

Since the left hand side of the equation is only a function of time and the right hand side depends only on spatial variations, they must both be equal to a constant. This separation process can be continued to show that both terms on the right hand side are constants. Hence,

$$\frac{1}{X}\frac{d^2X}{dx^2} = -a^2, \Rightarrow \frac{d^2X}{dx^2} + a^2X = 0, \Rightarrow X(x) = \sin m\pi x, \tag{4-4}$$

where the separation constant is chosen as $a = m\pi$ in order to satisfy the boundary conditions in x. Here m is an integer. Similarly,

$$\frac{1}{Y}\frac{d^2Y}{dy^2} = -b^2, \Rightarrow \frac{d^2Y}{dy^2} + b^2Y = 0, \Rightarrow Y(y) = \sin n\pi y, \tag{4-5}$$

where $b = n\pi$ and n is an integer so that the boundary conditions in y are satisfied. Combining these results we obtain the equation for T as

$$\frac{1}{T}\frac{d^2T}{dt^2} = -C^2(a^2 + b^2), \Rightarrow \frac{d^2T}{dt^2} + C^2(a^2 + b^2)T = 0. \tag{4-6}$$

Thus, we have

$$T(t) = A\cos\omega_v t + B\sin\omega_v t, \tag{4-7}$$

where the frequency ω satisfies the dispersion relation

$$\omega_v{}^2 = \omega_{mn}^2 = C^2(m^2 + n^2)\pi^2. \tag{4-8}$$

Thus, the general solution is obtained by adding together all the possible solutions, to give

$$z = \sum_{m=1}^{\infty}\sum_{n=1}^{\infty}\sin(m\pi x)\sin(n\pi y)[A_{mn}\cos\omega_{mn}t + B_{mn}\sin\omega_{mn}t]. \tag{4-9}$$

The constants A_{mn} and B_{mn} are determined by initial conditions on z and $\partial z/\partial t$. Each value of m and n corresponds to a different possible mode of oscillations. The fundamental mode is given by $m = 1$ and $n = 1$ with

$$z = \sin(\pi x)\sin(\pi y)[A_{11}\cos\omega_{11}t + B_{11}\sin\omega_{11}t] \tag{4-10}$$

and has

$$\omega_{11} = \sqrt{2}\pi C. \tag{4-11}$$

It corresponds to the whole membrane oscillating up and down. The mode $m=2$ and $n=1$ has a spatial form given by

$$\sin(2\pi x)\sin(\pi y), \tag{4-12}$$

and has

$$\omega_{21}=\sqrt{5}\pi C. \tag{4-13}$$

This kind of vibration in the membrane was used in some cases for exciting the bottom of the buckets full of sand. We used this equation for wave:

$$z=A\sin(m\pi x)\sin(n\pi y)\sin(\omega_v t). \tag{4-14}$$

Where A represents amplitude of wave, $m=17, n=13$ and ω_v is time-frequency of wave and calculates from this equation:

$$\omega_v=\pi C\sqrt{m^2+n^2}, \tag{4-15}$$

where C represents speed of the wave.

Figure (4-1) shows the displacement of the square plate in several times under excitation of the wave, explained by Eq. (4-14).

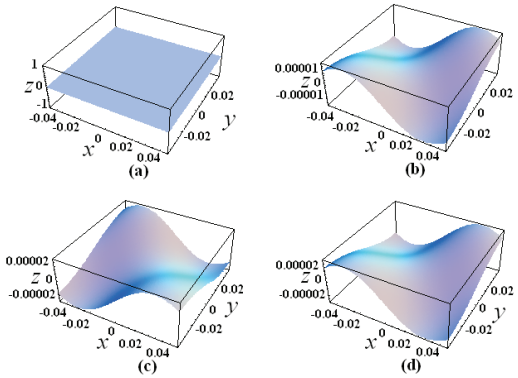

Fig. 4-1: *Displacement of the square surface in several times under excitation by the wave:* $z=A\sin(m\pi x)\sin(n\pi y)\sin(\omega t)$ *when A is amplitude of the wave and equal to 0.00003,* $m=17, n=13$, $\omega_v=\pi C\sqrt{m^2+n^2}$ *where C represents the speed of sound. The boundary conditions are z=0 for x-axis and y- axis. a)* $t=0s$, *b)* $t=0.2s$, *c)* $t=0.4s$, *d)* $t=0.6s$.

As shown in Fig. (4-1) the displacement of the plate in the center and along the main axis is zero and the boundary conditions designed according to this subject. But we used other boundary conditions on some other cases. In these cases we consider that the boundaries of the bottom remain stationary (simply supported plate) and the origin of Cartesian coordinate is in the center of the plate. So we can write the boundary condition for the square that $-a\le x\le a, -b\le y\le b$ as follow:

$$\begin{cases} x=\pm a, -b\le y\le b & \Rightarrow z=0 \\ y=\pm b, -a\le x\le a & \Rightarrow z=0 \end{cases}, \tag{4-16}$$

and the center of surface has a finite displacement. For these boundary conditions we can write the following equations for the wave,

$$z=A\cos(\frac{(2m+1)\pi}{2a}x)\cos(\frac{(2n+1)\pi}{2b}y)\cos(\omega_v t), \tag{4-17}$$

$$z=A\cos(\frac{(2m+1)\pi}{2a}x)\cos(\frac{(2n+1)\pi}{2b}y)\sin(\omega_v t). \tag{4-18}$$

Where A is amplitude of the wave, a and b are the length and width of the surface. We can calculate ω by using these equations in eq.4-1, so we will have:

$$\omega_v=\frac{C\pi}{2}\sqrt{(\frac{2m+1}{a})^2+(\frac{2n+1}{b})^2}. \tag{4-19}$$

The frequency of vibration in the circular plate can be explained by following equation (Yi-Yuan Yu, 1996):

$$f_{mn} = (2R)^{-1}\sqrt{T/\sigma}\beta_{mn}, \qquad (4\text{-}20)$$

Where R represents radius of the membrane and T, σ, β_{mn} represents tension, area density and Zero value of the m-th order Bessel function, respectively.

In Figures (4-2), (4-3) and (4-4) displacement of one square surface under certain conditions and excitation by waves, that is explained in Eq.4-17 and Eq.4-18, was shown.

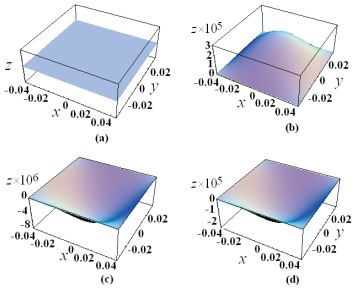

Fig. 4-2: *Displacement of the square surface in several times under excitation by the wave:* $z = A\cos(\frac{(2m+1)\pi}{2a}x)\cos(\frac{(2n+1)\pi}{2b}y)\sin(\omega_v t)$ *when A is amplitude of the wave and equal to 0.00003,* $m=0, n=0, a=0.045m, b=0.035m$,

$\omega_v = \frac{C\pi}{2}\sqrt{(\frac{2m+1}{a})^2+(\frac{2n+1}{b})^2} = 28.43$, *where C=0.5 represents the speed of sound. The boundary conditions are z=0 for all side. a)* $t=0s$, *b)* $t=0.06s$, *c)* $t=0.12s$, *d)* $t=0.18s$.

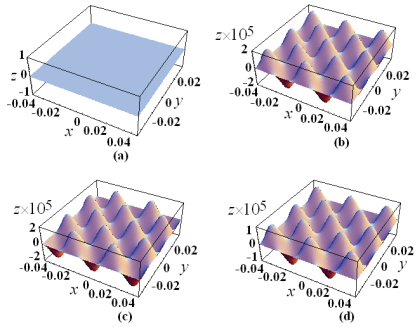

Fig. 4-3: *Displacement of the square surface in several times under excitation by the wave:* $z = A\cos(\frac{(2m+1)\pi}{2a}x)\cos(\frac{(2n+1)\pi}{2b}y)\sin(\omega_v t)$ *when A is amplitude of the wave and equal to 0.00003,* $m=2, n=2, a=0.045m, b=0.035m$,

$\omega_v = \frac{C\pi}{2}\sqrt{(\frac{2m+1}{a})^2+(\frac{2n+1}{b})^2} = 142.14$, *where C=0.5 represents the speed of sound. The boundary conditions are z=0 for x-axis and y- axis. a)* $t=0s$, *b)* $t=0.06s$, *c)* $t=0.12s$, *d)* $t=0.18s$.

In Fig. 4-5 some of the main principle modes of vibration for one rectangular plate have been shown.

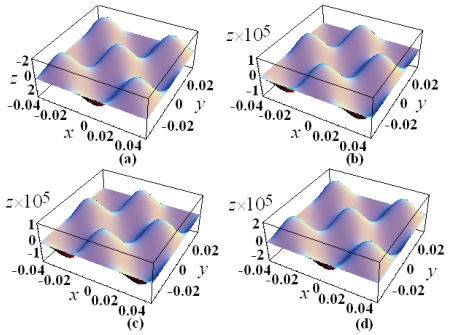

Fig. 4-4: *Displacement of the square surface in several times under excitation by the wave:* $z = A\cos(\frac{(2m+1)\pi}{2a}x)\cos(\frac{(2n+1)\pi}{2b}y)\cos(\omega_v t)$ *when A is amplitude of the wave and equal to 0.00003,* $m=1, n=1, a=0.045m, b=0.035m$,

$\omega_v = \frac{C\pi}{2}\sqrt{(\frac{2m+1}{a})^2+(\frac{2n+1}{b})^2} = 85.28$, *where C=0.5 represents the speed of sound. The boundary conditions are z=0 for all side boundaries. a)* $t=0s$, *b)* $t=0.025s$, *c)* $t=0.05s$, *d)* $t=0.075s$.

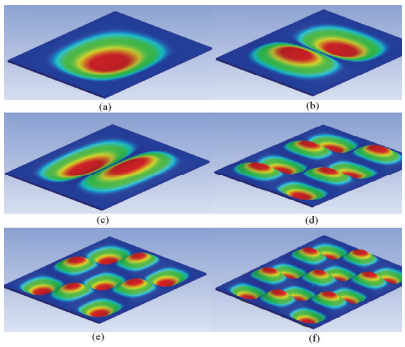

Fig. 4-5: *Principle mode of vibration in a square plate in which the boundary is fixed. a) First mode of vibration. b) Second mode of vibration. c) Third mode of vibration. D) Ninth mode of vibration. e) 12th mode of vibration. f) 19th mode of vibration.*

4-1-2. 2D-Vibration of a Circular Membrane

Consider the vibrations of a circular membrane inside the region $0 \le r \le R$ and $0 \le \theta \le 360^\circ$. The wave equation is

$$\frac{\partial^2 z}{\partial t^2} = C^2\left(\frac{\partial^2 z}{\partial r^2} + \frac{1}{r}\frac{\partial z}{\partial r} + \frac{\partial^2 z}{\partial \theta^2}\right), \tag{4-21}$$

describing the displacement, $z(r,\theta,t)$, of the membrane. We consider the symmetrical conditions in θ-direction, so we can write $\frac{\partial^2 z}{\partial \theta^2} = 0$. Suppose the boundary conditions are taken as $z = 0$ on the sides of the circle $r = R$ and $0 \le \theta \le 360^\circ$. Try a solution of the form

$$z = R(r)T(t), \tag{4-22}$$

Because z is just function of r, t.

So the wave equation may be expressed in the separable form as

$$\frac{1}{C^2}\frac{1}{T}\frac{d^2T}{dt^2} = \frac{1}{R}\left(\frac{d^2R}{dr^2} + \frac{1}{r}\frac{dR}{dr}\right). \tag{4-23}$$

This equation satisfies only if both sides equal to a constant. If we consider positive and zero value for this constant we will arrive at unacceptable equations, so we should consider a negative value for this constant, for example $-k^2$. By separating variables in both directions of Eq. (4-22) we will have the following ordinary differential equation for T (t):

$$\frac{1}{T}\frac{d^2T}{dt^2} = -k^2. \tag{4-24}$$

Thus, we have

$$T(t) = A\cos\omega_v t + B\sin\omega_v t, \tag{4-25}$$

and we can consider the following ordinary differential equation for R(r):

$$\frac{\partial^2 R}{\partial r^2} + \frac{1}{r}\frac{\partial R}{\partial r} + k^2 R = 0. \tag{4-26}$$

By considering the new variable which can define as $s = kr$, we can rewrite the above equation as follows:

$$\frac{d^2R}{ds^2} + \frac{1}{s}\frac{dR}{ds} + R = 0. \tag{4-27}$$

This equation has conformity with Bessel differential equation, so we can write the general solution for it as follows:

$$R(r) = C_1 J_0(s) + C_2 Y_0(s). \tag{4-28}$$

J and Y represent the first kind of Bessel functions and the second kind of Bessel functions, respectively.

The displacement of the center of the circle is finite, so

$$r \to 0 \Rightarrow s \to 0 \Rightarrow z = \text{finite value}. \tag{4-29}$$

By applying this boundary condition to Eq. (4-27) we will have $C_2 = 0$ because we know that $s \to 0 \Rightarrow Y_0(s) \to \infty$, now we can rewrite Eq. (4-27) as follows:

$$R(r) = C_1 J_0(s). \tag{4-30}$$

Now we should apply the following boundary condition for finding an exact solution:

$$r = R \text{ and } 0 \le \theta \le 360^\circ \Rightarrow z = 0 \Rightarrow R(r \to R) = 0 \tag{4-31}$$

$$R(r \to R) = C_1 J_0(kR) = 0 \Rightarrow \begin{cases} C_1 = 0 \\ or \\ J_0(kR) = 0 \end{cases} \tag{4-32}$$

$C_1 = 0$ is not acceptable, so by the second equation we should consider kR equal to zeros of the first kind of Bessel function of order 0, which representing by α_m. So we have:

$$k_m = \frac{\alpha_m}{R}. \tag{4-33}$$

These zeros were calculated numerically and are found in some mathematics reference books. For example in order zero, we have $\alpha_0 = 2.4048, \alpha_1 = 5.5201, \alpha_3 = 8.6537, ...$ choosing each one of these zeros defines the number of vibration mode. If $\alpha_0 = 2.4048$ is chosen, then the mode of vibration is zero. Behavior of the first kind of Bessel function is shown in Fig. 4-6 for five different orders.

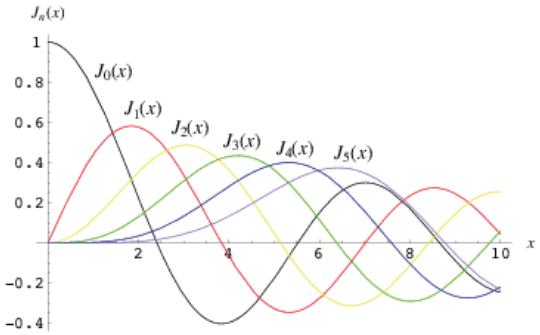

Fig. 4-6: *Orders zero to five of the first kind of Bessel function aspect x. The first kind of Bessel function has some zeros in each order. These zeros were calculated numerically and are found in some mathematics reference books. For example in order zero, we have* $\alpha_0 = 2.4048, \alpha_1 = 5.5201, \alpha_3 = 8.6537, ...$

In one case we consider $R = 4cm$ and you can see the resulting wave circle by choosing $\alpha_0 = 2.4048$.

From various mathematical reference books we can write the following series for the J kind of Bessel function of order m:

$$J_m(x) \equiv \sum_{l=0}^{\infty} \frac{(-1)^l}{2^{2l+m} l!(m+l)!} x^{2l+m}, \tag{4-34}$$

In Fig. (4-6), the principle nodes for first node of the circular plate have been shown.

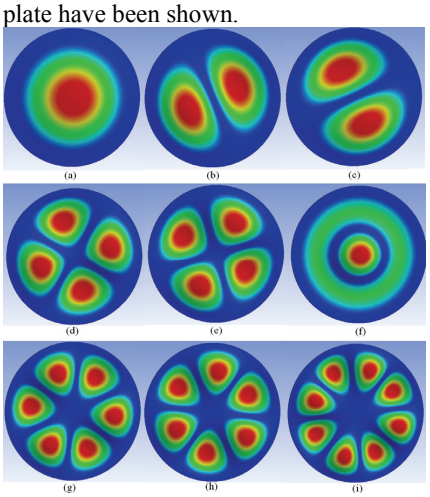

Fig. 4-7: *Principle mode of vibration in the circular plate in which the boundary is fixed. a) First mode of vibration. b) Second mode of vibration. c) Third mode of vibration. d) Fourth mode of vibration. e) Fifth mode of vibration. f) Sixth mode of vibration. g) Seventh mode of vibration. h) Eighth mode of vibration. i) Ninth mode of vibration.*

4-1-3. 2D-Vibrations of Plates with other Shapes

Well-known analogies (Conway, 1960; Seth, 1947) exist between the separate problems of transverse free vibration and buckling of a polygonal plate simply supported all around and the problem of the transverse vibration of a prestretched membrane having no deflection at its edges.

The governing differential equation for the vibrating membrane is

$$\nabla^2 W + (\frac{\rho_m \omega_m^2}{T}) W = 0. \tag{4-35}$$

Where $W = W(x, y)$ is the transverse deflection, ρ_m is the mass density per unit area, ω_m is the ferequancy, and T is the membrane tension (force per unit length). Operating on equation (4-35) by ∇^2 and substituting for $\nabla^2 W$ from equation (4-35) give the resulting equation:

$$\nabla^4 W - \left(\frac{\rho_m \omega_m^2}{T} \right)^2 W = 0 . \tag{4-36}$$

Furthermore, if $W = 0$ along the polygonal boundary of the membrane, then by equation (4-35), $\nabla^2 W$ is also zero, which satisfies the boundary conditions for a simply supported plate. Thus a complete analogy exists between the two problems, and the frequency of the plate can be obtioned from that of the membrane through the following correspondence,

$$\frac{\omega_v^2 \rho}{D} \sim \left(\frac{\rho_m \omega_m^2}{T} \right)^2 . \tag{4-37}$$

Again, operating on equation (4-35) by ∇^2 gives

$$\nabla^4 W - \left(\frac{\rho_m \omega_m^2}{T} \right) \nabla^2 W = 0 . \tag{4-38}$$

Which is of the same form as the differential equation governing the buckeling of a plate under the action of the inplane forces $N_x = N_y = N_0$ (a constant; i.e., hydrostatic pressure):

$$\nabla^4 W - \frac{N_0}{D} \nabla^2 W = 0 . \tag{4-39}$$

Again, the homogeneous boundary conditions for the simply supported polygonal edges of the plate are satisfied by the condition around the membrane. Thus the following correspondence exists:

$$\frac{(N_0)_{cr}}{D} \sim \frac{\rho_m \omega_m^2}{T} , \tag{4-40}$$

where $(N_0)_{cr}$ is the critical buckeling load of the plate; that is, the eigenvaues which satisfy the homogeneous boundary conditions.

Finally, from a comparison that exists between the plate vibration and plate buckeling problems (when of course, all edges are rectilinear and simply supported):

$$\omega_v \sqrt{\frac{\rho}{D}} \sim \frac{(N_0)_{cr}}{D} . \tag{4-41}$$

Kaczkowski(1961) analyzed the regular pentagons of side a (Fig.4-8) for the case when all edges are simply supported. He chose a deflection function of

$W(x, y) =$

$$\sum_{m=1,3,5}^{\infty} \left[A_m \sinh \sqrt{\left(\frac{m\pi}{a} \right)^2 + \sqrt{\frac{\rho \omega_v^2}{D}}}\, y + B_m \sinh \sqrt{\left(\frac{m\pi}{a} \right)^2 - \sqrt{\frac{\rho \omega_v^2}{D}}}\, y \right] \left(\sin \frac{m\pi x}{a} \right) . \tag{4-42}$$

Which exactly satisfies the symmetry conditions along AB and the simply supported conditions along OA. The symmetry conditions along OB yield a characteristic frequency that was found to be $\omega_v a^2 \sqrt{\rho / D} = 10.863$.

We found several nodal patterns for a completely free regular pentagon. These are exhibited in Fig.(4-9).

The fundamental frequency of a regular hexagon of side a that is simply supported along all sides was determined by Kaczkowski (1961) to be $\omega_v a^2 \sqrt{\rho / D} = 6.961$ by using the method described in eq.4-42.

Conway(1960) solved the problem with the point-matching method, using the solution in polar coordinates:

$$W_n = \left[A_n J_n(kr) + C_n I_n(kr) \right] \cos n\theta , \tag{4-43}$$

and by satisfying boundary conditions at all corners, midpoints, and quarter points of the sides.

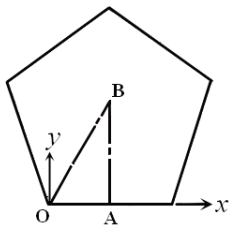

Fig. 4-8: *Regular pentagon.*

This gave the fundamental frequency as $\omega_v a^2\sqrt{\rho/D} = 7.129$. The problem is also discussed in the references (Seth , 1947; Hersch, 1958).

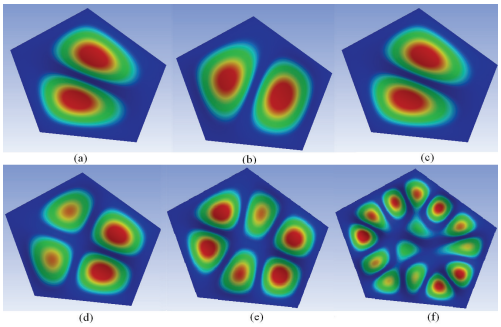

Fig. 4-9: *Nodal patterns of completely free regular pentagonal plates a) First mode of vibration. b) Second mode of vibration. c) Third mode of vibration. d) Fifth mode of vibration. e) Eighth mode of vibration. f) 20th mode of vibration.*

Nodal patterns for completely free regular hexagonal plates are shown in Fig. 4-10.

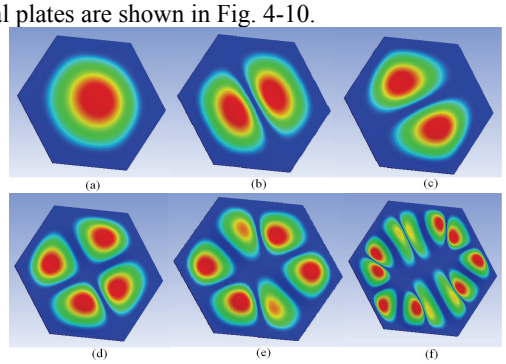

Fig.4-10: *Nodal patterns of completely free regular hexagonal plates. a) First mode of vibration. b) Second mode of vibration. c) Third mode of vibration. d) Fifth mode of vibration. e) Seventh mode of vibration. f) 20th mode of vibration.*

The fundamental frequency of a regular octagonal plate of side length a that is simply supported along all edges was computed to be $\omega_v a^2\sqrt{\rho/D} = 3.624$ by Kaczkowski (1961). The method used was that described in the discussion of pentagons (Section 4-3-1).

Nodal patterns for completely free regular heptagonal plates are shown in Fig. 4-11. Nodal patterns for completely free regular octagonal plates are shown in Fig. 4-12.

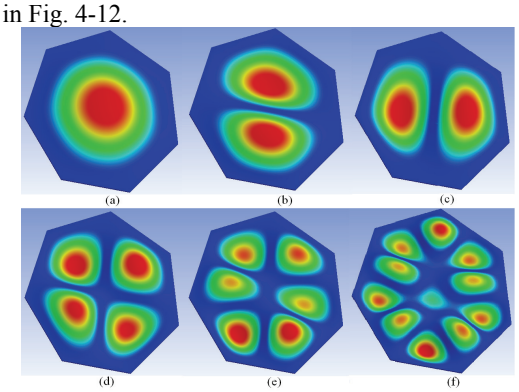

Fig.4-11: *Principle mode of vibration in heptagonal plate in which the boundary is fixed. a) First mode of vibration. b) Second mode of vibration. c) Third mode of vibration. d) Fifth mode of vibration. e) Eighth mode of vibration. f) 15th mode of vibration. .*

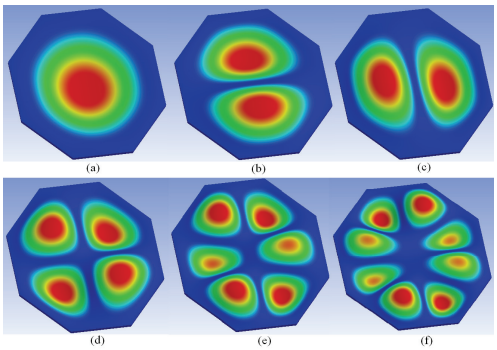

Fig.4-12: *Principle mode of vibration in octagonal plate in which the boundary is fixed. a) First mode of vibration. b) Second mode of vibration. c) Third mode of vibration. d) Fifth mode of vibration. e) Eighth mode of vibration. f) 10th mode of vibration.*

In the present work we choose a different deflection function given as

$$W(x,y)=\sum_{i=0}^{N}\sum_{j=0}^{M}a_{ij}x^{i}y^{j}, \tag{4-44}$$

where a_{ij} represent the coefficients of polynomial listed below. Note that deflection function (4-44) can be easily implemented into any multiphase code to describe the periodic motion of the base of container.

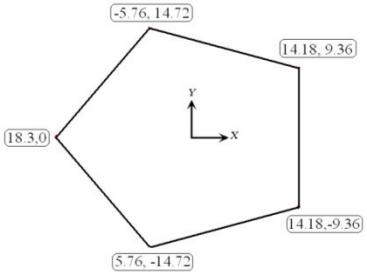

Fig. 4-13: *The geometry which used for pentagonal case in our numerical result.*

By using eq.4-44 we will arrive to more trustable answers for simply supported plates. For example we can consider the geometry shown in Fig. 4-13, by solving numerically eq.4-44 for the first mode of vibration, we will reach to the following coefficients matrix for a_{ij}, we consider $i, j = 1 to 25$:

Columns 1 to 5:

0.478773260023445	-0.054488013603077	-1.73142493228079	0.197166106982849	1.97278143861513
-0.000645407574623391	0.0011338178137521	0.00517679912773161	-0.0215339984629281	-0.0113744257208497
-2.12441424041754	-0.0713517553851091	5.07711681882185	3.57512630557109	-4.94306854806109
0.025957311525157	-0.0189113758516442	-0.136381893339199	0.380203538266926	0.271186496288487
2.59551569328323	-1.54921670217822	-1.73649623425581	-3.67016770534922	-7.81778251382752
-0.289555563162789	0.0743229906003648	0.950915356529038	-1.36244969859827	-0.823286619610312
1.16060012357684	4.0864490987041	-9.5240228302643	-3.06916785075129	29.363566553577
1.51531333496493	-0.168720710060565	-3.50516972640536	1.84253863652267	1.91223224604404
-9.75174750153678	-0.620676192378977	37.8985463338835	0.827565785444907	-56.8980753308261
-4.21184546814276	0.24936766400934	7.19686369790459	-0.980590188899778	-3.64270917858389
22.766370782308	0.127256467654978	-65.2154681953809	-0.16818623308513	42.9033080206014
6.34261301635735	-0.143208173616556	-8.0001623911069	0.136774921249459	4.01016091972259
-25.3690876329637	-0.0211034448722882	55.6914578511716	0.0280468267299086	-30.2005031119588
-4.99622894542469	0.0229708653714641	4.97972113588945	-0.0231821023292955	-2.49175951696606
10.1596386584736	0.00301507391395753	-14.3714717896277	-0.00400691874629168	7.61637280651594
2.0353635730039	-0.00326642043369555	-2.03482266094725	0.00332205797902697	1.01771670384122
1.98370415199601	-0.000376879281064394	-1.47377930735854	0.000500865577001168	0.670573031129811
-0.607404555499408	0.00040838962478697	0.607318656530952	-0.000415225995482494	-0.303702132260819
-2.23304632923398	4.18754828626295e-005	2.17839270500768	-5.56517360787191e-005	-1.08035735330169
0.141690558170097	-4.53778197572918e-005	-0.141679929937201	4.61354224168087e-005	0.0708452795605026
0.831282781008642	-4.18754821428783e-006	-0.826035938980888	5.56517361847532e-006	0.411977996832003
-0.027031356990364	4.53777774613965e-006	0.0270301730032055	-4.61354387998215e-006	-0.0135156784939312
-0.206100338058055	3.80686201362923e-007	0.20564499585087	-5.05924874452725e-007	-0.102712877550764
0.004353973132739	-4.12525217210396e-007	-0.0043538535874292	4.194131019029 87e-007	0.00217698656637264
0.039393402996989	-3.172385011315e-008	-0.0393574217691116	4.21604062044564e-008	0.0196682392344941

Columns 6 to 10:

-0.280973745879343	-0.281108063900319	-2.08725133059094	-4.24660944336858	11.1611020156292
0.0945255980834645	0.00593066507352115	-0.204564925790403	0.0103813910054831	0.249379689370937
-3.83672487390565	12.0061833851268	-6.05907297634543	-30.4963739584265	6.1723755700955
-1.35710786922859	-0.276515887147743	1.84253863652267	0.138292170828357	-0.968837372416546
1.51622983978915	20.9681702203762	3.04505864631446	3.51131130592796	-3.08607405215343
3.44748144683528	0.1122818402197	-2.72571434862584	-0.0608648473280235	0.392219027470541
-0.773922587019435	-67.4443174586947	-1.02464148598748	54.2609863553745	1.02853989365789
-2.70141470848966	-0.586451545175 19	1.84717980071035	0.159598724548729	-0.112046771372746
0.197943561131565	53.6285131190963	0.256351326170575	-17.7198783922578	-0.257131842025737
0.392219027470541	1.19943485851767	-0.113952767283543	-0.303555033639908	0.028454618213043
-0.039779151341611	-19.6295233700006	-0.0512768807791209	6.30109773296471	0.0514262577443651
-0.0678422573228409	-1.33336093021679	0.0232726615301591	0.334180121384034	-0.00571960734147399
0.00663109224183997	10.6670972058572	0.00854619357284534	-2.99050228772331	-0.00857104216080145
0.0114163399742723	0.829953518594056	-0.00387622992588848	-0.207646626089314	0.000952976766333031
-0.000947316039101874	-2.58185331861208	-0.0012208853844307	0.705192657056255	0.0012244345843487
-0.00163374024004815	-0.339137110181637	0.000553621468321884	0.0848097253218847	-0.000136132995282627
0.000118414563356315	-0.223707989062453	0.000152610675180345	0.0467181344594097	-0.000153054323006849
0.000204201656636455	0.101219776088393	-6.920308540371 79e-005	-0.0253085110217277	1.70166612352882e-005
-1.31571741 13103e-005	0.360785728002009	-1.695674170057 05e-005	-0.0889726631986311	1.70060358894105e-005
-2.26888795280868e-005	-0.0236133216562004	7.68924039643158e-006	0.00590377329670858	-1.89074060146706e-006
1.31571741216405e-006	-0.137460288404198	1.69567417008744e-006	0.0342218870628702	-1.70060358894052e-006
2.26888864224652e-006	0.00450502883386758	-7.68924022035584e-007	-0.00112630654116093	1.89074058494607e-007
-1.19610673836673e-007	0.0342562783481719	-1.54152197280798e-007	-0.00854908703328467	1.54600326267318e-007
-2.06262609287698e-007	-0.000725642264571534	6.99021835766418e-008	0.00018141554719772	-1.71885507592935e-008
0	-0.00655819787287491	1.28460164400667e-008	0.0016381304303669	-1.28833605222765e-008

Columns 11 to 15:

17.2265156411261	-23.8034712988753	-35.6508237940319	27.0622108149079	40.8906916484165
-0.0116712574432443	-0.145505753233183	0.000291770873055717	0.0229708663837	-0.000280142003557966
29.9206879217263	13.2196122087939	6.63321942151237	-27.1423915133143	-36.2691671226329
-0.016219535482338	0.136774921249459	0.00465392973509796	-0.0228003388970736	-0.000386610284807143
-20.2195877396863	-6.60980190168077	-3.894413472776	13.5711957776622	17.9755203549872
0.00539346457603879	-0.0689867414986875	-0.00202559986810 36	0.0114163399742723	0.000128377914866327
-1.91539707778428	2.20326551600376	3.23361396559663	-4.52373193836526	-6.18664630499561
-0.0293305362630417	0.0232726615301591	0.00532006221710173	-0.00381258476598939	-0.000698347422379513
0.671724646110334	-0.550816339839982	-0.966132002893514	1.13093298487027	1.54844679542652
0.0599715990044025	-0.00581507604017143	-0.0101184993297989	0.000952976766333031	0.00142789519063331
-0.555760592464877	0.110163266699201	0.289070947262559	-0.2261866596983282	-0.319161274578357
-0.0666680481608795	0.00116259488080149	0.0111393373992729	-0.000190585990099168	-0.00158733448028973
0.458472261211025	-0.0183605444404278	-0.113511076965432	0.0376977661639495	0.0618105281018293
0.0414976759171804	-0.000193768191275005	-0.00692155420283053	3.17644270350023e-005	0.000988039902787971
-0.117833379673209	0.00262293491994701	0.0255754289214844	-0.00538539516627934	-0.0100628276132034
-0.0169568555091519	2.76812676487096e-005	0.00282699084406363	-4.53777751121576e-006	-0.000403734654979819
-0.0126630289973847	-0.000327866864992949	0.00128694212898844	0.00067317439578492	0.000603986300782792
0.00506098880441937	-3.46015814821519e-006	-0.000843617034057586	5.67222176419867e-007	0.000120499733438556
0.0182112695589992	3.64296516658805e-005	-0.00293441853254994	-7.47971550872134e-005	0.000333177754713254
-0.00118066608281002	3.84462009535212e-007	0.000196792443223619	-6.30246861128844e-008	-2.81110972097625e-005
-0.00689099294588507	-3.64296516658805e-006	0.00113746584305744	7.47971550872134e-006	-0.000154047446894475
0.000225251441693379	-3.84462009676156e-008	-3.75435513720311e-005	0	5.36312956412807e-006
0.00171451925699608	3.31178651508004e-007	-0.000284661044078936	-6.79974137156486e-007	3.99123200442141e-005
-3.62821132285767e-005	0	6.04718490659067e-006	0	-8.63859838775636e-007
-0.000328057915956242	-2.75982209590003e-008	5.45776522574273e-005	5.66645114297071e-008	-7.73524623908388e-006

Columns 16 to 20:

-16.7145003315182	-26.1489674999129	6.23046109790307	10.1032584535301	-1.67050211573047
-0.0033209713534 3864	5.20517947367455e-006	0.000408389624810144	-3.89094317145942e-006	-4.61354869754841e-005
16.7140597781409	25.6392871530848	-6.23046293354132	-10.0381340502611	1.6705021097316 6
0.00332205797902697	8.310862652575e-005	-0.000408406981841668	-5.36960271384359e-006	4.61354224168087e-005
-8.3570298888737	-12.8341686535077	3.11523146677128	5.01638969328471	-0.835251054865825
-0.00166101644212087	-3.6171218522571e-005	0.000204201656636455	1.7830252612965e-006	-2.306771309706 27e-005
2.78567662955271	4.31402344055716	-1.03841048892404	-1.67467949557876	0.278417018288607
0.000553621468321884	9.50011178127428e-005	-6.80665847691109e-005	-9.69926980113154e-006	7.68924039643158e-006
-0.696419157386522	-1.08167350328006	0.259602622231017	0.418655658186897	-0.0696042545721518
-0.000138405996317661	-0.000180687487914371	1.70166612352882e-005	1.98318776468618e-005	-1.92231006640934e-006
0.139283831477252	0.218116429909053	-0.0519205244462036	-0.0838548839198444	0.0139208509144304
2.76812676487096e-005	0.000198916739274034	-3.40333311128081e-006	-2.20463122262555e-005	3.84462009535212e-007
-0.023213971912875	-0.037531094774726	0.00865342074103394	0.0140941939472739	-0.00232014181907173
-4.61354422716769e-006	-0.000123599182193393	5.67222176419867e-007	1.37227764276106e-005	-6.407700161015 54e-008
0.00331628170183928	0.00553039185998229	-0.00123620296300485	-0.00203039207186465	0.000331448831295961
6.590777304144 47e-007	5.04819793582792e-005	-8.10317392856134e-008	-5.6074257636086e-006	0
-0.00041453521272991	-0.000611438846830193	0.000154525370375606	0.000244694300247209	-4.14311039119951e-005
-8.238471635353 01e-008	-1.50645898938855e-005	1.012896741184 28e-008	1.67360740886884e-006	0
4.605946808110 11e-005	1.81139958439235e-005	-1.71694855972896e-005	-2.16261290840767e-005	4.60345599022168e-006
0	3.51415077185034e-006	0	-3.90431905691145e-007	0
-4.605946808110 11e-006	1.32581353234278e-005	1.71694855972896e-006	4.85553910537498e-007	-4.60345599022168e-007
0	-6.70420560214841e-007	0	7.44879106128899e-008	0
4.187224371009 19e-007	-4.44177140415305e-006	-1.56086232702632e-007	3.15715616738237e-007	4.18495999111062e-008
0	1.07985444760548e-007	0	-1.19980533163283e-008	0
-3.489353642507 66e-008	9.21128214705881e-007	1.30071860585527e-008	-8.75507499950446e-008	0

Columns 21 to 25:

-2.78066213357289	0.350710045855962	0.5945651338748 56	-0.0605800789126623	-0.104114585414 15
5.783521949666692e-008	4.53777774613985e-006	-3.53722116233812e-008	-4.1941310046394e-007	0
2.77509264515427	-0.350710045871749	-0.5939645824617 75	0.0605800789126281	0.104073101601705
9.23429233232124e-007	-4.53777716449526e-006	-4.88145703075334e-008	4.19413101902987e-007	0
-1.38775452476976	0.175355022935874	0.2969536961608 46	-0.0302900394563141	-0.0520384827310016
-4.01902424186438e-007	2.26888864224652e-006	1.6209320541666 8e-008	-2.0970655091538 5e-007	0
0.463000081609788	-0.0584516743119581	-0.0990063249856513	0.0100966798187714	0.0173494248816644
1.05556797582336e-006	-7.56296236064711e-007	-8.81751800108183e-008	6.99021835766418e-008	0
-0.115789117485644	0.0146129185779895	0.0247510973718942	-0.0025241699546928 4	-0.0043376819638413 3
-2.00763875460192e-006	1.89074058494607e-007	1.8028979678964 4e-007	-1.7475545894914 5e-008	-1.520938450456e-008
0.0231784006986284	-0.00292258371559791	-0.0049512735669 6603	0.0005048339909385 68	0.0008676981913386 21
2.21018599193373e-006	-3.7814811669251e-008	-2.00421020238687e-007	0	1.674383327222 53e-008
-0.00387628966758634	0.000487097285932984	0.0008262766212608 96	-8.41389984897613e-005	-0.0001447175237037 56
-1.37332424659325e-006	0	1.24752512978279e-007	0	-1.0403971565100 4e-008
0.00055564987535671 2	-6.95853265618549e-005	-0.0001181917903179 64	1.20198569271088e-005	2.0688422752998 9e-005
5.60910881758657e-007	0	-5.09765978509872e-008	0	0
-6.85712216317758e-005	8.69816582032186e-006	1.4690992614606 8e-005	-1.5024821158885 9e-006	-2.5793657931030 8e-006
-1.67384332154283e-007	0	1.5214612807898 5e-008	0	0
7.06568647825846e-006	-9.66462868914651e-007	-1.5817442712998 5e-006	1.6694245732095 5e-007	2.8240619816085 4e-007
3.9046119687226e-008	0	0	0	0
-5.39155171660488e-007	9.66462868914651e-008	1.4292609073223 8e-007	-1.6694245732095 5e-008	-2.6972531364743 2e-008
0	0	0	0	0
1.30554923031575e-008	0	0	0	0
0	0	0	0	0
0	0	0	0	0

Applying the above mentioned coefficients we will reach to the figure 4-14(a) for the first mode of pentagonal plates:

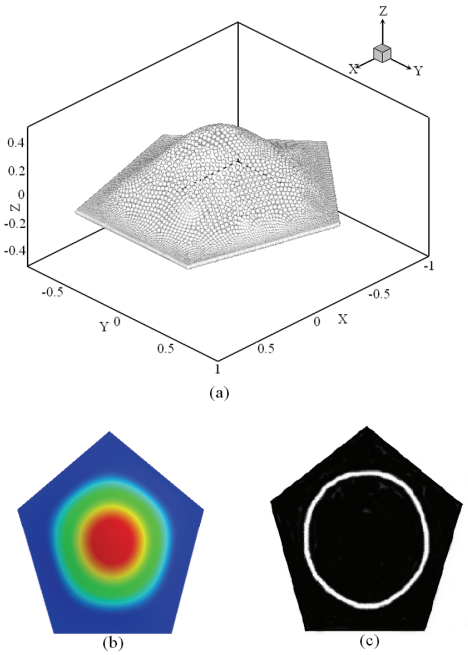

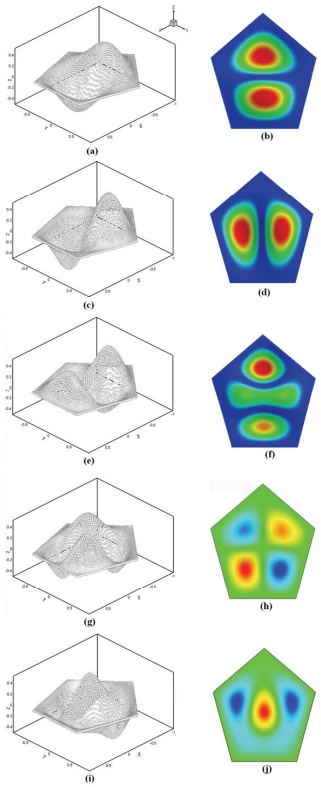

Fig.4-14:*(a) Our numerically calculated nodal pattern by using polynomial solution for the arbitrary pentagonal shape as shown in fig.4-13. (b)The nodal pattern of first mode for pentagonal plates. (c) Experimental pattern has been observed for the first mode of vibration in pentagonal case (Waller, 1952).*

Fig.4-15: *The nodal pattern for arbitrary pentagonal membrane shown in fig.4-13. (a,b)The second mode of vibrations in pentagonal plate,(c,d)The third mode of vibrations in pentagonal plates.(e,f)The fourth mode of vibrations in pentagonal plates.(g,h)The fifth mode of vibration in pentagonal plates.(i,j)The sixth mode of vibration in pentagonal plates.*

We also solve this problem for other modes of vibrations for pentagonal plates. You can compare our result with the nodal pattern in Fig.4-15.

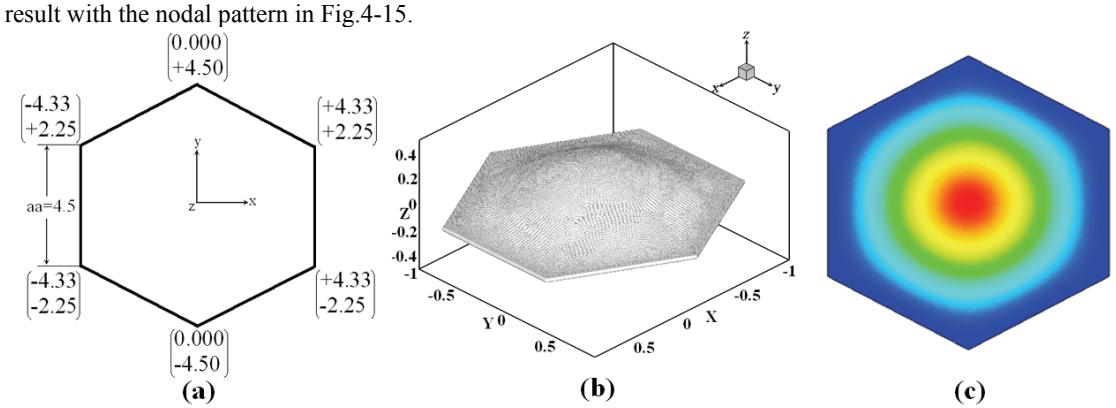

Fig.4-16: *(a) The coordinates that we used for arbitrary hexagonal membrane. (b)Our calculated nodal pattern by using polynomial solution for hexagonal membrane shown in (a). (c)The nodal pattern of first mode for membrane.*

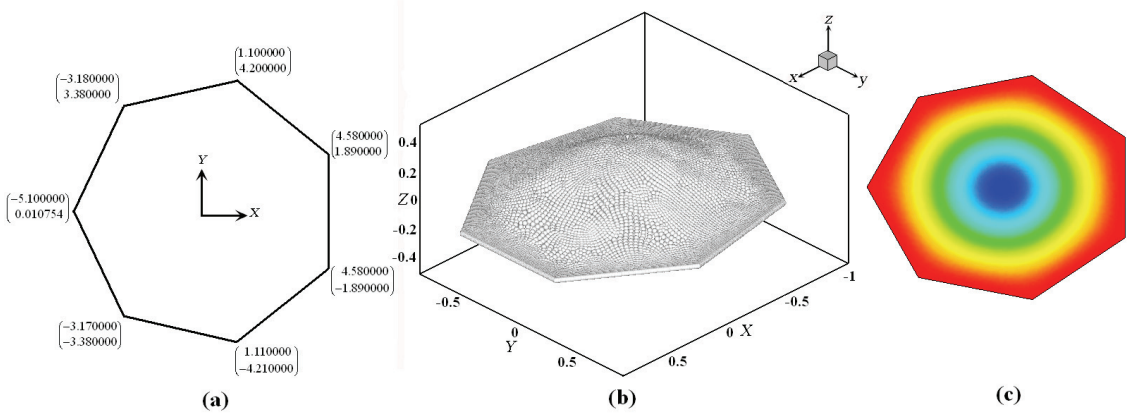

Fig.4-17: *(a) The coordinates that we used for arbitrary heptagonal membrane.(b)Our calculated nodal pattern by using polynomial solution for heptagonal membrane shown in(a).(c)The nodal pattern of first mode for heptagonal membrane.*

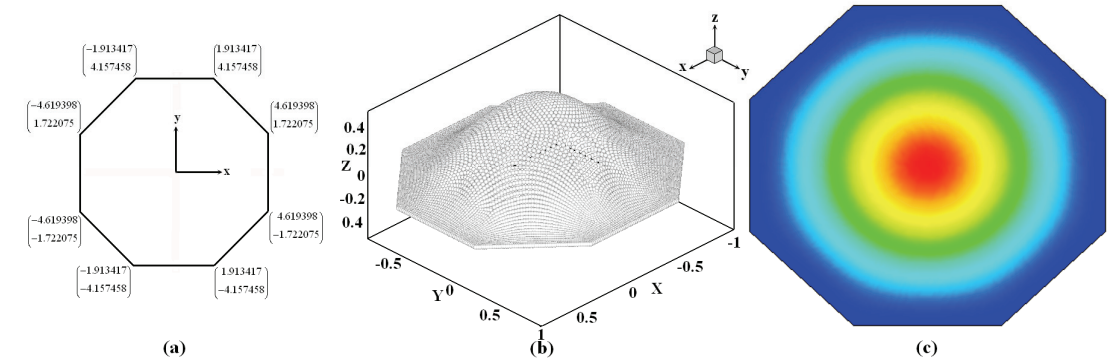

Fig.4-18: *(a) The coordinates that we used for arbitrary octagonal membrane.(b)Our calculated nodal pattern by using polynomial solution for octagonal membrane shown in(a).(c)The nodal pattern of first mode for octagonal membrane.*

By using this numerical method we can find all nodal patterns for the plates in polygonal shape and also some usual shape such as ellipse. The coordination that we used for illustration of result in hexagonal has been shown in figure 4-12+4. In Figures 4-16, 4-17, 4-18, 4-19 and 4-20 you can see the first mode that we found by new polynomial solution for hexagonal, heptagonal, octagonal, enneagon and ellipse, respectively.

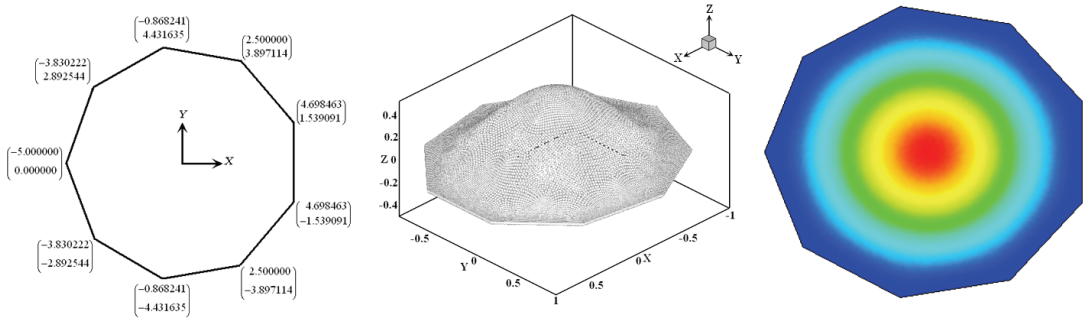

(a) (b) (c)

Fig.4-19: *(a) The coordinates that we used for arbitrary enneagon membrane. (b)Our calculated nodal pattern by using polynomial solution for enneagon membrane shown in (a). (c)The nodal pattern of first mode for enneagon membrane.*

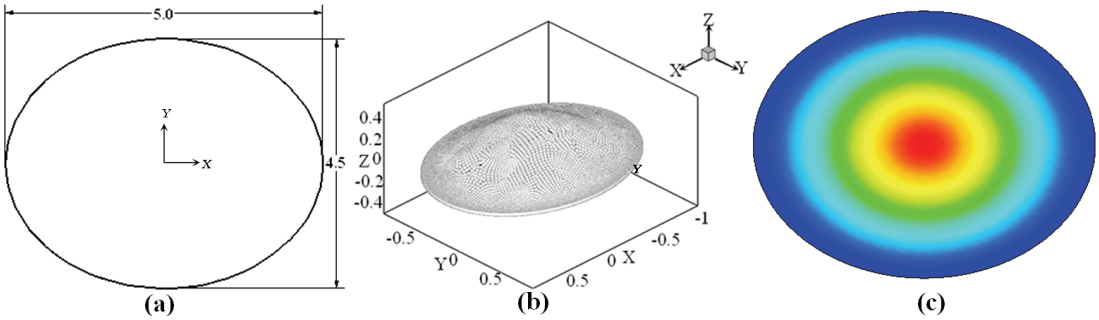

(a) (b) (c)

Fig.4-20: *(a) The coordinates that we used for arbitrary ellipse membrane.(b)Our calculated nodal pattern by using polynomial solution for ellipse membrane shown in (a).(c)The nodal pattern of first mode for ellipse membrane.*

4-2.Collective Processes in Gas-Particle Flows

In this section the question will be addressed of the effects of particle motion on the gas flow and vice versa. Here, particular interest is devoted to particles, which are small enough to participate in velocity fluctuations. In addition, particle volume fraction is large enough that their interaction mainly occurs through collisions, which lead the particulate phase with a collective behavior of its own.

In the following section fluid flow through stationary granular beds is investigated in order to examine induced fluctuations in the gas velocity due to the presence of particles. Information, as such, is required for understanding the collective processes in dense gas-particle flows.

4-2-1. Fluid Flow through a Stationary Irregular Array of Particles

Fluid flow in a granular bed, as illustrated in Fig. 4-21, has attracted attention due to its importance in many industrial processes, such as chromatographic separation technology (Lightfood et al., 1998), packed bed reactor and contacting device design (Strigle, 1994; and Billet, 1995) modeling of contaminant transport in hydro geological and environmental systems (Slichter, 1905), and studies of perfusion in biological media (Kostyuk and Krishtal, 1985).

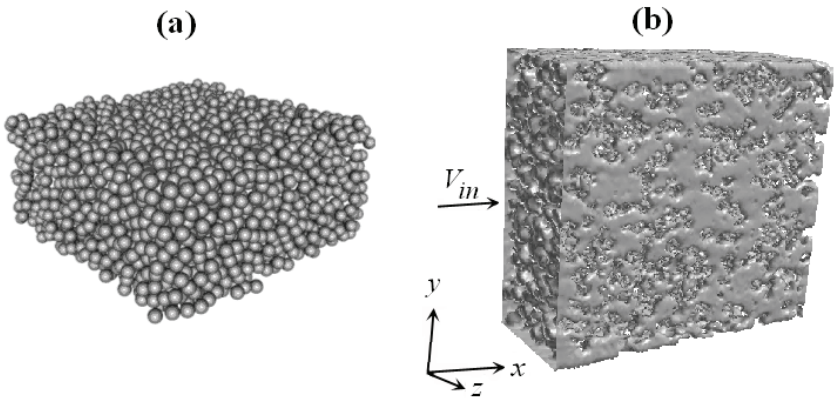

Fig. 4-21: *(a) An illustration of particles in an irregular cubic granular bed. The two different phases are named Carrier Phase (or continues phase) and Dispersed Phase. (b) A three dimensional view of the void region within an irregular array as shown in (a).*

In the geometry as that illustrated in Fig. 4-21, the gas flow is complex where the critical Reynolds number at which the transition takes place is several orders of magnitude lower than that of flow in pipes (Bear, 1988). The transition from laminar to turbulent flow in a granular bed seems rather subtle, compared to the rather sharp transition that occurs in pipe flow. The occurrence of relaminarization from turbulent to laminar regime is quite likely leading to the conditions at which combination of different flow types exists. The existing literature provides limited quantitative information on the criteria that can be employed for determining the flow regime. Demarcation implies that a significant challenge faces researchers to explore the complex behavior linked to the detection of the onset of turbulence, even in a stationary granular bed such as that illustrated in Fig. 4-21. Indeed turbulence in the aforementioned system is a controversial issue. Three-dimensional fluctuations occur on length scales that range from very small pores with the size of fraction of particle diameter to the scales much larger than particle diameter and on a correspondingly broad range of time scales. Hence it is necessary to describe fluid flow in a wide range of excited length and time scales. Modeling of the aforementioned system requires a mathematically rigorous, multi-scale, modeling methodology capable of predicting coupling behaviors from the very small scales such through full scale system. Performing Direct Numerical Simulation (DNS) in which all scales of the flow are properly resolved for simulating flows in models such as that illustrated in Fig. 4-21 is not currently feasible due to prohibitive computational requirements. Considering the current rates of increase of computational power, it is quite unlikely that DNS will become a popular tool for the aforementioned simulations in the near future. Therefore, the spatial resolution of the scheme (at least in some parts of the flow) may be insufficient to describe the smaller scales. In the following, the application of large eddy simulation (LES) (Sagaut, 1998; Mathieu and Scott, 2000) which has the less ambitious goal of describing the larger scales of the flow field through a stationary irregular array of particles is investigated.

4-2-1-1. Large Eddy Simulation (LES)

Attempts has been done for simulating turbulence in gas-particle systems(Ahmadi and Ma,1990;Ma and Ahmadi,1990; Abu-Zaid and Ahmadi,1996).Computations of turbulent flows using spatially filtered equations are know as Large Eddy Simulation (LES) by which large-scale unsteadiness can be captured. LES can be used to calculate flow statistics, which are determined by the larger scales, such as the mean velocity and second-order velocity moments. Indeed, these are the quantities that are often required in practice. Recent advances in physical models, numerical techniques, and computational power together have made LES (Ghosal and Moin, 1995) a useful tool for computing gas-particle flows in vertical channels (Yamamoto et al., 2001) where the dynamics of larger scales is influenced by the presence of small scales because of nonlinear interactions.

Using LES the dynamic range of scales to be resolved is reduced by filtering operation performed on the Navier-Stokes equations. The resulting equations that describes the space-time evolution of the large eddies contain the additional terms, namely apparent stresses, arising from fluctuations about the filtered mean. Thus, LES generates an approximation in which scales below the filter size are missing. The turbulent

energy cascade generates smaller and smaller scales and all scales of turbulence are dynamically significant. Given the lack of small scales below a certain size, the correction must be applied via the aforementioned additional terms (known as subgrid stress tensor) in the governing equations of LES. The subgrid scale (sgs) stress tensor describes the effect of the unresolved scales on the larger resolved scales. The replacement of sgs stress by an explicit physical model (matched to the particular flow) is required to close equations for the large scale fields on a grid small enough (but much larger than the Kolmogorov scale) to provide reasonable resolutions.

Such an approach is obviously approximate and imposes restrictions on the extracted information from computation. However, according to Reynolds (Reynolds, 1976) turbulence modeling such as LES based on spatial filtering is expected to be more general than time averaging Navier-Stokes (RANS) models. Note that in RANS wherein fluctuations at all scales are dealt with by the turbulence model, grid refinement does not increase the dynamic range of scales that is resolved. By contrast, in LES smaller spatial scales are resolved as the grid is refined.

Here, the governing equations of LES used in this thesis are presented. Filtered Navier-Stokes equations for an incompressible viscous Newtonian fluid in Cartesian coordinates may be obtained applying a spatial filter such as

$$G\left(x_i-\xi_i\right)=\left(\gamma/\pi\bar{\Delta}^2\right)^{1/2}\exp\left(-\gamma\left|x_i-\xi_i\right|^2/\bar{\Delta}^2\right), \tag{4-45}$$

where $\bar{\Delta}$ represents cutoff length and G represents spatial filter.

The results are the equations that will be resolved in the numerical simulation whose sample results are illustrated in Fig. 4-22. The filtered momentum equation may be given as

$$\frac{\partial\bar{u}_i}{\partial t}+\frac{\partial}{\partial x_j}\left(\overline{u_iu_j}\right)=-\frac{\partial\bar{p}}{\partial x_i}+\nu_g\frac{\partial}{\partial x_j}\left(\frac{\partial\bar{u}_i}{\partial x_j}+\frac{\partial\bar{u}_j}{\partial x_i}\right), \tag{4-46}$$

where u_i represents the velocity vector of the gas, ν_g represents kinematic viscosity and $\bar{p}$ represents the filtered pressure.

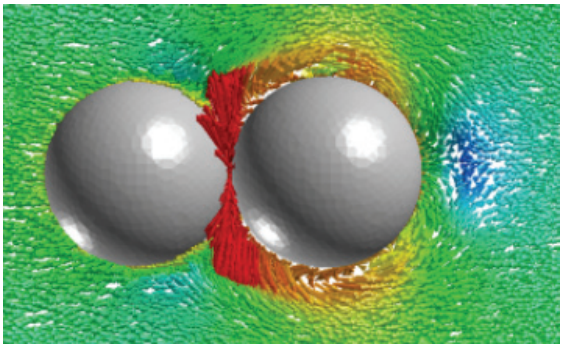

Fig. 4-22: *Vector plot of a velocity field of air at the instant of impact of two equal sized balls with the impact velocity of* $55.4\ cm/s$. *The velocity field is plotted in the plane passing through the center of the balls. Here the ball on the right-side is moving toward the one on the left. Vectors are color coded by their velocity magnitudes, where the red is for highest velocity and dark blue represents the lowest.*

Note that the resolved part of $\bar{\phi}\left(\mathbf{x},t\right)$ of a space-time variable $\phi\left(x_i,t\right)$ is defined as

$$\bar{\phi}\left(x_i,t\right)=\int_{-\infty}^{\infty}\int_{-\infty}^{\infty}\phi\left(\xi_i,t'\right)G\left(x_i-\xi_i,t-t'\right)dt'd\xi_1d\xi_2d\xi_3\,. \tag{4-47}$$

The filtered momentum equation includes the non-linear terms $\overline{u_iu_j}$, which have to be expressed as a function of $\bar{u}_i$ and u_i' defined as u_i-u_i'. The filtered continuity equation is given as

$$\partial\bar{u}_i/\partial x_i=0\,. \tag{4-48}$$

Using Leonard's decomposition (Leonard, 1974) the non-linear term in Eq. 4-47 may be given as

$$\overline{u_iu_j}=\overline{\bar{u}_i\bar{u}_j}+\overline{\bar{u}_iu_j'}+\overline{\bar{u}_ju_i'}+\overline{u_i'u_j'}. \tag{4-49}$$

Substituting Eq. (4-49) into (4-47), the filtered momentum equation may be expressed as

$$\frac{\partial\bar{u}_i}{\partial t}+\frac{\partial}{\partial x_j}\left(\overline{\bar{u}_i\bar{u}_j}\right)=-\frac{\partial\bar{p}}{\partial x_i}+\nu_g\frac{\partial}{\partial x_j}\left(\frac{\partial\bar{u}_i}{\partial x_j}+\frac{\partial\bar{u}_j}{\partial x_i}\right)-\frac{\partial\bar{\tau}_{ij}}{\partial x_j}, \tag{4-50}$$

where τ_{ij} is called the subgrid tensor defined as $\tau_{ij} = C_{ij} + R_{ij} = \overline{u_i u_j} - \overline{u}_i \overline{u}_j$. Here, $C_{ij} = \overline{\overline{u}_i u'_j} + \overline{\overline{u}_j u'_i}$ represents the interaction between large and small scales, and $R_{ij} = \overline{u'_i u'_j}$ represents the interaction between the subgrid scales.

Note that the $\overline{\overline{u}_i \overline{u}_j}$ term in Eq. (4-50) requires a second application of the filter. To remedy this further decomposition is required

$$\overline{\overline{u}_i \overline{u}_j} = \left(\overline{\overline{u}_i \overline{u}_j} - \overline{u}_i \overline{u}_j\right) + \overline{u}_i \overline{u}_j = L_{ij} + \overline{u}_i \overline{u}_j, \tag{4-51}$$

where L_{ij} represents interactions among the large scales. Using Eq. (4-51), the filtered momentum equation may be given as

$$\frac{\partial \overline{u}_i}{\partial t} + \frac{\partial}{\partial x_j}\left(\overline{u}_i \overline{u}_j\right) = -\frac{\partial \overline{p}}{\partial x_i} + \nu_g \frac{\partial}{\partial x_j}\left(\frac{\partial \overline{u}_i}{\partial x_j} + \frac{\partial \overline{u}_j}{\partial x_i}\right) - \frac{\partial \tau_{ij}}{\partial x_j}, \tag{4-52}$$

where $\tau_{ij} = L_{ij} + C_{ij} + R_{ij} = \overline{u_i u_j} - \overline{u}_i \overline{u}_j$. In order to model the subgrid tensor τ_{ij}, Smagorinsky (1963) postulated that $\tau_{ij} = -2\nu_{sgs}\overline{S}_{ij} + 1/3\,\tau_{kk}\delta_{ij}$ with $\nu_{sgs} = \left(C_s\overline{\Delta}\right)^2\left(2\overline{S}_{ij}\overline{S}_{ij}\right)^{1/2}$. The aforementioned expression is akin to a mixing-length formula with mixing-length $C_s\overline{\Delta}$. Here the resolved strain rate is defined as $\overline{S}_{ij} = 1/2\left(\partial\overline{u}_i/\partial x_j + \partial\overline{u}_j/\partial x_i\right)$ and the constant C_s for a case of shear flows is given as $C_s \approx 0.1$.[57] This coefficient must decrease for flows near solid boundaries by using the damping function given as $C_{sb} = C_s^2\left[1 - \exp\left(-\left(y^+/A^+\right)^3\right)\right]$, where $y^+ = yu_\tau/\nu$ characterize distances from the wall in viscous wall units, u_τ and ν are the friction velocity, and kinematic viscosity of the fluid, respectively. Here, A^+ represents a constant whose value is set to 26. To accommodate non-uniform meshes, $\overline{\Delta}$ may be specified as $\overline{\Delta} = V^{1/3}$, where V represents a computational cell.

Currently, the Dynamic Smagorinsky model is preferred for wall bounded and free shear flows. However, the model should be improved for pressure driven separation which would be likely the case in flows through an irregular array of particles. In addition, the Smagorinsky model cannot account for the energy transfer from small-scale to large-scale structures, which could be significant in a number of cases. The fact that the filter width $\overline{\Delta}$ be specified explicitly motivated the need for a more general model such as Dynamic Sub-Grid Scale model (DSGS) (Germano et al., 1991).

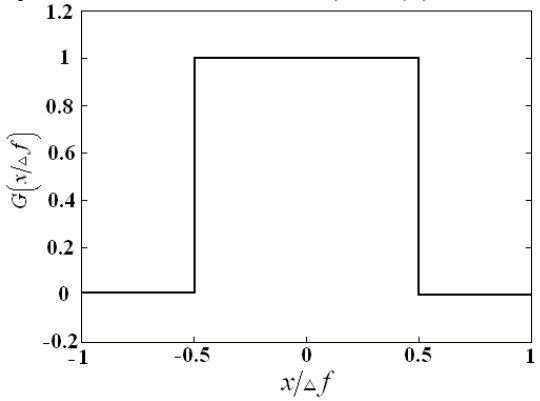

Fig. 4-23: Filter function, *G,* of top-hat filter.

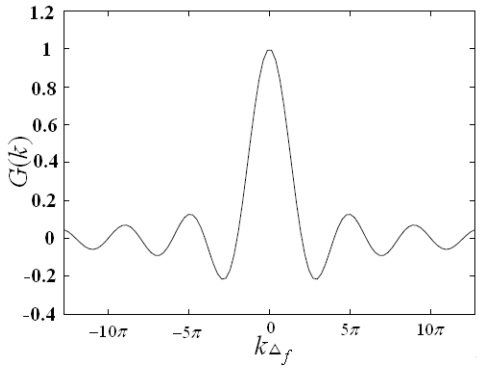

Fig. 4-24: Filter transfer function, $\hat{G}$, of top-hat filter.

A significant progress in the subgrid-scale modeling of non-equilibrium flows was made by the development of DSGS. In DSGS, two filters are introduced which are a grid filter, $\overline{\Delta}$, and a test filter (Cui and Neary, 2002), $\hat{\overline{\Delta}}$ where $\hat{\overline{\Delta}} > \overline{\Delta}$. Quantities filtered at the grid scale are denoted by the over bar while the

hat notation represents filtering at the larger scale. Thus $\overline{u}_i$ denotes the computed velocity delivered by the numerical method, and $\hat{\overline{u}}_i$ represents the LES-computed velocity field filtered at scale $\hat{\overline{\Delta}}$. In developing DSGS model, an exact relationship, namely Germano identity, may be used between the subgrid-scale stress tensors at the two different filter widths. Substitution of a Smagorinsky form for the sub-grid scale stress, namely $\tau_{ij} = -2C\overline{\Delta}^2\left(2\overline{S}_{mn}\overline{S}_{mn}\right)\overline{S}_{ij} + 1/3\,\tau_{kk}\delta_{ij}$, into the Germano identity, along with applying the least square method suggested by Lilly (1992), leads to an expression for the model parameter as

$$C = \frac{1}{2}\frac{\left\langle L_{ij}M_{ij}\right\rangle}{\left\langle M_{kl}M_{kl}\right\rangle}, \tag{4-53}$$

where $L_{ij} = \overline{\overline{u}_i\overline{u}_j} - \hat{\overline{u}}_i\hat{\overline{u}}_j$ and $M_{ij} = \overline{\Delta}^2\left(2\overline{S}_{ij}\overline{S}_{ij}\right)^{1/2}\overline{S}_{ij} - \hat{\overline{\Delta}}^2\left(2\hat{\overline{S}}_{ij}\hat{\overline{S}}_{ij}\right)^{1/2}\hat{\overline{S}}_{ij}$. Here, L_{ij} is a measure of the turbulent stress between the test and grid filter widths, and M_{ij} is a function of the resolved rate-of-strain. The angled brackets in (4-53) represent averages over the homogenous or periodical direction.

The aforementioned model improves on the model of Smagorinsky and can be applied to various turbulent flows. To improve numerical stability, it is necessary to smooth the distribution of *C* and set it to a positive value. However, there is a contradiction between the numerical stability and the backscatter. Note that the backscatter can only be obtained with a negative *C*. This may sometimes give rise to unphysical backscatter that tends to destabilize the numerical simulation.

4-2-1-2. Numerical Results

In order to visualize the velocity field of gas flowing through an irregular array of particles, the vector plot of velocity field is illustrated in Fig. 4-25. Here the flow of fluid interrupted by an array of spherical particles randomly positioned within a rectangular duct with the inlet velocity of air set to $V_{in} = 0.25\ m/\text{sec}$ to obtain the Reynolds number exceeding a critical value at which turbulence vortices begin to appear, namely $\text{Re}_c \approx 10$ (Clift et al., 1978). The predicted velocity field as illustrated in Fig. 4-25 is obtained using a sub-scale model of Smagorinsky, detailed in the previous section.

As suggested by Masuoka and Takatsu (1996), at least two types of vortices may be observed, namely the interstitial and pseudo vortices, in the geometry as illustrated in Fig. 4-25. Note that the mixing caused by an interstitial vortex contributes to Forchheimer flow resistance and that of a pseudo vortex to momentum dispersion.

Fluid structures with the size of the order of square root of permeability, which characterizes the gap thickness formed between particles, are clearly present in the flow field, as depicted in Fig. 4-25. As shown in Fig. 4-25, fluid flowing past each particle appears to produce a vortex. These vertical structures could play an important role in the transport mechanism such as momentum dispersion due to the solid obstructions. In the converging sections of the duct located on the top and bottom of each particle, the fluid layers close to the walls, as depicted in Fig. 4-26, tend to move faster resulting in a flattened velocity profile and therefore less mechanical energy may be converted to turbulence. However, when the flow crosses the enlarged sections in the back of each particle, the fluid particles close to the wall are subjected to an unfavorable pressure gradient resulting in a slower fluid motion than that in the core, which could lead to separation, which enhances turbulence production.

The behavior of fluid flowing in a system as illustrated in Fig. 4-25 appears to be analogous to that in a porous medium of conduit type where relaminarization could occur after diverging sections of tube, as well as turbulence enhancement after converging sections. In this light, LES is a potentially powerful tool for providing detailed and accurate resolution of flow in a porous medium.

In order to visualize the fluid mixing behavior in the duct, the fluid streamlines, as shown in Fig. 4-26 (a, b), were color-coded using a mixing parameter defined as, $\lambda = \|\mathbf{D}\|/\|\mathbf{D}\| + \|\boldsymbol{\omega}\|$, where $\mathbf{D}$ represents the rate of deformation tensor, $\boldsymbol{\omega}$ is the vorticity vector and the double-lines denotes the magnitude of quantity.

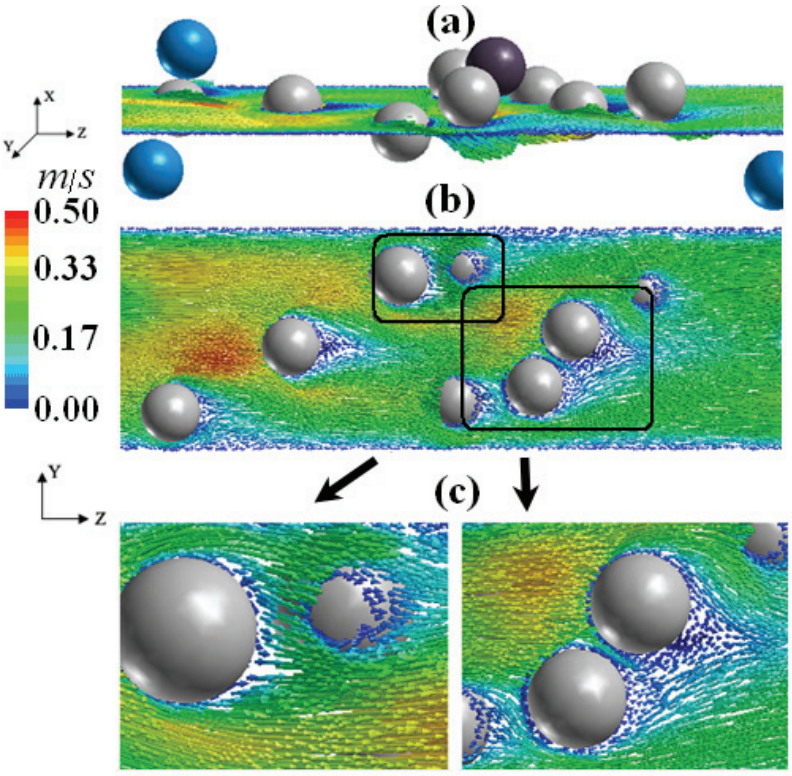

Fig. 4-25: *Illustration of velocity vector field for the flow of fluid interrupted by an irregular array of 25 spherical particles with diameter of 5mm randomly positioned within a rectangular duct with this dimensions* $1.5\times3\times12cm^3$ *. The uniform inlet velocity of air is* $V_{in}=0.25\ m/\sec$ *and the Reynolds number is approximately equal to 100. This system was modeled with 851666 triangular cells and 1754061 faces and 166192 nodes. (a) Isometric view of a part of system, velocity vector field was drawing for a surface that was in middle of height of duct. (b)* $y-z$ *view of the system has been shown in (a). (c) Two zoomed view of two different parts of the (b).*

The mixing parameter λ, can be interpreted as follows; $\lambda=0$, 0.5, and 1 represent simple rotation, simple shear and elongation regimes, respectively. To further quantify the extent of mixing in the duct, in Fig 4-26 the range of mixing parameter λ, is adjusted to 0 and 0.79. At $\lambda=0$ the fluid is essentially turning as a rigid body, whereas at $\lambda=0.79$ it is being stretched. As can be seen from Fig. 4-26, the mixing processes can be quite complex even in this simple geometry.

4-2-2. Fluid Flow in the Presence of Moving Bodies

In the preceding section the transport phenomena and collective processes involved in fluid flowing through stationary array of particles were investigated. In many industrial applications such as fluidized beds, solid body movements result in an increase of inertial instability in the fluid phase, which could be an origin of fluid turbulence, which in turn enhances the dispersion and mixing.

In dense gas-particle suspensions of massive particles where the particle collision time τ_c (which characterizes the mean time between successive collisions of a particle with its neighbors) is much smaller than the particle crossing time τ_i, the motion of the particles can be partitioned into three components. They are the local mean particle velocity, the fluctuating velocity associated with the organized motion of collections of particle, and the fluctuations at the level of individual particles. In this case particle-particle collisions generate a random component of particle velocity. The kinetic energy of particle random motion is characterized by a granular temperature, which is proportional to the mean square of the random component of particle velocity. Sinclair and Jackson (1989) suggested that the particle velocity fluctuations could generate an effective pressure in the particle phase.

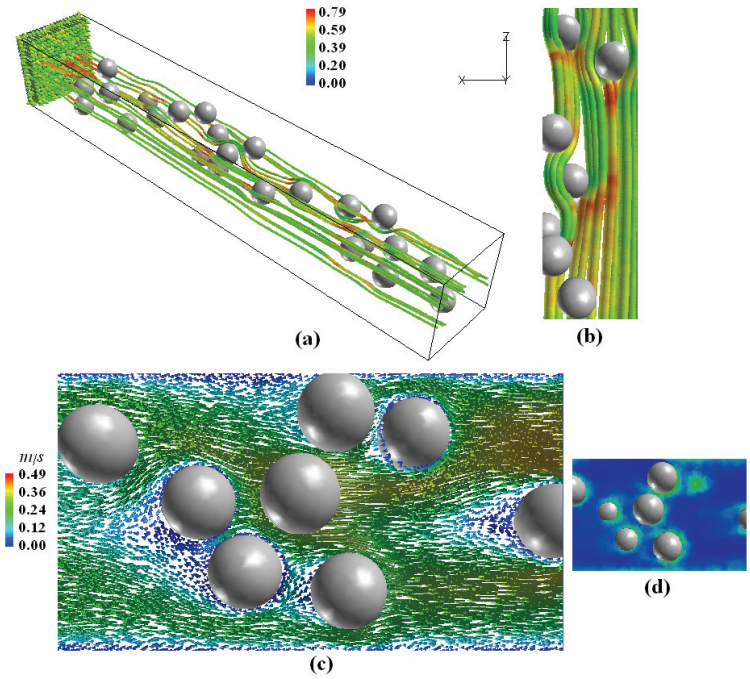

Fig. 4-26: *(a, b) Illustration of the system consists of 25 spherical particles with 5mm diameter has been arranged randomly in one* $1.5\times3\times12 cm^3$ *rectangular. The grid condition is the same as explained in caption of Fig.4-25. This right side part of this figure shows the isometric view of the whole system with the uniform velocity vectors in the inlet of the duct and stream line of the gas flow along a cut-surface in* $y-z$ *plane(*x *in the middle) duct has been colored by mixing parameter* λ*. (c) The velocity vector field in one part of system around the particles. (d) The contours of the velocity in the same part as (c).*

For dense gas-particle flows, number of mechanisms may be responsible for turbulence modulation including shedding of vortices behind the particles and enhancement of the gas velocity gradient between two particles.

4-2-2-1. Turbulence Enhancement

4-2-2-1-1. Shedding of Vortices

It is commonly accepted that when the particle Reynolds number exceed Re_c, turbulent kinetic energy enhances due to vortex shedding. To obtain a better understanding of turbulence enhancement of the gas, the interaction of a fluctuating object such as a solid wedge, as shown in Fig. 4-27 (a), with surrounding fluid is considered in the following. To this end, the flow of air is simulated through a $1.5\times3\times12\ cm^3$ duct in which a single wedge is placed at its center. As illustrated in Fig. 4-27 (a), the wedge is a right equilateral triangle prism with edge length of $2.2\ cm$ and height $1.5\ cm$ whose displacement along the y-axis is given by $A_0\sin(100t)$.

Using LES techniques large-scale structures is visualized in flow of air passing the fluctuating wedge. Here a stochastic component is superimposed to velocity in the z-direction given as $V_z = 50(1+0.1\psi)\ cm/s$, where ψ is a random number which has a Gaussian distribution with zero mean and a standard deviation of one. The pressure at the exit of duct is assumed to be fixed to the local atmospheric pressure. In addition, no-slip boundary condition is assumed at the entire solid fluid interface.

To divide the air space into discrete control volumes more than 10^6 3D tetrahedral computational cells are used, which are nonuniformly distributed in the grid with fine enough mesh near the solid surface. In addition, roughly 6×10^5 wall triangular elements as well as more than 1.3×10^4 boundary triangular elements are used at the inlet and exit.

The major challenge faced in simulating the aforementioned systems is resolving the interfacial motion. The remedy for this problem is to employ dynamic interfaces treatment for modeling the flow passing the fluctuating wedge. Generally speaking, natural framework for dynamic interface problems is the Lagrange method, in which the interface representation is embedded in the material description of flow. In

this case, the mesh convects and deforms with the flow, and therefore interfaces that are well-resolved initially remain sharp during simulations. In the simulations, described in the following, a Lagrangian framework is adopted that evolves the grid points at each time step. To maintain mesh quality required for LES techniques, and permit adaptively a Delaunay triangulation of the dynamically-evolving grid points is required at each time step as that proposed by Walkingtor et al. (2000).

Here, the central-differencing is used for spatial discretization of conservation equations, and time-advancement is treated using a first-order implicit scheme with a time step $dt = 4 \times 10^{-4}$ sec, which is much smaller than the life time of large structures in the gas flow. The small eddies were modeled and those fluid structures of a characteristic size greater than the cutoff length were resolved.

Figure 4-27 illustrates the instantaneous realizations each separated by $t \approx 0.005\,\text{sec}$. This shows considerable variation in flow pattern from instance to instance. Note that it is reasonable to assume that the relaxation time for the gas velocity to conform to that of the wedge is short compared with the shortest significant time scale of the fluctuations in wedge velocity. As depicted in Fig. 4-27, the flow in the duct evolves to a time dependent turbulent state. The duct flow of air is completely distorted and unsteady vortices are produced due to interruption caused by rotation of the solid wedge along its y-axis. Hence, the paths followed by fluid particles are not straight but tortuous similar to that in a porous medium, causing momentum diffusion which leads to dispersion of the gas within the duct. The reason for focusing attention to the back face of the wedge is that the nature of the wedge-induced gas flow is of interest as it passes the rotating wedge, unsteady state flow patterns are generated in the gas as evidenced in Fig. 4-27.

To obtain a better visualization, the vortices produced in the lower part of the channel beside the wedge, as shown in the Fig. 4-27 (b), are magnified in Fig. 4-27 (c). The overall flow is far more complicated with many intermediate and small-scale components.

Recall that Masuoka and Takatsu (1996) suggested that two types of vortices including pseudo vortices may be observed in flows through an irregular array of solid particles. Careful observation along the bottom wall of the wedge reveals what appear to be pseudo vortices, whose sizes are to be of order of height of the back face of the wedge. The pseudo vortices initially bend to the right and after a few time steps they turn to the left as illustrated in Figs. 4-27 (d-e). Note that other vortices can also be observed in the front side of the wedge, which appears to be arising from the instability of the boundary layers.

Moreover, flow accelerates within the lower part of channel formed around the wedge and separates after passing the wedge to form a strong recirculation pattern. Accordingly, it would be expected that even slight change in the shape of convergent and divergent passages could result in a significant change of flow patterns, as well as mixing processes in a duct flow.

Note that Particle Image Velocimetry (PIV), which easily provides instantaneous, velocity vector measurements in the cross-section of the duct flow, can be used to visualize the vortices and the turbulent flow around the wedge, as illustrated in Fig. 4-27. The PIV measurements would be of vast importance for the validation of numerical simulations, which may be of use in developing correlations for turbulent dispersion.

4-2-2-1-2. Enhancement of the Gas Velocity Gradient

Another mechanism responsible for turbulence modulation would be the enhancement velocity gradient between two particles. To obtain a better understanding of the aforementioned mechanics it is instructive to investigate macro-scale coherent structures in a duct flow of gas passing through an assembly of twenty five mono-dispersed spherical particles with diameter of $5\ mm$, which are set into a random translational motion initially. The initial configuration of particles is shown in Fig. 4-29 (a) where the solid volume fraction is roughly 0.05.

The classification of gas-particles flows (Elgobashi, 1991), Fig. (4-28) indicates that when the particle volume fraction ϕ_s exceeds a critical value, namely $\phi_s > 10^{-3}$, the relative distance between particles is small enough so that the particles may collide. This is called four-way coupling (Elgobashi, 1991).

Using LES the flow field around moving particles are calculated in detail. By using 10^6 3D tetrahedral computational cells nonuniformly distributed in the grid, the spatial resolution of LES required to resolve the particle movements is obtained. Note that the particle Stokes number is large, and therefore the effect of subgrid scale eddies on the particle movements appear to be insignificant.

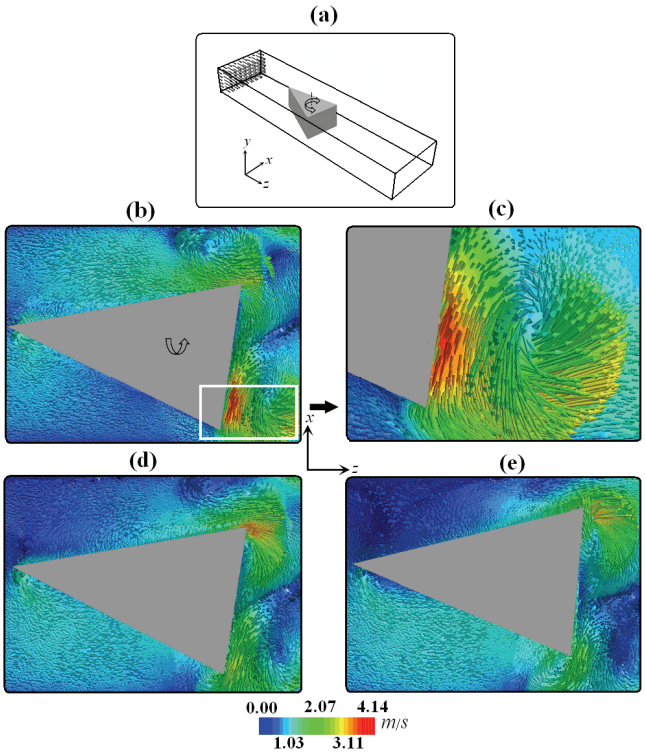

Fig. 4-27: *(a) View of the* $1.5\times3\times12\ cm^3$ *duct with wedge placed at the middle. The wedge is a right equilateral triangle prism of edge length* $2.2\ cm$ *and height* $1.5\ cm$*. In the carried out simulation the inlet average velocity of flow air is set to 50cm/s. Here the wedge is rotating with angular velocity 100 1/s along the y-direction. The grid condition is as follows: 675759 cells, 1381704 faces, 126174 nodes and we defined one cell zone and 8 face zones in this system. (b) Temporal evolution of the velocity field of fluid in the plane passing through the center of the duct, shown in (a). Here the simulation is carried out for the inlet average velocity of 50 cm/s. To obtain better visualization of flow field around the converging section of the duct, the flow patterns in the vicinity of the bottom of the wedge shown in (b) is magnified and presented in (c). The velocity vector field around the wedge is shown for several times of simulation in part (d-e). There is 0.005s between each frame from (d) to (e).*

A uniform velocity of 25 cm/s is used as the inlet condition of the air. Fig. 4-29 (b) and (c) represent the instantaneous velocity vector field and the pressure distribution around the particles. The integrated pressure distribution and the shearing stresses over the surface of the pth particle at time t is computed to obtain the total drag, D_i^p. The linear velocity vector of the pth particle at time $t, V_i^p(t)$, is calculated using an explicit Euler formula given as $V_i^p(t) = V_i^p(t-\Delta t) + D_i^p / m\,\Delta t$ .Obviously, modeling the flow passing the moving particles involves dynamic interfaces treatment. The Lagrange method is employed to resolve the interfacial motion. For the sake of simplicity, neither rotational degree of freedom for the particles nor the effect of gravity is taken into account in the present model.

The chain of events that lead to a binary collision of two spheres in a system, as shown in Fig. 4-29 (a), is predicted using the aforementioned model. The enhancement of the velocity gradient between particles is clearly presented in Figs. 4-29 (d-e) which depicts the instantaneous realizations of velocity vector fields each separated by $t \approx 0.05$ sec . It is likely that the growth of disturbances due to movement of particles induce a random behavior wherein the vortex field around the particles. As illustrated in Fig. 4-29 (f), a very complicated vortex pattern between the colliding particles can be developed causing the vorticity to increase which implies that collision among particles produce turbulence. Indeed, this mechanism of turbulence enhancement and the other one described in the preceding section may not be independent. Here, turbulence is viewed as a maze

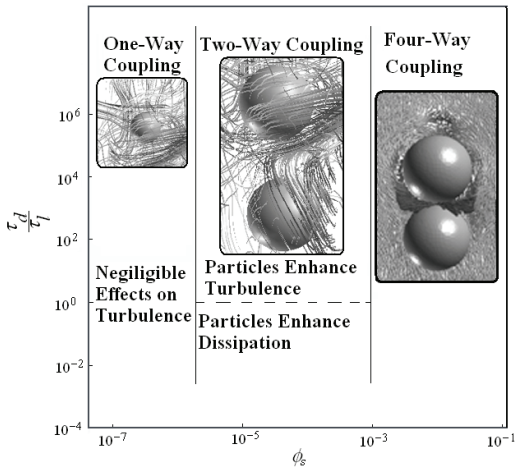

Fig. 4-28: *Classification of flow regimes for gas-solid flows according to Elgobashi (1991).*

of vortices interacting one with the other in a random manner and transferring vorticity to smaller and smaller length scales (Granger, 1995).

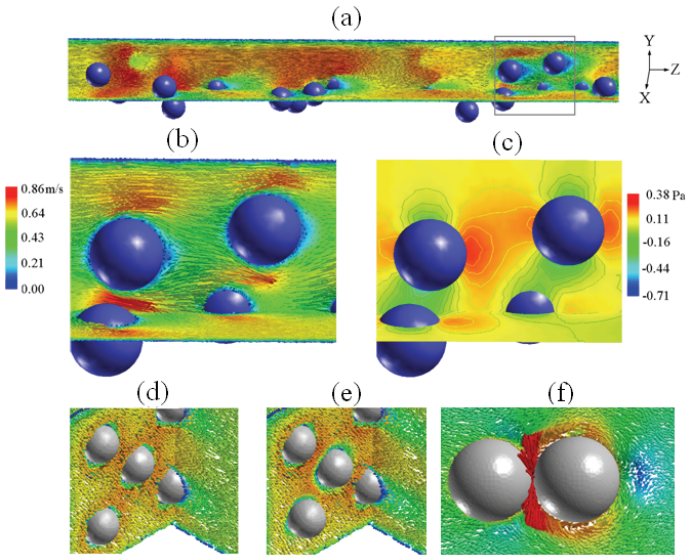

Fig. 4-29: *(a) An illustration of the air velocity field passing through an assembly of spherical particles, which are set into transitional and rotational motion. To obtain a better visualization of flow field, the flow patterns marked in (a) is magnified and represented in (b). Part (c) is the contours of pressure for the configuration, as illustrated in (b). (d-e) are an illustration of the chain of events ends to a binary collision of two spheres in a system, as shown in (a). The velocity vector field is plotted in the plane passing through the center of the colliding balls. Vectors are color coded by their velocity magnitudes where the red is for highest velocity and dark blue represents the lowest. Part (f) is an illustration of velocity vectors field around two particles that are in collision to each other. This collision induces turbulence in gas phase.*

Note that PIV enables simultaneous velocity measurements of both gas and particle phases in a dilute gas-particle flow where $\phi_s << 10^{-3}$. The image processing which implements the phase separation is rather simple, but has limitations. The method is restricted to low solid densities to avoid a quality drop in the measurements, and cross talk between measurements of the two phases. It must be emphasized that the PIV measurement capabilities are confined to particles solid volume fractions far below the range of interest from the point of view of dense suspensions. In this light, in dense suspensions the detailed experimental data available are limited due to the fact that gas-particle flows with appreciable particle loading are too opaque to permit optical measurements such as PIV. In contrast, computational simulations such as LES represent the promising avenue to investigate 3-D macro-scale structures in a dense gas-particle system such as that illustrated in Fig. 4-29 (a). The results outlined in this section would be of use in developing models to capture complex phenomena involved in dense gas-particle flows for which interparticle collisions could play an important role.

The simple lessons learned from analysis of the flow dynamics discussed in this section are summarized as follows. At high solids loading of large particles (whose Stokes number is large) the turbulent fluctuations are driven by the collective motion of the particle assembly, rather than the gas. The slip velocity will be small only if the relaxation time for the gas velocity to conform to that of the particles is short, compared with the shortest significant time scale of the fluctuations in particle velocity. Coherent structures in dense gas-particle flows can be captured only thought 3D transient simulations.

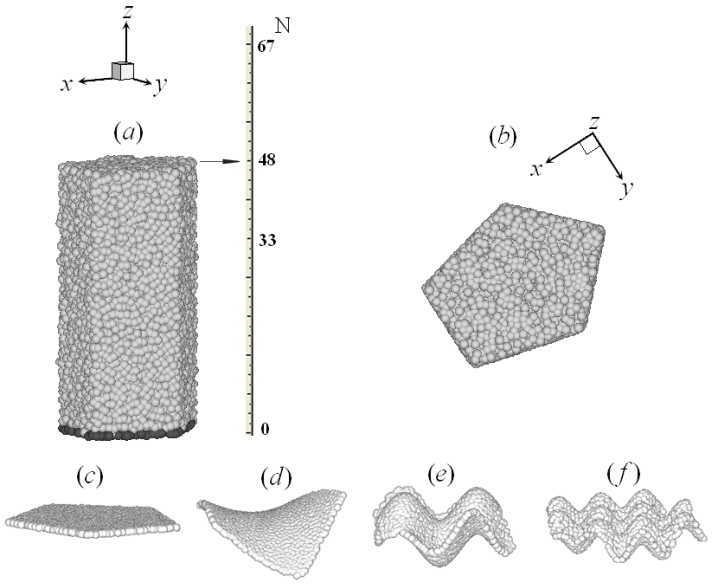

Fig. 4-30: *(a) A schematic of configuration of particle in pentagonal prism used in our molecular dynamics simulation. (b) Top view of the system has been shown in part (a) changes the particles position in the bottom of bucket during the time has been shown in parts (c-f).*

Note that one limitation of the scheme described in this section is that only a small number of moving particles can be studied, and especially simulations of a collision as illustrated in Fig. 4-29, could be quite costly. Hence, a more simplified scheme would be desired to treat the hydrodynamic interactions reliably among a large numbers of particles in a system such as a vertically vibrated granular material, as illustrated in Fig. 4-30 and Fig. 4-31.

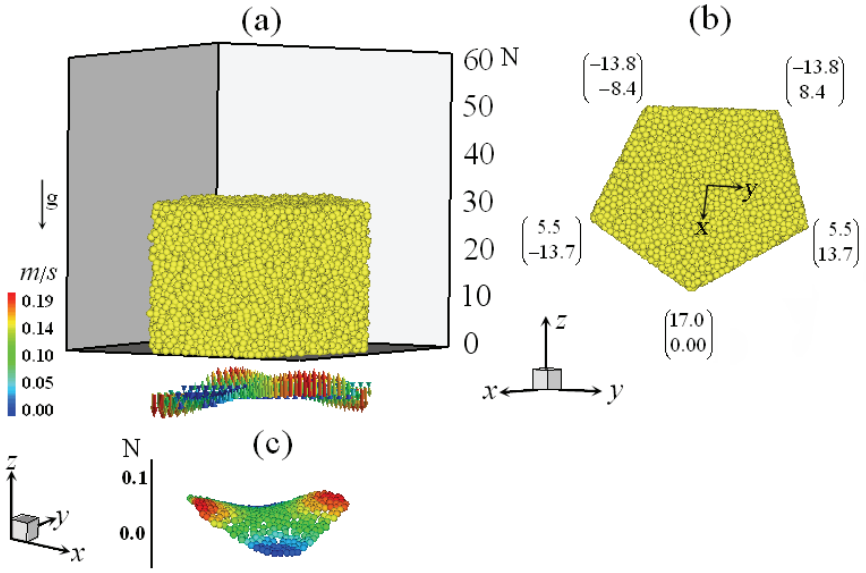

Fig. 4-31: (a) Schematic diagram of a dense mixture of gas-particles in a pentagonal prism under sinusoidal oscillation in the vertical direction given as $z = A\sin(kx)\sin(ly)\cos(\omega t)$,where $\omega = C\sqrt{l^2 + k^2}$, C characterizes speed of wave in bottom wall of the bucket, A is a constant, $k = m\pi$, and $l = n\pi$. An instantaneous velocity vectors for the particles at the bottom wall is shown below of (a). The numerical values used for the aforementioned parameters were $A/\sigma = 3\times10^{-2}$, $m = 17$ $1/m$, $n = 13$ $1/m$, and $C = 100\ m/s$. (b) Top view of the initial particle configurations. The initial solid fraction ϕ_s was 0.585. (c) The observed oscillon structure has been formed in molecular dynamics simulation of system has been shown in (a) the

particles have been colored by local granular temperature. The next oscillon will form in central region (red hole) that has high granular temperature. (d) An illustration of velocity vector field in outlet surface of bucket. It is observed that in region that oscillon formed the air tended to move more out of the bucket.

4-2-3. Simplified Discrete Model

The sophisticate discrete model outlined in the preceding section (which contains only a few empirical parameters) may not become feasible in the foreseeable future for producing detailed information for a vertically vibrated granular material. Hence, a more simplified model is used to generate the results as illustrated in Fig. 4-31.

The system as illustrated schematically in Fig. 4-31 (a) represents a virtual reality type vibro-ganular medium device. Roughly 2×10^4 identical, slightly overlapping, spherical glass particles with diameter $\sigma = 600\ \mu m$ are used to fill the bucket with sand. The initial configuration of sand particles in a pentagonal prism bucket more than one-half full is illustrated in Fig. 4-31 (a). The free surface, as depicted in Fig. 4-31 (b), located at $N = Z_0/\sigma \approx 30$, was nearly flat before vibration begins. Here, σ represents the particle diameter.

The base wall of the bucket is subjected to sinusoidal oscillation in the vertical direction given as $z = A\sin(k_v x)\sin(l_v y)\cos(\omega_v t)$, where $(\omega_v = C\sqrt{l_v^2 + k_v^2})$ and $k_v = m_v\pi$ and $l_v = n_v\pi$. The numerical values used for the aforementioned parameters were $A/\sigma = 3\times10^{-2}$, $m_v = 17\ \ 1/m$, $n_v = 13\ \ 1/m$, and $C = 100\ m/s$. The initial solid fraction ϕ_s was 0.585. The physical properties for the glass balls and the gas as well as model constants are presented in Table 3-1.

The system size and the values for parameters such as C (speed of wave in the bottom wall of bucket), A, k_v and l_v were selected based on limitations imposed by computational resources. The complexities of granular systems such as polydispersity, the Coulomb interaction between the particles, and the particle rotational motion are neglected.

4-2-3-1. Numerical Models

In general, solid particles with mass *m* in a fluid obey the Langevin equation given as

$$m\frac{dV_i^p}{dt} = F_i^f + F_i^g + F_i^i + F_i^b, \tag{4-54}$$

where F_i^f is the drag force from the gas, F_i^g is the gravitational force, F_i^i is the force due to particle-particle interaction, and F_i^b is the Brownian force due to thermal motion of the gas. To simplify the equation of motion for the solid particles it would be useful to define dimensionless quantities given below

$$\begin{aligned}
\mathrm{Re}_p &= (1-\phi_s)\frac{\sigma\left|u_i - V_i^p\right|}{\nu_g}, \\
\mathrm{St} &= \frac{2}{9}(1-\phi_s)\left(\frac{\rho_g}{\rho_p}\right)^{-1}\frac{\sigma\left|u_i - V_i^p\right|}{\nu_g}, \\
\mathrm{Fr} &= \frac{\left((1-\phi_s)\left|u_i - V_i^p\right|\right)^2}{gL},
\end{aligned} \tag{4-55}$$

where $\mathrm{Re}_p, \mathrm{St}, \text{and } \mathrm{Fr}$ are the Reynolds number, The Stokes number, and the Froude number, ρ_g and ρ_p are densities of the gas and the particle, respectively, u_i is the velocity of the gas at the particle position, *g* is the acceleration due to gravity, and *L* is the linear size of vibro-ganular medium device. Note that Fr is the ratio of the total kinetic energy of the particle to the gravitational potential.

Using the data presented in Table 1, the order of magnitude of dimensionless quantities listed in Eq. (4-55) for the vibro-ganular medium device are estimated as $\mathrm{Re}_p \sim 10, \mathrm{St} \sim 10^4$, and $\mathrm{Fr} \sim 1$. Since the work done by the drag force over the size of particle is much larger than thermal energy (equal to the product $k\,T_{th}$, where k is Boltzmann's constant and T_{th} is particle thermodynamic temperature in Kelvin), the random force F_i^b can be neglected. Thus for the case $\mathrm{Re}_p \sim 10$, and $\mathrm{St} \gg 1$ with non-linear visco-elastic particle-particle interactions, the Langevin equation for translational motion of the pth particle in the vibro-ganular medium device may be reduced to

$$\frac{dV_i^p}{dt} = \frac{3}{4}\frac{\rho_g}{\rho_p} C_D' \frac{\left|u_i - V_i^p\right|}{\sigma}\left(u_i - V_i^p\right)\left(1-\phi_s\right)^2 - g\delta_{iz} + \sum_{p=1}^{N_j} F_{i,jp}^{(n)}, \tag{4-56}$$

Where C_D' is the effective drag coefficient, defined as $C_D' = \left(1-\phi_s\right)^{-4.7} C_D$ (We and Chem, 1966), where C_D is the drag coefficient for an isolated particle depends on particle Reynolds number, and δ_{ij} represents Kronecker delta. An expression for the drag coefficient C_D is given as, $C_D = \frac{24}{\mathrm{Re}_p}\left(1 + 0.15\,\mathrm{Re}_p^{0.687}\right)$ (Rowe and Henwood, 1961), which is valid for particle Reynolds umbers up to about 40.

By employing a soft particle approach an expression may be obtained for the normal force per unit mass acting on the pth particle due to viscoelastic contacts between this particle and its N_j neighboring j^{th} particles forming a chain like structure at time *t*, given as (Bordbar and Zamankhan, submitted 2005a):

$$F_{i,jp}^{(n)} = \left(\left(2E/3\left(1-\nu_p{}^2\right)m\right)\sigma^{1/2}\hat{\delta}_{jp}^{3/2} + \frac{K_n\tau}{m}\left(\,G_0^2/\left(G_0-G_\infty\right)\right)\hat{\delta}_{jp}\frac{d\hat{\delta}_{jp}}{dt}\right)k_{i,jp}. \tag{4-57}$$

Here, E represents Young modulus, ν_p represents Poisson's ratio, $\hat{\delta}_{jp}$ represents overlapping between the pth and j^{th} particles, G_0 represents instantaneous (glassy) shear modulus, G_∞ represents long time shear modulus, K_n represents coefficient characterizing the viscous behavior of the grains, and τ is the relaxation time for the viscoelastic material (Phan-Thien, 2002). The above-mentioned model is capable of capturing chain like contacts, which are of importance in modeling dense granular flows. To obtain an expression appropriate to spherical particle-flat wall contact from Eq. (4) σ has to replace 2σ.

To predict the gas flow field in the vibro-ganular medium device, a generalized form of the Navier-Stokes equations for a gas interacting with a solid phase is used. That is

$$\left(\left(1-\phi_s\right)u_i\right)_{,i} - \phi_{s,t} = 0, \tag{4-58}$$

$$\left(\left(1-\phi_s\right)u_i\right)_{,t} + \left(\left(1-\phi_s\right)u_iu_j\right)_{,j} = -\frac{\left(\left(1-\phi_s\right)p\right)_{,i}}{\rho_g} + \left(\left(1-\phi_s\right)\sigma_{ij}\right)_{,j} - \left(1-\phi_s\right)g\delta_{iz} + \frac{f_i}{\rho_g}. \tag{4-59}$$

The last term on the right hand side of Eq. (4-58) represents the particle effect on the gas, which is given as the sum of all hydrodynamic forces on the particles in a computational cell, namely $f_i = -1/\left(V_c\left(1-\phi_s\right)\right)\sum_{s=1}^{N_c} f_i^p$. Here, V_c represents the volume of a computational cell, N_c is the number of particles in the cell, and $f_i^p = \frac{\pi\sigma^2}{8}C_D'\rho_g\frac{\left|u_i - V_i^p\right|}{\sigma}\left(u_i - V_i^p\right)\left(1-\phi_s\right)^2$ is the hydrodynamic force on the pth particle in the computational cell.

The governing equations of the gas phase are solved using LES technique. The filtered equations are similar to Eqs. (4-58, 4-59) with the difference that on the left-hand side of Eq. (4-59) the gradient of the subgrid scale stress tensor must be included given by $\tau_{ij,j}$ with $\tau_{ij} = \overline{\left(1-\phi_s\right)u_iu_j} - \overline{\left(1-\phi_s\right)u_i}\,\overline{\left(1-\phi_s\right)u_j}\Big/\overline{\left(1-\phi_s\right)}$. In order to achieve closure of the LES equations of the gas phase the subgrid-model is presented here. Note that an over bar represents a spatial filter.

By applying the Gaussian filter Eq. (4-45) with filter width $\Delta_i\,(i = x, y, z)$ (taken equal to the grid spacing) to equations (55, 56), the filtered equations are obtained given as

$$\left(\overline{(1-\phi_s)u_i}\right)_{,i} - \bar{\phi}_{s,t} = 0, \tag{4-60}$$

$$\left(\overline{(1-\phi_s)u_i}\right)_{,t} + \left(\overline{(1-\phi_s)u_i u_j}\right)_{,j} = -\frac{\left(\overline{(1-\phi_s)p}\right)_{,i}}{\rho_g} + \left(\overline{(1-\phi_s)\sigma_{ij}}\right)_{,j} - \overline{(1-\phi_s)} g\delta_{iz} + \frac{\overline{f_i}}{\rho_g}. \tag{4-61}$$

where an over bar represents the spatial filter. Note that any quantity such as u_i in the flow domain can be decomposed as $u_i = \bar{u}_i + u_i'$, where u_i' is the subgrid-scale part that accounts for the scales not resolved by the computational grid. As an alternative to this approach discussed in the preceding section, a sort of Favre filter can be defined as

$$\tilde{u}_i = \frac{\overline{(1-\phi_s)u_i}}{\overline{(1-\phi_s)}}. \tag{4-62}$$

This gives rise to the alternative decomposition $u_i = \tilde{u}_i + u_i''$, where u_i'' represents the subgrid-scale part of u_i based on Favre filtering. The Favre filtered governing equations are given as

$$\left(\overline{(1-\phi_s)}\tilde{u}_i\right)_{,i} - \bar{\phi}_{s,t} = 0, \tag{4-63}$$

$$\left(\overline{(1-\phi_s)}\tilde{u}_i\right)_{,t} + \left(\overline{(1-\phi_s)}\tilde{u}_i\tilde{u}_j\right)_{,j} = -\frac{\left(\overline{(1-\phi_s)}\tilde{p}\right)_{,i}}{\rho_g} + \left(\overline{(1-\phi_s)}\tilde{\sigma}_{ij}\right)_{,j} + \tau_{ij,j} - \overline{(1-\phi_s)} g\delta_{iz} + \frac{\overline{f_i}}{\rho_g}. \tag{4-64}$$

In Eq. (4-64), the molecular stress tensor, and the subgrid scale stress tensor are given as

$$\sigma_{ij} = -\frac{2}{3}\nu_g u_{p,p}\delta_{ij} + \nu_g\left(u_{i,j} + u_{j,i}\right) \tag{4-65}$$

$$\tau_{ij} = \overline{(1-\phi_s)}\left(\widetilde{\tilde{u}_i\tilde{u}_j} - \tilde{u}_i\tilde{u}_j + \widetilde{u_i''\tilde{u}_j} + \widetilde{\tilde{u}_i u_j''} + \widetilde{u_i''u_j''}\right). \tag{4-66}$$

As a tentative first attempt at closure, the LES equations Eqs. (4-63) and (4-64) may be closed with a subgrid-scale model for, τ_{ij}, given as (Speziale et al.,1998)

$$\begin{aligned}\tau_{ij} = {} & \overline{(1-\phi_s)}\left(\widetilde{\tilde{u}_i\tilde{u}_j} - \tilde{\tilde{u}}_i\tilde{\tilde{u}}_j\right) + 2C_1\overline{(1-\phi_s)}\Delta_i^2\left(\tilde{S}_{mn}\tilde{S}_{mn}\right)^{\frac{1}{2}}\left(\tilde{S}_{ij} - \frac{1}{3}\tilde{S}_{pp}\delta_{ij}\right) \\ & -\frac{2}{3}C_2\overline{(1-\phi_s)}\,\Delta_i^2\left(\tilde{S}_{mn}\tilde{S}_{mn}\right)^{\frac{1}{2}}\delta_{ij},\end{aligned} \tag{4-67}$$

where C_1 and C_2 are dimensionless constant whose values may be determined by correlating the results of analysis such as that detailed in Sec.4-2-2-1-2. However, a highly resolved flow field is required to estimate the aforementioned constant accurately. Note that Speziale et al. (1998) fund that the values of constants C_1 and C_2 for compressible turbulence are 0.012 and 0.0066, respectively.

Note that subgrid-scale model Eq. (4-67) was originally proposed for compressible turbulent flow. In the present study, the model Eq. (4-67) is tested to clarify its relevance for dense gas-particles flows in vibro-ganular medium device for which the fluctuating fields may not be small compared with those of the mean fields.

4-2-3-2. Simulation Procedure

By performing the simulations based on the model discussed in the preceding section, an increased understanding of the dynamics of dense gas-particle flows may be obtained in a vibro-ganular medium device.

The molecular dynamic type simulation is performed to calculate the motion of particles in the gas. The contact force as described in the preceding section is used to capture the major features of grain interactions. A particle dynamic model is employed to account for particle contacts of finite duration, in which the viscoelastic behavior of the particles is represented using a nonlinear Hertzian type model presented in the preceding section. Note that the use of nonlinear viscoelastic model is essential for capturing granular structure formation in the vibro-ganular medium device. The flow is driven by the oscillatory movements of the base wall in the vertical direction given as $z = A\sin\left(k_v x\right)\sin\left(l_v y\right)\cos\left(\omega_v t\right)$. Equation (4-56) is integrated using 4th and 5th order embedded formulas from Dormand and Prince (1980),

with $\Delta t = 10^{-7}\ s$. Note that the calculation of drag force acting on a particle requires knowledge of the local averaged values of the fluid velocity components at the position of the particle in Lagrangian grid. Due to the numerical solution method detailed below these variables are only known at discrete nodes in the domain. Hence, a mass weighted averaging technique (Zamankhan, 1995) has to be employed for calculating the averaged quantities in Lagrangian grid. Here, modeling the flow passing the moving particles does not require any dynamic interfaces treatment discussed in Sec. 4-2-2. The solution of the gas field requires the computational domain as depicted in Fig. 4-31 to be divided into cells. The calculation of the gas is based on the numerical solution of the set of partial differential equations (4-58, 4-59) and (4-67). The flow is resolved using 4×10^4 tetrahedral cells, non-uniformly distributed in the grid where only one-seventh of the computational cells are used between the free surface and the base wall of the device. Note that the mesh-spacing of this grid is larger than the particle diameter. The solution of Eqs. (4-58, 4-59) requires specification of the solids fraction at the appropriate grid nodes. The value of solids fraction is obtained from molecular dynamic simulations by counting the volume of particles within each computational cell divided by the volume of the cell. The governing equations are fully solved with a second-order finite volume method on a staggered grid. The central differencing scheme is used for spatial discretization and the time is advanced via a second-order implicit scheme. The time step for the gas phase equals $7\times10^{-6}\ s$. The linear interpolation routines are used to communicate the information from grid-nodes to particle positions and vice-versa.

Note that the required CPU time for simulation may be decreased by artificially increasing the duration of a contact between the particles as suggested by Silbert et al. (2001). However, the disadvantage of their approach is that the softer normal interactions between the particles have to be assumed.

4-2-3-3. Results of Molecular Dynamics Simulations

Deformation and flow of granular assembly in the surrounding gas in the system as illustrated in Fig. 4-23 is investigated using the models described in Sec. 4-2-3-1. To maintain motion in glass balls, which interact with each other through energy-dissipating contact force and interact with gas via drag forces, the energy is supplied via sinusoidal oscillation of the base wall in the vertical direction whose instantaneous configuration is illustrated Fig. 4-31 (c).

In this study, an important parameter is $\Gamma = A_{eff}\omega_v^2 / g$ that measures the acceleration of base relative to gravity. Here, A_{eff} the effective amplitude of the vibrating base is defined as $A_{eff} = A\iint_S \left|\sin(kx)\sin(ly)\right| dxdy \Big/ \iint_s dxdy$, S represents the surface of the pentagon as depicted in Fig. 4-31 b, and A is a constant. As Γ exceeds a critical value Γ_c, the free surface of glass balls in the device becomes unstable. When Γ increases well above Γ_c for N (dimensionless height of layer of glass balls) of 30 additional instability, which appears to be subharmonic bifurcation type, occurs as illustrated in Fig. 4-32.
The structures, as illustrated in Fig. 4-32 (a), are somewhat small with the typical diameter of 8 particles and height of 20 particles. Figure 4-32 (a) and (b) represent two instantaneous realizations of the structures separated by $1/10f$, where f is oscillation frequency of the base. The particles are color-coded using the values of their granular temperature, T, where red represents the highest value whereas blue shows the lowest values. To obtain the particle granular temperature, the time averaged velocity of particles, $\overline{V}_i^p$, is calculated within a sampling volume using a large number of realizations whose sample is shown in Fig. 4-32 (a). Then the granular temperature is calculated using an expression given by $T = \left(V_i^p - \overline{V}_i^p\right)\left(V_i^p - \overline{V}_i^p\right)$.
Note that because the structures are subharmoic, peaks and depressions can coexist in a configuration as illustrated in Fig. 4-32 (a).

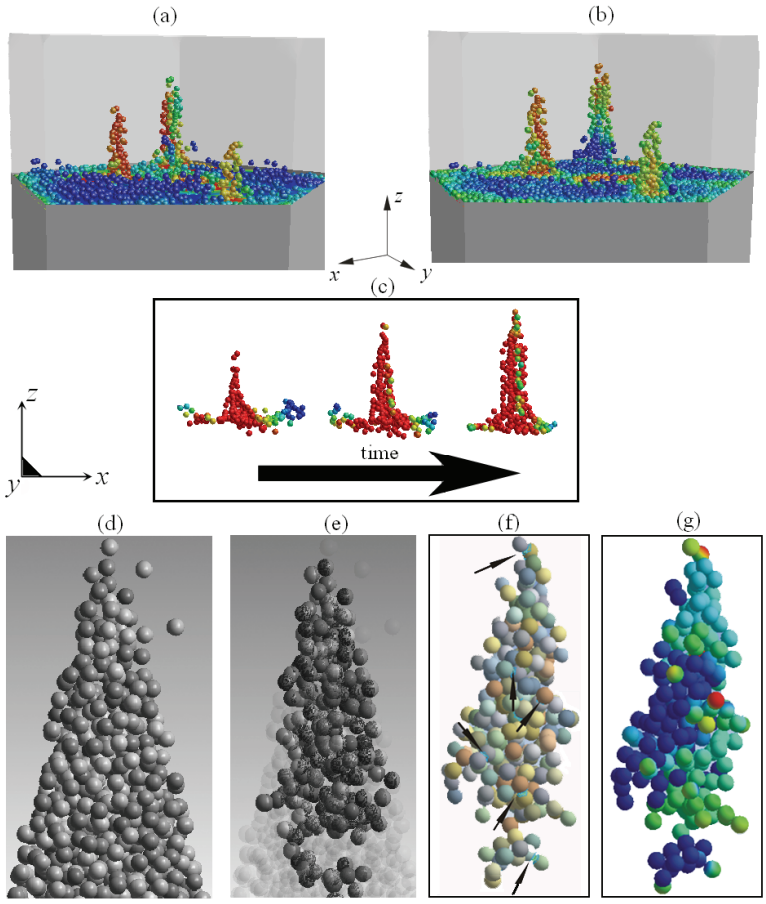

Fig. 4-32: *(a-b) Observed oscillon structure that has been formed in the molecular dynamics simulation of the system; shown at two different times. The particles have been colored by local granular temperature. The next oscillon will form in the central region of part (b) (red hole) that has a high granular temperature. (c) Changing an oscillon structure shape during the time (d) represents a snapshot of a single structure. (e) The chains within an oscillon like structure are highlighted. (f) Some of the most recent contacts occurred between the chains and single particles in the structure are marked by arrows. (g) Represents the deformations in the oscillon type structure caused by the contacts marked in (f).*

Figure 4-32 (c) represents the time evolution of a single structure. As it can be seen from Fig. 4-32 (a-c), steep gradients of granular temperature are present in the system implying the existence of solid-like and liquid-like qualities side-by-side.

The structures as shown in Fig. 4-32 form with equal probability at all locations and are very stable. Figure 4-32 (d) represents a snapshot of a single structure which is very similar to oscillons observed by Umbanhowar et al. (1996). In Fig. 4-32 (e) the chains within an oscillon like structure are highlighted. As it can be seen from Fig. 4-32 (e), the oscillon like structure is a well connected, stable, network of long chains. In Fig. 4-32 (f) some of the most recent contacts occurred between the chains and single particles in the structure are marked by arrows. Figure 4-32 (g) represents the deformations in the oscillon type structure caused by the contacts marked in (f). It appears that dissipation at the scale of large chains, which are highly dissipative, keeps the structure localized. This observation highlights the importance of using an accurate scheme such as that detailed in Sec.4-2-3-1 for treatment of visco-elastic collisions between particles.

An important question remains concerning the role played by the surrounding gas. Figure 4-33 (a) shows a configuration of the glass balls in the device. The oscillon-like structure drifts around leading to a convective motion as illustrated in Fig. 4-33 (b) in the gas phase, since the gas does not slip freely at the

surface of the balls. Consequently, a corresponding profile of particle velocity may be induced by the drag forces exerted by the gas on the particles. As a result of gas-particle interactions, particles in adjacent layer of the gas (which move slower) collide with the chains located in the core of osillon-like structure generating a random component of particle velocity characterized by a granular temperature as illustrated in Fig. 4-32 (a-c).

An obvious question is what would be the role of the surrounding gas deep inside the device. Figure 4-33 (a) shows two regions marked using arrows where small bubbles appear to be formed. To obtain a better visualization, the wall regions are magnified in Fig.4-33 (c) and the vector plot of gas velocity filed is depicted in Fig.4-33 (d). Note that the overall flow is far more complicated than that illustrated in Fig. 4-33 (d) with many intermediate and small-scale components.

Recall that the results presented in Sec.4-2-2-1-2 suggest that the gas forced from beneath during particle-particle collision can be collected into large cavities generated during free-flight of particles. In fact, the effect of quantities such as local gas velocity and pressure is very important in the dynamics of bubble formation. The bubbles created in cavities as illustrated in Fig. 4-33 (c), are observed to be compressed and expanded during each vibro-device cycle. However, the mean bubble size appears to grow. Generally speaking, the bubbles near each other tend to coalesce and become one large bubble. However, large bubbles have not been observed in the vibro-granular device with pentagonal prism shaped bucket.

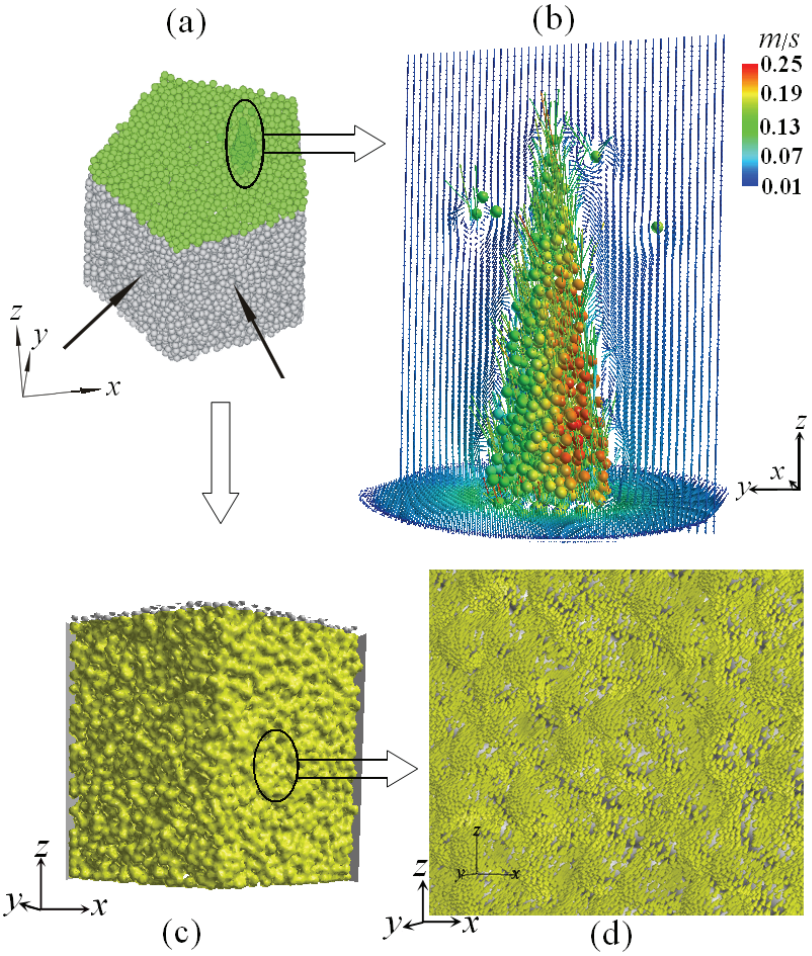

Fig. 4-33: *(a) Shows a configuration of the glass balls in the device. (b) Convective motion in the gas phase around the oscillon structure. (c) An illustration of small bubbles formed in the system. (d) A better visualization of small bubbles introduced by the vector plot of gas velocity filed.*

In Figures (4-34) and (4-35) one oscillon structure has been shown in two period rising up and coming down. The velocity field around this structure has been shown in these two figures.

Due to limitations in the available computational resources no details such as flow dynamics of granular materials in the vibro-granular device with different bucket shapes can be provided using even the

simplified approach described above. In order to simulate such systems in the following section, as an alternative approach, a continuum approach is to be proposed, which appears to retain the essential features that characterize the gas-particles flows in vertically vibrated granular materials.

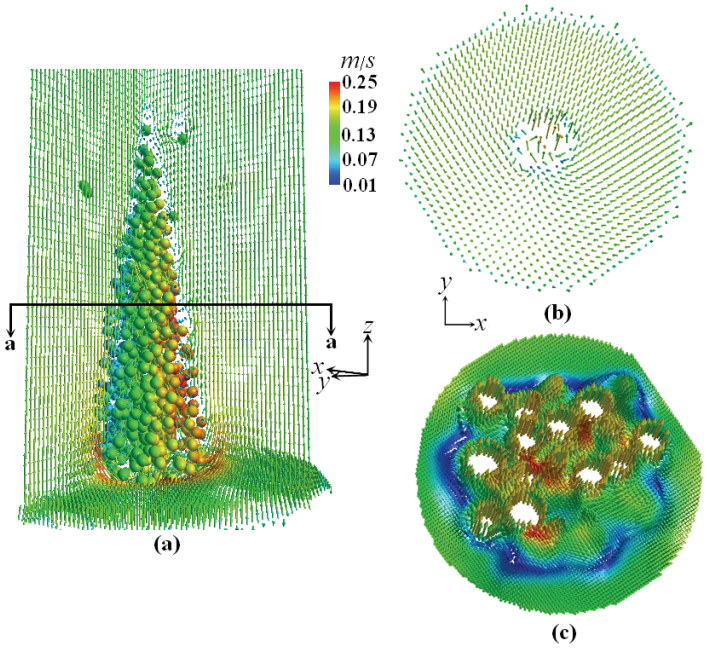

Fig. 4-34: *(a) An oscillon structure has been observed in simulation with a velocity field of gas around it. This picture takes in the rising period of oscillon. (b) Top view of velocity vector of the gas in a cut section (a-a) on oscillon structure shown in part (a). (c) A better visualization of velocity vectors around particles in the oscillon structure in a central region of cut section (a-a) has been defined in part (a).*

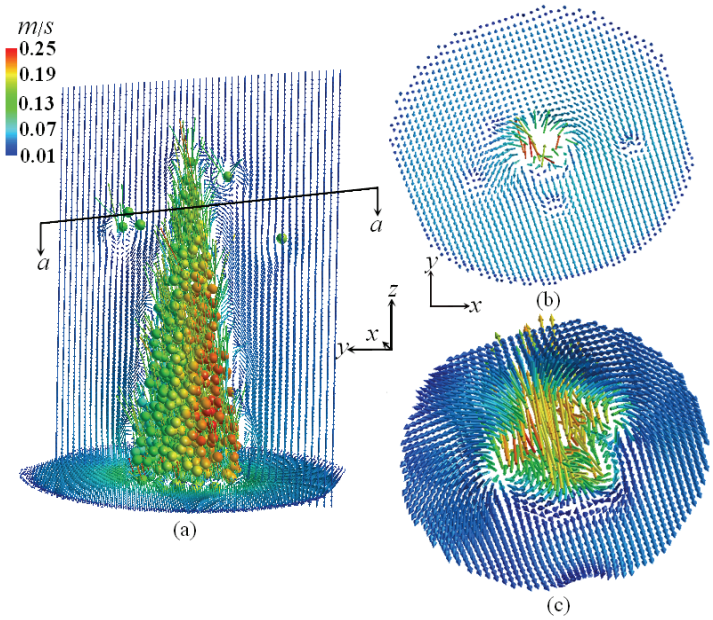

Fig. 4-35: *(a) An oscillon structure has been observed in simulation with a velocity field of gas around it. This picture is taken when the oscillon is coming down. (b) Top view of velocity vector of the gas in a cut section (a-a) on oscillon structure shown in part (a). (c) A better visualization of velocity vectors around particles in the oscillon structure in a central region of cut section (a-a) has been defined in part (a).*

4-3. Continuum Approach in Simulating Vibrated Granular Bucket

As told in the previous section the simplified desecrate model that was explained has some limits in modeling a vibrating granular system. For example, molecular dynamic approach is an expensive method for modeling a complex system and needs a long time for simulating, so we also used continuum approaches to model the buckets that are full of granular material and under the effect of vertical vibration. This method let us model vibrating granular materials in the buckets with different cross area shapes. In the following sections, we first developed more about the different flow regimes that occur in granular materials under

shearing and then after that we will explain the continuum constitutive equations in these regimes. Finally we will present some of our interesting results, which have been taken by using the continuum approach.

4-3-1. Different Regimes on Granular System under Shearing

The concept of Newtonian fluid includes mass and momentum balances and constitutive equations and the combination of these correlations yields the well-known Navier-Stokes equations. There is a similar developed equation for the granular materials moving in the rapid-granular regime. This regime occurs when particle-particle contacts are not very extensive and therefore friction is not prevalent. By using a similarity between the movement of molecules and flow of small elastic (or elasto-plastic) particles and resemble, for certain limiting cases, the fluid flow equations will be resulted.

Slow, frictional (which are usually named Coulomb) flows of grains are different with rapid flow regime because in this state, particles are in contact for longer times and friction is the overwhelming interaction. In this regime the mass and momentum balances govern flow but the form of constitutive equations are different with a rapid flow regime. Schaeffer (1987) combined these general equations to yield a set of differential equations that replace the Navier-Stokes equations. There are many research works in the field of solving these equations for the several different geometry and systems (i.e. (Tardos, 1997) and (Tardos et. al., 1998)).

Figure 4-36 shows a schematic of different regimes in granular flow as a function of the shear rate. The dimensionless shear rate (γ^*) can be defined by the following equation:

$$(\gamma^*) = \gamma \left[d_p / g \right]^{1/2} \quad , \tag{4-68}$$

where d_p and g represent the particle diameter and gravity acceleration.

At the shear rate equal to zero, the particles are in a stationary state and we can using the equations of static equilibrium together with a yield condition calculate stresses in the system. This regime, also includes very slow particle flows when the particles proceed from one static state to the next, this regime is named a "quasi-static regime". The yield condition defines the point where the particles start to deform (flow), so as shown in Fig. 4-28, at low γ^*, of the order of 0.2 or lower, the so-called "slow, frictional regime" can be identified.

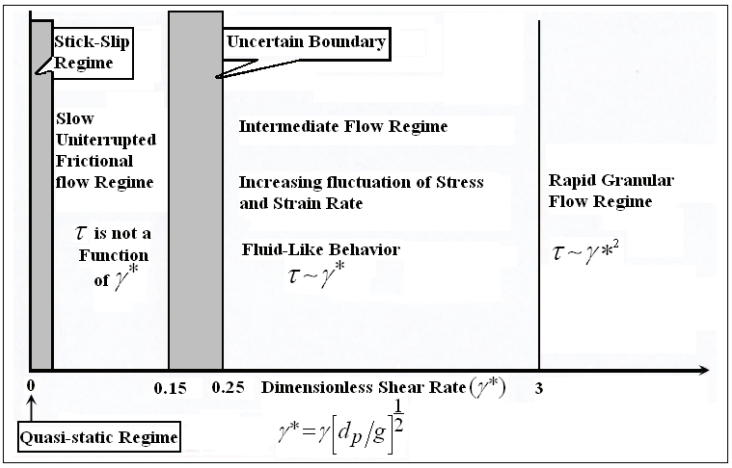

Fig. 4-36: *Schematic representation of different flow regimes in granular material under the effect of shearing.*

In this regime frictional forces between particles have the main role in the system and so they are predominant. The main things that can be said about these regimes are the uninterrupted character of the flow, the existence of a continuous shear field and the fact that the shear stress is independent of the shear rate to within experimental error (Tardos et.al, 1998). A narrow range of very low shear rates in which the flow exhibits a stick-slip character separates the frictional and the quasi-static regimes. The large vacillations in stresses are the main characteristics of this regime.

The rapid granular flow regime can be recognized at the other end of the spectrum, in fact this regime occurs in very high shear rates (i.e. $\gamma^* > 3$). In this regime particles are moving so fast that friction between them can be neglected and the character of the flow has been determined by only short collisions between the particles. This regime has been studied extensively and many theoretical and experimental results are available (i.e. (Campbell, 1990; Dufty, 2000, Dufty and Brey, 1999; Tan and Goldhirsch, 1998)). One other

regime can be recognized between the "slow" and the "rapid" flow regimes, which is named the "intermediate" regime and in this regime both the collisional and frictional interactions between particles must be considered.

4-3-1-1. Rate-Independent Quasi-Static Regime

At very high concentrations and low rate-of-strain, collisions cannot be seen as instantaneous anymore, since grains suffer longer and permanent contacts in rubbing and rolling on each other. Therefore, a kinetic stress model based on the Boltzmann equation is irrelevant and a frictional stress model must be taken into account. This can be done using plasticity and similar theories in which the material behavior is assumed to be independent of the velocity gradient or the rate-of-strain. Needless to say, this is atypical for a viscous Newtonian flow where stress specifically depends on rate-of-strain and, again, this shows that a Newtonian rheology cannot be chosen for granular flow whatever the concentration. Under a normal stress, a well-compacted granular material will shear only when the shear stress attains a critical magnitude. This is described by a Mohr-Coulomb law based on the laws of sliding friction. However, the Mohr-Coulomb law says nothing about how the granular material deforms and flows, rather it describes the onset of yielding. The Plastic Potential theory will provide the required constitutive equations for describing the deformation of a granular material under frictional motion. According to this theory, the concept of critical state plays a key role. However, a critical state described by a simple Mohr-Coulomb theory leads to physical inaccuracies (such an infinite dilatancy of the granular material). Actually, the Mohr-Coulomb law should only be seen as an asymptotical solution after the granular material has endured long and permanent plastic-frictional deformation. The Plastic Potential theory allied with the critical state approach can successfully describe the phenomenon of dilatancy, consolidation, the independence between the rate-of-strain-tensor and the stress tensor.

Granular materials are neither solid nor liquid as commonly understood. Under certain conditions, a granular material can behave like a solid. How-ever, when the stress state satisfies the yield condition, the so-called quasi-static flow occurs and the material yields along stress characteristics and flows as blocks, each consisting of many granules, moving relative to one another along thin slip lines. In quasi-static flows of granular materials, there often exist stress and velocity discontinuities in the material.

The double-shearing flow theory is based on the Mohr-Coulomb yield condition. If the stress state in a granular material reaches the yield condition, flow occurs by shearing along two families of planes, namely the $\alpha-$ and $\beta-$ characteristics. These two planes are inclined at angles $\pm\varepsilon$ $(\varepsilon=\pi/4+\phi/2)$ to the direction of the principal stress σ_1 where ϕ is the angle of material internal friction, as shown in Figure 4-29. The double shearing theory assumes that the complete deformation at any point of the material consists of two shearing motions occurring simultaneously on the $\alpha-$ and $\beta-$ lines and which are superposed one on another.

More specifically, in the rectangular Cartesian coordinate systems as shown in Fig.4-37, the double-shearing assumption can be formulated by

$$\frac{\partial \mathrm{v}}{\partial s_\alpha}=ae_\beta,\quad \frac{\partial \mathrm{v}}{\partial s_\beta}=be_\alpha, \tag{4-69}$$

where the first set of coordinate system O_{xy} is fixed in space while the second set $O_{\varepsilon\eta}$ is fixed on the particle and is in motion relative to the first set with rotating speed Ω and translational velocity $(\mathrm{v}_x,\mathrm{v}_y)$, s_α and s_β are measured along the slip-line, e_α and e_β denote unit vectors along the direction of α and β respectively.

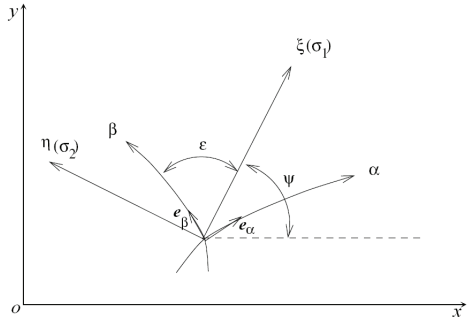

Fig. 4-37: *Coordinate System, $\alpha-,\beta-$ lines.*

Consider the plane flow in a rectangular Cartesian coordinate system with the x-axis being vertical upward. The equations of motion for the quasi-static flow are

$$\frac{\partial \sigma_{xx}}{\partial x}+\frac{\partial \sigma_{xy}}{\partial x}-\rho g=0,\quad \frac{\partial \sigma_{xy}}{\partial x}+\frac{\partial \sigma_{yy}}{\partial x}=0 \tag{4-70}$$

If σ_1 and σ_2 represent the maximum and minimum principal stress components namely ($\sigma_1 \geq \sigma_z \geq \sigma_2$) and if we assume that the direction of σ_1 makes an angle of ψ with the x-axis, then we have:

$$\sigma_{xx} = -p + q\cos 2\psi, \quad \sigma_{yy} = -p - q\cos 2\psi, \quad \sigma_{xy} = q\sin 2\psi, \tag{4-71}$$

We can write following relation for p and q:

$$p = -\frac{\sigma_1 + \sigma_2}{2}, \quad q = \frac{\sigma_1 - \sigma_2}{2}, \tag{4-72}$$

Suppose that the material is cohesionless and obeys the Coulomb yield criterion. Then, the stress state satisfies:

$$q = p\sin\phi \tag{4-73}$$

where ϕ is a material parameter, namely the angle of internal friction. On substituting equations (4-71) into equations (4-70), we can deduce in the usual way the stress equations in terms of the arc lengths s_α and s_β along the α and β characteristics defined respectively by:

$$\frac{dy}{dx} = \tan(\psi - \varepsilon) \quad -\alpha\text{line} \tag{4-74}$$

$$\frac{dy}{dx} = \tan(\psi + \varepsilon) \quad -\beta\text{line} \tag{4-75}$$

So we can rewrite (4-69) as follow:

$$\frac{\partial p}{\partial s_\alpha} + 2p\tan\phi\frac{\partial \psi}{\partial s_\alpha} = -\frac{\rho g}{\cos\phi}\sin(\psi + \varepsilon) \tag{4-76}$$

$$\frac{\partial p}{\partial s_\beta} - 2p\tan\phi\frac{\partial \psi}{\partial s_\beta} = \frac{\rho g}{\cos\phi}\sin(\psi - \varepsilon) \tag{4-77}$$

By using these later two equations with Eq. (4-74) and (4-75), we have a system of four equations for the determination of the characteristic field and the p and ψ values along the characteristic lines.

In order to calculate the velocity field corresponding to the stress field, we adopt the so-called double shearing assumption as formulated in Eq. (4-69). The velocity equations based on this assumption have been shown to be

$$\frac{\partial u}{\partial x} + \frac{\partial v}{\partial y} = 0 \tag{4-78}$$

$$(\frac{\partial u}{\partial x} - \frac{\partial v}{\partial y})\sin 2\psi - (\frac{\partial v}{\partial x} + \frac{\partial u}{\partial y})\cos 2\psi = \sin\phi(\frac{\partial u}{\partial y} - \frac{\partial v}{\partial x} + 2u\frac{\partial \psi}{\partial x} + 2v\frac{\partial \psi}{\partial y}) \tag{4-79}$$

4-3-1-2. Transition Regime

Equations to characterize this regime were first proposed by Savage (1983). The idea behind the new approach is to assume that the strain rate in this regime fluctuates around an average value and that the fluctuations are distributed according to a Gaussian distribution with a standard deviation of strain rate. He showed in high granular temperature limit, the averaged equations yield solutions that smoothly merge with those of rapid granular flow solutions while the granular flow also exhibits liquid-like behavior in the sense that a viscosity can be calculated. The flow dynamics is strongly affected by gravitational and centrifugal forces fall into an intermediate regime between two limiting flow regimes (fully dynamic rapid flow and quasi-static, rate-independent plastic regimes) where both collisional and frictional interaction between particles should be taken into account. In fact, the total stresses are as the linear sum of the rate-independent, dry friction part plus a rate-dependent viscous part obtained from the high shear rate granular flow kinetic theories. The magnitude of the rate-independent contribution was chosen such that the sum of the two parts satisfied the overall momentum equation perpendicular to the flow direction. When the concentration is high and the deformation rate are low as in quasi-static or transitional regimes, the particle typically experience multiple contacts that are long lasting rather than identifiable, short term, collision. At higher shear rates

fluctuations exist in stress due to fluctuations in the strain rate which may be even larger the mean strain rates. Therefore the effect of viscosity associated with the pseudo-thermal motion of grain can not be neglected. This likely the case in the granular flow in a spinning bucket at high frequencies (Walker, 1966) in which the grains in the center of bucket is pulled down by gravitational force and pushed out and up along the sidewalls by centrifugal forces to maintain a weak convective In fact, the average velocity field suggest the presence of local convective motion in the spinning bucket.

4-3-1-3. Rapid Flow Regime

The mechanical behavior of flowing granular material results from force exerted at the many points of contact between different particles. These contact points are not permanent, but are continually forming and breaking as the assembly of particles moves.

Unless the particle surface is perfectly smooth the forces have both tangential and normal components, and the surface of contact may, or may not, be slipping into each other. When the assembly of particles is widely spaced and in vigorous motion, individual contacts are of short duration and may be treated as 'collision', analogous in many ways to the encounters between molecules in a liquid or gas (Umbanhowar, 2003). The kinetic energy associated with the relative motion of macroscopic particles; called granular temperature by physicists, plays a central role in this regime and is not constant. When it increases in viscosity it also increases in gas. Instead, it is continually and irrevocably transferred by collisions to internal (thermal or non-kinetic) degree of freedom (Savage, 1998). The individual grains which randomly fluctuate and translate has some energy dissipation in which it should be small in some sense for the analysis of kinetic theory, it is usually based on a hard sphere model, to be valid (Walton and Braun,1986). The particles posses a well-define thermodynamic temperature which the associated thermal energy (equal to the product $k_B T$ where k_B *is* Boltzmann's constant and T is the temperature in Kelvin) is too small to allow relative particle motion, as it does in ordinary liquids. We might at first be temped to view any granular flow as that of a dense gas since gases, too, consist of discrete particles with negligible cohesive forces between them. In contrast to ordinary gases, however, the energy scale is the potential energy mgd of a grain of mass m raised by its own diameter d in the Earth's gravity g. For typical sand, this energy is at least 10^{12} times $k_B T$ at room temperature. Because the $k_B T$ is irrelevant, ordinary thermodynamic argument become useless. So, dynamic collections of grains require a continuous external source of energy to prevent them from getting struck in a particular configuration. However, numerous comparison (Walton and Braun, 1986; Lun and Bent, 1994; Savage, 1992; Lan and Rosato, 1995; Savage, 1983; Ma and Ahmadi,1998) of the kinetic theory results with experimental measurements and granular dynamic computer simulations (which are free of the questionable assumptions made in kinetic theories) have shown quite good agreement for cases when dissipation is relatively small and the particle concentration range from small to moderate.

4-3-2. Continuum Approach Analysis in Gas-Particle System

In most of the granular flow examples, the flow dynamics fall into an intermediate regime where both collisional and frictional interactions between particles should be taken into account. In addition in some examples (such as granular materials under vertical vibration) gas trapped in the granular material was found to be a major source of heaping (Pak and Behringer, 1994).

Computational experiments as detailed in the preceding section may lead to scale-dependent closures for quantities such as the drag, stresses and effective dispersion. These quantities represent important frontiers in this class of problems.

However, the most practical approach to simulating the flow dynamics of the aforementioned systems is to treat the gas and particle phases as interpenetrating continua. Here, the aim is to extend the previous approach (Zamankhan et al., 1997) to more general types of flow regimes by which in-depth analysis can be handled of complex gas and particle flows.

Consideration is given to a granular material consisting of a binary mixture of differently colored, monosized, spherical particles as illustrated in Fig.4-38. For this system, light and dark colors are represented by subscripts l and d, respectively. Recall that the balance of mass of particles of kind l in a curvilinear coordinates system may be given as (Zamankhan et al., 1997):

$$\frac{\partial \rho^l}{\partial t}+V_i\frac{\partial \rho^l}{\partial x_i}+\rho^l\frac{\partial V_i}{\partial x_i}+\frac{\partial}{\partial x_i}\left(\rho^l u_i^l\right)=0. \tag{4-80}$$

where ρ^l is the apparent density of particles of kind l, defined as $\rho_s\left\langle\phi_s^l\right\rangle$, ρ_s represents the particle material density, $\left\langle\phi_s^l\right\rangle$ is the average solids fraction of particles of kind l, x_i represent curvilinear coordinates, V_i is slowly varying mean velocity and u_i^l is a rapidly fluctuating velocity of particles of kind l.

In Eq. (4-80), subscript *i* is a free index for which the summation convention is applied.

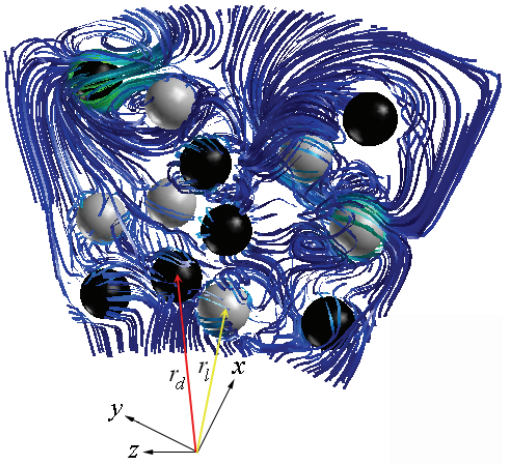

Fig. 4-38: *Schematic of a granular bed under shear composed of a binary mixture of differently colored, monosized, spherical particles.*

4-3-2-1. Constitutive Equations in Rate-Independent Quasi-Static Regime

The third term on the left hand side of Eq. (4-80) includes the divergence of the velocity field which is known as the phase space compressibility of the granular assembly. This term does not vanish for the vibrating packed grains as illustrated in Fig. 4-31 where the grains must first dilate if they are to deform. Here, the aim is to develop an approximate theory by which both dilatancy and contractancy of the granular material, as illustrated in Fig. 4-31, can be predicted. To this end, following Savage (1998), an attempt is made to obtain a representation of the behavior for slow flow dynamics of granular assembly at high solid fractions (as depicted in Fig. 4-31) that can be merged with the kinetic theory results at moderately high shear rates for an assembly as illustrated in Fig. 4-30. In light of the above, it is useful to define a yield function, *Y*, as follows

$$Y\equiv\frac{\sigma_1^2+\sigma_2^2+\sigma_3^2-\sigma_1\sigma_2-\sigma_2\sigma_3-\sigma_3\sigma_1}{3}+\sin^2\theta_f\left[\left(\frac{\sigma_1+\sigma_2+\sigma_3}{3}+P\right)^2-P^2\right]=0. \tag{4-81}$$

Where θ_f corresponds to the value of the angle of internal friction, σ_i, $i=1,2,3$ are principal stresses (which are the eigenvalues of the stress tensor $\mathbf{P}_{ij}$), and $P\left(\phi_s,T\right)$ is the pressure at solids fraction ϕ_s and granular temperature T.

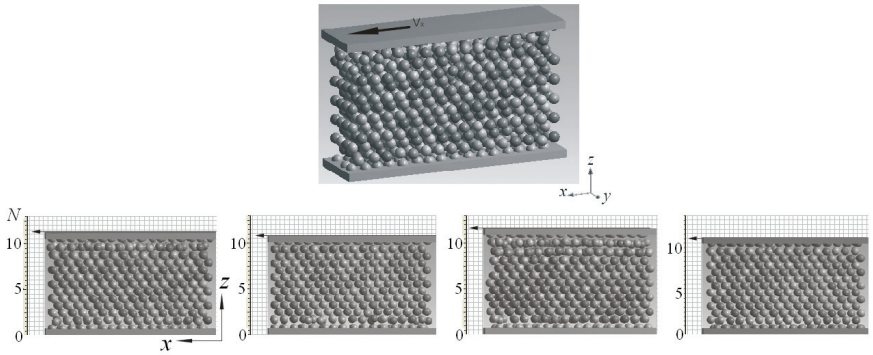

Fig. 4-39: *A layer of granular material under shearing.*

Using the Finite Element approach as described in an earlier article (Zamankhan, 2005), the pressure distribution can be conveniently predicted for the assembly, as depicted in Fig. 4-39. As illustrated in Fig. 4-39(a), the stress chains developed in the assembly due to the gravitational acceleration can clearly be observed.

Note that the yield surface as described in Eq. 4-81 is convex and whose size grows with increasing ϕ_s, and T. Using the principle of coaxially, the rate of strains defined as $\varepsilon_{ij} = \frac{1}{2}\left(\partial V_i/\partial x_j + \partial V_j/\partial x_i\right)$, may be derived from a plastic potential function. In the simplest case when the yield and plastic potential functions are identical, the rate of strains may be given by

$$\varepsilon_{ij} = \lambda \frac{\partial Y}{\partial \sigma_{ij}}. \tag{4-82}$$

Where λ is a scalar . Equation 4-82 states that the plastic strain increment of the granular assembly is in the direction of the outward normal to the yield surface.

By solving Eq. 4-81 for stress components in terms of the rate of strains and then substituting the results in the yield function, relations between stress and rate of strain tensors may be found as

$$\sigma_{ij} = \frac{P}{\left[\left(\frac{4}{3}\sin^2\theta_f + 1\right)\mathrm{I}_1^2 - 4\sin^2\theta_f \mathrm{I}_2\right]^{\frac{1}{2}}} \times \left[2\sin^2\theta_f \varepsilon_{ij} + \left(1 - \frac{2}{3}\sin^2\theta_f\right)\varepsilon_{kk}\delta_{ij}\right] - P\delta_{ij}, \tag{4-83}$$

where I_1 and I_2 are the first and second invariants of rate of strain tensor, respectively. Equation 4-83 represents the stress tensor for a rate-independent, plastic behavior of the granular assembly.

Making use of the expressions for rate of strains, the divergence of the velocity may be expressed as

$$\frac{\partial V_i}{\partial x_i} = -\frac{\left[\left(\frac{4}{3}\sin^2\theta_f + 1\right)\mathrm{I}_1^2 - 4\sin^2\theta_f \mathrm{I}_2\right]^{\frac{1}{2}}}{P}\left(\frac{1}{3}\sigma_{ii} + P\right), \tag{4-84}$$

where $\frac{1}{3}\sigma_{ii}$ represents the average normal stress.

Using expression 4-84 it is convenient to realize that in dilatancy of granular assembly a decrease of solids fraction, ϕ_s, occurs during deformation characterized by a positive divergence of the velocity. On the other hand, for the contractancy of granular assembly an increase of solids fraction, ϕ_s, during deformation would be expected. At the critical state where $\frac{1}{3}\sigma_{ii} = -P$, a deformation without change in specific volume can be predicted.

4-3-2-2.Constitutive Equations in Transitional Regime

Equation 4-80 is somewhat more generalized than that used by Savage (1998). The particle diffusive motion, which can be observed even at high solids fraction (Hsiau and Hunt, 1993; Polashenski et al., 2002), is accounted for in Eq. (4-80). If color of particles is ignored, Eq. (4-80) becomes similar to that used by Dasgupta et al. (1994), in which the particle diffusive motion was regarded as correlated fluctuations in solids fraction and solids velocity. In this case, the time-smoothing of volume-averaged continuity equation for the gas phase may be given by (Dasgupta et al., 1994),

$$\frac{\partial\left\langle\phi_g\right\rangle}{\partial t} + U_i\frac{\partial\left\langle\phi_g\right\rangle}{\partial x_i} + \left\langle\phi_g\right\rangle\frac{\partial U_i}{\partial x_i} + \frac{\partial}{\partial x_i}\left(\left\langle\phi_g' U_g'\right\rangle\right) = 0., \tag{4-85}$$

where $\left\langle\phi_g\right\rangle$ and U_i represent the averaged values of volume fraction and velocity of the gas phase for which $\phi_g = 1 - \phi_s$. The primes designate the fluctuation parts about the averaged values. As illustrated in Fig. (4-

40), the particles displace the gas during their diffusive motion, it may be assumed that $\rho_g \left\langle \phi'_g U'_g \right\rangle$ balances the net diffusive drift of particles.

Polashenski et al. (2002) show that the net diffusive drift of particles in a collision dominated regime in which fluctuations are driven by the collective motion of the particle assembly may be expressed as

$$\rho u_i = \rho D_{ij}^T \frac{\partial \ln T}{\partial x_j} + B_{ij} \frac{\partial \rho \Pi}{\partial x_j} + D_{ij} \frac{\partial \rho}{\partial x_j}., \tag{4-86}$$

where ρ is particle apparent density, defined as $\rho_s \left\langle \phi_s \right\rangle$, D_{ij}^T, B_{ij}, and D_{ij} are thermal diffusion, particle mobility and ordinary diffusion tensors, respectively, and Π is a potential whose expression was given by Polashenski et al.(2002). Here, the suffix "l" is dropped assuming that the color label plays no role in particle dynamics.

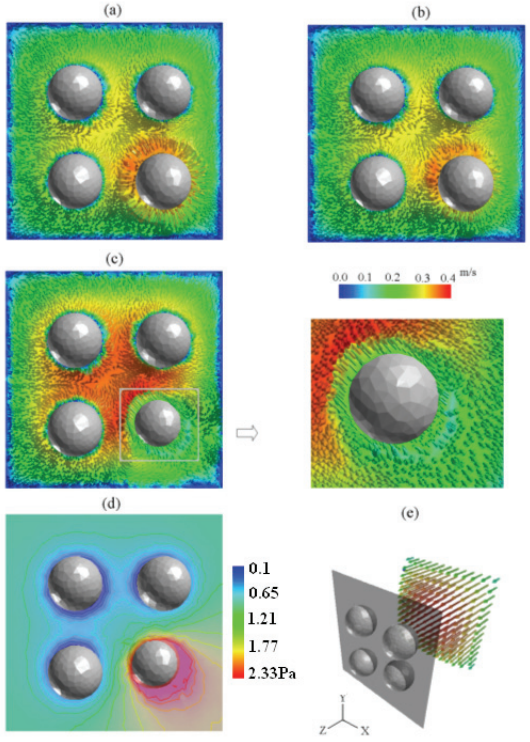

Fig. 4-40: *Velocity contours combined with velocity vectors representing an air flow in the presence of moving spherical particles in a duct of square cross section. The vectors are color-coded to represent the magnitude of velocity. (a-c) Instantaneous realizations of a velocity field in the plane as shown in (e) at three different instances in time separated by* $\delta t \approx 0.005\, sec.$ *Flow field around a moving particle in (c) is magnified in order to visualize the displacements of the surrounding gas by a moving particle. (d) Contour of the pressure field for the configuration in (c). The arrows in (e) represent the upstream, undisturbed duct flow.*

By analyzing a perturbation solution of the Boltzmann equation through the first order in the gradient of solids fraction, Garzo (2002) has derived the elements of D_{ij} for granular shear flows. Note that in the absence of shearing motion diffusion tensor, D_{ij}, may be reduced to $D_0 \delta_{ij}$, where D_0 represents the diffusion coefficient (Savage,1993; Zamankhan et al., 1998) and δ_{ij} is the Kronecker delta.

The significance of the first and the second terms on the right side of Eq. (4-86) far from the solid walls is not quite clear. Moreover, no analytical expressions exist for the diffusion coefficient in dense granular flows for which frictional contact between the particles plays a key role in flow dynamics. In this light, more rigorous theoretical studies are required to further examine the significance of diffusion processes in the systems such as those studied in vertically vibrated granular layers. In this case, as a predictive method the results of previous molecular dynamic type simulations (Polashenski et al., 1998; Zamankhan et al., 1998; Zamankhan et al., 1999) can be used to characterize particle diffusive motion.

4-3-2-3.Viscous-like Behavior

Here, the somewhat standard form of the linear momentum equation is used for the particle phase that in a curvilinear coordinates system is given as (Zamankhan et al., 1997):

$$\rho_s\left(\frac{\partial\left(\phi_s V_i\right)}{\partial t}+\frac{\partial\left(\phi_s V_i V_j\right)}{\partial x_j}\right)=\frac{\partial\sigma_{ij}}{\partial x_j}+F_i+\rho_s\phi_s g_i, \tag{4-87}$$

where σ_{ij} represents the stress tensor for the particle phase. Here, F_i is the total force of the interphase interaction per unit volume, which includes the drag force as well as the buoyancy contribution to the overall hydrodynamic force.

By averaging Eq. (4-87) over the ensemble of the spheres, an equation for balance of momentum may be obtained similar to that of the time-smoothing of volume averaged momentum equation suggested by Dasgupta et al. (1994) that is:

$$\rho_s\left(\frac{\partial\left(\phi_s V_i\right)}{\partial t}+\frac{\partial}{\partial x_j}\left(\phi_s V_i V_j\right)\right)+\left(\frac{\partial\rho u_i}{\partial t}+\frac{\partial}{\partial x_j}\left(\rho u_j V_i+\rho u_i V_j\right)\right)=\frac{\partial\left\langle\sigma_{ij}\right\rangle}{\partial x_j}+\left\langle F_i\right\rangle+\rho_s\phi_s g_i, \tag{4-88}$$

where the third correlation $\left\langle\phi_s' V_i' V_j'\right\rangle$ has been neglected and the fluctuations are assumed to be relatively small as suggested by the molecular dynamics type simulations presented in section 4-2-3.

Note that for very low shear rates where the strain-rate fluctuations are very small, the constitutive behavior of the granular assembly may be predicted by using Eq. 4-83 for $\left\langle\sigma_{ij}^s\right\rangle$, which have a rate-independent form. However, as suggested by Savage (1998), at higher shear rates fluctuations exist in σ_{ij} due to fluctuations in the strain rate ε_{ij} which may be even larger than the mean strain rates $\left\langle\varepsilon_{ij}\right\rangle$. Therefore, it is not permissible to neglect the effect of viscosity associated with the pseudo-thermal motion of grains. By assuming that the strain rate fluctuations are isotropic and they are distributed according to a Gaussian distribution with a standard variation of ε, namely $f\left(\varepsilon_{ij}\right)=1\Big/\varepsilon\left(2\pi\right)^{\frac{1}{2}}e^{-\left(\varepsilon_{ij}-\left\langle\varepsilon_{ij}\right\rangle\right)^2\Big/2\varepsilon^2}$, a stress-strain rate relation can be developed similar to that of a Newtonian viscous fluid. Note that the variance of the strain rate fluctuations, ε^2, characterizes the pseudo-thermal motion of grain. Therefore, it is analogous to the granular temperature *T*, which is a term that measures the energy of the random motion of the grains.

The aim in this section is to provide a concise framework within which the seemingly complex behavior (such as the existence of solid-like and fluid-like qualities side-by-side in the continuous flow of granular material) involving very large strains can be described. To proceed, it may be conjectured that the mean value of stress can be calculated from the fluctuating strain rate by multiplying the Eq. 4-83 for σ_{ij} by $f\left(\varepsilon_{ij}\right)$ and integrating over the strain rate space. It is convenient to evaluate the resulting integral over e_1, e_2, e_3 which represent principal strain rates. That is

$$\left\langle\sigma_i\right\rangle=1\Big/\varepsilon^3\left(2\pi\right)^{\frac{3}{2}}\times\int e^{-\left[\left(\varepsilon_1-\left\langle\varepsilon_1\right\rangle\right)^2+\left(\varepsilon_2-\left\langle\varepsilon_2\right\rangle\right)^2+\left(\varepsilon_3-\left\langle\varepsilon_3\right\rangle\right)^2\right]\Big/2\varepsilon^2}\sigma_i d\varepsilon_1 d\varepsilon_2 d\varepsilon_3, \tag{4-89}$$

where σ_i (i=1,2,3) represent the principal stresses in a three-dimensional system whose expressions are given by

$$\sigma_i=\frac{P}{\left[\left(\frac{4}{3}\sin^2\theta_f+1\right)\mathrm{I}_1^2-4\sin^2\theta_f\mathrm{I}_2\right]^{\frac{1}{2}}}\times\left[2\sin^2\theta_f\varepsilon_i+\left(1-\frac{2}{3}\sin^2\theta_f\right)\mathrm{I}_1\right]-P. \tag{4-90}$$

Following the approach of Savage (1998), which is valid only for a two dimensional case, the right hand side of Eq. 4-89 can be expanded in powers of $\left\langle e_i\right\rangle\Big/\varepsilon$ which is a small parameter when the values of ε are

large compared to the mean strain rates. Transforming to spherical coordinates by introducing $e_1 = \varepsilon r \cos\varphi \sin\theta, e_2 = \varepsilon r \sin\varphi \sin\theta, e_3 = \varepsilon r \cos\theta,$ into Eq. 4-90 and integrating over $0 < r < \infty, 0 < \theta < \pi, 0 < \varphi < 2\pi$ the mean principal stresses as a linear function of the mean principal strain rates may be found as

$$\langle \sigma_i \rangle = 2\mu \langle \varepsilon_i \rangle + (\zeta - \mu)\langle \mathrm{I}_1 \rangle - P, \tag{4-91}$$

where μ and ζ are the coefficients of viscosity, which have the form of $\mu = PA_1/\varepsilon$, $\zeta = PB_1/\varepsilon$. The coefficients A_1 and B_1 as well as the ratio of viscosities, ζ/μ , depend on the angle of repose θ_f whose variations in terms of θ_f are given by Bordbar and Zamankhan (2005a).

Note that the angle repose, θ_f, is that made between the flat surface and the outside of the cone as illustrated in Fig.4-41. Figure 4-41 depicts a spill of particles onto a flat surface collected in a pile. The spill takes on the shape of a flat cone. In Fig. 4-41 numerical results are obtained using the finite element approach detailed by Bordbar and Zamankhan (2005a). The resulting shape of the spill of particles could be affected by the distance between the leak and the flat surface where the leak collects. The roughness of the flat surface upon which the material collects is another important factor that affects the shape of spill. The physical properties of the glass balls are listed in Table 3-1. In order to obtain an angle of repose of $\theta_f \approx 30^\circ$, the sliding coefficient of friction is set to 0.6 in the present simulations. Note that a theory of contact mechanics has been developed recently (Persson, 2001) valid for randomly rough surfaces. This theory can be applied to viscoelastic solids in order to take into account more precisely the adhesive force between glass balls in direct contact.

In a straightforward way the expressions for the mean stress components referred to a curvilinear coordinate systems, x_i, may be given as

$$\langle \sigma_{ij} \rangle = 2\mu \langle \varepsilon_{ij} \rangle + (\zeta - \mu)\langle \varepsilon_{kk} \rangle \delta_{ij} - P\delta_{ij}. \tag{4-92}$$

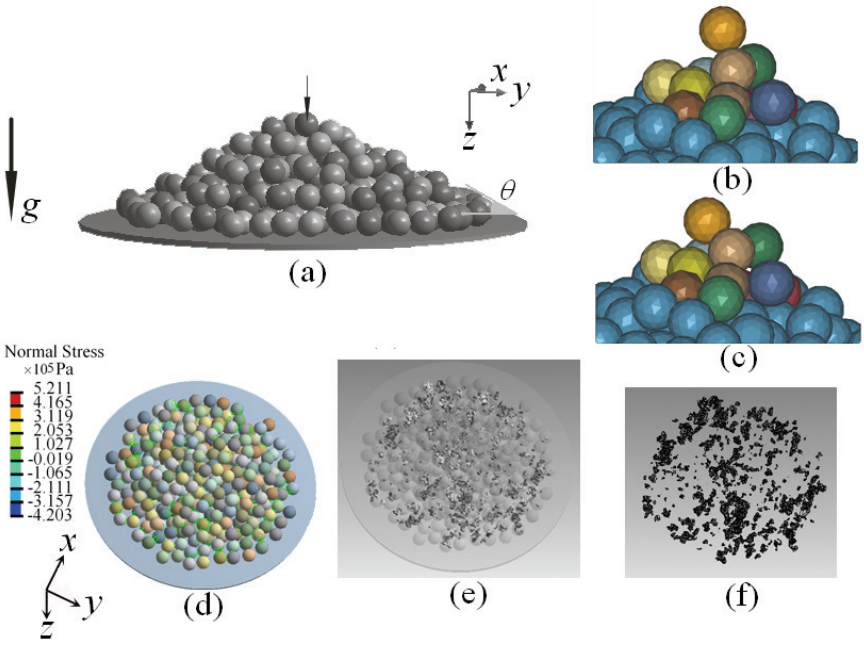

Fig. 4-41: *(a) Illustration of a conical spill using computer simulations. Note that a leak approaches the spill. The angle made between the surface and the outside of the cone is referred to as the angle of*

repose, θ_f. *(b, c) Configuration of the particles in the spill at two different times after the collision. (d-f) Top view of the stress field developed in the spill* $t = 10^{-4}$ sec *after the collision.*

Equation (4-92) resembles a viscous-like character for a liquid granular material in the sense that the viscosity decreases with increasing the strain rate fluctuations. Following Savage(1998) it may be reasonably straightforward to shown that the above averaged equations for a three-dimensional case can smoothly merge with those describing rapid granular flows at the limiting case of large fluctuations. To proceed, an explicit form for *P* is required. Without a firm physical basis, Savage (1998) suggested that P is composed of a pressure density contribution for quasi-static deformation as well as a collisional stress contribution which depends on granular temperature. Hence

$$P\left(\phi_s, T\right) = P_0 \log \frac{\phi_\infty - \phi_0}{\phi_\infty - \phi_s} + \rho_s \phi_s \left[1 + 2(1+e)\phi_s g_c\right] T. \tag{4-93}$$

Where P_0 is a reference value of P, ϕ_∞ is the solids fraction at close packing, and ϕ_0 is the minimum solids fraction, e is the coefficient of restitution, g_c is the equilibrium value of the radial distribution function at contact, and T is the granular temperature defined as $T = \left\langle u^2 \right\rangle / 3$. A simple representation of the radial distribution function g_c follows from the Enskog approximate model of dense gases of identical rigid spheres, which is based on a heuristic concept of the free volume of each sphere to be smoothed over so as to present a regular sphere of a concentration dependent radius. Hirschfelder et al. (1954) suggested that

$$g_c = \frac{1}{1 - \left(\phi_s / \phi_\infty\right)^{\frac{1}{3}}}. \tag{4-94}$$

The value of P_0 in Eq. (4-93) may be determined using the numerical method for predicting the stress distribution in a system. The bulk density ρ_b can easily be measured by filling a rectangular container with glass balls of diameter $1\ mm$. The physical properties of the material are given in Table 3-1. Note that the bulk density can be increased with the application of elevated stresses or when the material is vibrated. The bulk density is related to solid volume fraction by $\rho_b = \left(1 - \phi_s\right)\rho_g + \phi_s \rho_s$ where ρ_g is the density of the gas. Apparently, an unequal transmission of the vertical force components occurred which could imply a purely diffusive large-scale behavior for the force.

The data obtained using numerical simulations can be fit according to $P_0 \log\left(\phi_\infty - \phi_0 / \phi_\infty - \phi_s\right)$ with $P_0 = 0.5\ kPa$, $\phi_\infty = 0.63$ and $\phi_0 = 0.487$. Here, ϕ_0 represents the solid volume fraction of the initially loose sample and ϕ_∞ is the maximum solid volume fraction and P_0 is determined from a least-square fit of the numerical simulations data.

Equations (4-92) and (4-93) may not predict the anisotropy caused by an anisotropic distribution of collision directions due to presence of a chain-like granular structure. Moreover, the present approach regarded the grains as possessing no rotational motion. However, as will be shown in the following section these constitutive equations could be of use for interpretation of previously unexplained hydrodynamic phenomena in transitional regimes that are observed in three-dimensional granular flows.

The total force of the interphase interaction per unit volume in Eq. (4-86) may be approximated by Buyevich et al. (1994),

$$F_i = \rho_s \phi_s \left[\beta_1 K_1\left(\phi_s\right) + \beta_2 K_2\left(\phi_s\right)\left\|W\right\|\right] W_i - \phi_s \left[\rho_g \phi_g + \rho_s \phi_s\right] g_i, \tag{4-95}$$

where W_i is the interstitial slip velocity of the gas, namely $U_i - V_i$, whose norm is denoted by $\left\|W\right\|$ and expressions for the coefficients $\beta_1, \beta_2, K_1\left(\phi_s\right)$, and $K_2\left(\phi_s\right)$ are given as (Buyevich, 1994; Buyevich et al., 1994):

$$\beta_1=\frac{18\nu_g}{\sigma^2},\ \beta_2=\frac{3}{8\sigma},\ K_1=\frac{1}{\phi_s^{\frac{5}{2}}},\ K_2=\left(\frac{\phi_s}{1-1.17\phi_s^{\frac{2}{3}}}\right)^2. \tag{4-96}$$

In addition an approximate expression for $\left\langle F_i\right\rangle$ is given by

$$\left\langle F_i\right\rangle=F_i+\rho_s\phi_s\times\left[\beta_1\left.\frac{\partial K_1}{\partial\phi_s}\right|_{\phi_S}\left\langle\phi_s' W_i'\right\rangle+\beta_2K_2\left(\phi_s\right)\left\langle W_j' W_j^0 W_i'\right\rangle+\right.$$
$$\left.\beta_2\left.\frac{\partial K_2}{\partial\phi_s}\right|_{\phi_S}\left(\left\langle\phi_s' W_j^0 W_j'\right\rangle W_i+\left\langle\phi_s' W_i'\right\rangle\left\|\langle W\rangle\right\|\right)\right] \tag{4-97}$$

Where $W_i'=U_i'-V_i'$, $W_j^0=\left\langle W_j\right\rangle\Big/\left\|\langle W\rangle\right\|$.

4-3-2-4. Fluctuation Energy

Note that by introducing the link between ε and T in the preceding section an additional equation is required for calculation of the granular temperate. The conservation of fluctuation energy for the particle phase (Zamankhan et al., 1997) includes the work performed by $\left\langle\sigma_{ij}\right\rangle$, the divergence of a pseudo-energy flux owing to the fluctuating motion as well as the production and dissipation of the fluctuation energy due to the interaction with the interstitial fluid, and to the energy dissipation due to strain-rate fluctuations. Following Savage (1998) the rate of energy dissipation due to strain-rate fluctuations, γ, may be given as

$$\gamma=1\Big/\varepsilon^3\left(2\pi\right)^{\frac{3}{2}}\times\int e^{-\left[\left(\varepsilon_1-\left\langle\varepsilon_1\right\rangle\right)^2+\left(\varepsilon_2-\left\langle\varepsilon_2\right\rangle\right)^2+\left(\varepsilon_3-\left\langle\varepsilon_3\right\rangle\right)^2\right]\Big/2\varepsilon^2}\sigma_i'\varepsilon_i' d\varepsilon_1 d\varepsilon_2 d\varepsilon_3, \tag{4-98}$$

where $\sigma_i'=\sigma_i-\left\langle\sigma_i\right\rangle$, $\varepsilon_i'=\varepsilon_i-\left\langle\varepsilon_i\right\rangle$. Variations of $\gamma/P\varepsilon$ with the angle of repose is presented by Bordbar and Zamankhan (2005a).

The flux of the fluctuation energy is expressed using the kinetic theory type approach (Jenkins and Richman, 1985). That is

$$Q_i=-\lambda\frac{\partial T}{\partial x_i}, \tag{4-99}$$

where λ being the coefficient of the fluctuation energy transfer which characterizes processes of mean flow energy being converted into the energy of the fluctuations. This coefficient is defined as $\lambda=\alpha PA_1/\varepsilon$ where the parameter α is a function of the average solid volume fractions given as

$$\alpha=\frac{30\left(-3+e\right)\left\{8\left(1+e\right)^2\left(-49+33e\right)g_c^2\phi_s^2-\pi\left[5+6\left(1+e\right)g_c\phi_s\right]\left[5+3\left(1+e\right)^2\left(-1+2e\right)g_c\phi_s\right]\right\}}{\left(-49+33e\right)\left\{96\left(-3+e\right)\left(1+e\right)^2g_c^2\phi_s^2-\pi\left[5+4\left(1+e\right)g_c\phi_s\right]\left[5+2\left(1+e\right)^2\left(-1+3e\right)g_c\phi_s\right]\right\}} \tag{4-100}$$

The remaining mechanisms have relevance to production and dissipation of the fluctuations due to interaction with the interstitial fluid. The former can be considered as energy inflow to the fluctuations due to the mean relative flow and the latter characterizes the dissipated energy per unit volume, per unit time caused by hydrodynamic resistance to the fluctuations. Consideration of these mechanisms may be of interest recalling that the presence of a complex motion reported by Pak et al. (1994).

To obtain the rate of generation of the granular temperature due to hydrodynamic interactions, it would be necessary to determine the response of particles to fluid velocity fluctuations. Buyevich (1994) suggested reliable expressions for the energy supply, which is caused by both the hydrodynamic drag and buoyancy, and the dissipation power, which is due the drag alone. They are

$$\tilde{Q}_+ = \rho_s \phi_s \left[\beta_1 K_1(\phi_s) \langle U_i' V_i' \rangle + \beta_1 \frac{dK_1}{d\phi_s}\bigg|_{\phi_s} \langle \phi_s' V_i' \rangle W_i \right] +$$

$$\rho_s \phi_s \left\{ \beta_2 K_2(\phi_s) \left[\langle U_i' V_i' \rangle + \left\langle \left(W_i^0 V_i' \right) \left(W_j^0 U_j' \right) \right\rangle \right] \| \langle W \rangle \| + \beta_2 \frac{dK_2}{d\phi}\bigg|_{\phi_s} \langle \phi_s' V_i' \rangle W_i \| \langle W \rangle \| \right\} - \tag{4-101}$$

$$\phi_s (\rho_s - \rho_g) \langle \phi_s' V_i' \rangle g_i,$$

and

$$\tilde{Q}_- = \rho_s \phi_s \left(3\beta_1 K_1(\phi_s) + 4\beta_2 K_2(\phi_s) \| \langle W \rangle \| \right) T. \tag{4-102}$$

These formulae appear to be suffice to develop a conservation of "translational" fluctuation energy for the particle phase, which is given as

$$\frac{3}{2}\rho_s \left(\phi_s \frac{\partial T}{\partial t} + \phi_s V_i \frac{\partial T}{\partial x_j} \right) = \langle \sigma_{ij} \rangle \frac{\partial V_i}{\partial x_j} - \frac{\partial Q_i}{\partial x_i} + \tilde{Q}_+ - \tilde{Q}_- - \gamma. \tag{4-103}$$

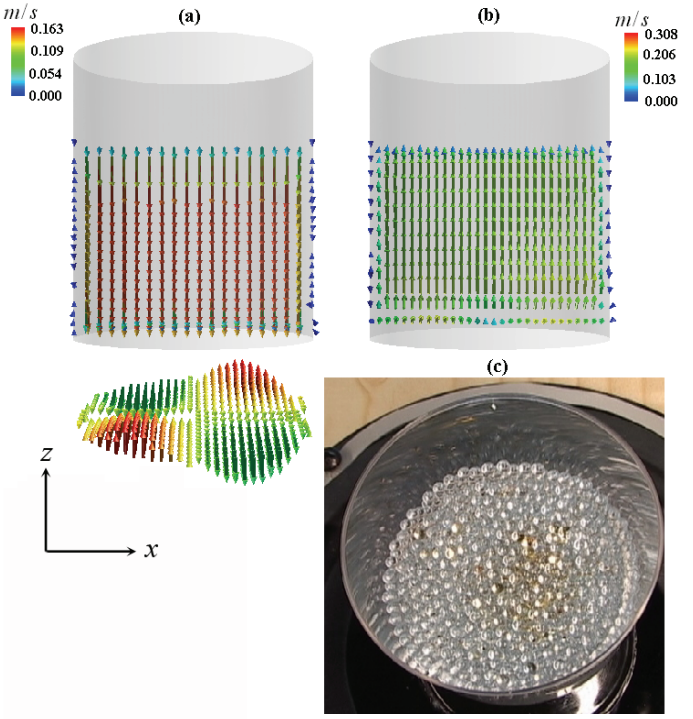

Fig. 4-42: *(a) Instantaneous velocity vector field for glass ball movement in a circular vibro-granular media device at an early stage of vibrations in a xz plane at* $y = 0$. *As can be seen, some particles are flowing up near the wall region and others are flowing down in the core region. Note that the initial solids fraction is set to* $\phi_s = 0.58$. *Shown also is the instantaneous the solid velocity field at the base of container. (b) Velocity vector field for the gas in the same plane. It is likely that the gas turbulent fluctuations are driven by the collective motion of the particle assembly. (c) Photograph of a circular vibro-granular media device in which glass balls are subjected to oscillation in the vertical direction. Top view of free surface shape seems to support results presented in (a).*

4-3-2-5. Continuous Phase

Turning attention to the flow of the interstitial fluid, on average the momentum conservation equation can be approximately written as

$$\rho_g \left(\frac{\partial \left(\phi_g U_i \right)}{\partial t} + \frac{\partial \left(\phi_g U_i U_j \right)}{\partial x_j} \right) = \phi_g \frac{\partial E_{ij}^g}{\partial x_j} - F_i + \rho_g \phi_g g_i, \tag{4-104}$$

where E_{ij}^g is the stress tensor for the fluid phase. Time-smoothing of Eq. 4-104 can be approximately written as

$$\rho_g\left(\frac{\partial\left\langle\phi_g U_i\right\rangle}{\partial t}+\frac{\partial}{\partial x_j}\left(\phi_g U_i U_j\right)+\frac{\partial}{\partial x_j}\left(U_j\left\langle\phi_g' U_i'\right\rangle+U_i\left\langle\phi_g' U_j'\right\rangle\right)\right)=$$
$$\left(\left\langle\phi_g\frac{\partial E_{ij}^g}{\partial x_j}\right\rangle-\frac{\partial}{\partial x_j}\left(\phi_g\left\langle U_i' U_j'\right\rangle\right)\right)-\left\langle F_i\right\rangle+\rho_g\phi_g g_i. \tag{4-105}$$

The approximate expression for the time smoothed total force of the interphase interaction per unit volume, $\left\langle F_i\right\rangle$, is given in Eq. (4-97).

A Newtonian stress-strain rate type constitutive equation is conjectured for the time smoothed stress tensor for the gas phase, given as

$$\left\langle E_{ij}^g\right\rangle=-p_g\delta_{ij}+\mu_{eg}\left[\frac{\partial U_i}{\partial x_j}+\frac{\partial U_j}{\partial x_i}\right], \tag{4-106}$$

where the effective viscosity of the gas phase is given as $\mu_{eg}=\mu_g\left(1+2.5\phi_s+7.6\phi_s^2\right)\left(1-\phi_s/\phi_m\right)$ (Dasgupta, 1994). Here, μ_g represents the molecular viscosity of the gas.

It may be speculated that Eqs. (4-105) can be closed by a turbulence model such as the $k-\omega$ model. Given the form of the conservation of momentum Eq. 4-105 the modeling of turbulence in gas particle flows is quite complex. For example, as depicted in Fig. 4-42, at an earlier stage of shaking, particles fall through the air enhance the gas turbulence, as discussed in some detail in previous parts of this section. In this case, consideration of turbulence may be important in order to improve predictions of air heaping and bubbling. In this light, the important features of turbulence in a vibrated granular material might be captured using a highly simplified model which is integrable up to the wall such as that proposed by Wilcox (2000). Hence, by neglecting the anisotropy of the fluid velocity fluctuations, the simplified transport equations of $k-\omega$ for the continuous phase whose density and velocity are defined as $\rho_m=\rho_g\left\langle\phi_g\right\rangle$ and $U_i^0=\left\langle\phi_g\right\rangle\langle U_i\rangle$, respectively, are given as:

$$\frac{\partial}{\partial t}\left(\rho_m k\right)+\frac{\partial}{\partial x_i}\left[\rho_m U_i^0 k-\rho_m\left(\nu_g+\varsigma^*\nu_T\right)\frac{\partial k}{\partial x_i}\right]=E_{ij}^g\frac{\partial U_i}{\partial x_j}-\chi^* k\omega+\left(\tilde{Q}_- -\tilde{Q}_+\right),$$
$$\frac{\partial}{\partial t}\left(\rho_m\omega\right)+\frac{\partial}{\partial x_i}\left[\rho_m U_i^0\omega-\rho_m\left(\nu_g+\varsigma\nu_T\right)\frac{\partial\omega}{\partial x_i}\right]=\Sigma\frac{\omega}{k}E_{ij}^g\frac{\partial U_i}{\partial x_j}-\chi\omega^2+C_\omega\chi^*\omega\left(\tilde{Q}_- -\tilde{Q}_+\right). \tag{4-107}$$

Here, $k=\left\langle U_i U_i\right\rangle/2$, the kinematic eddy viscosity is defined as, $\nu_T=k/\omega$ and the closure coefficients and auxiliary relations are listed as

$$\Sigma=\frac{13}{25}\ ,\ \chi=\chi_0 f_\beta,\quad \chi^*=\chi_0^* f_{\beta^*},\quad \varsigma=\frac{1}{2},\quad \varsigma^*=\frac{1}{2},\quad \chi_0=\frac{9}{125},\quad f_\beta=\frac{1+70\chi_\omega}{1+80\chi_\omega},\quad \chi_\omega\equiv\left|\frac{\Omega_{ij}\Omega_{jk}S_{ki}}{\left(\chi_0^*\omega\right)^3}\right|,$$
$$\chi_0^*=\frac{9}{100},\quad C_\omega=1.2,\quad f_{\beta^*}=\begin{cases}1, & \chi_k\le 0\\ \dfrac{1+680\chi_k^2}{1+400\chi_k^2}, & \chi_k>0\end{cases},\quad \chi_k\equiv\frac{1}{\omega^3}\frac{\partial k}{\partial x_j}\frac{\partial\omega}{\partial x_j},\quad \varepsilon=\chi^*\omega k\ \text{ and }\ l=k^{\frac{1}{2}}/\omega \tag{4-108}$$
$$\Omega_{ij}=\frac{1}{2}\left(\frac{\partial U_i}{\partial x_j}-\frac{\partial U_j}{\partial x_i}\right),\quad S_{ij}=\frac{1}{2}\left(\frac{\partial U_i}{\partial x_j}+\frac{\partial U_j}{\partial x_i}\right)$$

In formulating the turbulence model (4-107), a number of correlations appear in the balances of k and ω mainly due to the influence of the particle phase on the gas phase. These terms are modeled on an ad hoc basis. However, the value of parameter C_ω has been estimated using the molecular dynamic type simulations presented in the section 4-2-3.

By applying the equations derived heuristically in this section deformation and the flow of dense gas-particle assembly in a vibrated sandbox will be predicted in the following sections.

4-4. Continuum Model for Vibro-Granular Medium Device

The more fascinating behavior of the granular materials occurs when grains are vibrated vertically. In fact, the effects of high frequency oscillations, namely above $100\ Hz$, have been ignored in the previous works (Umbanhowar et al., 1996; Pak et al., 1994). Here, high frequency, vertically vibrated, granular material is investigated using the model developed in the preceding section in order to determine whether oscillon structures can be developed at high frequency vibrations.

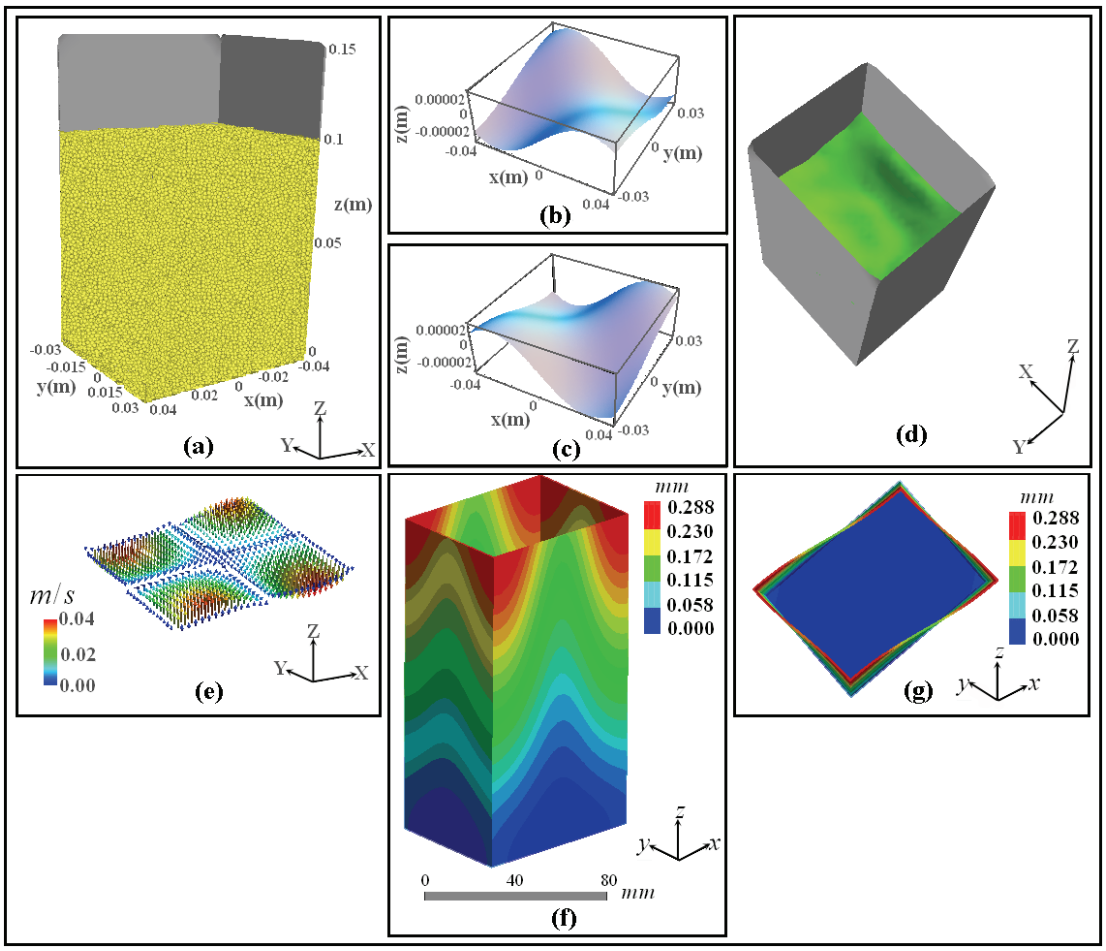

Fig. 4-43: *(a) Schematic diagram of granular material under vertical vibrations. Initially the free surface was flat and the average solids fraction was* $\phi_s = 0.58$. *The container dimensions are* $9.2 \times 7.78 \times 15\ cm$. *The mono-dispersed glass particles were used, where particle diameter was* $1\ mm$. *(b-c) The shape of the base of the container at two different time steps. (d) Top-view of surface shape of glass balls in the vibro-device. A long kink on the granular surface separates a heap in the core from the elevated solids adjacent to the wall. The free surface snapshot was taken after* $0.2\ \text{sec}$ *of simulations. (e) The instantaneous velocity vector field of glass balls at the base wall at* $t = 0.2\ \text{sec}$. *(f) Side-view of the instantaneous elastic deformation of sidewalls of the vibro-device made of steel. The finite element approach as described by Bordbar and Zamankhan (2005a) is used to calculate deformations. (g) Top-view of the instantaneous deformation of container.*

Recall that Danna et al. (2003), concluded that the vibro-fluidized granular matter can be treated (to a first approximation) with the equilibrium formalism. In this light, the many-particle problem as such as that presented in Fig. 4-43 can be represented by just two macroscopic parameters: viscosity and granular temperature which are found to be anisotropic and inhomogeneous.

Indeed, the aforementioned observation justifies the use of a set of hydrodynamic equations with a local velocity, a density and a granular temperature as local variables such as those developed in the preceding section to describe the behavior of granular material in the vibro-granular medium.

In Fig. 4-43, the vibro-granular medium is a driven environment, with continuous injection of energy, via membrane type deformation of the base of the container and dissipation of energy due to inelastic collisions between the particles.

As illustrated in Fig. 4-43 (a), a dense bed with a height of $H = 0.1\ \ m$ of glass balls with diameter of $\sigma = 10^{-3}\ \ m$ and material density $\rho_p = 2390\ kg/m^3$ is placed on the top of a large vibrated square plate whose center is fixed. The height of container is $H_0 = 0.15\ m$ and the initial solids fraction is selected to be $\phi_s = 0.58$. The free surface of granular material is flat as illustrated in Fig. 4-43 (a). The displacement $z(x,y,t)$ of the square elastic membrane, as illustrated in Fig. 4-43 (b) may be described as $z = A\sin(k_v x)\sin(l_v y)\cos(\omega_v t)$ where $(\omega_v = C\sqrt{l_v^2 + k_v^2})$, C is speed of wave in the vibrated wall, A is a constant, and $k_v = m_v\pi$ and $l_v = n_v\pi$. The mode illustrated in Fig. 4-43 (b) is produced by $m = 17\ \ 1/m$, $n = 13\ \ 1/m$, and $A = 10^{-4}\ \ m$. A high frequency vibration, namely $f > 1\ \ kHz$, may be obtained by setting $C = 100\ m/s$. Note that the nondimensional peak acceleration, $\Gamma = A(2\pi f)^2/g$, is large to assure that the glass balls are in loose contact with the container base. In this case, a shock wave (Soleymani et al., 2004) could occur through which kinetic energy transfers to glass balls, which in turn allows the assembly to rearrange.

As illustrated in Fig. 4-43 (c), the predicted free surface shape with a heap in the central region as well as formation of kinks between the central region and side walls, and elevation of solids at the walls after 0.1 sec of vibrations indicates the presence of impact regime in the vibro-granular medium as described in the above.

To obtain results such as that presented in Fig. 4-43 (c), the hydrodynamic equations (4-80), (4-85), (4-88), (4-103), (4-105) and (4-107) with the constitutive equations (4-86), (4-93), (4-99), and (4-106) are solved numerically in a Cartesian coordinates system x, y, z using the appropriate boundary conditions at the side walls, bottom wall, and the top face of container which is open to the atmosphere.

It is clear that the boundary conditions are crucial to predict the behavior of a vibro-granular medium correctly. Jenkins and Louge (1997) calculated the flux of fluctuation energy in the limit that the granular material is agitated but the mean velocity of the contact points with respect to the wall is zero. Given the simulation results shown in Fig. 4-43 (e), the scenario mentioned above might describe the condition near the container base in a high frequency vibro-granular medium.

Assuming that the fluctuations in the velocity of the contact point is Maxwellian, an approximate expression for the energy transfer between the container base and the glass balls in the limit of zero mean slip, may be given as

$$Q_i n_i = -\left(\frac{\rho_p \phi_s}{2}\right) g_c (1+e) T^{3/2} \left(\frac{\pi}{18}\right)^{1/2} \times$$

$$\left\{ \frac{2}{\pi}(1-e) + \frac{\mu}{2}\left[\pi - \frac{2\bar{\mu}_0}{1+\bar{\mu}_0^2} + \frac{4\bar{\mu}_0}{\left(1+\bar{\mu}_0^2\right)^2} - 2\phi_0 \right] - \mu\mu_0 \left[1 - \frac{2\bar{\mu}_0^2}{1+\bar{\mu}_0^2} + \frac{4\bar{\mu}_0^4}{\left(1+\bar{\mu}_0^2\right)^2} \right] + \frac{2}{7}\frac{\left(1-\beta_0^2\right)}{(1+e)} \frac{\bar{\mu}_0^4}{\left(1+\bar{\mu}_0^2\right)^2} \right\}, \tag{4-109}$$

where $\mu_0 = 7/2(1+e)\mu$, $\bar{\mu}_0 = \mu_0/(1+\beta_0)$, and $\phi_0 = \tan^{-1}(\bar{\mu}_0)$.

For the stress variable, the boundary conditions for the solid phase may be obtained using the law of sliding (Zamankhan et al., 2004). Therefore, the magnitude of tangential stress is proportional to the magnitude of the normal stress at any point on the wall. That is,

$$\left(\tau_i \tau_i\right)^{1/2} = \mu \left| \sigma_{pq} n_p n_q \right|, \tag{4-110}$$

where $\tau_i = \left(\sigma_{ij} n_j - \sigma_{pq} n_p n_q n_i\right)$.

The shape of side walls could become quite complex in a vibro-granular medium container, as illustrated in Fig. 4-43 (f-g). The container may even be distorted for small amplitude vibration of the container base. However, the magnitudes of deformations are somewhat small. In this study, the deformations of sidewalls are neglected and the sidewalls are assumed to be stationary. The latter assumption appears to simplify the problem greatly. However, a more accurate prediction of gas-particle dynamics in a vibro-granular medium device requires a detailed description of elastic container –granular material interactions, which will be addressed in a future article.

In order to apply $k-\omega$ model to the vibro-granular medium device appropriate boundary conditions should be specified for the velocity and two turbulence parameters at the solid walls. An advantage of the $k-\omega$ model is that it does not require calculation of wall distances for use in low-Re damping functions.

No slip condition is assumed for the gas at the walls. In addition, k is assumed to vanish at the walls. Following Wilcox, ω at the wall is set to $\omega = 2500\nu_w/\kappa_s$, where κ_s is a roughness factor whose value is unity for a smooth wall. Finally for the gas pressure at the top face the atmospheric value is used.

Note that the treatment of the gas-particle flows in a container with a deforming bottom, as depicted in Fig. 4-43(b), requires a grid which must be moved accompanied with the plate movement and deformation. In this case, the dynamic mesh method is required. The method proposed for the dynamic mesh in Part I can easily be utilized for the problems with small amplitude vibration as that presented in Fig. 4-35. In brief, the approach is to apply the tension spring analogy to tetrahedron cell shape in the grid. In addition, the internal angles of triangle faces and the angles between two faces that construct the cell, is controlled in order to prevent generating squashed invalid elements. In this light the entire container is discretized using tetrahedral elements.

The numerical results for the fields of gas velocity, solid velocity, and solids fraction in the geometry such as that illustrated in Fig. 4-43, are obtained through discretization using the control volume formulation (Patankar, 1980). The integral form of the governing equations (4-80), (4-85), (4-88), (4-103), (4-105) and (4-107) is considered at each element of a large number of tetrahedral elements, to produce a set of coupled, nonlinear, algebraic equations using the QUICK differencing scheme (Versteeg and Malalasekera, 1995) for spatial discretization, and the time-advancement via a second-order, implicit scheme. These equations are linearized and by using an extension of SIMPLE algorithm (Patankar, 1980) the velocities are solved coupled by phases. Here staggered grids are used for which the velocities are calculated at the cell faces whereas the scalar quantities such as pressure and solids fraction are evaluated at the cell centers. The continuity equation is turned into an equation for pressure correction.

The convergence criteria are defined in terms of residuals for the aforementioned continuity equation, velocity components of the gas and the solid phase, granular temperature, solids fraction, k and ω. These quantities are computed by summing the imbalance in corresponding equations in the domain at each iteration in a time step. They provide a measure of the degree to which each of the hydrodynamic equations listed earlier is satisfied. In the present attempt, convergence is considered to be achieved only when each of the normalized residuals fall below 10^{-3}.

The physical properties of the gas used in the simulations are $\rho_g = 1.225\ kg/m^3$ and $\nu_g = 1.461 \times 10^{-5}\ m^2/s$.

The numerical results of the hydrodynamic equations (4-80), (4-85), (4-88), (4-103), (4-105) and (4-107) using the constitutive equations (4-86), (4-93), (4-99), and (4-106) are presented in the following section in vibro-granular medium containers with different kind of cross sections. Apparently, the vibro-device provides a somewhat simple geometry in which to test the proposed theory presented in the preceding section for dense gas-particle mixtures.

As a reference case, in the following section sample numerical results are presented for flow dynamics of a simple liquid-gas in the vibro-device using a modified volume-of-fluid method (Chen et al., 1999) incorporating surface tension stresses. The physical properties of the simple liquid used in the aforementioned simulations are $\rho_w = 998.2\ kg/m^3$ and $\nu_w = 1.0\times10^{-6}\ \ m^2/s$.

In all cases listed above, the base wall of the prism shaped container is subjected to sinusoidal oscillation in the vertical direction given as $z = A\sin\left(k_v x\right)\sin\left(l_v y\right)\cos\left(\omega t\right)$.

4-4-1. Results and Discussions in Continuum Model

Vibrated granular material exhibits fluid-like behavior, examples of which are heaping, bubbling and free-surface excitation. As shown in Fig. 4-44, at high frequencies and small amplitude vibrations, fluidization of glass particles can be observed due to the presence of interstitial gas. The results presented in this section are obtained using a time step of $10^{-5}\ s$. Grid independence solution is found using slightly less than 10^6 tetrahedral elements.

As depicted in the inset of Fig. 4-44(a), the glass balls are clearly lifted off by the bubble of the gas. During the lift off process, the glass balls tend to dilate, making the movement of the bubble easier. It is likely that the glass balls compact later when the shape of the base of container changes. In this case, the bubble between the glass balls and base is compressed, which provides an upward force on the grains. Fig. 4-44 (b) represents the complex flow field of the gas around the bubble. The bubble is depicted in Fig.4-44 (c).

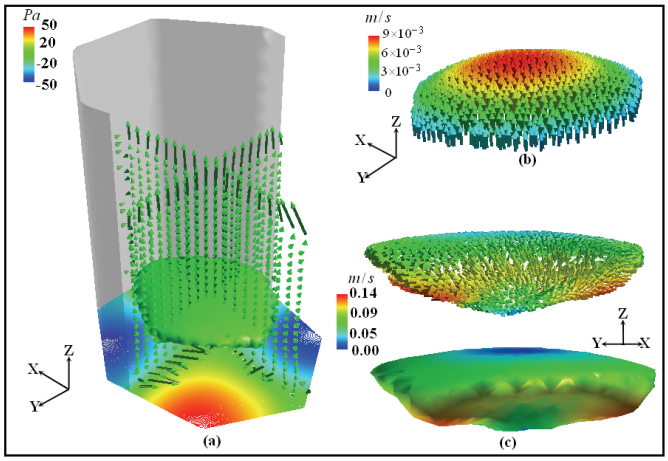

Fig. 4-44: *(a) Shown is a large bubble color-coded with the local gas pressure in the middle of a heptagonal vibro-granular media device. The snapshot is taken at* $t = 0.228\ \text{sec}$. *The contours of pressure are shown at the base of the container. Vector velocity field of glass balls slightly higher than the top side of bubble is magnified and presented in the inset of (a). (b) Vector velocity field of gas phase around the bubble. (c) To obtain a better visualization, the single, large bubble in (a) is magnified. The glass particle diameter is* $1\ mm$ *and initially* $10\ cm$ *of a heptagonal prism is poured with them.*

Note that the additional gas pressure at the base could significantly change the dynamics of bubbling in the container, as illustrated in Fig. 4-45. Here, a heptagonal prism is used as the container of the vibro-granular device. In this case, the bubbles, which are color-coded with local gas pressure, are formed close to the container base as illustrated in Figs. 4-45 (a-c).

Figures 4-45 (d-e) illustrate time evolution of the free surface shape of the granular material in which oscillon type structures can easily been observed. Realizations presented in the aforementioned Figs. are each separated by $10^{-2}\ \text{sec}$. Hence, the observed oscillons are sub harmonically excited structures in agreement with those observed in (Umbanhowar et al., 1996). Recall that the oscillion type structure reported in Section 4-2-3 was also a sub-harmonically excited structure in qualitative agreement with the predictions of the continuum type model proposed in this part.

Note that one of oscillons shown in Fig. 4-45 is somewhat similar to those generated experimentally by Thrasher (1997). He named them rouge oscillons, which are peaks of granular materials over twenty-five times the height of the granular layer. The long oscillons such as those shown in Fig. 4-45, may bend due to drag force imposed by the gas. To obtain better visualization of the flow field around a long and bend

oscillon, the flow field in the corner of contained is magnified and presented in the inset of (a). As it can be seen from Fig. 4-45 (a) the glass balls within the oscillon are falling due to gravitational acceleration and large vortices can be observed in the gas flow field.

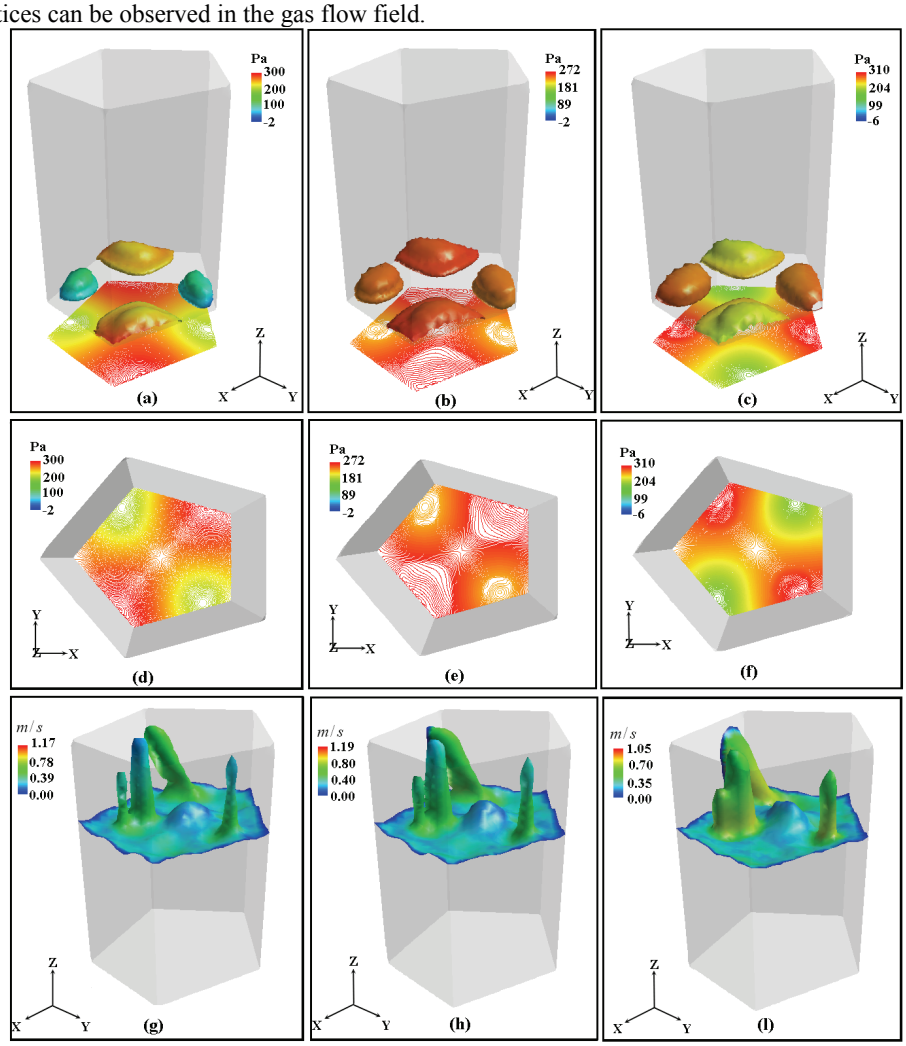

Fig. 4-45: *(a-f) Temporal evolution of the pressure distribution of gas at the base of pentagonal vibro-granular media device. Realizations each separated by* 10^{-2} sec *and the first one, namely (a), is taken at* $t = 0.185$ sec. *Note that the bubbles are formed adjacent to the base wall and they are color-coded with the local gas pressure. (g-l) Side views of the free surface shape of glass balls at different time steps. Again, realizations each separated by* 10^{-2} sec *and the snapshot shown in (g) is taken at* $t = 0.185$ sec. *Temporal evolution of the long, bend oscillon and its interaction with the side wall of container is clearly presented.*

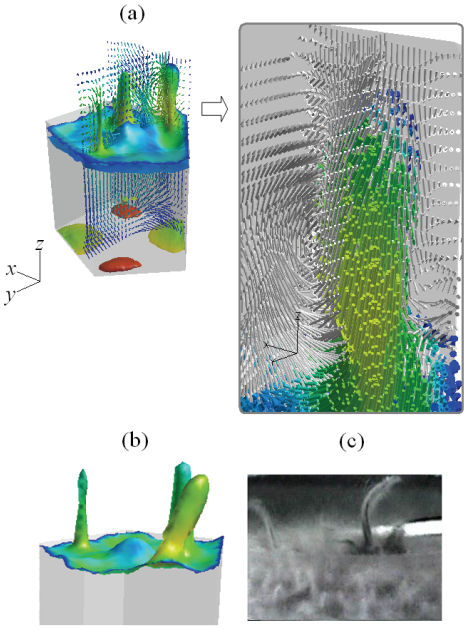

Fig. 4-46: *(a) Side-view of instantaneous surface shape of glass balls in a pentagonal vibro-granular media device taken after* $0.185\,\text{sec}$. *Three oscillons can be observed, and the fourth one is taking shape in the central zone of free surface. (Inset) Velocity vector fields of gas in* xz *and* yz *planes passing through the center of a long, bend oscillon. (b) A view of (a) excluding the details of velocity vector fields. (c) Photograph of rouge oscillon (*Thrasher, 1997). *Note that the oscillon captured by camera is likely to bend due to gas-oscillon interaction.*

Recall that Fineberg (1996) suggested that the vibro-granular media may be an example of a driven dissipative nonlinear system having many degrees of freedom. In order to compare complex behavior of granular material already presented in this section with that of ordinary liquid-gas mixture in the vibro-device, numerical results were obtained by replacing glass balls with a viscous fluid. The container shape is selected to be an octagonal prism. Using the modified VOF method and LES the free surface of water is visualized as illustrated in Fig. 4-47. Recall that LES has been previously discussed in section 4-2-3-1. The results presented in Fig. 4-47 are obtained using a time step of $10^{-4}\ s$ and grid independence solutions are found using more than 27×10^{6} tetrahedral elements. The disorder top view of the free-surface of the vibro-liquid-gas mixture, as shown in Fig. 4-47 (h), is quite different than that presented in Fig. 4-46 (c). However, the differences between the nonlinear systems with little dissipation and the granular media deserve further study.

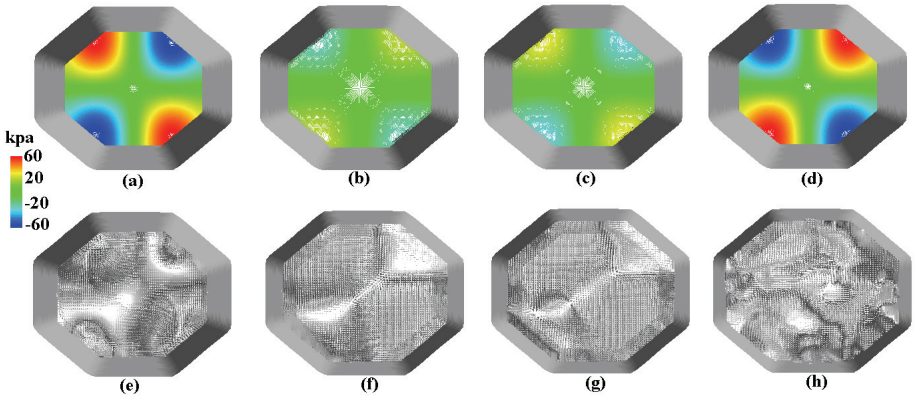

Fig. 4-47: *(a-d) Temporal evolution of the pressure distribution of liquid at the base of octagonal vibro-device. Realizations each separated by* $2\times10^{-4}\,\text{sec}$. *Here, the glass balls are replaced by a viscous liquid, namely water. (e-g) Views of velocity field of liquid at different heights of the container. Kinks and stripes can clearly been observed. (h) Top view of free-surface instabilities of liquid. Patterns are disordered dissimilar to those illustrated in Fig. 4-46 glass particles.*

5. Concluding Remarks

Existing works on the shaken sand have been largely confined to the experimental front. Indeed, the discoveries of experimentalist are spurring theorists in their search for a comprehensive, hydrodynamic type description for granular materials. Here, the development of a comprehensive molecular dynamics type model was considered for studying the deformation and flow of dense mixtures of gas and particles. The achievements are summarized as follows.

- The collisions of viscoelastic, mono-sized and multi-sized glass balls have been studied experimentally using a modified Newton's Cradle device. A numerical model based on finite element methods was developed to analyze the measurement data in order to obtain a better understanding of the processes during a collision. For example, a quantity such as the viscous damping coefficient, which is lacking in the literature, was determined for the glass balls. To obtain detailed information about the interparticle interactions in dense granular flows, a simplified model based on dimensional analysis has been developed for collisions between glass particles.

- A detailed overview has been provided of collective processes in gas-particle flows to obtain insight into the hydrodynamics of a shaken sandbox and to arrive at a simplified but realistic model for shaken sand. The simplified model includes an equation of motion for spherical sand particles having repulsive and dissipative interactions with its neighbors. In addition, the gas-particle interactions are taken into account using an empirical formula for drag force exerted by the gas on the particles. The hydrodynamic model of the gas phase is based on generalized Navier-Stokes equations for a gas interacting with a solid phase. The governing equations of the gas phase were solved using LES technique.

- The model is tested through its application to describe the influence of periodic vertical vibrations of the base of a pentagonal prism shaped container on the dynamics of granular media for which interactions with the surrounding gas plays an important role in dynamical pattern deformation. The base wall of the container is subjected to sinusoidal oscillation in the vertical direction given as $z = A\sin(k_v x)\sin(l_v y)\cos(\omega_v t)$, where $(\omega_v = C\sqrt{l_v^2 + k_v^2})$, C is speed of wave in the base wall of the container, A is the derived amplitude, and $k_v = m_v\pi$ and $l_v = n_v\pi$. The parameter, Γ, was defined that measures the acceleration of the container base relative to gravity. The parameter, Γ, is varied by changing the derived amplitude. As Γ increased above a critical value Γ_c, the free surface of shaken particles became unstable. When Γ increased well above Γ_c, the structures were observed with some degree of symmetry. The structures are subharmonic, therefore, both peaks and depressions can coexist. The incomplete structures have also been observed. The generation of incomplete structures has been linked to the formation of bubbles in the upper layers of shaken particles. Limitations in the available computational resources urged that further exploration of a shaken sandbox requires a different routine along with the present approach.
- To this end, an alternative approach a continuum approach was developed to describe granular flow dynamic behavior in the intermediate regime where both collisional and frictional interactions between particles may occur. The model successfully reproduced localized structures such as oscillon and results were presented indicating the role of the gas in the dynamics of oscillons.

While progress on the computational and theoretical fronts has been encouraging and even oscillon-type structures similar to those observed by Umbanhowar et al.[1] have been generated, there are still many, many open problems. An example of open problems includes the connection between bubbling and the downward convective flow induced by the collapse of the structures. In addition, the exact role of the gas in the development, growth and propagation of the cavities merits further investigation. Note that due to limitations in the available computational resources, currently no details such as flow dynamics of granular materials in containers with different bucket shapes can be provided.

The present models provide greater insight toward the explanation of poorly understood hydrodynamic phenomena in the field of granular flows and dense gas-particle mixtures. This attempt might help in overcoming the difficulties which lie in building a comprehensive hydrodynamic theory for the next generation of reactor models. The present models can be generalized to investigate the granular material-container wall interactions which would be an issue with high interests in the industrial systems. By using this approach ideal processing conditions and powder transport can be created in industrial systems.

References

-Abramowitz M. and Stegun A.,Handbook of Mathematical Functions.,Dover publications,NewYork,(1965).
-Abu-Zaid, S. and Ahmadi, G.,Powder Technology Vol.89, pp. 45-56 (1996).
-Ahmadi, G. and Ma, D., Int. J. Multiphase Flows Vol. 16, 323-340 (1990).
-Anderson K., Sundaresan S., Jackson R., Journal of Fluid Mechanics, 303, 327-366(1995).
-Anderson T.B., Jackson R., I&EC Fundamentals, 6, No. 4 ,527-539(1967).
- Anderson T.B., Jackson R., I&EC Fundamentals, 7, No. 1,12-21(1968).
- Aoki K. and Akiyama T., Phys. Rev. Lett. 77, 4166 (1996).
-Assenheimer M. and Steinberg, V., Phys. Rev. Lett., 70, 3888 (1993).
-Babic M and Shen H., Journal of Fluid Mechanics, 219, 81-118, (1990).
-Bagnold, R.A., Proc. Royal Soc. London, 49, 225 (1954).
- Batchelor G.K., Journal of Fluid Mechanics, 193, 75-110, (1988).
-Bayon A. and Drucker-Colin R., "In Vivo Perfusion and Release of Neuroactive Substances: Methods and Strategies", Academic Press, Orlando (1985).
-Bear J., "Dynamics of Fluids in Porous Media" Dover Publications Inc., Mineola, New York (1988).
-Behringer, R., Rev. Mod. Phys., 57, 657 (1985).
-Behringer, P.R., Pak, H.K., Nature, 371,231-233,(1994)
-Benjamin T. and Ursell F., Proc.R.soc.London A 225, 505 (1954).
-Billet R.,"Packed Towers:In processing and Environmental Technology",VCH,New York (1995).
-Bizon C., Shattuck M.D., Swift J.B., McCormick W.D., and Swinney H.L., Phys. Rev. Lett. 80, 57 (1998).
-Bordbar M.H. , Zamankhan P.," Theoretical Analysis and Numerical Simulations of Vertical Vibrated Granular Materials", Accepted with revision in the "Journal of Applied Physics" (2005b).
-Bordbar M.H. and Zamankhan P., Complex flow dynamics in dense granular flows,Part II:Simulation, accepteed in journal of Applied Mechanics(2005a).
-Bridges F.G., Hatzes A. and Lin D.N.C., Nature 309, 333 (1984).
-Brilliantov N. V., Spahn F., Hertzsch J.-M., and Pöschel T., Model for collisions in granular gases , Phys. Rev. E, 53,5382-5392,(1996a).
-Brilliantov N. V., Spahn F., Hertzsch J.-M., and Pöschel T., Physica A, 231,417, (1996b).
-Busse, F.H. and Whitehead, J.A., J. Fluid Mech., 47,305 (1971).
-Buyevich Yu.A., Chem.Eng.Sci.,49,1217(1994)
-Buyevich Yu.A. and Kapbasov Sh.K., Chem.Eng.Sci.,49,1245(1994).
-Campbell, C.S., Annu. Rev. Fluid Mech., 2, 57 (1990).
-Campbell C.S., Journal of Fluid Mechanics, 465:261-291,(2002).
-Cao, J., Ahmadi, G. and Massoudi, M., J. Fluid Mechanics Vol. 316, 197-221 (1996).
-Cerda E., Melo F., and Rica S., Phys. Rev. Lett. 79, 4570 (1997).
-Chen L., Garimella S.V., Reizes J.A. and Leonardi E., J. Fluid Mech., 387, 61 (1999).
-Clift R., Grace J.R., and Weber M.E., Bubbles, Drops and Particles, (Academic Press, New York, 1978).
-Clement, E., Vanel, J., Rajchenbach, J., and Duran, J., Phys. Rev. E 53,2972(1996).
-Conway H.D., Analogies Between the Buckling and Vibration of Polygonal Plates and Membranes., Can.Aeron .J.,Vol.6,No.7,Sept.1960,p.263.
-Conway,H.D., The Bending, Buckling,and Flexural Vibration of Simply Supported Polygonal Plates by point-Matching.J.Appl.Mech.,vol.28,no.2, pp.288-291,(1961).
-Cross, M.C.& Hohenberg, P.C., Rev.Mod.Phys.65, 851-1112 (1993).
-Cui J. and Neary V.S., "Large eddy simulation (LES) of fully developed flow through vegetation." IAHR's 5th International Conference on Hydroinformatics, Cardiff, Wales, July 1-5, (2002).
-Cundall P, Strack O. A , Geotechnique, 29:47-65,(1979).
-Danna G., Mayor P., Barrat A., Loreto V. and Nor F., Nature, 424, 909 (2003).
-Dasgupta S., Jackson R. and Sundaresan S., AICHE J.40,215(1994)
-De Bruyn, J.R., Bizon, C., Shattuck, M.D., Goldman, D., Swift, J.B. and Swinney, H.L., Phys. Rev. Lett., 81, 1421 (1998).
-De Bruyn, J.R., Lewis, B.C., Shattuck, M.D., Swift, J.B. and Swinney, H.L., Phys. Rev. E, 63, 041305(2001).
-De Gennes, P.G., Rev. Mod. Phys., 71, S374 (1999).

-Deng R., Wang Chi-Hwa ,Symposium 2003,MEBCS Technical Parallel Session, (2003).
-Dubois-Violette, E., Dunrand, G., Guyon, E., Manneville, P. and Pieranski, P., in Liquid Crystals, edited by L. LIEBERT (Academic Press, New York)
p. 147,(1978).
- Dufty J.W., *J. Phys.: Condens. Matter* 12 ,A47-A56(2000)
- Dufty J.W. and Brey J.J. Physical Rev.Lett.82(1999)
-Duran, J., "Sands, Powders, and Grains: An Introduction to the Physics of Granular Materials." ,Springer-Verlag, New York, Inc., New York, (2000).
-Eggers, J., Riecke, H., Physical Review E, 59,4476,(1999).
-Elata D, Berryman J G., Mechanics of materials, 24:229-240,(1996).
-Elgobashi S.E., Appl. Scient. Res., 48, 301 (1991).
-Ennis, B.J., Green, J., and Davies, R, "The Legacy of Neglect in the U.S.", Chem. Eng. Prog., Vol. 90, No. 4, pp. 32-43 (1994).
-Evesque, P. and Rajhenbach, J., Phys. Rev. Lett., 62, 44 (1989).
-Falcon E., Laroche C., Fauve S. and Coste C. ,The European Physical Journal B,3:45-57,(1998).
-Faraday, M., Philos. Trans. R. Soc. London, 121, 299 (1831).
-Fauve, S., Douady, S. & Laroche, C.J., Phys.Colloque, Paris 50 C3, 187-191(1989).
-Findley W. N., Lai J.S., and Onaran K.,Creep and relaxation of nonlinear viscoelastic materials (with an introduction to linear viscoelasticity), Dover Publications, Inc., New York, (1989).
-Fineberg J., Nature, 382, 763 (1996).
-Foerster, S. F., Louge, M. Y., Chang, H., and Allia, K. , Physics of Fluids, 6(3):1108-1115,(1994).
- Garg S.K., Pritchett J.W., Journal of Applied Physics, 46, No. 10, 4493-4500(1975).
-Garzo V., Phys.Rev.E.66,021308 (2002)
-Germano M., Piomelli U., Moin P., and Cabot W. H., Phys. Fluids, A, 3, 1760 (1991).
-Ghosal S. and Moin P., J. Comput. Phys. 118, 24 (1995).
-Goh, Y.K., and Jacobs, R.L., New J. Phys. 4, 81 (2002).
-Goldman, D.I., Moon, S.J., Swift, J.B. and Swinney, H.L., Phys. Rev. Lett., 90, 104302 (2003).
-Gorham D A and Kharaz A H. The measurement of particle rebound characteristics. Powder Technology, 112:193-202,(2000).
-Granger R.A., Fluid Mechanics, (Dover Publications, New York, 1995).
-Gugan, D., American J. of Phys., 68, 920-924 (2000).
-Halabia A.,"M.S. Thesis",Lappeenranta University of Technology,2005.
- Harris S.E., Crighton D.G., Journal of Fluid Mechanics, 266, 243-276(1994).
-Harry L. Swinney., E.C. Rericha., "Pattern Formation and Shocks in Granular Gases.", Center for Nonlinear Dynamics and Department of Physics, University of Texas at Austin, Austin, Texas 78712 USA.
-Happel J. and Brenner H.,"Low Reynolds Number Hydrodynamics", Noordhoff International Publishing Leyden,(1973).
- Hellwege K-H. and Madelung O.,Landolt-Bornstein, physical properties of rocks, ,New Series,Group V,Vol.1,Pt. a(Springer,Berlin,1982).
- Hernandez J.A., Jimenez J., "Proc.NATO Advanced Research Workshop on the Global Gerentry of Turbulence"(J. Jimenez, ed.), pp. 133-142, (1991).
-Hersch,J.:Contribution ä la Methode dcs Equations aux differences.ZAMP,vol.9a,no.9,pp.129-180,(1958).
-Hertz H., J.reine und angewandte Mathematik, 92: 156-171,(1882).
-Hirschfelder J.O., Curtiss Ch.F., and Brid R.B., `"Molecular Theory of Gases and Liguids,New York",Wiley(1954)
- Homsy G.M., El-Kaissy M.M., Didwania A., Int. Journal Multiphase Flow, 6,305-318(1980).
-Howard, J.R.,Fluidized Bed Technology, Principles and Applications. Hilger, NewYork, (1989).
-Hsiau S.S. and Hunt M.L.,J.Fluid Mech.,251,299(1993).
-Hunt K.H., and Crossley F.R.E., J. Appl. Mech. 97, 440, (1975).
-Jaeger H.M., Nagel S.R., and Behringer R.P., Rev. Mod. Phys. 68,1259 (1996).
-Jaeger, H.M., Nagel, S.R., and Behringer, R.P., Phys. Today 49,No.4, 32(1996).
-Jenkins J.T. and Louge M.Y., Phys. Fluids 9, 2835 (1997).

-Johnson K.L., Contact mechanics, 2nd ed. New York: Cambridge University Press, (1985).
-Kaczkowski,Z.:stabilität und Eigenschwingungen einer Platte von der form eines regelmässigen Polygons.Ost.Ingr.-Arch.,vol.15, pp.103-109,(1961)
-Knight, J.B., Jeager, H.M.&Nagel, S.R. Phys.Rev.Lett.70, 3728-3730 (1993).
-Knowlton, T.M., Carson, J.W., Klinzing, G.E., and Yang, W-C.,"The Importance of Storage, Transfer, and Collection.", Chem. Eng. Prog., Vol. 90, No. 4, pp. 44-54(1994).
-Kostyuk D.G. and Krishtal O.A., "Intracellular Perfusion of Excitable Cells", Wiley, New York (1984).
-Kozlov, V., Ivanova, A., and Evesque, P., Europhys. Lett. 42, 413 (1998).
-Kudrolli, A. and Gollub, J.P., Physica D, 97, 133 (1996).
-Kumar, K., Falcon, E., Bajaj, K., and Fauve, S., Physica (Amesterdam) 270A, 97 (1999).
-Kuo H. P., Knight P. C., Parker D. J., Tsuji Y., Adams M. J. and Seville J. P. K. , Chemical Engineering Science, 57:3621-3638,(2002).
-Kuwabara G., Kono K. , Japanese Jouranl of Applied Physics, 26(8): 1230-1233,(1987).
-Labous L., Rosato A. D. and Dave R. N. ,Physical Review E, 56(5): 5717-5725,(1997).
-Lan, Y., Rosato, A.D., Physics of Fluid, 7, 1818-1831(1995)
-Landau L.D. and Lifsitz E.M.,Theory of Elasticity.Oxford University Press,Oxford,(1965).
-Laroche, C., Douady, S. & Fauve, S.J. Phys., Paris 50, 699-702 (1989).
-Leonard A., Adv. Geophys. 18A, 237 (1974).
-Lightfood E.N., Chiang A.S., and Noble P.T., Ann. Rev. Fluid Mech., 13, 351 (1981).
-Lilly D.K., Phys. Fluids A, 4, 633 (1992).
-Lioubashevski, O., Hamiel, Y., Agnon, A., Reches, Z., and Fineberg, J., Phys.Rev.Lett.83, 3190 (1999).
-Liu Q., Roux B., Proc. VIII European Symposium on Materials and Fluid Sciences in Microgravity, Brussels, Belgium, ESA SP-333, pp. 735–740,(1992).
- Lun, C.K.K., Bent, A.A., Journal of Fluid Mechanics, 258, 335-353(1994).
-Ma, D. and Ahmadi, G., Powder Technology Vol. 56, 191-207 (1988).
-Ma, D. and Ahmadi, G., Int. J. Multiphase Flows Vol. 16,340-351 (1990).
-Marghitu D. B., Hurmuzlu Y., ASME Journal of Applied Mechanics, Vol.62, No.3, pp. 725-732(1995).
-Masuoka T. and Takatsu Y., “International Journal of Heat and Mass Transfer”, 39, 2803 (1996).
-Mathieu J. and Scott J., An Introduction to Turbulent Flow, (Cambridge University Press, Cambridge, 2000).
-Mehta, A. and Luck, J.M., Phys. Rev. Lett., 65, 393 (1990).
-Melo F., Umbanhowar, P.B. and Swinney, H.L., Phys. Rev. Lett., 75, 3838 (1994).
-Melo, F., Umbanhowar, P.B. and Swinney, H.L., Phys. Rev. Lett.,72,172-175 (1994).
-Mena, F., National Autonomous University of Mexico (UNAM.), (1993).
-Meneveau C., Phys. Fluids, 6, 2, 815 (1994).
-Metcalf, T., Knight, J., and Jaeger, H., Physica (Amsterdam) 236A, 202 (1997).
-Mindlin T. D. , ASME Journal of Applied Mechanics, 16: 259-268,(1949).
-Mishra B. K. and Murty C. V. R. , Powder Technology, 115:290-297,(2001).
-Moon, S.J., Shattuck, M.D., Bizon, C., Goldman, D.I., Swift, J.B. and Swinney, H.L., Phys. Rev. E, 65, 011301(2002).
-Morgado W.A.M. and Oppenheim I., Phys. Rev. E 55, 1940 (1997).
-Mukerjee M., Scientific American, November 1996, 19-21, (1996).
-Nedderman, R.M.,“Statics and Kinematics of Granular Materials.” Cambridge University Press (1992).
-Ouyang, Q. and Swinney, H., Nature, 352, 610 (1991).
-Pak H. K. and Behringer R. P., Nature, 371, 231 (1994).
-Pak H.K, Behringer R.P. Phys. Rev. Lett., 71, 1832-1835 (1993).
-Pak, H.K., Van Doorn, E., and Behringer, R.P., Phys. Rev. Lett. 74, 4644, (1995).
-Patankar S.V. , Numerical Heat Transfer and Fluid Flow, New York: Hemisphere 1980.
-Persson B.N.J., J. Chem.Phys.,115,3840(2001).
-Polashenski Jr. W., Zamankhan P., Mäkiharju S., And Zamankhan P.,Phys.Rev.E.66,021303.,(2002).
-Pope S. B., Turbulent Flows, (Cambridge University Press, Cambridge, 2000).
-Poschel, T. and Brilliantov, N. (Editors), Granular Glass Dynamics (Springer,Berlin) (2003).
-Reynolds W.C., Annual Review of Fluid Mech. 8, 183 (1976).
-Rosa R., Thorsten P., Nikolai T.B. and Thomas S.,Physical Review E., 60(4):4465-4472(1999).

-Rothman D., Phys. Rev. E 57, 1239 (1998).
-Sagaut P., Large Eddy Simulation for Incompressible flows, (Springer, Berlin, 1998).
-Savage S.B., J. Fluid Mech., 377, 1-26 (1998).
-Savage S.B. and Dai R., Mech.Mater.16,225(1993).
- Savage, S. B., In Mechanics of Granular Material : New model and constitutive relations (ed. J.T. Jenkis & M. Satake), pp. 261-282, Elsevier,(1983).
-Schager T., Poschel T. , Physical Review E, 57(1):650-654,(1998).
-Schleier-Smith, J.M., and Stone H.A., Phys. Rev. Lett. 86, 3016 (2001).
-Schwager T. and Pöschel T., Phys. Rev. E 57, 650 (1998).
-Sellgren U.,Björklund S. and Andersson S., Wear 254 , 1180–1188, (2003).
-Seth, B.R.: Transverse Vibrations of Rectilinear Plates.Proc.Indian Acad.Sci.,sec.A,vol.25, pp.25-29,(1947).
- Shinbrot T., Nature 389, 574 (1997).
-Sinclair J.L. and Jackson R., AIChE J, 35, 1473 (1989).
-Slichter C.S., "Field Measurments of the Rate of Movement of Underground Water," Water Supply Papers 14 R, US. Geological Survey (1905).
-Smagorinsky J., Monthly Weather Rev.,91,99 (1963).
-Sobral Y.D.and Cunha F.R.,Tendências em Matemática Aplicada e Computacional, 3, No. 2 ,197-206 (2002).
-Soleymani A., Zamankhan P. and Polashenski Jr. W., Appl. Phys. Lett., 84, 4409 (2004).
-Strigle Jr. R.F., "Packed TOWER Design and applications:random and Structured Packings",Gulf Pub.Co.,Houston (1994).
- Tan M.L. and Goldhirsch I. ,Phys. Rev. Lett. 81, 3022–3025 (1998)
-Thornton C, Ning Z. , Power Technology, 99: 154-162,(1998).
-Thrasher M. E., Still playing in a sand box, http://oas.ucok.edu/OJAS/97/T97/MTHRA.HTM, (1997).
-Tomas, B. and Squires, A., Powder Technol.100, 200 (1998).
-Tsimring L. and Aranson I., Phys. Rev. Lett. 79, 213 (1997).
-Tsinontides, S.C. & Jackson, R.Proc.Joint DOE/NSF Workshop on Flow of Particulates and Fluids (eds Plasynski, S.I. et al.) 254-286 (Pittsburgh Energy Technology Center, Pittsburgh,1991).
-Tsuji Y., Kawanuchi T. and Tanaka T., Power Technology, 77,79-87(1993).
-Tsuji Y., Tanaka T. and Ishida T., Power Technology, 71,239-250,(1992).
-Umbanhowar P. B., Nature, 389, 541-542 (1997).
-Umbanhowar P.,Nature 424, 886 - 887 (2003).
-Umbanhowar, P. and Swinney, H.L., Physica A, 288,344 (2000).
-Umbanhowar P., Melo F. and Swinney H., Nature, 382, 739 (1996).
- Venkataramani S. and Ott E., Phys. Rev. Lett. 80, 3495 (1998).
-Versteeg H.K. and Malalasekera M.,"An Introduction to Computational Fluid Dynamics.", Edinburgh: Longman 1995.
-Vu-Quoc L. and Zhang X. , Mechanics of Materials, 31: 235-269,(1999).
-Vu-Quoc L., Zhang X. and Lesburg L.,38: 6455-6489,(2001).
- Walker, D. M., Chem. Eng. Sci., vol. 21, pp. 975-997,(1966).
-Walkingtor N.J., Antaki J.F., Blelloch G.F., Ghattas O., Melcevic I., and Miller G.L., Proceedings of the 2000 ACM/IEEE conference on Supercomputing, Dallas, Texas, Article No. 26 (2000) .
-Walton O. R., Braun R. L. , Journal of Rheology, 30(5): 949-980,(1986).
-Wang C. H., Jackson R., Sundaresan S., J. Fluid Mech., 342, 179-197 (1997).
-Wang C. H., Jackson R., Sundaresan S., J. Fluid Mech., 308, 31-62 (1996).
-Wilcox D.C.,"Turbulence Modeling for CFD",DCW Industries,Inc. a La Canada, California (2000).
-Wong P., "Phys. Today," 41, 24, (1998).
-Xu, H., Louge, M. and Reeves, A., Continuum Mech. Thermodyn., 15, 321(2003).
- Yamamoto Y., Potthoff M.,Tanaka T., Kajlshima T. and Tsuji Y., J. Fluid Mech. 442, 303 (2001).
-Yi-Yuan Yu,"Vibrations of Elastic PlatesLinear and Nonlinear Dynamical Modeling of Sandwiches, Laminated Composites, and Piezoelectric Layers ",Springer-Verlag New York, 1996.
-Zamankhan P., Tynjala T., Polashenski Jr. W., Vahedi Tafershi H., ShakibManesh A., and Sarakoma P., J..Phys.Rev.E,58,R5237(1998).

-Zamankhan P., Tynjala T., Polashenski Jr. W., Zamankhan P. and Sarakoma P., Phys.Rev.E,60,7149,(1999).
-Zamankhan P., Vahedi Tafreshi H., and Chen J.C., Phys. Rev. E, 56, 2972 (1997).
-Zamankhan P., Soleymani A., Polashenski Jr. W.and Zamankhan P., Chem. Eng. Sci., 59, 235 (2004).
-Zhang D. Z., Rauenzahn R. M. , Journal of Rheology, 44(5):1019-1041,(2000).
-Zhang D.Z. and Whiten W J. , Power Technology, 88:59-64,(1996).
-Zhang D. Z. and Rauenzahn R. M. ,Journal of Rheology,41(6): 1275-1298(1997).

ACTA UNIVERSITATIS LAPPEENRANTAENSIS

184. HALME, TAPANI. Novel techniques and applications in generalised beam theory. 2004. 101 s. Diss.

185. LOISA, ANTTI. Studies on integrating kinematic design method with mechanical systems simulation techniques. 2004. 143 s., liitt. Diss.

186. 2nd Workshop on Applications of Wireless Communications. 2004. 74 s.

187. LI, XIAONING. Conflict-based method for conceptual process synthesis. 2004. U.s. Diss.

188. LAURILA, LASSE. Analysis of torque and speed ripple producing non-idealities of frequency converters in electric drives. 2004. 124 s. Diss.

189. NIKULA, UOLEVI. Introducing basic systematic requirements engineering practices in small organizations with an easy to adopt method. 2004. 207 s., liitt. Diss.

190. TANNINEN, JUKKA. Importance of charge in nanofiltration. 2004. U.s. Diss.

191. VIHTONEN, TIINA. Tuote- vai liiketoimintaosaamista? Pienten ja keskisuurten leipomoalan yritysten strategiset valinnat, liikkeenjohdon käytännöt ja menestyminen. 2004. 238 s. Diss.

192. TURUNEN-SAARESTI, TEEMU. Computational and experimental analysis of flow field in the diffusers of centrifugal compressors. 2004. 103 s. Diss.

193. SOLEYMANI, AZITA. Advanced topics in deformation and flow of dense gas-particle mixtures. 2004. U.s. Diss.

194. SALLINEN, PETRI. Modeling dynamic behavior in tilting pad gas journal bearings. 2004. 157 s. Diss.

195. HEILMANN, PIA. Careers of managers, comparison between ICT and paper business sectors. 2004. 262 s. Diss.

196. AHMED, MOHAMMAD. Sliding mode control for switched mode power supplies. 2004. U.s. Diss.

197. HUPPUNEN, JUSSI. High-speed solid-rotor induction machine – electromagnetic calculation and design. 2004. 168 s. Diss.

198. SALMINEN, PIA. Fractional slot permanent magnet synchronous motors for low speed applications. 2004. 150 s. Diss.

199. VARIS, JARI. Partner selection in knowledge intensive firms. 2004. U.s. Diss.

200. PÖYHÖNEN, AINO. Modeling and measuring organizational renewal capability. 2004. U.s. Diss.

201. RATAMÄKI, KATJA. Product platform development from the product lines´ perspective: case of switching platform. 2004. 218 s. Diss.

202. VIRTANEN, PERTTU. Database rights in safe European home: the path to more rigorous protection of information. 2005. 425 s. Diss.

203. Säädöksiä, systematiikkaa vai ihmisoikeuksia? Oikeustieteen päivät 19. – 21.8.2003. Toim. Marjut Heikkilä. 2004. 350 s.

204. PANTSAR, HENRIKKI. Models for diode laser transformation hardening of steels. 2005. 134 s., liitt. Diss.

205. LOHJALA, JUHA. Haja-asutusalueiden sähkönjakelujärjestelmien kehittäminen – erityisesti 1000 V jakelujännitteen käyttömahdollisuudet. 2005. 201 s., liitt. Diss.

206. TARKIAINEN, ANTTI. Power quality improving with virtual flux-based voltage source line converter. 2005. U.s. Diss.

207. HEIKKINEN, KARI. Conceptualization of user-centric personalization management. 2005. 136 s. Diss.

208. PARVIAINEN, ASKO. Design of axial-flux permanent-magnet low-speed machines and performance comparison between radial-flux and axial-flux machines. 2005. 153 s. Diss.

209. FORSMAN, HELENA. Business development efforts and performance improvements in SMEs. Case study of business development projects implemented in SMEs. 2005. 209 s. Diss.

210. KOSONEN, LEENA. Vaarinpidosta virtuaaliaikaan. Sata vuotta suomalaista tilintarkastusta. 2005. 275 s. Diss.

211. 3rd Workshop on Applications of Wireless Communications. 2005. 62 s.

212. BERGMAN, JUKKA-PEKKA. Supporting knowledge creation and sharing in the early phases of the strategic innovation process. 2005. 180 s. Diss.

213. LAAKSONEN, PETTERI. Managing strategic change: new business models applying wireless technology as a source of competitive edge. 2005. 142 s. Diss.

214. OVASKA, PÄIVI. Studies on coordination of systems development process. 2005. U.s. Diss.

215. YANG, GUANGYU. Control and simulation of batch crystallization. 2005. U.s. Diss.

216. MUSTONEN–OLLILA, ERJA. Information system process innovation adoption, adaptation, learning, and unlearning: a longitudinal case study. 2005. U.s. Diss.

217. SAINIO, LIISA-MAIJA. The effects of potentially disruptive technology on business model – a case study of new technologies in ICT industry. 2005. 205 s. Diss.

218. SAINIO, TUOMO. Ion-exchange resins as stationary phase in reactive chromatography. 2005. 175 s. Diss.

219. CONN, STEFFEN. Software tools to support managers: development and application to new product development and strategic alliance management. 2005. 168 s. Diss.

220. TYNJÄLÄ, TERO. Theoretical and numerical study of thermomagnetic convection in magnetic fluids. 2005. U.s. Diss.

221. JANTUNEN, ARI. Dynamic capabilities and firm performance. 2005. 210 s. Diss.

222. KOLA-NYSTRÖM, SARI M. In search of corporate renewal: how to benefit from corporate venturing? 2005. 190 s. Diss.

223. SARÉN, HANNU. Analysis of the voltage source inverter with small DC-link capacitor. 2005. 143 s. Diss.

224. HUUHILO, TIINA. Fouling, prevention of fouling, and cleaning in filtration. 2005. U.s. Diss.

225. VILJAINEN, SATU. Regulation design in the electricity distribution sector – theory and practice. 2005. 132 s. Diss.

226. AVRAMENKO, YURY. Case-based design method for chemical product and process development. 2005. U.s. Diss.

227. JÄRVINEN, KIMMO. Development of filter media treatments for liquid filtration. 2005. U.s. Diss.

Appendix A

- Coefficient Matrixes for Polygonal Plates and Ellipse Membrane

Appendix A-Coefficient Matrixes for polygonal plates and ellipse membrane:

A-1: Coefficient matrix (23×23) of the second mode of vibration in pentagonal membrane:

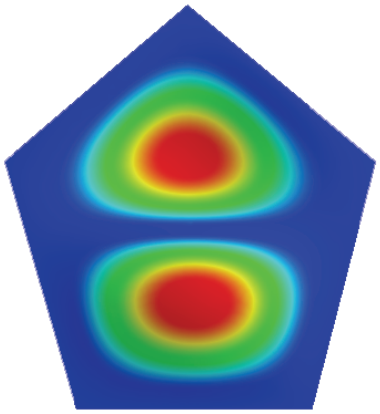

Columns 1 to 5:

-0.0298325805742934	-2.26903526733915	0.245778323525883	9.06371555368329	-0.411679983840713
-2.26903526733915	9.06371555368329	-12.9598281733475	10.536505358196	-10.8200770555827
0.245778323525883	-12.9598281733475	-5.11048820372541	10.3203614568399	0.682570367610922
9.06371555368329	10.536505358196	10.3203614568399	1.76283421347828	0.0885474991006234
-0.411679983840713	-10.8200770555827	0.682570367610922	0.0885474991006234	-0.00101420729348423
-12.9598281733475	10.3203614568399	-0.442129308011297	0.000641744231178118	8.82004474829322e-005
2.04243062216511	-5.249867416018 59	0.00289320763445802	-0.000134587700444392	-6.72091727400867e-008
10.536505358196	1.76283421347828	0.000641744231178118	-2.31679540308238e-005	-1.38416319112538e-008
-5.11048820372541	-0.442129308011297	-0.00303709400229531	-7.751241582745 2e-007	0
-10.8200770555827	0.0885474991006234	8.82004474829322e-005	-1.38416319112538e-008	-27.950038035178
4.24427184422603	-0.0147651603222589	5.55731087639733e-006	0	-21.0753418508962
10.3203614568399	0.000641744231178118	-7.751241582745 2e-007	10.7254637678376	5.24986753411008
-1.54742479433569	-0.00117542062138237	0	17.8267015564097	-0.00612937205692415
-5.24986741601859	-0.000134587700444392	0	9.95156097988303	-0.0363106527610253
0.682570367610922	8.82004474829322e-005	0	5.24986753411008	-0.00186405931439875
1.76283421347828	-2.31679540308238e-005	10.7254637678376	0.442129308014262	0.000647106701704178
-0.10123347815059	4.64983295720882e-006	-18.5916332053422	0.0147651603222589	0
-0.442129308011297	-7.751241582745 2e-007	-1.93047965855039	0.0779417043005426	-2.13990258752451e-008
0.0014342032774043	1.10733016846254e-007	-4.90763640129965	0.0129429334026938	2.99410029740943
0.0885474991006234	-1.38416319112538e-008	5.24986753411008	0.000647106701704178	1.00711647497254
0.00289320763445802	0	0.143489997886254	1.54072986368045e-005	-1.12187433104582
-0.0147651603222589	0	-0.0885474991006334	2.13990258752539e-007	-0.221064654008659
-0.000825919084880558	0	0.000783235732361492	0	-0.00040668010102533

Columns 6 to 10:

-12.9598281733475	2.04243062216511	10.536505358196	-5.11048820372541	-10.8200770555827
10.3203614568399	-5.24986741601859	1.76283421347828	-0.442129308011297	0.0885474991006234
-0.442129308011297	0.00289320763445802	0.000641744231178118	-0.00303709400229531	8.82004474829322e-005
0.000641744231178118	-0.000134587700444392	-2.31679540308238e-005	-7.751241582745 2e-007	-1.38416319112538e-008
8.82004474829322e-005	-6.72091727400867e-008	-1.38416319112538e-008	0	-27.950038035178
-7.751241582745 2e-007	0	10.7254637678376	-1.93047965855039	5.24986753411008
0	-1.04281115867889	9.95156097988303	0.143489997886254	-0.0363106527610253
10.7254637678376	9.95156097988303	0.442129308014262	0.0779417043005426	0.000647106701704178
-1.93047965855039	0.143489997886254	0.0779417043005426	1.39479163041643e-008	-2.13990258752451e-008
5.24986753411008	-0.0363106527610253	0.000647106701704178	-2.13990258752451e-008	1.00711647497254
-0.0885474991006334	6.64107421286881e-005	2.13990258752539e-007	-112.966656493712	-0.221064654008659
0.0779417043005426	1.54072986368045e-005	26.9853374102005	0.881417107446142	0.374554707257854
-0.00323554704364676	0	5.16019655974756	0.00556340368255944	-0.000148632342630425
1.54072986368045e-005	-10.1180182976644	0.0442737495503217	-0.00624255839842576	10.1163641511365
-2.13990258752451e-008	-1.12187433104582	0.374554707257854	0	-1.72006613178032
26.9853374102005	0.0442737495503217	0.00104042639847097	3.47645607507119	0.00246086005370983
-4.97654536121107	-0.00185242580209939	2.06433809208463e-007	-0.0906557357092679	-0.102892142057062
0.881417107446142	-0.00624255839842576	3.47645607507119	-1.45829453945763	6.8050358492064e-006
-0.00738258016112947	0	0.874779748891581	0	-0.872562732691064
0.374554707257854	10.1163641511365	0.00246086005370983	6.8050358492064e-006	0.0734514256274167
-0.00624255839842576	-20.1335663241028	0.411568569115424	34.6769462200093	-3.46268035313086
1.8579042828763e-005	-0.293805702506827	0.000489962581142869	-0.218744487355463	0.00480927826160246
-1.87667099280421e-008	0.000140570611504795	6.18639622655128e-008	-3.56819462285717e-005	-8.67474433910973e-008

Columns 11 to 15:

4.24427184422603	10.3203614568399	-1.54742479433569	-5.24986741601859	0.682570367610922
-0.0147651603222589	0.000641744231178118	-0.00117542062138237	-0.000134587700444392	8.82004474829322e-005
5.55731087639733e-006	-7.751241582745 2e-007	0	0	0
0	10.7254637678376	17.8267015564097	9.95156097988303	5.24986753411008
-21.0753418508962	5.24986753411008	-0.00612937205692415	-0.0363106527610253	-0.00186405931439875
-0.0885474991006334	0.0779417043005426	-0.00323554704364676	1.54072986368045e-005	-2.13990258752451e-008
6.64107421286881e-005	1.54072986368045e-005	0	-10.1180182976644	-1.12187433104582
2.13990258752539e-007	26.9853374102005	5.16019655974756	0.0442737495503217	0.374554707257854
-112.966656493712	0.881417107446142	0.00556340368255944	-0.00624255839842576	0
-0.221064654008659	0.374554707257854	-0.000148632342630425	10.1163641511365	-1.72006613178032
-0.110080960607358	1.8579042828763e-005	-97.3221110096265	-0.293805702506827	6.58567653525284e-005
1.8579042828763e-005	3.47645607507119	0.0736882180029886	0.411568569115424	6.8050358492064e-006
-97.3221110096265	0.0736882180029886	1.30849428991454e-007	-6.8050358492064e-007	-0.808932494040337
-0.293805702506827	0.411568569115424	-6.80503584920064e-007	0.430016551047416	-3.46268035313086
6.58567653525284e-005	6.80503584920064e-006	-0.808932494040337	-3.46268035313086	0
0.000489962581142869	0.0848445736474173	2.67078427654243	8.58799689571863e-005	0.0829456081812169
-17.7728431339459	0.00368947912919357	0	-0.0169706673440126	-6.61599743003903e-008
-0.218744487355463	0.14427834784831	-0.531627983071601	0.000123043002685491	-5.82734530799183e-005
5.46498141370404e-006	9.54221877302071e-007	0.000307195549603726	-0.00326331337247543	0.625791031805781
0.00480927826160246	0.0829456081812169	0.391597604697172	0.0886158286760966	0.999249111887535
-17.8961666401893	0.000123043002685491	0	-0.000614068483358343	0
-0.0860033105056952	0.0195798802348526	-0.0138242683304954	0.0416353796619574	-0.000404066339453853
7.42449417267194e-006	5.88620738180993e-008	-1.44680669603033e-006	-2.50332970550489e-008	2.8948810521168e-007

Columns 16 to 20:

1.76283421347828	-0.10123347815059	-0.442129308011297	0.0014342032774043	0.0885474991006234
-2.31679540308238e-005	4.64983295720882e-006	-7.7512415827452e-007	1.10733016846254e-007	-1.38416319112538e-008
10.7254637678376	-18.5916332053422	-1.93047965855039	-4.90763640129965	5.24986753411008
0.442129308014262	0.0147651603222589	0.0779417043005426	0.0129429334026938	0.000647106701704178
0.000647106701704178	0	-2.13990258752451e-008	2.99410029740943	1.00711647497254
26.9853374102005	-4.97654536121107	0.881417107446142	-0.00738258016112947	0.374554707257854
0.0442737495503217	-0.00185242580209939	-0.00624255839842576	0	10.1163641511365
0.00104042639847097	2.06433809208463e-007	3.47645607507119	0.874977948891581	0.00246086005370983
3.47645607507119	-0.0906557357092679	-1.45829453945763	0	6.8050358492064e-006
0.00246086005370983	-0.102892142057062	6.8050358492064e-006	-0.872562732691064	0.0734514256274167
0.000489962581142869	-17.7728431339459	-0.218744487355463	5.46498141370404e-006	0.00489278261602 46
0.0848445736474173	0.00368947912919357	0.14427834784831	9.54221877302071e-007	0.0829456081812169
2.67078427654243	0	-0.531627983071601	0.000307195549603726	0.391597604697172
8.58799689571863e-005	-0.0169706673440126	0.000123043002685491	-0.00326331337247543	0.0886158286760966
0.0829456081812169	-6.61599743003903e-008	-5.82734530799183e-005	0.625791031805781	0.999249111887535
2.34958562822574	6.47482811999093e-006	0.014333885087363	0.499624555943512	2.75366267605538e-007
6.47482811999093e-006	0.0144659025834545	-0.16654151864783	-5.01416000192573	8.77240690511919e-005
0.014333885087363	-0.16654151864783	0.0131453543754841	-1.75689482342551e-005	6.04785999434745e-005
0.499624555943512	-5.01416000192573	-1.75689482342551e-005	0	0.000255962233705798
2.75366267605538e-007	8.77240690511919e-005	6.04785999434745e-005	0.000255962233705798	0.0030025111571022
0.00104164041603262	0	-0.000246861934757936	0	5.77308093848602e-005
0.0508020239525186	-0.000519577283425701	0.0360301338852264	-0.000175826312582042	0.0138689497804205
0	-5.82607928750613e-008	0	1.09508756565383e-008	0

Columns 21 to 23:

0.00289320763445802	-0.0147651603222589	-0.000825919084880558
0	0	0
0.143489997886254	-0.0885474991006334	0.000783235732361492
1.54072986368045e-005	2.13990258752539e-007	0
-1.12187433104582	-0.221064654008659	-0.00040668010102533
-0.00624255839842576	1.8579042828763e-005	-1.87667099280421e-008
-20.1335663241028	-0.293805702506827	0.000140570611504795
0.411568569115424	0.000489962581142869	6.18639622655128e-008
34.6769462200093	-0.218744487355463	-3.56819462285717e-005
-3.46268035313086	0.00480927826160246	-8.67474433910973e-008
-17.8961666401893	-0.0860033105056952	7.42449417267194e-006
0.000123043002685491	0.0195798802348526	5.88620738180993e-008
0	-0.0138242683304954	-1.44680669603033e-006
-0.000614068483358343	0.0416353796619574	-2.50332970550489e-008
0	-0.000404066339453853	2.8948810521168e-007
0.00104164041603262	0.0508020239525186	0
0	-0.000519577283425701	-5.82607928750613e-008
-0.000246861934757936	0.0360301338852264	0
0	-0.000175826312582042	1.09508756565383e-008
5.77308093848602e-005	0.0138689497804205	0
0	-1.82574649501461e-005	0
-1.82574649501461e-005	0.0224765984137422	0
0	0	0

A-2: Coefficient matrix (23×23) of the third mode of vibration in pentagonal membrane:

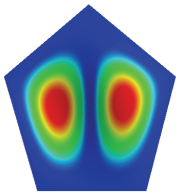

Columns 1 to 5:

-0.0317322388291359	-2.29372749532922	0.29257794842124	9.7940063861206	-0.557980862446129
-2.29372749532922	9.7940063861206	-20.4053812795514	48.1370957637457	-114.20198861446
0.29257794842124	-20.4053812795514	9.19599066949013	164.658223207233	-63.9986477765195
9.7940063861206	48.1370957637457	164.658223207233	41.3825116579864	2.12953643603054
-0.557980862446129	-114.20198861446	-63.9986477765195	2.12953643603054	-0.619253534110612
-20.4053812795514	164.658223207233	-10.5223124833524	2.56621074676514	-4.35890688511206
0.4595900664717 19	-121.539254142259	0.5089449013392	13.4419670980446	0.545761520952394
48.1370957637457	41.3825116579864	2.56621074676514	-2.64516245436871	-0.00313931534699742
9.19599066949013	-10.5223124833524	3.75648286906653	-0.175363767352269	-2.22852033692585e-005
-114.20198861446	2.12953643603054	-4.35890688511206	-0.00313931534699742	-35.2212696341066
-44.9243234460025	-0.358007335769051	-2.9786987 6586008	-3.48814483766786e-005	-63.7336242531592
164.658223207233	2.56621074676514	-0.175363767352269	11.1304723858484	121.095785185308
81.4937471461373	-10.33935611477 86	0.0130128040606073	59.7956549231708	3.66617984826073
-121.539254142259	13.4419670980446	0.00034881447416453 1	235.458651759263	-12.5444205403328
-63.9986477765195	-4.35890688511206	-2.22852033692585e-005	121.095785185308	-24.8311366975728
41.3825116579864	-2.64516245436871	11.1304723858484	10.5223047193383	-2.60289031840716
17.851502132966	1.04478919290187	3.54001776420046	0.358007335714998	-0.0130126631037637
-10.5223124833524	-0.175363767352269	-127.297950193508	35.3702507433545	8.67279052716532e-005
-3.42382275788188	0.0251140185383792	200.070398329954	-2.16772898650111	27.2653940200107
2.12953643603054	-0.00313931534699742	121.095785185308	-2.60289031840716	79.1636489969903
0.5089449013392	0.00034881447416453 1	-20.0807349045517	-0.0624428619574453	77.8109761257656
-0.358007335769051	-3.48814483766786e-005	-2.1295364587223	-0.000867279030539921	-5.26115235969962
-0.0623378926932552	3.17104077707231e-006	0.0645354325126114	-7.88435502558538e-006	-0.0317878456286227

Columns 6 to 10:

-20.4053812795514	0.459590066471719	48.1370957637457	9.19599066949013	-114.20198861446
164.658223207233	-121.539254142259	41.3825116579864	-10.5223124833524	2.12953643603054
-10.5223124833524	0.5089449013392	2.56621074676514	3.75648286906653	-4.35890688511206
2.56621074676514	13.4419670980446	-2.64516245436871	-0.175363767352269	-0.00313931534699742
-4.35890688511206	0.545761520952394	-0.00313931534699742	-2.22852033692585e-005	-35.2212696341066
-0.175363767352269	0.00034881447416453 1	11.1304723858484	-127.297950193508	121.095785185308
0.00034881447416453 1	-4.0846547819674	235.458651759263	-20.0807349045517	-12.5444205403328
11.1304723858484	235.458651759263	10.5223047193383	35.3702507433545	-2.60289031840716
-127.297950193508	-20.0807349045517	35.3702507433545	-0.54248788750002	8.67279052716532e-005
121.095785185308	-12.5444205403328	-2.60289031840716	8.67279052716532e-005	79.1636489969903
-2.1295364587223	7.46766890340196	-0.000867279030539921	420.11832079728 9	-5.26115235969962
35.3702507433545	-0.0624428619574453	53.6692410017986	20.6923115105021	-13.3811829550268
12.8566773804522	2.22852033793827e-005	116.913364928534	-1.56520100952878	0.0537042153683564
-0.0624428619574453	-87.3402260999129	1.06476822936371	2.25469504450276	17.0696537213227
8.67279052716532e-005	77.8109761257656	-13.3811829550268	9.03669411531524e-005	-38.9711446088109
53.6692410017986	1.06476822936371	-0.375907979438395	115.814059651304	0.0596678892858341
-117.751949870391	-31.6268259721608	-7.45892600323438e-005	9.42321946442038	3.07816082543433
20.6923115105021	2.25469504450276	115.814059651304	7.63416726345895	-0.000203633001554393
-0.179003667857499	-0.00100283408736231	20.1826365543528	0.561460801957627	-30.0781887115 71
-13.3811829550268	17.0696537213227	0.0596678892858341	-0.000203633001554393	1.72435929368845
2.25469504450276	772.660208279219	-12.1384489517928	-339.447932810546	160.945778743825
-0.00671303272176646	-6.89743717110308	-0.0146615723899559	-5.04565919507288	-0.223790323479141
6.78084182179008e-006	0.0102269694745028	-1.85120910564083e-006	-0.00248719686980808	4.0366222399079e-006

Columns 11 to 15:

-44.9243234460025	164.658223207233	81.4937471461373	-121.539254142259	-63.9986477765195
-0.358007335769051	2.56621074676514	-10.33935611147786	13.4419670980446	-4.35890688511206
-2.97869876586008	-0.175363767352269	0.0130128040606073	0.000348814474164531	-2.22852033692585e-005
-3.488144837667 86e-005	11.1304723858484	59.7956549231708	235.458651759263	121.095785185308
-63.7336242531592	121.095785185308	3.66617984826073	-12.5444205403328	-24.8311366975728
-2.12953645872 23	35.3702507433545	12.8566773804522	-0.0624428619574453	8.67279052716532e-005
7.46766890340196	-0.0624428619574453	2.228520337938 27e-005	-87.3402260999129	77.8109761257656
-0.000867279030539921	53.6692410017986	116.913364928534	1.06476822936371	-13.3811829550268
420.118320797289	20.6923115105021	-1.56520100952878	2.25469504450276	9.03669411531524e-005
-5.26115235969962	-13.381182955026 8	0.0537042153683564	17.0696537213227	-38.9711446088109
23.2907489601572	-0.0067130327217 6646	420.066624621607	-6.89743717110308	7.46766890340196
-0.0067130327217 6646	115.814059651304	1.75371745335462	-12.1384489517928	-0.000203633001554393
-420.066624621607	1.75371745335462	-1.76187122925298	2.03633001620212e-005	58.1803861650667
-6.89743717110308	-12.1384489517928	2.03633001620212e-005	9.74280753369627	160.945778743825
7.46766890340196	-0.000203633001554393	58.1803861650667	160.945778743825	-8.35695126359283e-005
-0.0146615723899559	6.72910241165779	-62.196798481571	-0.0039962560170922	1.96565228644932
-125.60708988646	0.0887306857803253	-0.00467989099839426	-1.34607578664323	0.673156814614774
-5.04565919507288	-6.71360550965205	-9.29139714654146	0.00298339446429171	0.00389967785241176
-2.97462468701935	-4.44028446389824e-005	-0.133881677415405	0.218381959715177	1.53442076851452
-0.223790323479141	1.96565228644932	-26.2057979603184	1.55620580626663	-80.496027281384
-99.1010325208995	0.00298339446429171	-1.50611568628 76e-006	-0.0146143121113474	1.80733882353782e-005
-1.94856155776751	-1.31029174563546	-0.327608885636589	-3.33979861065442	-0.0320528915175351
0.000502192488417054	-3.93906853779027e-006	-8.98102624897416e-005	2.00805592811462e-006	1.47578997299118e-005

Columns 16 to 20:

41.3825116579864	17.851502132966	-10.5223124833524	-3.42382275788188	2.12953643603054
-2.64516245436871	1.04478919290187	-0.175363767352269	0.0251140185383792	-0.00313931534699742
11.1304723858484	3.54001776420046	-127.297950193508	200.070398329954	121.095785185308
10.5223047193383	0.358007335714998	35.3702507433545	-2.16772898650111	-2.60289031840716
-2.60289031840716	-0.0130126631037637	8.67279052716532e-005	27.2653940200107	79.1636489969903
53.6692410017986	-117.751949870391	20.6923115105021	-0.179003667857499	-13.3811829550268
1.06476822936371	-31.6268259721608	2.25469504450276	-0.00100283408736231	17.0696537213227
-0.375907979438395	-7.45892600323438e-005	115.814059651304	20.1826365543528	0.0596678892858341
115.814059651304	9.42321946442038	7.63416726345895	0.561460801957627	-0.000203633001554393
0.0596678892858341	3.07816082543433	-0.000203633001554393	-30.078188711571	1.72435929368845
-0.0146615723899559	-125.60708988646	-5.04565919507288	-2.97462468701935	-0.223790323479141
6.72910241165779	0.0887306857803253	-6.71360550965205	-4.44028446389824e-005	1.96565228644932
-62.196798481571	-0.00467989099839426	-9.29139714654146	-0.133881677415405	-26.2057979603184
-0.0039962560170922	-1.34607578664323	0.00298339446429171	0.218381959715177	1.55620580626663
1.96565228644932	0.673156814614774	0.00389967785241176	1.53442076851452	-80.496027281384
-157.231400461566	-0.000433297539156917	0.324760264560417	-40.0775762299107	-2.20886152092608e-005
-0.000433297539156917	0.314796549407164	13.3591943435011	-96.8970152309362	0.00208775887304963
0.324760264560417	13.3591943435011	0.085203327642235	-0.000422527075144407	-0.00538832461186882
-40.0775762299107	-96.8970152309362	-0.000422527075144407	-2.5819126050625e-006	0.00579929043949826
-2.20886152092608e-005	0.00208775887304963	-0.00538832461186882	0.00579929043949826	-0.286285781444259
0.0240269486457767	-0.000108443929306991	-0.00585015922228098	0.000271100823283716	0.00201442667822259
-4.52619267238154	-0.0181298385642964	-3.43542937716494	-0.00308788632648811	-1.38637497856831
-6.80344016650108e-007	-2.25184429162064e-006	1.72129498222984e-007	3.17418387771349e-007	-3.47316162260167e-008

Columns 21 to 23:

0.5089449013392	-0.358007335769051	-0.0623378926932552
0.000348814474164531	-3.488144837667 86e-005	3.17104077707231e-006
-20.0807349045517	-2.12953645872 23	0.0645354325126114
-0.0624428619574453	-0.000867279030539921	-7.88435502558538e-006
77.8109761257656	-5.26115235969962	-0.0317878456286227
2.25469504450276	-0.0067130327217 6646	6.78084182179008e-006
772.660208279219	-6.89743717110308	0.0102269694745028
-12.1384489517928	-0.0146615723899559	-1.85120910564083e-006
-339.447932810546	-5.04565919507288	-0.00248719686980808
160.945778743825	-0.223790323479141	4.03662223990 79e-006
-99.1010325208995	-1.94856155776751	0.000502192488417054
0.00298339446429171	-1.31029174563546	-3.93906853779027e-006
-1.50611568628 76e-006	-0.327608885636589	-8.98102624897416e-005
-0.0146143121113474	-3.33979861065442	2.00805592811462e-006
1.80733882353782e-005	-0.0320528915175351	1.47578997299118e-005
0.0240269486457767	-4.52619267238154	-6.80344016650108e-007
-0.000108443929306991	-0.0181298385642964	-2.25184429162064e-006
-0.00585015922228098	-3.43542937716494	1.72129498222984e-007
0.000271100823283716	-0.00308788632648811	3.17418387771349e-007
0.00201442667822259	-1.38637497856831	-3.47316162260167e-008
-0.000180733879890986	-0.000118339803548655	-4.09845140061246e-008
-0.000118339803548655	-0.232622017355663	0
-4.09845140061246e-008	0	0

A-3: Coefficient matrix (25×25) of the fourth mode of vibration in pentagonal membrane:

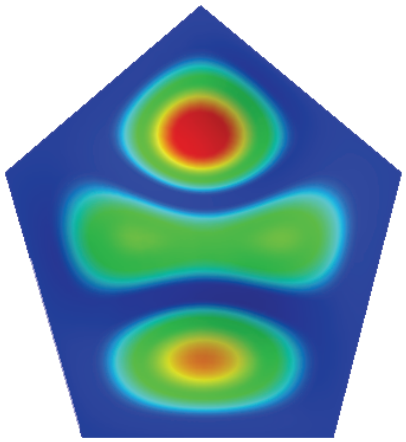

Columns 1 to 5:

-0.270735956728458	0.212831715655739	9.46494770236313	-2.97975607027661	-39.0172090143897
0.212831715655739	-2.97975607027661	9.19523407576683	-12.7982621401479	-9.01397091682901
9.46494770236313	9.19523407576683	-32.4310524736236	71.9142038764538	-246.097246186859
-2.97975607027661	-12.7982621401479	71.9142038764538	86.7770396441812	9.55338971312435
-39.0172090143897	-9.01397091682901	-246.097246186859	9.55338971312435	0.765423496154554
9.19523407576683	71.9142038764538	-34.5186548255476	0.357237786375023	-0.0657859096783291
62.8665545009499	-115.664687593545	19.4723494571167	0.0334882397564513	-1.23940385406739
-12.7982621401479	86.7770396441812	0.357237786375023	-0.0105264415815387	-0.00133146540602352
-32.4310524736236	-34.5186548255476	0.0562635002861498	-0.0554867503518 45	0.000163121945824191
-9.01397091682901	9.55338971312435	-0.0657859096783291	-0.00133146540602352	0
-67.6970348005918	-2.04326107286382	1.17947413481638	-1.84929515563 23e-005	143.021818788373
71.9142038764538	0.357237786375023	-0.0554867503518 45	-1.68117745890 91e-007	-146.465242108209
197.648309241822	-0.00332086188740277	-0.0755041494358102	2.12021650150359	227.901407367311
-115.664687593545	0.0334882397564513	5.15721859932178e-005	-5.92902382740685	-9.55338965788547
-246.097246186859	-0.0657859096783291	0.000163121945824191	-146.465242108209	-0.76533260626674
86.7770396441812	-0.0105264415815387	-1.68117745890 91e-007	116.403014647947	1.02260979270945
168.890182104012	0.0941466870326722	-1.65416547190398	34.5186717286386	3.18503169278454
-34.5186548255476	-0.0554867503518 45	5.36818877809321	2.04326107300919	-0.00165090699400334
-68.2705749650824	0.00288935878370837	-236.450106484663	0.0557282593578705	-0.00016312174083800 1
9.55338971312435	-0.00133146540602352	-146.465242108209	1.02260979270945	2.86508875639442e-008
19.4723494571167	5.15721859932178e-005	-109.216862957537	0.566439393676171	-133.650195520604
-2.04326107286382	-1.84929515563 23e-005	-86.7729829000512	0.0190602482372001	73.2346436876949
-4.27784692763312	5.73023779040417e-007	67.9994113818161	0.000340372526515271	-110.969384817897
0.357237786375023	-1.68117745890 91e-007	2.04326107300919	3.78191715825648e-006	4.77669482894273
0.765423496154554	0	-0.76533260626674	2.86508875639442e-008	0.382682548166396

Columns 6 to 10:

9.19523407576683	62.8665545009499	-12.7982621401479	-32.4310524736236	-9.01397091682901
71.9142038764538	-115.664687593545	86.7770396441812	-34.5186548255476	9.55338971312435
-34.5186548255476	19.4723494571167	0.357237786375023	0.0562635002861498	-0.0657859096783291
0.357237786375023	0.0334882397564513	-0.0105264415815387	-0.0554867503518 45	-0.00133146540602352
-0.0657859096783291	-1.23940385406739	-0.00133146540602352	0.000163121945824191	0
-0.0554867503518 45	5.15721859932178e-005	-1.68117745890 91e-007	5.36818877809321	-146.465242108209
5.15721859932178e-005	1.48292540080926e-006	-5.92902382740685	-109.216862957537	-9.55338965788547
-1.68117745890 91e-007	-5.92902382740685	116.403014647947	2.04326107300919	1.02260979270945
5.36818877809321	-109.216862957537	2.04326107300919	4.17585803747301	-0.00165090699400334
-146.465242108209	-9.55338965788547	1.02260979270945	-0.00165090699400334	2.86508875639442e-008
-86.7729829000512	-0.270425148325103	0.0190602482372001	-1.48292540537 61e-006	73.2346436876949
2.04326107300919	0.566439393676171	3.78191715825648e-006	-30.0137025426996	4.77669482894273
-0.337607392209499	-0.0117456321952389	-40.8771591124348	83.7664056046053	-1.85111514255139
0.566439393676171	-2.08448529792437e-007	-12.7725353015372	-0.594500567207671	-4.08568570128313e-005
-0.00165090699400334	-133.650195520604	4.77669482894273	-1.23071946907753	0
3.78191715825648e-006	-12.7725353015372	1.351771111157314	-5.67462829409324e-007	-24.408607111113
-8.96350010555329	-33.9490842492477	-0.00170823711127575	50.6183564047678	-1.59223160964756
-30.0137025426996	-0.594500567207671	-5.67462829409324e-007	4.25754630109097	2.82025178165584
-58.2015072312334	9.32055937617942	11.2103617193454	-3.24544676076524	-0.000886359169207517
4.77669482894273	-4.08568570128313e-005	-24.408607111113	2.82025178165584	1.18258416978 93e-008
-0.594500567207671	-7.4696071088 43e-006	5.75311195477839	0.0125517312017104	6.10212394090142
-0.0125750060195263	83.732723686094 1	3.15171476656324	-1.11914038532978e-007	0.398057902411889
-0.00405592051857038	-32.4368349802507	0.236012400731453	-161.585399003325	-5.56707885085509
-5.67462829409324e-007	5.75311195477839	0.000140490999326466	3.6155409537541	0.00214125164079761
0	-0.127577982865855	1.1825841697893e-008	0.031894807461712 6	-2.32436751144712e-008

Columns 11 to 15:

-67.6970348005918	71.9142038764538	197.648309241822	-115.664687593545	-246.097246186859
-2.04326107286382	0.357237786375023	-0.00332086188740277	0.0334882397564513	-0.0657859096783291
1.17947413481638	-0.0554867503518 45	-0.0755041494358102	5.15721859932178e-005	0.000163121945824191
-1.84929515563 23e-005	-1.68117745890 91e-007	2.12021650150359	-5.92902382740685	-146.465242108209
143.021818788373	-146.465242108209	227.901407367311	-9.55338965788547	-0.76533260626674
-86.7729829000512	2.04326107300919	-0.337607392209499	0.566439393676171	-0.00165090699400334
-0.270425148325103	0.566439393676171	-0.0117456321952389	-2.08448529792437e-007	-133.650195520604
0.0190602482372001	3.78191715825648e-006	-40.8771591124348	-12.7725353015372	4.77669482894273
-1.48292540537 61e-006	-30.0137025426996	83.7664056046053	-0.594500567207671	-1.23071946907753
73.2346436876949	4.77669482894273	-1.85111514255139	-4.08568570128313e-005	0
9.73047706369428	-0.0125750060195263	-0.000672268278972486	83.732723686094 1	37.2030012784174
-0.0125750060195263	-5.67462829409324e-007	1.44028030301508	5.75311195477839	2.82025178165584
-0.000672268278972486	1.44028030301508	11.3162501627647	-0.743768821453767	-2.718696632063 74e-005
83.7327236860941	5.75311195477839	-0.743768821453767	1.56101110412141e-006	6.10212394090142
37.2030012784174	2.82025178165584	-2.718696632063 74e-005	6.10212394090142	0.0318948074617126
3.15171476656324	0.000140490999326466	-2.54762146209086	0.0148849077656129	0.00214125164079761
-0.0822707940341972	-21.6313147371604	0.811326037371795	-0.0154635522061353	-233.763264674457
-1.11914038532978e-007	3.6155409537541	-0.463906779268671	1.24814157716359	-0.0796115804823778
-17.3698928404893	10.7932528172102	-6.22467269894298e-007	-0.723108190749792	0.0188299895262504
0.398057902411889	0.00214125164079761	-1.22042261364454	7.8216482411327	3.26581389520389e-008
-1.23071946907753	1.24814157716359	0.0356135929595359	-4.28947298796632e-005	-0.43044492995921
-0.000276134860360695	0.970025133608894	-0.129713663101414	-0.0849423317360256	-5.50804928247689
712.682037423333	13.4181222221101	-1.23577117016 15e-008	-0.00283786260140165	2.26558047842835e-007
0.970025133608894	0.0217268066817267	-0.0354795688897214	0.0916788830397236	-0.0290576799980584
-0.00638046390523036	3.26581389520389e-008	0.00106473189852521	-2.29980412035955e-008	-0.000152480926323365

Columns 16 to 20:

86.7770396441812	168.890182104012	-34.5186548255476	-68.2705749650824	9.55338971312435
-0.0105264415815387	0.0941466870326722	-0.0554867503518 45	0.00288935878370837	-0.00133146540602352
-1.68117745890 91e-007	-1.65416547190398	5.36818877809321	-236.450106484663	-146.465242108209
116.403014647947	34.5186717286386	2.04326107300919	0.0557282593578705	1.02260979270945
1.02260979270945	3.18503169278454	-0.00165090699400334	-0.00016312174083800 1	2.86508875639442e-008
3.78191715825648e-006	-8.96350010555329	-30.0137025426996	-58.2015072312334	4.77669482894273
-12.7725353015372	-33.9490842492477	-0.594500567207671	9.32055937617942	-4.08568570128313e-005
1.351771111157314	-0.00170823711127575	-5.67462829409324e-007	11.2103617193454	-24.408607111113
-5.67462829409324e-007	50.6183564047678	4.25754630109097	-3.24544676076524	2.82025178165584
-24.408607111113	-1.59223160964756	2.82025178165584	-0.000886359169207517	1.18258416978 93e-008
3.15171476656324	-0.0822707940341972	-1.11914038532978e-007	-17.3698928404893	0.398057902411889
0.000140490999326466	-21.6313147371604	3.6155409537541	10.7932528172102	0.00214125164079761
-2.54762146209086	0.811326037371795	-0.463906779268671	-6.22467269894298e-007	-1.22042261364454
0.0148849077656129	-0.0154635522061353	1.24814157716359	-0.723108190749792	7.8216482411327
0.00214125164079761	-233.763264674457	-0.0796115804823778	0.0188299895262504	3.26581389520389e-008
0.0838560877549242	0.0170271756084099	0.0217268066817267	-0.729182650846 59	0.0132685967470 63
0.0170271756084099	0.000627444842606687	-0.0139879624268097	-0.00594985344168474	0.00218283054855496
0.0217268066817267	-0.0139879624268097	0.000496163592187095	-0.000273216729498715	-0.0290576799980584
-0.729182650846 59	-0.00594985344168474	-0.000273216729498715	2.18317824974796	2.40945565775166
0.0132685967470 63	0.00218283054855496	-0.0290576799980584	2.40945565775166	1.00603240483429e-008
0.0916788830397236	46.8607720851813	-4.81655823710162	0	0.000236939227626124
0.0298463341466775	-7.0880513169585e-005	1.32796277438126e-006	-0.000856117850413498	0.000297572640884422
0.00684894280330799	-2.33031134803363e-006	-0.00288697956432594	1.22341347859679e-005	-0.000403578888817588
0.200787971486352	-0.00151682880079346	0.249961018342943	2.77585760666391e-005	0.179999814217366
1.00603240483429e-008	1.90896250532987e-005	0	-2.10715043682215e-006	0

Columns 21 to 25:

19.4723494571167	-2.04326107286382	-4.27784692763312	0.357237786375023	0.765423496154554
5.15721859932178e-005	-1.84929515563323e-005	5.73023779040417e-007	-1.68117745899091e-007	0
-109.216862957537	-86.7729829000512	67.9994113818161	2.04326107300919	-0.76533260626674
0.566439393676171	0.0190602482372001	0.000340372526515271	3.78191715825648e-006	2.86508875639442e-008
-133.650195520604	73.2346436876949	-110.969384817897	4.77669482894273	0.382682548166396
-0.594500567207671	-0.0125750060195263	-0.00405592051857038	-5.67462829409324e-007	0
-7.469607108843e-006	83.7327236860941	-32.4368349802507	5.75311195477839	-0.127577982865855
5.75311195477839	3.15171476656324	0.236012400731453	0.000140490999326466	1.182584169789 3e-008
0.0125517312017104	-1.11914038532978e-007	-161.585399003325	3.615540953754 1	0.0318948074617126
6.10212394090142	0.398057902411889	-5.56707885085509	0.00214125164079761	-2.32436751144712e-008
-1.23071946907753	-0.000276134860360695	712.682037423333	0.970025133608894	-0.00638046390523036
1.248141577716359	0.970025133608894	13.4181222221101	0.0217268066817267	3.26581389520389e-008
0.0356135929595359	-0.129713663101414	-1.23577117016 15e-008	-0.0354795688897214	0.0010647318985 2521
-4.28947298796632e-005	-0.0849423317360256	-0.00283786260140165	0.0916788830397236	-2.299804120359 55e-008
-0.43044492995921	-5.50804928247689	2.26558047842835e-007	-0.0290576799980584	-0.000152480926323365
0.0916788830397236	0.0298463341466775	0.00684894280330799	0.2007879714863 52	1.0060324048342 9e-008
46.8607720851813	-7.0880513169585e-005	-2.33031134803363e-006	-0.00151682880079346	1.9089625053298 7e-005
-4.81655823710162	1.32796277438126e-006	-0.00288697956432594	0.2499610183429 43	0
0	-0.00085611785041349	1.22341347859679e-005	2.77585760666391e-005	-2.10715043682215e-006
0.000236939227626124	0.00029757264088442 2	-0.00040357888881758 8	0.1799998142173 66	0
2.91288918647196e-007	7.03959700510031e-005	-2.71869663206374e-005	-0.00014468507999896	2.04263881691225e-007
7.03959700510031e-005	0.0149999845181139	-2.77585761511827e-006	0.0700820591692827	0
-2.71869663206374e-005	-2.77585761511827e-006	1.63121786649532e-005	3.76851903649183e-006	-1.69704769053049e-008
-0.00014468507999896	0.0700820591692827	3.76851903649183e-006	0.0114616407102527	0
2.04263881691225e-007	0	-1.69704769053049e-008	0	0

A-4: Coefficient matrix (25×25) of the fifth mode of vibration in pentagonal membrane:

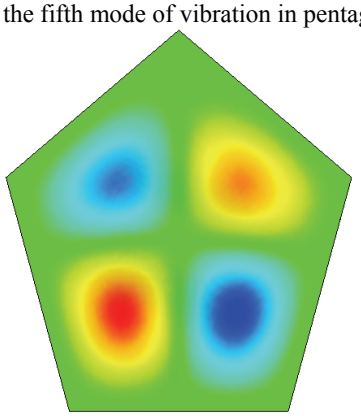

Columns 1 to 5:

0.0010269561316818	-0.00610820662222977	-0.0363372508436441	0.0539020974829327	-0.0223035155795515
0.267011200776324	13.5159806311131	1.44517275581893	-62.4861420067027	-4.07837691545137
0.00668590143322945	0.0061174715647212	0.519883525557816	0.133608982017904	-1.52872977871448
-3.10602160432609	-71.6203531349311	-4.78873565577669	247.808081523282	75.770174045756
-0.145952046848834	0.014473676232484	-4.90566644072533	-2.137264906659 88	30.5424875878962
10.5512165614045	140.500905633147	-44.5262290220817	-370.195225377101	-9.00287624815792
2.01998735169764	0.126484968598252	19.1649192139739	3.125269634324 11	-135.46373940687
-21.3004445842896	-144.518575319808	98.9693641112677	345.11146792915	-85.1055809184614
-13.5823076465244	-0.300389319984405	-26.5610640167079	0.866261661887261	239.951796042779
72.291177657914	115.990567341664	-26.9503514930631	-141.524236591276	-16.6518350479637
45.9463996391828	0.0243814788034587	-16.2116308748032	0.129259528312176	-183.4249159992471
-235.888325954965	-69.0856250496709	167.266431901191	56.167160492675 7	-78.7244638346295
-83.8412368430617	-0.00432790373110571	88.582430287692	-0.0158563704317 5	38.2726861406274
425.548671741984	10.8062382918805	-428.063028126608	-7.801836334936 16	213.070350432115
84.2210341890465	0.000614023757775869	-99.0006957964276	0.00231294279408749	31.6713066018787
-406.464209011855	-1.53780770650874	406.769318663013	1.124452420008 1	-203.230485391354
-46.4831432910531	-7.67682593278458e-005	50.3666422591325	-0.00028889328254048	-22.074323975393
209.282340900066	0.192290585381939	-209.325580879661	-0.140652103125084	104.641177160442
14.9885399010406	8.529693766055 15e-006	-15.6726249759456	3.209965770917 69e-005	7.37960432228914
-72.0670599236693	-0.0213661327573648	72.072426908929	0.015627691225 5184	-36.03352994004
-3.42251711830785	-8.529696194039 21e-007	3.51907859707381	-3.209967183287 29e-006	-1.70129538897583
18.5222029993788	0.00213661011946828	-18.5228008328851	-0.0015627638062561	9.26110149974635
0.608102739961162	7.754269161833 09e-008	-0.619725617193563	2.918151841158 37e-007	0.303282303586071
-3.78935371358111	-0.000194237270091553	3.78941407600282	0.000142069448845654	-1.89467685679043
-0.0886096375316918	0	0.08984097669367	-2.43179320697 54e-008	-0.0442521196005653

Columns 6 to 10:

0.256143142520102	1.61341423359409	-4.24774452015907	-9.17054412307385	19.3022137642351
119.654997581703	-9.13817438308052	-141.655291674092	20.2201740311368	115.978159063061
-1.13564408156253	-6.63208135694731	4.67038847424695	40.0187005298521	-17.9881733690587
-340.541608563493	-92.05666319907	345.11146792915	3.3276550187429	-264.980276777626
8.61007101750494	-50.9568203006347	-10.8925899678008	1.99101279808701	9.57996804059059
376.863601088626	-66.9944754503372	-300.872076957447	164.785420635109	181.751558707333
-4.41868606712053	198.0574768262 17	5.80953505552538	51.3748891695053	-3.17208027325964
-646.885335303242	-60.7715983062708	1005.3397381213	-39.0623533452433	-55.2846684958049
-18.697877024674	-115.649147084226	2.06958823191941	-473.874919086508	0.718834577243038
181.751558707333	-8.877281554863 31	-41.1242122317129	-1.9038752320874 3	-916.419108294733
3.7317545621064	-62.5050965144437	0.203069672248689	24.5292396695325	-0.21356659542892
-32.0830266796358	27.802414762880 9	7.737295629666 13	-6.541835509009 08	-2.69691412562154
-0.623925203628434	19.5958799605659	-0.0342654447156345	-4.171648497010 07	0.026132172440 9257
5.36993911438846	-71.3446490828591	-1.31423958665618	17.7560840146414	0.448664520280973
0.0890948984703434	-17.4258047665859	0.00488951426894941	3.78506783252429	-0.00373337386173201
-0.769345232491003	67.7948804521116	0.187533174239919	-16.9358720235624	-0.0640983996147807
-0.0111372340260724	8.52821191851615	-0.000611236483852522	-1.99394664262036	0.000466670004349912
0.0961477068831189	-34.8875968455333	-0.0234414652897 66	8.72009810669492	0.00801228384730534
0.00123746801099337	-2.62899992214604	6.79148827024116e-005	0.6333779666986 89	-5.18522329144809e-005
-0.0106830465096565	12.012071151356	0.00260460580603074	-3.00279416162733	-0.000890254179141437
-0.000123746812569762	0.588405903141481	-6.79148952316645e-006	-0.1437409964232 11	5.18522324653177e-006
0.00106830495874119	-3.08713347214794	-0.00026046066059774	0.771758458312338	8.90254158230922e-005
1.12497101925274e-005	-0.103478152865823	6.174081341642 37e-007	0.0254636768824813	-4.71383931656082e-007
-9.71186355553227e-005	0.631569012667136	2.367824167272e-005	-0.1578897380658 69	-8.09321961749128e-006
-9.37475849493302e-007	0.0149909150190829	-5.14506778588155e-008	-0.0037044717402555	3.92819943042563e-008

Columns 11 to 15:

26.975348149008	-43.8131917393296	-46.5634613115587	55.4092655098656	47.0427953421483
-4.53737228178531	-50.9554895403333	-0.0740771867565912	10.8062372474126	-0.109301393879804
-79.0928695087195	43.0664058096749	81.24298328066953	-55.4149052748274	-54.3386052626912
-0.324415847786592	56.1671604926757	0.799535922311506	-10.6848891436736	0.0232358015881178
33.1454720936513	-21.5335110397165	-16.8296073889061	27.7075148693618	25.813094977085
-46.041572904177	-23.5066974446933	6.89963980168801	5.36993911438846	-1.06942534213201
-124.43209769615	7.17601251343215	17.8733865931718	-9.235857074355535	-11.2218140869164
-2.35444911828882	7.73729562966613	0.591760837153675	-1.796381109478814	-0.0536240380370992
58.9445338000501	-1.79433801120001	-8.102504115458l5	2.3089603588965	3.57415012366671
0.631179444053982	-1.97360680450853	-0.0110122966108333	0.448664520280973	-0.00732363664434394
1205.34929454562	0.35971520576218	1.52030031926238	-0.46179225l0735	-0.763524724961592
1.41246698719441	88.9336373992373	-0.228443989868362	-0.089737957889705	0.0331584452798947
2.86976741100975	-0.0591792784750403	-99.9954679998324	0.0769575260324885	0.142661941172667
-3.56720430000007	-0.065636510580326	0.591689757763203	-4.90392378075299	-0.0848541000117249
-1.14744687939948	0.00854414316379494	0.14844362380908	-0.0109998239519331	4.23824788658034
3.3897442396774	0.0093765691630431l	-0.564529059885658	-0.00213661013409665	0.0807093546235817
0.461853121445988	-0.00106801792890186	-0.0696247714438417	0.0013743816373341	0.0123673662345427
-1.7443798410686	-0.00117207303494577	0.290669936931772	0.00026707624750848l	-0.0415328533580487
-0.135489631609283	0.000118668658572237	0.0215054612735115	-0.000152709070817122	-0.00338068130584067
0.600603557572883	0.000130230329422474	-0.100093138720735	-2.96751385957613e-005	0.0143000847041193
0.0298344212324322	-1.18668658580715e-005	-0.00483482899865841	1.52709070817025e-005	0.000726059091062487
-0.15435667360738	-1.30230329135163e-005	0.0257252819437452	2.96751385980134e-006	-0.00367515889541381
-0.00521247930931342	1.07880598709454e-006	0.000853120018021848	-1.38826428015481e-006	-0.000125557349040649
0.0315784506333568	1.18391208309935e-006	-0.00526299126886623	-2.69773987257057e-007	0.000751867872222782
0.000752837043293736	-8.99004989245526e-008	-0.000123874928446126	1.15688690012901e-007	1.80474160951411e-005

Columns 16 to 20:

-40.5966913979148	-26.7003991043205	18.2623944218941	8.39547990700917	-5.799993937583
-1.12474012385777	-0.00139046529253856	0.192290585358028	-0.00151812715412433	-0.0156276665088067
40.596660568315	27.5405396315794	-18.26239454888919	-8.50927666434301	5.79999393716815
1.1244524200081	0.0146288998826984	-0.192299158904723	0.000325806350355513	0.0156276912255184
-20.2983303671629	-13.5001199243059	9.13119727539831	4.2419848363607	-2.89999696858839
-0.562742391477703	0.123496699440483	0.0961477068831189	-0.0148510018263353	-0.00781381733600333
6.76610988467477	4.76928277129037	-3.04373242641852	-1.45232719497295	0.966665656189448
0.187533174239919	0.0105930960503352	-0.0320491458041135	-0.000744590835435207	0.00260460580603074
-1.691527505696656	-1.26762602808311	0.760933106410359	0.374271821169553	-0.241666414048238
-0.0468830612737785	-0.000195757009561069	0.00801228384730534	-0.000101171077932335	-0.00065115166457404
0.338305499662067	0.254024642909726	-0.152186621290377	-0.0756320699665392	0.048333282809611 4
0.00937656916304311	-0.00389237579152098	-0.00160245756489552	0.000460534077914376	0.000130230329422474
-0.0563842499741055	-0.0430742892816191	0.025364436881559	0.012836284842422 2	-0.00805554713493596
-0.0015627640903221	0.0105691154292394	0.000267076247508482	-0.00117963081110643	-2.17050548553115e-005
0.00805494314378424	0.00815990362207124	-0.00362349098308193	-0.0020824596511318	0.00115079244784799
0.179091616901873	-0.0100813118838325	-3.815374962240 24e-005	0.001120947171042 8	3.1007221223458e-006
-0.001006835393174 46	-0.121839142482474	0.000452936133405646	0.000366210810665514	-0.000143849055980998
-2.790649900992769e-005	0.0051905290723 1685	-0.00458159911227908	-0.000576843369629103	-3.87590265304516e-007
0.000111873511848547	0.000462033214424107	-5.032637287667 49e-005	0.00234379307260989	1.59832293227728e-005
3.1007221223458e-006	-0.001787377477155 95	-5.299131892554723e-008	0.000198612307835736	8.74024623656492e-005
-1.118735118485 47e-005	-9.421151955552 3e-005	5.0326263653914e-006	1.225133995067 23e-005	-1.59832248729619e-006
-3.100722122435 42e-007	0.000459380034709735	5.299131892554723e-008	-5.104387354741 4e-005	0
1.017031925895 89e-006	1.595700084058 84e-005	-4.575114877628 54e-007	-1.941174474066 1e-006	1.45302076748483e-007
2.818838293120 98e-008	-9.398198694396 96e-005	0	1.044260933642 75e-005	0
-8.475266049132 38e-008	-2.272843492635 07e-006	3.812595731357 12e-008	2.671275491581 6e-007	-1.21085063957069e-008

Columns 21 to 25:

-1.79977857764151	1.41195808877877	0.291347951761068	-0.277822091631368	-0.036910481996134
-1.5451061191548e-005	0.00213661011946808	-1.38011566031 41e-005	-0.000142069449372961	-1.17053505190616e-007
1.81212114921561	-1.41195808877985	-0.292493327204692	0.27782209163 1366	0.0370267656828453
0.000162559646017 64	-0.00213660804884 73	2.96194609442 65e-006	0.000142069448845654	1.23151268812092e-006
-0.904561325978558	0.70597904438992 1	0.146187059840201	-0.138911045815683	-0.0185134146156845
0.00137219662419647	0.00106830495874119	-0.000135009063 42182	-7.103472510716 86e-005	1.03954291073173e-005
0.305013417910172	-0.235326348129996	-0.0490959711339719	0.046303681938 5609	0.00620139671396304
0.000117702038309834	-0.000356101665835956	-6.769003768153 95e-006	2.367824167272e-005	8.91682120198 1e-007
-0.0772153399481054	0.058831587032496	0.012380339613 8253	-0.011575920484 6402	-0.00155858608829321
-2.175044829574 04e-006	8.902541582309 22e-005	-9.246433185977 94e-007	-5.919560415389 75e-006	-1.64776119459063e-008
0.015473675946 7113	-0.011766317406 4993	-0.00248406181 104734	0.002315184096 92805	0.000312138924461164
-4.324861930875 58e-005	-1.780508315798 41e-005	4.186673437925 12e-006	1.183912083099 35e-006	-3.27641055362167e-007
-0.002591309393 81065	0.001961052901 08322	0.000416263728 776085	-0.000385864016 154675	-5.21484542720479e-005
0.000117434615887 119	2.967513859801 34e-006	-1.072391646457 78e-005	-1.973186805185 55e-007	8.896561809631 03e-007
0.000393773679 34962	-0.000280150441 44046	-6.174919478430 8e-005	5.512343087923 92e-005	7.627710355796 33e-006
-0.000112009734 088854	-4.239305514040 63e-007	1.019042882766 2e-005	2.818838293120 98e-008	-8.485585915822 29e-007
-5.941662227892 06e-005	3.501880180505 75e-005	8.684156644032 99e-006	-6.890428859904 9e-006	-1.03192233007822e-006
5.767260653416 7e-005	5.299131892547 23e-008	-5.244047141167 27e-006	0	4.369136858649 01e-007
9.350438198039 12e-006	-3.890977798339 72e-006	-1.218866984989 24e-006	7.656032066561 01e-007	1.355434717898 96e-007
-1.985975568048 87e-005	0	1.805566250520 12e-006	0	-1.504526495922 52e-007
-3.825629461053 66e-005	3.890977795259 587e-007	1.709365567986 73e-007	-7.656032066561e-008	-1.760799607952 7e-008
5.104222548592 02e-006	-1.284108219047 13e-006	-4.640351984507 91e-007	0	3.866835309004 51e-008
2.157846286986 74e-007	-3.537252801512 38e-008	4.182557290612 78e-007	0	0
-1.044244299377 44e-006	0	9.493281229051 71e-008	1.502925517995 65e-008	0
-2.846714558970 4e-008	0	0	0	0

A-5: Coefficient matrix (28×28) of sixth mode of vibration in pentagonal membrane:

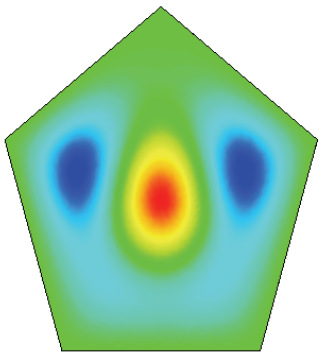

Columns 1 to 5:

0.562506292015314	-0.0839466966572218	-6.34406870603561	-1.72745345998555	23.5394341628999
-0.935109083937985	-0.5938740101160367	-0.00470757855509873	-0.014106841001194	0.0945703574188883
5.67672356147094e-006	1.389830654084445e-008	-4.64690381078097e-007	1.86988113766842e-008	-13.8276451230049
27.6013295099368	19.450504983882	-5.565200808381	-3.73106375516128	0.935109083937985
-0.00062444065770915	2.892544534052e-005	6.13391256231421e-005	-6.22734571869445e-006	-5.67672355828579e-006
-165.054677857229	-121.873131184376	54.8695378486428	40.0844837500171	-13.8006647549671
0.0224839009824368	-0.00534645805917815	-0.00276026952289959	0.000823030169727909	0.000312219692950778
140.228956953524	0.832513294243954	-114.200523703649	-68.055928726445	55.0182259921414
-0.311823525251083	-0.0508609377801623	0.0515627715284246	0.000965961439239832	-0.00749329977052375
-11.5104860833507	1530.9653420578	21.8544799109195	-282.146913608655	-35.0571499788667
1.592152941205	-0.593103949797766	721.873255752945	0.135090938202833	0.0787891110982479
41.323352175446	-3614.63633748595	3.72723984824687	1694.32802984164	0.421259605053148
-2.07291068265042	6.13475153532202	0.918844946313327	-2.37990156200025	-0.311823525251083
-1.37195009639075	-393.2320497264	2.54079281129436	-109.803051243305	-6.74802404629725
-0.000821774688360119	1.86244726173333	-0.310115346941626	-1.54294848430672	0.312603950366643
0	0	0	-162.240407503307	0.195907516039096
0.00380305458693291	-0.00110420605959941	-0.000734955890972606	0.000185537516654362	0.000117357432563128
-6.89923370311551e-007	1.21704623630813e-008	6.115349900392 44e-008	0	0
-0.00589616390968879	0.00272170326628606	0.00195914545272856	-0.000684556783480563	-0.0004791646877724 52
1.6730959791227e-005	0.037388310018436	-1.83495618516183e-006	1.54870931039523e-008	1.85900004132021e-007
0.0222766780531606	-0.00188823620737866	-0.00372903118039 77	0.000909691100717537	1.20827378344082
-6.25929549428107e-005	8.51932365337403e-007	8.72588756683981e-006	-1.23896744829722e-007	-1.11773133826654e-006
-0.38532869550533	0.000144531949863205	0.0628466337981321	-0.000231859548984543	-0.0091556976240443
-0.00105622743787329	-2.55579709709586e-006	0.000212255845098194	5.203663282629 03e-007	-3.520758126248e-005
2.07669520472161	1.104744976091 65e-005	-0.512616009272563	4.052367171278 84e-006	0.102776692707919
0.00548453382012987	2.788143229054981e-006	-0.00183021822846701	-9.46120597108847e-007	0.000457044485010798
-2.52225373575978	3.786543824253 47e-006	1.256060237702	-1.01582413487013e-005	-0.418752072249267

Columns 6 to 10:

5.11434636673494	-42.0634207362309	33.5472253757007	55.71760064115 19	-224.812358583082
0.2920890292832	-0.5471545080845 42	-1.52426053082 9	1.500759162844 99	3.4858571901772 8
9.40665253363841	81.789420261979 1	-50.92519042745 7	-177.170820839703	96.412725067548 3
0.593654131551412	0.112683189514428	0.246427407795636	-0.989533291892258	-3.1235102202343
2.1913214689812 4e-007	4.646903812075 46e-007	-3.99188828508934e-008	67.851879563182 6	-31.418296802769 9
-9.715205041051052	2.782600404190 5	1.8645235345718	-0.467554541968993	-0.2967328369875
-5.940581185146 61e-005	-3.066956439611 04e-005	7.48208958061869e-006	2.838361794440 99e-006	-4.500440380095 59e-007
39.3163936308626	-18.28984549439 58	-13.2197041342042	4.600221584989 53	3.2249601946 0934
-0.000909916012568426	0.000920086555336731	1.3403976219678 3e-005	-0.000104073249567769	-1.011024064190 18e-005
21.2666648814299	28.550131555311 1	13.9992940697698	-13.7545564945563	-9.488031411607 04
-0.019728667574154	-0.012880797217 2724	0.0046216381709 0384	0.001873319529 5622	-0.000352355194 700991
38012.7021622938	-4.303291872627 23	70.180659530175 8	7.0114330748611 7	-6.177456483249 96
0.509973516770798	0.077396808009225 7	-0.119011158560 57	-2186.625903025 63	0.017651760154 6269
482.66252480534	-0.611767922096 532	-295.9252228975 69	-0.224640438676 345	61.516683768 46
0.966097759856532	-0.154241194822 509	-0.257108506285 627	0.052490920627 3036	0.080493315226 7587
265.839842644105	-0.359673932578 682	-28.784741847539	0.965525996733 36	-48.643570333 7722
-2.50397495825623	0.044149262633 58748	2.441051522236 06	-0.044944740104 63563	-1.251795383 09397
0	0	209.920764435092	-0.024480935155 0506	-230.27424787 965
0.000138025813699926	9.216251711747 09e-005	-2.31921895817953e-005	-1.469244893284 13e-005	0.674592347 326783
0	-1.668038191694 69e-008	0	0	0
-0.000302411405344564	-0.000246003298 254567	7.606186483117 36e-005	5.582596116587 09e-005	-1.533620152 2214e-005
1.521307795385 43e-008	1.211930320663 51e-007	-0.000745067433626411	-1.241886397323 05e-008	0
0.000188823620737867	0.001234578297 43985	-9.096928398877 5e-005	-0.000190175412 02563 8	3.024115325014e-005
-8.519323654089 78e-008	5.053710597575 42e-006	1.238967448315 97e-008	-6.287068085585 79e-007	0
-1.313926816934 76e-005	-0.016978598748 3402	2.107814081677 7e-005	0.002443509337 3714	-1.716578370344 24e-005
2.323451905614 87e-007	-9.151091142335 35e-005	-4.730602984452 7e-008	1.523481616702 65e-005	0
-9.206208132464 65e-007	0.104066795317 69	-3.376972643429 47e-007	-0.020842969874 2161	1.094939014112 39e-006

Columns 11 to 15:

-130.907385592482	589.047639839083	346.689973634743	-840.884081636037	-558.504131257961
-1.96834089546147	-3.92098955467146	0.961957868023363	2.00890249400791	0.00886839073930564
119.751103196526	-87.0539434356599	151.9070703183 97	167.149925947288	-265.681687852374
3.1535607735855	10.886306401799 6	-6.185981427786 74	-15.46776469506 12	6.30366971615592
-299.744180530 31	139.733604882844	517.604151336476	-208.068704979 77	-356.309125852305
-0.924713549192916	-1.282929024053 83	5.00210394977421	10.638296415437	-5.273304008963 18
-2.32345190576348e-007	4.796211267415 25e-008	-140.621484493371	46.105936429 59	468.157352490583
-0.9275334680635	-0.620318574702871	0.155851513989664	0.098814841609 5168	3.36656344684059
1.02231884522854e-005	1.218540823419 64e-007	-9.461205971088 47e-007	-7.659273289473 7e-008	7.74483968552205e-008
4.5724614873628	3.267632002950 21	-1.150055396247 34	-0.802751748989941	0.231883367015875
-0.000230021655348349	6.418900658516 93e-005	2.601831694089 91e-005	-3.915059845094 46e-006	-2.555797097095 86e-006
-5.71002628882107	-2.484985338468 64	2.750911299033 08	1.862359782192 86	-0.914492297472067
0.00257624796050031	-0.002837179780 20706	-0.000374663453213645	0.000303453575630695	4.600434969748 1e-005
0.738757337997106	-72964.9417195427	-1.16918417525429	1.150147294290 38	0.951671048549949
-0.012880797212724	-0.012857264366 6243	0.002622650709946 29	0.002681717293708 04	44.091020070806 4
0.087502013683079	41.432317229048	0.032099489905562	-2.553846450768 97	-0.104063000477 745
0.022086147239071 6	0.406842287724636	-0.007493299770 52375	-0.104316398800 544	0.001840174692 67635
0.044985411376739 1	94.261568746343 8	-0.120679372909 672	-25.232135352046 2	-0.010936936311 5905
-0.005520410796497 07	-0.665827471163 067	0.005620075161 7835	0.337296976400 277	-0.002760269522 89959
0	-130.651760196926	0.002721001632 4986	133.905800585364	-0.004998231888 4825
-1.045292558793 8e-005	2.576909953532 81e-006	1.648903297991 47e-006	-0.045066932747 4503	0.000613392191 944164
0	0	0	0	0
-0.0184617161854868	-7.606186683957 19e-006	-6.452219226019 95e-006	1.533620152221 4e-006	1.117443517901 86e-006
7.0190424966325e-008	0	0	1.061258898238 31e-005	0
-0.000313194362182859	8.269935362615 91e-006	3.964043858193 32e-005	-2.749195218470 77e-006	-5.335093702087 23e-006
-2.17883122436556e-006	0	2.720502886969 02e-007	0	-3.026154478285 5e-008
0.00345888388063911	-1.756511734731 41e-006	-0.000495811112345397	1.430481975286 87e-006	6.258241384358 23e-005

Columns 16 to 20:

685.205840700204	495.863276205929	-330.109344713878	-246.659358186399	109.73907573321
-0.310115359033352	0.023102207520 4208	0.044944653664034	0.000165098907472645	-0.0055204107967739
-524.539604115082	-90.0103249818661	841.373086812886	508.467745827969	-685.203154615753
8.95093171002256	-1.9682450041463	-2.07291068265042	0.147206598667525	0.307043341937 74
70.1282038757784	-227.610443771264	-67.683144890228	320.435894770629	262.418603290089
-22.2410380305446	3.772320733873 76	22.4025414009819	-6.10935919174272	-5.19705862016757
-139.413241587435	-90.2729959560093	80.10817860174 34	-1979.02075235718	325.794859036661
3.17771910218244	-14.551799915723 9	-15.467764695061 2	2.864607826665 14	21.928216125549
0	152.087089571607	-44.361426036331 7	-483.245159322192	124.780313399938
0.154768338158144	-0.038962878497416	-0.024678864336 2441	-5.598019408235 89	-3.920845904965 04
5.83536415160407e-007	2.365301492174 84e-007	-2.96595443066773e-008	-1.936209923954 4e-008	0
-0.649268109690182	0.230011079249 469	0.160152389902573	-0.046376734031 75	-0.030915652822 793
-3.940528216322 84e-005	-5.203663288534 08e-006	3.371706357582 36e-006	5.111594192198 4e-007	-3.582298379975 78e-007
0.385111393333718	-0.458485216503256	-0.307297033842283	0.152415382912 02	0.107761933207 526
-0.0003111135852111 929	6.244396316162 39e-005	4.791153683370 08e-005	-7.667391293790 8e-006	-4.251756359401 2e-006
1.87663334775377	0.166860724351 521	2817.472994881 08	-0.135949083516 92	-0.052240482052 74
0.0203421002660157	-0.000374663453 213645	-0.003477213781 37666	6.133913406435 92e-005	0.000484344234 094616
2.03649830675771	-0.004011842240 98335	-0.444394693982 715	0.013007875509 2526	-0.005447090856 61761
-0.110971243210688	0.000936658983 291529	0.028108080706 6016	-0.000230021655 348349	-0.005548562238 88038
-63.68148985805286	0.013408881043 8232	20.68628938963 38	0.001215219655 63375	-4.622283369774 79
0.0439784733284496	-0.000624440657 70915	-0.022533463741 6594	0.000306695548 340822	0.007329745562 88718
48.172553881747 4	-0.000272100172 222249	-48.614896527 1629	0.000499823806 337984	23.876259136793 3
-2.57690995332 81e-007	-1.704484005958 24e-007	-0.025349458522 6401	-6.133913391740 11e-005	0.025470701411 7552
0	0	0	0	-12.515177928 6314
6.91471483078474e-007	0.000218912013 858571	-1.394200133601 19e-007	-1.184669949039 57e-007	2.342645412302 55e-008
0	0	0	0	-1.232137141097 63e-007
-6.89161280217993e-007	-7.35936280296 727e-006	2.290996015392 31e-007	8.497662050344 68e-007	-5.762264872101 2e-008

Columns 21 to 25:

80.564240670709	-27.6013295098402	-19.4755015668644	5.56520080838121	3.73342276253322
0.000320871593039712	0.000624440487774578	1.83457631473035e-006	-6.133913391740 35e-005	2.91701457468925e-006
-484.247974524554	330.109355925039	244.9332196461	-109.739075696605	-80.3440107682342
-0.0493046202217766	-0.0449447401040563	0.00260339141429025	0.00552063978076721	-0.00068500749578 3129
85.3297510004387	-420.68373682405	-248.511431684605	342.601591901366	238.347137380645
2.56545752532451	0.935465093683878	-0.298336728606294	-0.154241194822509	0.0592682386731276
5182.47186626472	28.6794907716781	-3364.80839782529	-87.3862236363965	524.495818037502
6.38091045158821	-91.2104094679174	2.05833016092078	1.56456570175232	0.0472647695962444
-1121.40316707463	-166.857644168121	6455.44371789766	35.9243677204485	-14887.7965009597
22.7784582811965	9.14782983133 64	-6.23259691953893	-5.19705862016757	4.06300092933404
-100.77423 64063	8.16120833020 51	486.138897067377	-13.6531441163223	994.589259692371
0.00779257569948321	0.00493272480811135	3.08193725617156	1.97485908756295	-14.306947533998
-4.7306029844527e-008	2.55432299812237e-008	0	0	81.427871356176
-0.0383351798749115	-0.026650994245 4113	0.00772944556719584	0.00514824495725889	-0.00129876261658053
8.67277213742233e-007	5.32350408835202e-007	-8.519323654089 78e-008	-3.8652330541686e-008	0
0.0654978880719195	0.0436373166401391	-0.0217736261302885	-0.0153456360133778	0.0054764542678445
-1.12725012803847	-6.2065701496302 6e-005	1.0953416125517e-006	6.726884890433 06e-006	-1.2389674829722e-007
-0.0208673594083722	-0.0125445864996095	0.0169945552672609	-62.94299075867 97	-0.00818725469191387
4.68329715180155e-005	0.00093693602852936	-7.6673912937908e-006	-0.00013210862478 1968	1.1150707033576 5e-006
0.00044576039482 4613	0.934985323102008	-0.00144531949852 68	-0.1466213768569 4	0.00231859548984658
-0.00010407324956 7769	-0.00187778866 4794497	2.5557971486782 1e-005	0.00036648727785 1476	-5.2036632885340 8e-006
-0.00134088784921245	-7.92229056002968	-0.00012152194668 9344	1.91743922914282	-4.4576038871 93e-005
6.2443954682566e-005	-0.0126747292543676	-3.0669563496110 4e-005	0.0042451169019855	1.0407326633439e-005
2.4736379271644 6e-005	12.5677623758142	-4.5438525827453 2e-005	-6.2343528385 7041	0.00012189889621 0362
1.6794871118175e-008	0.0109690676402295	5.5762845538375 6e-006	-0.0109813093708025	-5.6767235582857 9e-006
0	0	0	2.5166837630165	-2.0613649393 5808e-006
-1.0264741725172 1e-007	1.16183345198304e-008	-2.0620467379608 2e-006	0	0

Columns 26 to 28:

-0.935109083937985	-0.593874010160367
5.67672356147094e-006	1.38983065408445e-008
27.6013295099368	19.450504983882
-0.00062444065770915	2.89254453405206e-005
-165.054677857229	-121.873131184376
0.0224839009824368	-0.00534645805917815
140.228956953524	0.832513294243954
-0.311823525251083	-0.0508609377801623
-11.5104860833507	1530.9653420578
1.592152941205	-0.59310394979766
41.323352175446	-3614.63633748595
-2.07291068265042	6.13475153532202
-1.37195009639075	-393.2320497264
-0.000821774688360119	1.86244726173333
0	0
0.00380305458693291	-0.00110420650959941
-6.89923370311551e-007	1.21704623630813e-008
-0.00589616390968879	0.00272170326628606
1.67309597912 27e-005	0.037388310018436
0.0222766780531606	-0.00188823620737866
-6.25929549428107e-005	8.51932365337403e-007
-0.38532869550533	0.000144531949863205
-0.00105622743787329	-2.55579709709586e-006
2.07669520472161	1.10474497609165e-005
0.00548453382012987	2.78814229054981e-006
-2.52225373575978	3.78654382425347e-006
-0.00262843621436186	-4.64690381078097e-007

A-6: Coefficient matrix (27×27) of the first mode of vibration in hexagonal membrane:

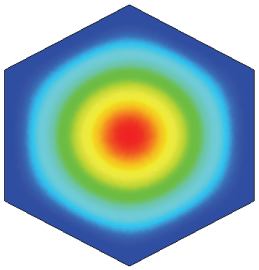

Columns 1 to 5:

0.351113008800894	-8.45026803588667e-005	-0.841419766031322	0.00441750217970349	0.771248813882266
0.000174790970846495	0.000508417587695931	-2.54278785445372e-005	0.000329670184 17196	0.000156120199329715
-0.977277930825949	-0.00153212830970217	1.31528597671422	-0.00209028403284245	0.572055277595609
-0.00425074290824023	-0.00242262914204794	0.00287380254450 77	-0.00525553595194631	0.00231292088844151
0.853933895938098	0.00620415669425428	-1.53433422492708	-0.0136509010667048	-0.157918437670787
0.0301101919320892	-0.00093489428544687	-0.0305131157989 99	0.0408893085333046	0.0131419566038302
-0.182880542124622	-0.00747940922944502	1.86859064417411	0.0115571278193932	0.954336422001205
-0.100092821526216	0.011525826951929 6	0.105170792476049	-0.0622535260783503	-0.0499408619696393
-0.119899205493311	0.00336359777830739	-2.17457981123191	-0.00252757528159224	1.35954631240718
0.18416046780823	-0.01255897837799 92	-0.195892271337367	0.0293924120157722	0.0972468386415752
0.353560840631815	-0.00065847649631 7198	2.68432379335925	0.00051164484846 1431	-1.37007560759424
-0.198223857402101	0.00420831427080372	0.209469936581989	-0.00428716901980234	-0.104575132317902
-0.766620814166846	0.00011013000975 5126	-1.0723488417974 8	-8.51761553796882e-005	0.633824959309148
0.126935899972899	-0.00067622671521574	-0.126913336843188	0.00072396965573461 7	0.0634265620796851
0.923604924533002	-1.57310364420487e-005	-0.578195797008352	1.21686055918985e-005	0.260155362072826
-0.0508553280873337	9.63640709988489e-005	0.0508654658911944	-0.00010370242236462 7	-0.0254278914500334
-0.631422859544272	1.96639729438443e-006	0.594112288050435	-1.52107107715378e-006	-0.291244352407779
0.0149638354862 47	-1.20479498544463e-005	-0.0149651908496706	1.29620577138514e-005	0.00748191679559709
0.253627275502787	-2.1848853865999e-007	-0.250132285618211	1.69007911658083e-007	0.124138838930143
-0.00345286713949507	1.33868095334111e-006	0.00345303566441896	-1.44020711629389e-006	-0.00172643357284403
-0.0705545493614 84	2.18488541216521e-008	0.070278607672894 1	-1.69007910984474e-008	-0.0350143158795053
0.00065308132121951	-1.33867978366769e-007	-0.000653100092502628	1.44020751341708e-007	0.000326540660601606
0.0150829941157425	0	-0.0150654029924912	0	0.00751800228785743
-0.00010446248772 89789	1.21698156861186e-008	0.000104464383041326	-1.30927961666054e-008	-5.22312438644122e-005
-0.00262857610140031	0	0.00262780761183131	0	-0.00131236436887404
1.44598131079 91e-005	0	-1.44599879671409e-005	0	7.22990650899546e-006
0.000387567217172463	0	-0.000387567811656646	0	0.000193638265034052

Columns 6 to 10:

-0.0368275773994348	-1.18935487463477	0.125888737590846	4.08722875715266	-0.219617465546614
-0.00795586616985844	-0.00113744728662928	0.0157844399134049	0.00121028386022413	-0.0125631575279304
0.0616886236431635	-0.687856905439389	-0.210281375262233	-2.42015940587464	0.317612378327515
0.0463402924072538	-0.00323786462584241	-0.0622535260783503	0.00209187153577916	0.0278024753700057
-0.0222421604964427	0.488684631339311	0.105386340906684	1.45604708253068	-0.158799689695817
-0.120375124141727	-0.00688582787545968	0.0793575704375485	0.00122165726501944	-0.010854040559389
0.00794167391274181	-5.2961218696094	-0.0351011088858351	2.05795384907638	0.0529336728478546
0.0760312083994621	0.017460294993929	0.00647078724586798	-0.00415852837045991	0.00331173146840954
-0.00194135942884187	2.32550448338616	0.00877666382449791	-1.13047687130576	-0.0132333903643964
-0.0108540045593 89	-0.0326501925855192	0.00356696935816815	0.00810395823439803	-0.0008411972706 17547
0.000388753637190731	-0.151572906350821	-0.00175531304109162	0.136011555515588	0.00264667840477801
0.00200348909547487	0.0349116394409328	-0.000726362008601502	-0.00871459383464999	0.000168727397316042
-6.47822568276784e-005	-0.0869231912358724	0.00029255249563163	0.00904804852601108	-0.0004411130612971 21
-0.000337040404082064	-0.021152229450799	0.00012100044483005	0.00528554684394803	-2.81129685601855e-005
9.254654779672 08e-006	-0.108408766271421	-4.1793211884417e-005	0.028202417928045	6.30161516443427e-005
4.81962282476282e-005	0.00847757764777829	-1.7282396844011e-005	-0.00211899095414976	4.01603043746998e-006
-1.15683140439367e-006	0.100388530659234	5.22415149994098e-006	-0.0251195948711259	-7.87701895527289e-006
-6.02408548339331e-006	-0.00249419847494842	2.16030930570675e-006	0.00062349306299841	-5.0200483375525e-007
1.2853682 38856693e-007	-0.0418258614738087	-5.80461277729046e-007	0.0104430260656151	8.75224328364385e-007
6.69339664113997e-007	0.000575505944069817	-2.400346011703e-007	-0.000143869464403669	5.57783224994158e-008
-1.2853682 3794241e-008	0.011723510509 9923	5.80461277731085e-008	-0.00292804831101848	-8.75224328364347e-008
-6.69339854934083e-008	-0.000108850015411 7105	2.400345969136 6e-008	2.72117217168005e-005	0
0	-0.00251187356626471	0	0.000627460647611369	0
0	1.74107305068877e-005	0	-4.35260365536768e-006	0
0	0.000438037619048761	0	-0.0001094658678992	0
0	-2.40999799452348e-006	0	6.02492209082955e-007	0
0	-6.45991182397544e-005	0	1.61431175236927e-005	0

Columns 11 to 15:

-9.94581623112198	0.208943644278335	14.8866422467096	-0.109345685450758	-13.6215620631678
-0.00038829140391741	0.00451649872312526	3.86923020554714e-005	-0.00067622706699603 8	-9.307377296772 44e-006
8.5484242854994	-0.248172992975605	-14.5360883693839	0.109048493351171	13.66726889128 48
-0.00023611652679 0852	-0.00428716901980234	7.03280872178436e-005	0.00067281817961 4501	-5.63551048980144e-006
-4.02553691755653	0.124086560730459	7.17727051247101	-0.0545242460838428	-6.83152975447309
-0.00035173485282 9032	0.00215679509230269	4.07642298830056e-005	-0.00033704040402064	-8.37589919605485e-006
0.923176218686071	-0.041362180975636 4	-2.30765036915385	0.0181747487360723	2.26817612493857
0.000872759746469662	-0.00072636200805 03	-0.00013861644236778 1	0.000112471899494396	2.07799513165602e-005
-0.108595220527435	0.010340545539692 3	0.554067120261379	-0.00454368718162 15	-0.564409402439034
-0.00163251440521174	0.000181520391931091	0.000270131961486695	-2.81129685601855e-005	-3.88693913828841e-005
0.0391643380817772	-0.00206810910387908	-0.113443865434561	0.0009087374363537	0.113351359596961
0.00174558191880859	-3.62927824436004e-005	-0.00029048646409495 93	5.62243716939624e-006	4.15614742486354e-005
-0.01252120005941 75	0.000344684850713 28	0.019901206500609 9	-0.00015456239391758	-0.01904363628831 16
-0.00105761114766719	6.04885397048402e-006	0.000176184894799823	-9.37075573057124e-007	-2.51812178016666e-005
-0.00419842534679762	-4.92406929586572e-005	-0.00185083070847467	2.16366056273966e-005	0.00257925825652462
0.000423878882386647	-8.64124618732223e-007	-7.0633031804984e-005	1.338679758 1101e-007	1.00923543425388e-005
0.00485989997120719	6.15508661983509e-006	-0.00048958503640238 3	-2.70457570342455e-006	-0.00021935199390 5547
-0.00012470992374743	1.08015569934814e-007	2.07831022099947e-005	-1.67334966276729e-008	-2.96928389874835e-006
-0.00207281515704643	-6.83898513315001e-007	0.000309589127032853	3.00508411491617e-007	-1.21054973541399e-005
2.87752972034908e-005	-1.20017298060712e-008	-4.79564881345563e-006	0	6.85126123892638e-007
0.000584342459405196	6.83898513315001e-008	-9.37629819229918e-005	-3.00508411491617e-008	1.01863990038435e-005
-5.44250077085524e-006	0	9.07057390560018e-007	0	-1.29583351687029e-007
-0.00012541201099 3164	0	2.05675292197 84e-005	0	-2.64706308496655e-006
8.70536525344383e-007	0	-1.45086788512256e-007	0	2.07270601272472e-008
2.1886171748292e-005	0	-3.61932912808219e-006	0	4.92840984970744e-007
-1.20499899726174e-007	0	2.00830736360985e-008	0	0
-3.22870364545289e-006	0	5.35888887601501e-007	0	-7.46991332427841e-008

Columns 16 to 20:

0.0329101216487078	7.69450646734866	-0.00745842801698484	-2.8104116191578	0.00134545394841045
0.000103673869971608	6.9077229241 42e-007	-1.20479498534999e-005	-1.29271395323881e-007	1.44020881313174e-006
-0.0329117545709112	-7.69591600055148	0.00745842121314068	2.81109441305045	-0.00134545397064522
-0.000103702422364627	1.25589226047887e-006	1.20483053773119e-005	-7.82714732547547e-008	-1.44020711629389e-006
0.0164558772884308	3.84592383211673	-0.00372921060655625	-1.40556316763241	0.000672726985322652
5.18512647641425e-005	7.27935130084599e-007	-6.02408548339331e-006	-1.16331977359472e-007	7.20103586624632e-007
-0.00548529242922128	-1.28032596850277	0.00124307020218642	0.468411100159022	-0.000224242328440881
-1.7282396844011e-005	-2.47529354279217e-006	2.00801755149501e-006	2.886104333467012e-007	-2.400346011703e-007
0.00137132310731803	0.319639633761367	-0.000310767550546549	-0.11706994638578	5.60605821102203e-005
4.32061390276159e-006	4.82378502778959e-006	-5.0200483375525e-007	-5.39852658122646e-007	6.00086495338761e-008
-0.000274264621463435	-0.0639681247480983	6.21535101093104e-005	0.0234212626017605	-1.12121164220441e-005
-8.641246187322 23e-007	-5.18725823122986e-006	1.00400981265738e-007	5.77242697897413e-007	-1.20017298060712e-008
4.57107702439087e-005	0.0106779731372192	-1.03589183515517e-005	-0.00390577677474158	1.86868607034068e-006
1.44020760710372e-007	3.14615883571122e-006	-1.67334966276729e-008	-3.49739136134261e-007	0
-6.53011003484408e-006	-0.00150754559603073	1.4798454787931e-006	0.000556024071864673	-2.66955152905811e-007
-2.05743939479279e-008	-1.26130413937471e-006	0	1.40171588090817e-007	0
8.1626375435551e-007	0.000175549128229279	-1.84980684849138e-007	-6.80739258467306e-005	3.33693941132264e-008
0	3.71126825178477e-007	0	-4.12400541492826e-008	0
-9.069597270616 78e-008	-1.49462399951381e-005	2.0553409427682e-008	7.05738039076276e-006	0
0	-8.56365859545648e-008	0	0	0
0	3.72898732416411e-007	0	-5.81098358240445e-007	0
0	1.61974534028575e-008	0	0	0
0	1.81185156196527e-007	0	2.8926236509762e-008	0
0	0	0	0	0
0	-4.9124895216996e-008	0	0	0
0	0	0	0	0
0	0	0	0	0

Columns 21 to 25:

0.756238897721392	-0.000200304458803901	-0.159932407346089	2.52170536550277e-005	0.0278692997672317
0	-1.33867978366838e-007	0	1.30927961287867e-008	0
-0.756245687614246	0.000200304458745388	0.159939435253086	-2.52170536551543e-005	-0.0278692827757006
1.39543590208396e-008	1.33867966527997e-007	0	-1.30927961666054e-008	0
0.378095725330401	-0.000100152229372694	-0.0799702733156802	1.26085268275772e-005	0.0139344017291953
0	-6.69339854934083e-008	0	0	0
-0.1260120847221	3.33840764575646e-005	0.0266558950369965	-4.20284227585905e-006	-0.00464463899147508
-2.75032615853112e-008	2.23113288786946e-008	0	0	0
0.0314977352704232	-8.34601911439116e-006	-0.00666370953670674	1.05071056896476e-006	0.00116111685179123
5.35976114199066e-008	0	0	0	0
-0.00629991842406669	1.66920382287823e-006	0.00133281487078049	-2.10142113792953e-007	-0.000232225613506395
-5.76362025692204e-008	0	0	0	0
0.00105015851396808	-2.78200637146372e-007	-0.000222157252389104	3.50236856321588e-008	3.87054777375751e-005
3.49573203967913e-008	0	0	0	0
-0.000149822195517027	3.97429481637674e-008	3.17192401928441e-005	0	-5.52782182930007e-006
-1.40144904374968e-008	0	0	0	0
1.85842829499909e-005	0	-3.95193372568696e-006	0	6.89888974718049e-007
0	0	0	0	0
-2.0142374499177e-006	0	4.34502472531325e-007	0	-7.62701807500166e-008
0	0	0	0	0
1.88957641679229e-007	0	-4.2317385539505e-008	0	0
0	0	0	0	0
-1.47879073429507e-008	0	0	0	0
0	0	0	0	0
0	0	0	0	0
0	0	0	0	0
0	0	0	0	0

Columns 26 to 27:

-2.72845969371866e-006	-0.00412611093544668
0	0
2.72845969371843e-006	0.00412616125007609
0	0
-1.36422984685921e-006	-0.00206308681912085
0	0
4.54743282286404e-007	0.000687690953346032
0	0
-1.13685820571601e-007	-0.000171921263933341
0	0
2.27371641143202e-008	3.43847643672377e-005
0	0
0	-5.73093881193685e-006
0	0
0	8.18594344454732e-007
0	0
0	-1.02241274262219e-007
0	0
0	1.13306607396428e-008
0	0
0	0
0	0
0	0
0	0
0	0
0	0
0	0

A-7: Coefficient matrix (27×27) of the first mode of vibration in heptagonal membrane:

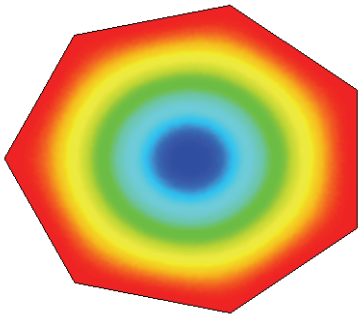

Columns 1 to 5:

-0.345036724582314	0.00182394113062401	0.858131141489139	0.0127792881066853	-0.730371837737039
0.000846410968279088	0.000864600886416156	-0.00603393780903616	0.022962226154732	0.0180519476729515
1.10963099589571	-0.0214210526388001	-1.82166178128682	0.412358141963523	1.62516064930242
0.00498385400982215	0.0184352560261516	-0.0103774826208003	-0.264325419673071	0.0443155579557928
-1.13108123332495	-0.1539327205085	1.83098394423723	2.09509943165307	-6.64996333364979
-0.0610581172612914	-0.0969587292651255	0.175232750521144	0.797863118525839	-0.340163732187685
0.765259314899595	-0.301746386791814	-4.68845653921744	-2.60364853744956	27.398343253788
0.246545553714319	0.179454124795642	-0.577539118921624	-0.956812298704693	0.526206576807581
-2.05758141731832	0.908863848216909	10.5777629391062	-0.67797678811597	-45.4891756781484
-0.48803770231078	-0.147933860833671	0.922148168702227	0.42952923934624	-0.545726420066949
5.562507829415	-0.180166113579763	-15.8643604677079	0.136064441383102	44.2240215684067
0.465870698781085	0.0541373383897499	-0.680011551253341	-0.0489478738666516	0.358950993737822
-9.35759874268375	0.030230530271638	14.6660759401917	-0.0216016182457725	-22.8014326873132
-0.158383273877001	-0.00860490306642337	0.149329790386371	0.00866378165629344	-0.0782368997840257
9.255712179091125	-0.00431844728654101	-9.688946168355566	0.00310613461489382	8.66515412150999
-0.0389908561289855	0.00122617663459371	0.0401291780594498	-0.00124167606345343	-0.0194901816892035
-5.240672093267 57	0.000539815123940058	5.18255193475645	-0.000388051583282944	-3.28505660529542
0.0385328965498199	-0.000153311146253367	-0.0386939689505145	0.000155169503450622	0.0192664701378289
1.738798995910 63	-5.99794528215246e-005	-1.7158042332901	4.31182705456941e-005	0.961077880974677
-0.0146311548557708	1.70348408221636e-005	0.0146511482134659	-1.72406928085498e-005	-0.00731557735642599
-0.398962115259473	5.99794513850 19e-006	0.394562588377749	-4.31182011103071e-006	-0.210431888171026
0.0037826001553620 1	-1.70348219360437e-006	-0.00378482723152952	1.7240712577558e-006	0.00189130007786909
0.0694089976102995	-5.45267764844623e-007	-0.0687739711109367	3.91983671566642e-007	0.0358621187226025
-0.000759082269797523	1.54862010542743e-007	0.000759307134602074	-1.56733760496566e-007	-0.000379541134898354
-0.0096355955617721 9	4.54389804044924e-008	0.00955910566812246	-3.26653058915997e-008	-0.00492777357068595
0.000125524651113 94	-1.29051675804979e-008	-0.000125545407536181	1.30611466703167e-008	6.27623255569708e-005
0.00109677826062457	0	-0.00108875024057135	0	0.000557887842109884

Columns 6 to 10:

-0.160882702701542	0.378293899928394	0.748267247606417	-0.097089265206705	-1.96381070851977
-0.104230441998823	-0.045845841704819	0.180963318202071	0.0578299907406018	-0.147938189234108
-1.89821346902789	-4.19422286592453	1.30782916609579	9.83498024737355	1.50622219303513
0.807670483668623	-0.0382781009669932	-0.956812298704693	-0.0103188289319302	0.425359431274828
-0.850196572525093	20.6400966693454	0.238646341186636	-30.4014292946134	-0.750836231481618
-1.55650514453452	0.299267239302308	1.09474082429075	-0.123813270332105	-0.145146567905526
0.519502583486505	-87.236418949418	0.225164735141597	118.413208944773	0.310167656297577
1.08354831757316	-0.141148495832476	-2.63168027280006	0.0417180493202063	0.040619370922043
-0.371504697979681	101.701010248067	0.11341162322304	-79.7982217771273	-0.0401796562481684
-0.145146567905526	0.154401730205417	0.0411294454543837	-0.0439195094112689	23.9102032244966
0.161445450478413	-59.6714710765498	0.0356889234263226	39.7410728241295	0.00983694651884059
0.0252200744613813	-0.11332310164512	-0.00874222329000924	0.0299117782325851	0.00214612120173372
-0.0248967747881283	15.8607570474634	-0.0057404366063603	-8.70063976446875	-0.00235232056457 54
-0.00429162702965222	0.0248884274413795	0.00144823434974003	-0.00651975390500251	-0.000357753841405251
0.00358258453324758	-4.03429190749 93	0.000822607753365115	1.79628195178902	0.000336135134991563
0.000613287721413 46	0.00668819728039595	-0.000206887193710 63	-0.00162418191953885	5.11042171686796-005
-0.000447605454006832	1.23121778643375	-0.000102805283502762	-0.421416398005557	-4.20161717069015-005
-7.66572055026362e-005	-0.0064489948201266	2.5861020885266e-005	0.0016055391774 5313	-6.38805770608648-006
4.97352241624853e-005	-0.334010340997795	1.14229289009492e-005	0.0798265095681 64	4.66846766467314e-006
8.51740670134604e-006	0.0024418580355976 5	-2.87345256766578e-006	-0.0006096314463720 26	7.09784222055894e-007
-4.9735167522442e-006	0.0712861151760 11	-1.14229237122154e-006	-0.0194738555989465	-4.66846748584618e-007
-8.51741050494646e-007	-0.0006308045385881 89	2.87345227608371e-007	0.0001576083398224 13	-7.09784217370032e-008
4.52137905885058e-007	-0.0120302440475676	1.03844762769949e-007	0.0031781868878769	4.24406135677963e-008
7.7431005556539e-008	0.0001265511891003 46	-2.61222933328652e-008	-3.16284279081962e-005	0
-3.76781587710781e-008	0.0016459756273911 1	0	-0.0004275798357 27122	0
0	-2.09242345893636e-005	0	5.23019379641424e-006	0
0	-0.0001859396353213 47	0	4.7879704289084 6e-005	0

Columns 11 to 15:

-1.40237826658934	3.30172593864658	4.63515126719818	-3.54174948777862	-7.07639432005278
-0.025912215877059 3	0.0547823313419828	0.00121329467943044	-0.00860490343076684	-0.000621426006964384
-12.7016244500907	-3.26612787156235	6.58716632587126	3.54201440640001	2.93247927082884
0.0228509085745 24	-0.0489478738666516	-0.000182363450367568	0.00856027850531911	0.000549389940053748
20.6829915915436	1.63442920134078	-8.4121455802655	-1.77099365972618	0.325166254348025
0.0125442875181195	0.0255284571018212	-0.00419942214091629	-0.00429162702965222	0.000297275537271785
-62.9351950361841	-0.543437166752591	14.1256682839872	0.5903472688226 1	-2.022061681066
-0.00387600488645713	-0.00874222329000924	0.00145937882058316	0.00143093616597101	-9.24774592860758e-005
37.9488649911021	0.136029056462994	-7.54344291216903	-0.147584862298484	1.15170131567654
0.00775418301772362	0.00217207124004554	-0.00151706533004366	-0.000357753841405251	0.000183609877902792
-146.3808729099 55	-0.0275990717397649	2.21622278920272	0.0295170509035148	-0.343963520835912
-0.00568828663743288	-102.070702928215	0.000996581840310195	7.1545709640260 4e-005	-0.000134912951145208
2.3368400308001 1	0.00458130772441 09	241.226860417 19	-0.00491586935263464	0.0726567203027128
0.00124441907173793	7.241045519550 68e-005	-0.000217125689530278	164.445934347854	2.96325804580442e-005
-0.448460417823808	-0.000647611844068455	0.0883242089780 2	0.000702422984764805	-9.35371154207485
0.000334409845151587	-1.034443350959 84e-005	-5.413939805881 58e-005	1.703482144912 78e-006	7.96086008957499e-006
0.0956485358027514	8.095149375739 13e-005	-0.0180490356235224	-8.784834002173 39e-005	0.00273583109173453
-0.000322449741115891	1.293053535101 85e-006	5.3517972577578e-005	-2.129352655137 13e-007	-7.67737478854837e-006
-0.0208487348924331	-8.994610341640 25e-006	0.0037602620885 4802	9.760926669935 45e-006	-0.000555929178922628
0.000122092901779407	-1.436726132222 38e-007	-2.032104821241 87e-005	2.365947389658 09e-008	2.90697385189032e-006
0.00401519686967157	8.994610344903 78e-007	-0.000703498630773844	-9.760926669898 76e-007	0.000102411792742153
-3.154022692941 11e-005	1.436726133452 81e-008	5.253611327413 72e-006	0	-7.50957784033598e-007
-0.000645781336712447	-8.176918495257 66e-008	0.000111332549063182	8.873569699909 19e-008	-1.607307899113 84e-005
6.327559455017 29e-006	0	-1.054280930273 21e-006	0	1.506561775004 12e-007
8.626112865851 67e-005	0	-1.473959743434 8e-005	0	2.118453488010 2e-006
-1.046211729468 18e-006	0	1.743397932138 08e-007	0	-2.490980308257 57e-008
-9.622797154575 29e-006	0	1.636329872551 2e-006	0	-2.345852263901 67e-007

Columns 16 to 20:

2.39620811695477	6.10253190906375	-1.06668551806569	-3.17684759214946	0.340802779804006
0.00124099792157458	2.160097203436 58e-005	-0.000153311146261708	-8.631079502051 19e-006	1.724073339018 57e-005
-2.39620669578112	-5.545333367718 35	1.066685523791 01	3.07610886882884	-0.340802779785601
-0.00124167606345343	-3.249409252140 19e-006	0.000153316445351195	7.630532317408 36e-006	-1.724069280854 98e-005
1.19810351475012	2.518825839285 55	-0.533342761007966	-1.49153435840523	0.170401389897436
0.000620700378747668	-7.501116703560 41e-005	-7.665720550263 62e-005	4.128668627649 96e-006	8.620352870485 21e-006
-0.399367704107196	-0.586659844153878	0.177780921091378	0.463373168881664	-0.056800463295827
-0.000206887193710 63	2.605801316051 64e-005	2.555218258174 86e-005	-1.284426218354 62e-006	-2.873452567665 78e-006
0.0998419415162 64	0.0614920722579 604	-0.0444452301862 195	-0.1050661977180 12	0.014200115824 3267
5.172189311547 68e-005	-2.709053808709 77e-005	-6.388057706086 48e-006	2.550136567465 19e-006	7.18363071912025e-007
-0.019968387691 7817	0.003006628261 92694	0.008889046040 64849	0.019074404291 3486	-0.002840023164 85094
-1.034443350959 84e-005	1.780448617612 54e-005	1.277611605252 34e-006	-1.873790999873 4e-006	-1.436726132222 38e-007
0.003328064627 39986	-0.002640894264 91695	-0.001481507673 3742	-0.002906043383 97782	0.000473337194 142106
1.724071384823 88e-006	-3.880807590871 73e-006	-2.129352655137 13e-007	4.115142195918 74e-007	2.394543555616 93e-008
-0.000475461121 500563	0.000833903814 950326	0.000211643953 33997	0.000360065901 846018	-6.761959916315 47e-005
-6.079883458222 356	-9.667945074460 07e-007	3.041932358000 16e-008	1.105852660682 06e-007	0
5.943172402519 4e-005	0.207692714317 694	-2.645538313067 87e-005	-2.976901033737 93e-005	8.452449895394 36e-006
3.078698857089 18e-008	9.556841725388 51e-007	0.138231749911 283	-1.066301239716 54e-007	0
-6.603302832026 25e-006	5.859256485627 03e-005	2.939491024640 14e-006	-0.003978150013 35047	-9.391615077118 33e-007
0	-3.628758609360 52e-007	0	4.037461443917 33e-008	-0.002622225330 798867
6.603302830262 8e-007	-1.179542003193 39e-005	-2.939499351943 36e-007	6.932784725155 5e-007	9.391613716225 4e-008
0	9.381448798953 07e-008	0	-1.042996922268 89e-008	0
-6.003002572966 17e-008	1.926389070402 49e-006	2.672272138130 33e-008	-1.580390411303 31e-007	0
0	-1.882644518345 02e-008	0	0	0
0	-2.587360965458 1e-007	0	2.408014588423 53e-008	0
0	0	0	0	0
0	2.892784826758 89e-008	0	0	0

Columns 21 to 25:

1.07483709900404	-0.083808454009452	-0.267456989314828	0.0166621476290389	0.0524506067052773
2.400094074981 16e-007	-1.703482193604 5e-006	-7.846436104313 6e-008	1.567337595835 96e-007	0
-1.065081857092 6	0.083808454009 4983	0.266147696140 392	-0.016662147629 0388	-0.0523496883847 694
-3.610489635924 24e-008	1.703482019158 22e-006	6.936847490470 25e-008	-1.567337604965 66e-007	0
0.527937506686 279	-0.041904227004 7342	-0.132454196737 123	0.008831073814 51947	0.026126462318 3722
-8.334583516172 68e-007	-8.517410504946 46e-007	3.753334742176 67e-008	7.836688007955 14e-008	0
-0.172574259181 216	0.013968075668 2557	0.043778500428 6096	-0.002770246048 3979	-0.008678523517 09496
2.895333861490 54e-007	2.839136876830 47e-007	-1.167660235607 65e-008	-2.612229333286 52e-008	0
0.042048611748 9597	-0.003492018917 06271	-0.010830256376 7953	0.000694256151 209952	0.002160210158 38477
-3.010059820889 e-007	-7.097842173700 32e-008	2.318305969099 29e-008	0	0
-0.008209950262 39314	0.000698403783 41259	0.002145146466 09467	-0.000138851230 24199	-0.000430303482 378814
1.978276241171 08e-007	1.419568433876 93e-008	-1.703446363545 78e-008	0	0
0.001339596862 48771	-0.000116400630 568764	-0.000354495869 167854	2.314187170699 84e-005	7.146208859411 43e-005
-4.312008434372 58e-008	0	0	0	0
-0.000185589744 28496	1.662866150982 34e-005	5.006343886974 57e-005	-3.305981672428 34e-006	-1.015971245161 95e-005
-1.074194406089 89e-008	0	0	0	0
2.163125715753 73e-005	-2.078582688727 93e-006	-6.109632400669 55e-006	4.132477090535 42e-007	1.257419339750 98e-006
1.061864535268 5e-008	0	0	0	0
-2.035641982325 35e-006	2.309536320880 81e-007	6.448677623960 07e-007	-4.591641211706 02e-008	-1.368522153236 14e-007
0	0	0	0	0
6.105694565521 64e-005	-2.309536201445 19e-008	-5.835843487126 7e-008	0	1.317065528670 13e-008
0	3.928521492386 83e-005	0	0	0
0	0	-7.137574972464 85e-007	0	0
0	0	0	-4.598332069798 93e-007	0
0	0	0	0	0
0	0	0	0	0
0	0	0	0	0

Columns 26 to 27:

-0.0027734157866251	-0.00849947492749963
-1.29051675804979e-008	0
0.0027734157866251	0.00848855968939977
1.2905167583242e-008	0
-0.00138670789331255	-0.00423904655417659
0	0
0.000462235964437516	0.0014102047542953 5
0	0
-0.000115558991109379	-0.000351712958471139
0	0
2.31117982218758e-005	7.01875670634277e-005
0	0
-3.85196637031263e-006	-1.16750108735765e-005
0	0
5.50280910044662e-007	1.66364779640569e-006
0	0
-6.87851137555828e-008	-2.06942791952955e-007
0	0
0	2.2768870354953e-008
0	0
0	0
0	0
0	0
0	0
0	0
0	0
0	0

A-8: Coefficient matrix (27×27) of the first mode of vibration in octagonal membrane:

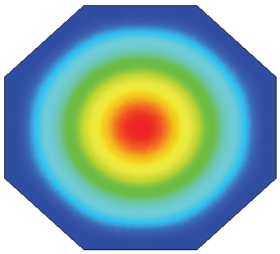

Columns 1 to 5:

0.609469648450613	0.000311280998738894	-1.30638380721211	-0.00907733398372557	0.929917397850659
-0.000167171911243713	-0.0015731415410869	0.00324951533794859	0.00545343846222579	-0.0198017530123948
-1.54169948038179	-0.00779141576775899	2.09031201258767	0.0672113074622871	-1.1061788732768
0.00762139833115327	0.0117047940236166	-0.0352088561035657	-0.0072708635539982	0.124276636790066
1.2316252689925	0.0405910880415918	-0.261265052929048	-0.233591690234696	-7.26763942366961
-0.0711427753621194	-0.0155014213927598	0.191706470542614	-0.138215553574213	-0.253001475959016
-0.666225582187508	-0.0724500019420565	0.823738773985497	0.313246041986564	16.6071052566562
0.279209016609418	-0.00295977501547304	-0.564009741342766	0.213194354068843	0.309464523703632
1.32870770595201	0.0483363499917986	-3.17511910116169	-0.162486197307911	-21 0579888885771
-0.564035642591113	0.011640376266815	0.89846644989773	-0.0830249949931812	-0.423171844778932
-2.74310144184477	-0.0096687213798168 2	6.22791619264667	0.0287995685809016	21.0785405839977
0.634564532966765	-0.0032154229512232 8	-0.78227816028552	0.000990331283785985	0.386543488060281
3.60801249403494	0.0016186754775504 4	-8.72288141706382	-0.00486863877714662	-7.36586666982308
-0.417304442701027	0.000516307385866319	0.418032080264045	-0.000595088112603734	-0.20812687946519
-2.86564250637216	-0.0002312382594857 7	5.67155842664295	0.00069465672315473	0.261357602507927
0.180267111240497	-7.3654815810911e-005	-0.180558379544606	8.4270883712044e-005	0.0901364463157812
1.48385813966188	2.89051082284267e-005	-2.13943962207169	-8.68388538732409e-005	0.486382555188464
-0.0641796784062499	9.2087844145244e-006	0.064219674229878	-1.0506491126881e-005	-0.03208982713808
-0.554777192503402	-3.2116786514976e-006	0.666525584338653	9.64872172833797e-006	-0.244134974312147
0.0184818620153923	-1.0232074704757 9e-006	-0.018486830999144	1.16733436731413e-006	0.00924093104720108
0.159715568526615	3.2116786979038 1e-007	-0.175327722286579	-9.6487234276466e-007	0.0760461918448252
-0.00433181277988224	1.0232065569115 1e-007	0.00433236626598097	-1.16734976425179e-007	-0.00216590638983693
-0.0366039166171057	-2.91970790714193e-008	0.038480487357775	8.77156669438117e-008	-0.0179112472444985
0.00084298850898744	0	-0.000842554735656572	1.0612271824384e-008	0.00042124925449598
0.00688180578014615	0	-0.00708115361339768	0	0.00340466008515098
-0.000138920337374 64	0	0.000138925495885857	0	-6.94601686873194e-005
-0.00109019633402569	0	0.00110923995715368	0	-0.000542026908974518

Columns 6 to 10:

0.0916195622732285	-0.423431975523272	-0.446906446809509	0.685636309610572	1.1982388196815
0.000309406799073653	0.0368672398893484	-0.0126766246696096	-0.0266912016933253	0.0116497874740721
-0.257635836785716	1.992151734855572	0.685509615613177	-1.799931947500 08	-1.37775545870768
-0.146668266583722	-0.180945974543276	0.213194354068843	0.105778032702608	-0.0812619540091473
0.383651349529811	13.0423388107092	-0.422598374470366	-15.0197340483483	0.685288831620245
0.911234157481083	0.167766083762823	-0.342042257877619	-0.074413908763669	0.00494401648463988
-0.0928968718532885	-24.5582166746937	-0.0553238456966304	24.714679122026	-0.230028738132712
-0.339644335673323	-0.0160258884481736	-5.92459294997933	0.0378506763225715	-0.00210515910513073
-0.114684111007834	12.5798111410085	-0.0178467794230813	-14.7404574902206	0.0609476139820637
0.00494401648463988	0.152098323953798	-0.00247146699545048	-0.0359214901365744	42.1863062232164
0.0207862636735883	-16.1560423535443	0.00555407765564476	15.0921413963925	-0.0116685166493186
-0.0015104586776668	-0.130339128682256	0.000618555609421124	0.0322009552202774	-0.000128395052960443
-0.00350574836721139	2.1733451299617	-0.000929208396858647	-3.026953454 19908	0.00191240328529994
0.000258535497657794	0.0696724516616165	-9.79042127785 68e-005	-0.0173440365619586	2.14948410947346e-005
0.000500329422150676	0.236631669692161	0.000132702218303584	0.395196809832828	-0.00027320186943617
-3.68287388815747e-005	-0.0300930600095985	1.40066566126324e-005	0.00751136950211762	-3.06955363136176e-006
-6.25450637756457e-005	-0.2449802739418 75	-1.65881084807841e-005	-0.0097893968340433	3.41502246670125e-005
4.60450757811529e-006	0.0107032790558449	-1.75101437713416e-006	-0.0026741522679 2273	3.83702766714622e-007
6.9494293344755e-006	0.0961308558046799	1.84312127856713e-006	-0.0143480650303663	-3.79446947107286e-006
-5.11602789155335e-007	-0.0030811384997853 3	1.94558502223018e-007	0.000770077587242147	-4.26336044110583e-008
-6.94943028388019e-007	-0.0274698581475441	-1.84312135923978e-007	0.0056970120950817 8	3.794469468354e-007
5.11603274279921e-008	0.000722061044330394	-1.94558298054242e-008	-0.000180492199153159	0
6.31766386262785e-008	0.0062309431649810 8	1.67556486933965e-008	-0.00143072306514321	-3.44951769859438e-008
0	-0.000140425789276095	0	3.51041187874663e-005	0
0	-0.001163048771148 18	0	0.000278257971972 56	0
0	2.31542493143094e-005	0	-5.78834739060995e-006	0
0	0.000183405553428138	0	-4.47250118307451e-005	0

Columns 11 to 15:

-1.66389203169885	-1.90115732961533	3.022131340212O3	1.86354277647453	-3.70684417856898
0.006703283043007O4	-0.0036424919161822	-0.0003475853757976 22	0.000516308178055481	0.000160754419837894
0.800108994662211	1.95610794629823	-1.55891138097105	-1.8631266517348 6	2.87083290627424
-0.0222314354459983	0.000990331283785986	0.00295457768338158	-0.000522346604450513	-0.000550242189168279
10.740496157472	-0.978104873312671	-2.22419346681257	0.931562690563185	-0.797561779800912
0.0237429327786553	-0.0017294265390361	-0.003310703178792 65	0.000258535497657794	0.000549644876613428
-22.5430972441809	0.326006866305186	4.91885815229198	-0.310521218290016	-0.362254088405942
-0.003196035343376O6	0.000618555609421124	0.0003415587128828 11	-8.57973522293224e-005	-7.74930395967478e-005
11.7499416696602	-0.0815046365826789	-2.61525361738549	0.0776302715927646	0.286233105829927
0.00707662042307583	-0.000146554337859427	-0.0011966648815430 7	2.14948410947346e-005	0.000179186254828508
119.356586183755	0.0162507758822678	0.760006515426385	-0.015526055569546	-0.0885987235361002
-0.006516947235252 48	-145.400737573454	0.00107832897921464	-4.29730915843698e-006	-0.000155200351487 12
0.591309400674271	-0.0027146561892017 2	-275.368126382165	0.00258813081320311	0.017337152201814 7
0.00348360645937307	-4.90271175428684e-006	-0.000578148121793057	196.25738754354	8.29050201883473e-005
-0.0662580724057624	0.000388114947532949	0.0212115244380388	-0.000369684264014053	10.6213292272207
-0.0015046531243535 3	7.00413428055038e-007	0.000250378979116098	-1.0232064188519 4e-007	-3.58249910701406e-005
-0.0013364785481090 5	-4.85143686429074e-005	-0.0014526376075236 9	4.62084983196588e-005	8.11643065546299e-005
0.000535163952104623	-8.75512290035696e-008	-8.9138408933489e-005	1.27900817501521e-008	1.27419988592232e-005
0.00346616310293013	5.3904854036250 2e-006	-0.000339615268281588	-5.1342775910859 6e-006	6.69290628148915e-005
-0.000154056924992154	0	2.56692529079721e-005	0	-3.66802202362443e-006
-0.00122666710402874	-5.3904854036738 2e-007	0.000174684412202433	5.13427759108541e-007	-2.73420247434672e-005
3.61030522165102e-005	0	-6.016406638438 97e-006	0	8.595964813454 76e-007
0.000297036829097917	4.90044127606548e-008	-4.618471194260 04e-005	-4.667525082804 94e-008	6.87514120622439e-006
-7.021289463804 76e-006	0	1.17013729291554e-006	0	-1.671735586620 18e-007
-5.684636705225 51e-005	0	9.139528908940 38e-006	0	-1.334747970794 81e-006
1.157712465715 47e-006	0	-1.929449130203 32e-007	0	2.756458251703 51e-008
9.062358524151 97e-006	0	-1.479605350332 33e-006	0	2.141517053588 68e-007

Columns 16 to 20:

-1.16575626775467	2.93926879357927	0.489402019414264	-1.46781024991809	-0.150023524248476
-8.403416858083 03e-005	-6.157741823162 27e-006	9.208784432660 59e-006	2.232745076745 5e-006	-1.167350667826 4e-006
1.16575855523367	-2.82185132001381	-0.489402009886002	1.44083301236602	0.150023524279627
8.427088371204 4e-005	5.253853336850 05e-005	-9.209211446254 76e-006	-7.644167346138 31e-006	1.167334367314 13e-006
-0.582879282076659	1.31260766458308	0.244701004916946	-0.703876543208008	-0.075011762139918 4
-4.201770289097 12e-005	-5.928647558980 16e-005	4.604507578115 29e-006	7.632731876441 47e-006	-5.836744295580 72e-007
0.194293091594649	-0.348423511449616	-0.0815670016525574	0.223347320026113	0.025003920713249 5
1.400665662632 4e-005	6.084469692777 93e-006	-1.534799382393 81e-006	-1.076398901181 03e-006	1.945585022230 18e-007
-0.048573273149609 8	0.058763178957147 8	0.020391750411748 4	-0.052479518247589 3	-0.006250980178318 19
-3.501983858941 13e-006	-2.136952138170 02e-005	3.837027667146 22e-007	2.488694360567 84e-006	-4.863957356898 46e-008
0.009714654620406 15	-0.006789491901 63 7	-0.004078350082 40226	0.009932592380 31522	0.001250196036 5642
7.004134280550 38e-007	1.916633883595 42e-005	-7.674048455851 78e-008	-2.155560502690 55e-006	0
-0.001619109103 58526	0.000587388827 153285	0.000679725013 732694	-0.001598414582 83421	-0.000208366005 943907
-1.167349677715 26e-007	-1.032384139526 33e-005	1.27900817501 521e-008	1.151986126871 99e-006	0
0.000231298384 425585	-7.128402839023 4e-005	-9.710357339039 67e-005	0.000228279446 115839	2.976657277701 e-005
-7.250636778729 36	4.471261884528 43e-006	0	-4.975704786686 e-007	0
-2.891257312729 19e-005	-0.237334673047 806	1.213796055991 58e-005	-3.095454255501 44e-005	-3.720821534712 63e-006
0	-1.591757699500 42e-006	0.164979132478 501	1.769713368497 03e-007	0
3.212518062640 88e-006	-1.183303986664 43e-005	-1.348661114185 26e-006	0.004562252711 96898	4.134245639161 71e-007
0	4.583795162137 7e-007	0	-5.094474886814 52e-008	-0.003130034285 45954
-3.212518062640 89e-007	3.672094174710 11e-006	1.348660741533 28e-007	-7.277575397505 75e-007	-4.134246027899 e-008
0	-1.074358328292 67e-007	0	1.193884001867 22e-008	0
2.920470966037 17e-008	-8.727825618517 57e-007	-1.226055219575 71e-008	1.267406559718 57e-007	0
0	2.089530880206 32e-008	0	0	0
0	1.670277878602 54e-007	0	-2.111051205269 31e-008	0
0	0	0	0	0
0	-2.670146247714 72e-008	0	0	0

Columns 21 to 25:

0.481661661209332	0.0357924170763664	-0.117858394985682	-0.0069549603989444	0.0228304299047891
-6.841830199050 69e-008	1.023206556913 07e-007	2.029768306500 35e-008	-1.061227089 6788e-008	0
-0.479385059430439	-0.035792417076 2844	0.11747364376496	0.006954960398 94458	-0.022805815813 3649
5.837516345441 96e-007	-1.023206500647 61e-007	-6.949247259124 41e-008	1.061227118243 84e-008	0
0.238113930435521	0.017896208538 1419	-0.058516707175 0096	-0.003477480199 47229	0.011387265270 7788
-6.587449563873 24e-007	5.116032742799 21e-008	6.938844641971 5e-008	0	0
-0.078219060563622 6	-0.005965402846 04747	0.019379789470 0263	0.001159160066 49076	-0.003785798077 20571
6.760466780247 12e-008	-1.705344213606 18e-008	0	0	0
0.019199329015 3175	0.001491350711 51185	-0.004808613698 02681	-0.000289790016 622691	0.000943449858 9391 05
-2.374391451505 39e-007	0	2.262449411367 08e-008	0	0
-0.003776615905 97962	-0.000298270142 30237	0.000955439199 498483	5.79580033245382e-005	-0.000188149413 40603
2.129593200626 42e-007	0	-1.959600457123 33e-008	0	0
0.000622038760 358349	4.971169038372 84e-005	-0.000158527771 027312	-9.659667220756 36e-006	3.129196390995 69e-005
-1.147093488400 24e-007	0	1.047260115336 7e-008	0	0
-8.852941373237 92e-005	-7.101670054818 34e-006	2.261854977014 58e-005	1.379952460108 05e-006	-4.466294087698 44e-006
4.967836886353 06e-008	0	0	0	0
1.125579752775 68e-005	8.877087568522 93e-007	-2.845855309166 03e-006	-1.724940575135 06e-007	5.595405665059 37e-007
-1.768619224875 62e-008	0	0	0	0
-1.344693127718 82e-006	-9.863430631692 14e-008	3.250265851044 85e-007	1.916600639038 96e-008	-6.286336441165 48e-008
0	0	0	0	0
-6.970403649463 95e-005	0	-3.503298360479 13e-008	0	0
0	4.688647555785 45e-005	0	0	0
-2.067808624674 14e-008	0	8.278042350298 61e-007	0	0
0	0	0	-5.487950969022 91e-007	0
0	0	0	0	0
0	0	0	0	0
0	0	0	0	0

Columns 26 to 27:

0.00113723698424604	-0.00366736423753549
0	0
-0.00113723698424604	0.00366400363054557
0	0
0.0005686184921230l9	-0.00183014369704847
0	0
-0.000189539497374 34	0.000609092577436915
0	0
4.738487434358 49e-005	-0.000152002975 67952
0	0
-9.476974868716 99e-006	3.035286392425 94e-005
0	0
1.579495811452 83e-006	-5.053003920875 94e-006
0	0
-2.256422587789 76e-007	7.214990239945 36e-007
0	0
2.8205282347372e-008	-9.028402338667 46e-008
0	0
0	1.008563511226 89e-008
0	0
0	0
0	0
0	0
0	0
0	0
0	0
0	0

A-9: Coefficient matrix (27×27) of the first mode of vibration in enneagon membrane:

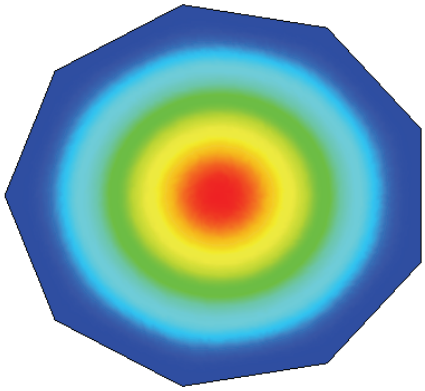

Columns 1 to 5:

0.601285248994827	0.000710680848015954	-1.25082947313786	-0.00864589961565798	0.777734372997656
-0.000126058331154866	0.00242417287972785	0.000688493185549532	-0.0205889030683011	-0.00385742388626276
-1.47891933610663	-0.0298001295889776	2.1832175208255 6	0.241331564760912	-3.09986734611448
0.00853011855276087	-0.0284638778927331	-0.026453368886261 6	0.226697300444869	0.0737652637333825
1.0615328727 29	0.221254256768901	-3.79529097722843	-0.221368372878999	33.3096999625559
-0.0672174210617246	0.0888578332148384	0.151438016614776	-0.603229782324505	-0.163808286611558
0.469976985325047	-0.881854523000815	10.1798547514845	4.43237414418392	-115.609819700738
0.216472678796937	-0.122138875101415	-0.436427051161202	0.625887149320581	0.25520346940267
-4.19615314363728	0.871287143040347	-9.53479116153494	-5.28258205927448	170.856878864934
-0.325990803664454	0.086102132717876 6	0.602789566656476	-0.251868006643468	-0.30542059242597
12.7070354743592	-0.175326573226879	-11.9951236034057	1.02320487866556	-121.223775301007
0.188519750909541	-0.0314693766859168	-0.313956541020729	0.0270647656753814	0.158102302375344
-22.3763059463612	0.0293687105004849	35.8699637181583	-0.168628132844013	32.9590331914719
0.0609030666280623	0.00500478573753543	-0.0622872771036951	-0.00487220154534248	0.0309352691748197
24.2470326951983	-0.00419563938651779	-34.6723894988568	0.0241344562927598	3.64568944514775
-0.134687422300857	-0.000713169347579896	0.134749190314055	0.00069814237242234 2	-0.0673410527254631
-16.5424964688539	0.000524461449733379	19.0452521891917	-0.00301630519495405	-6.94326406301713
0.0731849482553694	8.916854837315 09e-005	-0.0731943731875593	-8.72402001627751e-005	0.0365924852070632
7.35006280585712	-5.827349715323 99e-005	-7.78143057120049	0.000335148505156475	3.49779586394101
-0.0247941282863629	-9.907772853923 22e-006	0.0247952956751445	9.693141490610 85e-006	-0.0123970641069646
-2.29521853695162	5.827349800730 75e-006	2.3558468111037	-3.351483330093 33e-005	-1.12691650794247
0.00620485561120352	9.907762022441 72e-007	-0.00620498565487599	-9.693155505495 96e-007	0.00310242780569709
0.543656451951438	-5.297590734157 88e-007	-0.550971364619423	3.046803090878 09e-006	0.269677137964335
-0.00123700174195 82	-9.007055973642 04e-008	0.00123701487227082	8.811960109721 97e-008	-0.000618500870978892
-0.103265510818158	4.414658945185 14e-008	0.104044576271734	-2.539002573888 2e-007	-0.0514310040866576
0.000205285118003568	0	-0.000205286330013251	0	0.000102642559001784
0.0163571846127342	0	-0.0164317480784 48	1.953078903033 95e-008	0.00816134266713776

Columns 6 to 10:

0.0350251799570493	0.369815962738357	0.00497904547709283	-2.42569918221034	-0.351636017259624
0.0702023034727617	0.00507315932247755	-0.111803581968392	-0.000495188641461174	0.0860910283358873
-1.26269404473794	6.55508365453716	3.48045792152441	-2.52062687503212	-2.81751568957621
-0.589218208723288	-0.103724254686068	0.625887149320581	0.0536572128025407	-0.255028951966261
-3.32421276937899	-110.897116421038	0.881385553959316	158.459707587258	1.35203347680397
1.07847772575496	0.097761267359439	-0.683066601023474	-0.0154671004048251	0.0830089284559496
1.20491476488694	328.628053075768	0.00118780613351843	-366.935033556222	-0.304307519620467
-0.689157804433018	-0.0570419297607089	0.846412016407936	0.0201961036105445	-0.0236770680465196
0.428499459792621	-348.069488347687	0.0930689084232571	185.521987810605	0.181226947480693
0.0830089284559496	0.100739449366284	-0.0231359818214931	-0.0257020452557481	-3.49691360902285
0.131187265438482	168.917433402888	0.0806927536022625	-106.473102133319	-0.0252305390501403
-0.0146883458989582	-0.0523212948218863	0.0049187266553359	0.0131737066074586	-0.0012482074968785
-0.0166940660283097	-21.6121627433086	-0.0128925089626504	19.8709461144962	0.00314120887649887
0.00249596170083627	-0.0103811605395186	-0.000814228253712874	0.00257792184324813	0.000208076335254795
0.00245280063676563	-1.0096025446738	0.00184864915469504	-2.32360293832115	-0.000448502027106047
-0.000356699402458159	0.0224581987760743	0.000116316622726458	-0.00561175452839059	-2.97231405512925e-005
-0.000306023989589869	2.485546333687 34	-0.000231025176893122	-0.0279671351335 97	5.606471115991 63e-005
4.458522233096 67e-005	-0.0121990621958077	-1.453970551072 04e-005	0.00304937376650022	3.715410468800 41e-006
3.400609389465 16e-005	-1.21008793159393	2.566978879159 14e-005	0.250048401936019	-6.229401063216 83e-006
-4.953878556579 95e-006	0.0041325492791994 8	1.615526216294 56e-006	-0.001033088675583 58	-4.128234027649 48e-007
-3.400594209625 99e-006	0.382929474372192	-2.566977468039 73e-006	-0.089518817523173 8	6.229401551399 28e-007
4.953880741782 95e-007	-0.001034164275812 64	-1.615526019142 97e-007	0.000258535650474 747	4.128234001640 77e-008
3.091449801400 85e-007	-0.090852049516 3677	2.333615927713 27e-007	0.022051428889 3849	-5.663092303022 27e-008
-4.503528003171 35e-008	0.000206169145 37869	1.468660012511 04e-008	-5.154173924824 1e-005	0
-2.576208153620 38e-008	0.017251584032 6689	-1.944679938471 72e-008	-0.004248903679 86255	0
0	-3.421438833554 19e-005	0	8.553546583482 02e-006	0
0	-0.002731164570 45851	0	0.000677120517 672264	0

Columns 11 to 15:

5.54168256143 47	0.90392656582898	-7.427058528093 63	-1.10509901925557	6.41650987869064
-0.00120043851893558	-0.0308221856897399	1.83860694520167e-005	0.00500478480281472	-2.88475927251799e-005
-12.2534172944013	-0.0852112103611808	18.2765307335322	1.11128796789717	-10.0575260002877
-0.00861002556775067	0.0270647656753814	0.001672912470562	-0.00498037136446974	-0.000208144895955106
-100.732114848028	0.0459066229332692	21.47555003255536	-0.555617044613804	1.92589300692924
0.00311344467768795	-0.0143637685408906	-0.000627009540580691	0.00249596170083627	7.20757910971012e-005
186.743773529498	-0.0117246374545262	-40.1197124761343	0.185247337049558	3.52343563683351
-0.00350459017741511	0.00491872665553359	0.000632878924581734	-0.000832254963928754	-8.36224544308316e-005
-81.6564900282768	0.00338486315109274	18.94842162922188	-0.0463066000446297	-1.96439841791821
0.00501075650300052	-0.00122116756274138	-0.000851310266067208	0.000208076335254795	0.000119682681118852
328.344120575296	-0.00180803703336458	-5.001687295611 14	0.0092615323872142 2	0.521003433823707
-0.00261384245372802	5.85123083760745	0.000439296897995424	-4.16122819117966e-005	-6.22917383741645e-005
-3.39102982201751	0.000182357978281664	-367.945752718259	-0.00153313327527065	-0.0933424252048383
-0.000519060098211363	-4.07109386439128e-005	8.59087847279289e-005	-0.0551634454945915	-1.2359936389016e-005
0.315573358232399	-1.57253120423215e-005	-0.123503266385439	0.000219964775888149	16.6595154282346
0.00112290992294785	5.8158971897956e-006	-0.000187058484825182	-9.90776172909209e-007	2.67360907416136e-005
0.0738782144403448	1.965700185695 01e-006	-0.00110068165923854	-2.75640144036831e-005	0.00131331071912461
-0.000609953109878176	-7.26986714397577e-007	0.000101645792213 66	1.23847020228348e-007	-1.45226930923895e-005
-0.0543895562981897	-2.184109242645 97e-007	0.00753044229722863	3.06266826941498e-006	-0.00123320642239685
0.000206627463959606	8.077630060876 2e-008	-3.44362891861318e-005	-1.37607799962339e-008	4.91970152284755e-006
0.0184834913519714	2.184109332020 08e-008	-0.00289526235367596	-3.06266826931438e-007	0.000432678680890907
-5.17082137906331e-005	0	8.617855015824 87e-006	0	-1.23114794739603e-006
-0.00447764970771496	0	0.000726234345 3511	2.78424388119827e-008	-0.000105826108089282
1.03084572689235e-005	0	-1.71805797494137e-006	0	2.45439458783892e-007
0.000856776333886608	0	-0.000140833199770683	0	2.03247642734781e-005
-1.71071941677709e-006	0	2.85118219449401e-007	0	-4.07314146851689e-008
-0.000136081843537013	0	2.25045757539253e-005	0	-3.23358533793152e-006

Columns 16 to 20:

0.765531461246346	-3.91928294557337	-0.3283774289244 89	1.84603293933975	0.1017893283336 76
-0.000697717654064423	3.31469964044095e-007	8.916854835175 16e-005	-4.00670573733067e-007	-9.693167348256 87e-006
-0.765497560141311	3.603146503519 94	0.3283775695550 25	-1.83450945117327	-0.1017893278749 18
0.000698142372422342	2.984095203637955e-005	-8.917164853007 49e-005	-2.89116723291798e-006	9.693141490610 85e-006
0.38274919662565	-0.98046111209715	-0.164188782683584	0.843164662799602	0.0508946639493024
-0.00034897329154	-1.12183016127604e-005	4.458522233096 67e-005	1.00089453861855e-006	-4.84657579839872e-006
-0.127582709603059	-0.355117853510149	0.0547295962286721	-0.21295414778845 1	-0.0169648879742 123
0.000116316622726458	1.12995134901293e-005	-1.48616137941892e-005	-1.16143659640687e-006	1.61552621629456e-006
0.0318957192221988	0.26954804982787 3	-0.0136823988230 7	0.0356094130231535	0.0042412219945 5746
-2.90793239554565e-005	-1.52020334563893e-005	3.71541046880041e-006	1.66225899959557e-006	-4.03881506356201e-007
-0.006379142181 48087	-0.0800384818256083	0.0027364797738 8426	-0.00482761479519454	-0.000848244398872153
5.8158971897956e-006	7.84137732582119e-006	-7.4308212792847e-007	-8.6516304126046e-007	8.0776300608762e-008
0.00106319039666202	0.0160322795569042	-0.000456079962130376	0.000628371420771972	0.000141374066479468
-9.693156215396 83e-007	1.53447599871236e-006	1.23847020228348e-007	-1.71646875165354e-007	-1.3462716782507e-008
-0.000151951336 82993	-0.0021965312761 0879	6.51542803065267e-005	-0.000121093422190389	-2.01962952113433e-005
0.000709841843990449	-3.34032260613227e-006	-1.76924314229624e-008	3.71332646345789e-007	0
1.89885501276715e-005	-0.418135789792442	-8.14396601520378e-006	4.95463922764035e-005	2.52453690141799e-006
-1.73092072910273e-008	1.81510276474497e-006	-4.80419488944 85e-005	-2.01704101894847e-007	0
-2.10950475005428e-006	0.000131649940880359	9.04908029073446e-007	0.0081920750242 1157	-2.80505273036578e-007
0	-6.14933735466641e-007	0	6.83291902718905e-008	1.00657393535204e-006
2.10950475005505e-007	-5.12716070984378e-005	-9.04920559811031e-008	6.32321060068361e-006	2.80504509658782e-008
0	1.5389026813973e-007	0	-1.7099277047167e-008	0
-1.91773159095911e-008	1.29160353056293e-005	0	-1.49678475538281e-006	0
0	-3.06796066953816e-008	0	0	0
0	-2.50939318488356e-006	0	2.84407520654769e-007	0
0	0	0	0	0
0	4.01359642973824e-007	0	-4.50639931932874e-008	0

Columns 21 to 25:

-0.673262473487371	-0.0245846004936089	0.180990463142887	0.00483958398599273	-0.0377374934651666
0	9.90776202243988e-007	0	-8.81196005191356e-008	0
0.66381283158233	0.0245846004948093	-0.180323907932571	-0.00483958398599014	0.0376209172882249
3.31564778432971e-007	-9.90776101977035e-007	-2.62833441586938e-008	8.81196010972197e-008	0
-0.319814269224604	-0.0122923002473675	0.089207511978914 6	0.00241979199299518	-0.0186963574798824
-1.24648611400517e-007	4.95388074178295e-007	0	-4.40598004231849e-008	0
0.0980376421517176	0.0040974334158185 9	-0.0290231073635765	-0.000806597330998314	0.006159718781345 59
1.25550079692339e-007	-1.65129360478562e-007	-1.0558514788538e-008	1.46866001251104e-008	0
-0.0222534649738911	-0.0010243583539513 3	0.007072103720228 82	0.000201649332749587	-0.0015209647000848 7
-1.68911485219978e-007	4.12823400164077e-008	1.51114454415793e-008	0	0
0.00411088429346393	0.000204871670790396	-0.0013888821245052 1	-4.03298665499171e-005	0.0003012437318636 94
8.7126414688696e-008	0	0	0	0
-0.0006469825829506 8	-3.41452784650634e-005	0.000229097979445 8	6.7216444249862e-006	-4.9855678077973e-005
1.70497333185501e-008	0	0	0	0
9.22899861987824e-005	4.87789692358051e-006	-3.29015975570852e-005	-9.60234917855171e-007	7.1122825013831e-006
-3.71147787362579e-008	0	0	0	0
-1.45231511164671e-005	-6.09737115447564e-007	4.41158181422591e-006	1.20029364731896e-007	-9.10547591309053e-007
2.01678159154026e-008	0	0	0	0
3.05082401390958e-006	6.77485683830627e-008	-6.243626394314e-007	-1.33365960813218e-008	1.11935408249044e-007
0	0	0	0	0
-0.0001273333176097 03	0	1.0118698976332e-007	0	-1.43763732228092e-008
0	-1.35851610805609e-008	0	0	0
1.57650753813918e-007	0	1.5000442567272 2e-006	0	0
0	0	0	0	0
-2.90480198869391e-008	0	0	0	-1.49261098928881e-008
0	0	0	0	0
0	0	0	0	0

Columns 26 to 27:

-0.000801464654535915	0.00639848855654344
0	0
0.00080146465453592	-0.0063906145013913
0	0
-0.00040073232726796	0.00318738840013462
0	0
0.00013357744242 2653	-0.00105729380737008
0	0
-3.33943606056633e-005	0.000262996007323424
0	0
6.67887212113267e-006	-5.24054818212445e-005
0	0
-1.11314535352211e-006	8.71397358060093e-006
0	0
1.59020764788873e-007	-1.24524982407278e-006
0	0
-1.98775955986091e-008	1.57482821937323e-007
0	0
0	-1.8348339527131e-008
0	0
0	0
0	0
0	0
0	0
0	0
0	0
0	0

A-10: Coefficient matrix (27×27) of the first mode of vibration in ellipse membrane:

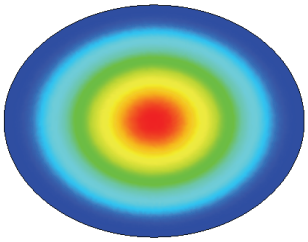

Columns 1 to 5:

0.3775384407490 49	0.000209021337052917	-0.919670291244984	-0.00684736682072185	0.666989407502115
-0.000720535061191185	0.00165536571830671	0.00633233619872442	-0.00976751624889971	-0.0221363088794533
-1.3678852654993 5	-0.00646531548021656	2.02319755870849	0.0756587752222089	-0.0189625935163349
0.0223769107095961	-0.0138066993285904	-0.0475011140220261	0.0587051682639128	0.151781111433082 4
1.37764843739569	0.035493437409439 1	0.554988963063806	-0.298256401368533	-13.5583289489 15
-0.237515985043618	0.034563813900 31479	0.145661757475489	-0.146517444241994	-0.209350024799074
0.5964017416699 79	-0.0757112318533914	-9.11390071090136	0.493960793814003	65.0322966858839
1.21126793661376	-0.0237281079957082	-0.55133822140031	0.0993758411213095	0.327601496541797
-6.0825863353908	0.0629656474716736	24.21041843223 16	-0.320099677345284	-121.795179337494
-3.42318921716168	-0.00752221692886136	2.1177006772262	-0.0201340572194482	-1.13104724545573
21.9322521871621	-0.0127907463539382	-40.5786446836987	0.0584870810434765	99.1483001193336
5.729654981419	0.00452366962969409	-4.83688793040709	-0.00704848778211518	2.43206119729769
-47.4376203488403	0.00214111190350766	59.46253163017 55	-0.00982095193403	-47.4113949413 31
-5.83371265527792	-0.00070265901889611	5.83503690011162	0.000783452947191877	-2.92013645051352
60.9261564027733	-0.00030589523443 3802	-67.919546221032	0.00140225384395837	37.2801613715828
3.66007474010439	9.99951867132636e-005	-3.65919781034088	-0.000113239197353571	1.83001933683943
-44.3780362716749	3.82373045733444e-005	45.849053545998	-0.000175286348510828	-23.4235062563458
-1.47980556925205	-1.25042097534655e-005	1.47968784822382	1.41807936302 3e-005	-0.739902859816039
17.9825884665588	-4.24858997119725e-006	-18.2160944998121	1.94762369331176e-005	9.17103799437401
0.43559790352992	1.3893899269363e-006	-0.435583268034105	-1.57563815931238e-006	0.217798951519047
-5.02119309599355	4.24859002671016e-007	5.05193837483712	-1.94762378085578e-006	-2.53283090249801
-0.100269511352204	-1.38938760359918e-007	0.100267881160417	1.5756241937942e-007	-0.0501347556767496
1.07482103546975	-3.86235457026709e-008	-1.07832614820453	1.77056707074197e-007	0.539819092037101
0.0189014060162682	1.26307955220607e-008	-0.0189012414178937	-1.43238571292171e-008	0.00945070300813271
-0.187255139680691	0	0.187609819526513	-1.47547255901759e-008	-0.0938605567533016
-0.00301258871334524	0	0.00301257351989024	0	-0.00150629435667262
0.0275722805845 33	0	-0.0276046618041117	0	0.0138065448543694

Columns 6 to 10:

0.056110406883497	0.510855925676879	-0.214849958913077	-3.41935260065293	0.447819561016963
0.0171564805677189	0.021629257031115	-0.00585511931440999	0.00311762457736723	-0.00753257843679911
-0.27676221848803	-3.64148864489107	0.571569322445	9.25674750998724	-0.750142743843991
-0.134095607551587	-0.186435793058059	0.0993758411213095	0.0513981704699986	-0.0217274288579552
0.520771880204637	47.1621739794537	-0.430643178844905	-78.4425957446706	0.370826911470772
0.74888708379034	0.114189905888872	-0.087480449797366	0.205955391194715	-0.0115643579609923
-0.192980517624771	-191.420451830303	-0.160194575185263	255.3941820707 33	-0.124444881147062
-0.0873595676694276	-0.205047191303234	-8.26514994210291	-0.0249310490805544	0.00411069292673443
-0.255377067275576	293.5066423417 09	0.00581476868869347	-286.631701845033	0.037512281092247 9
-0.0115643579609923	0.346661108998578	0.00458942478069441	-0.0949433946751781	55.3237086451849
0.0500425906984093	-172.958470724986	0.00587722874624397	94.97939691542 87	-0.00684713234690858
0.00214232433084498	-0.806255968819602	-0.000759736536931944	0.202698376882413	0.000175938048821 353
-0.00835587598693173	44.3540393993281	-0.000980501934700469	-20.2415100998306	0.00103551581454369
-0.000348078227699967	0.972505002451323	0.000132628525393806	-0.24334438605985	-2.916880702459 2e-005
0.00119353553361082	-17.0894560764925	0.000140061295609576	5.67999921479058	-0.00014793113909183
5.00405289995499e-005	-0.6098663103118 2	-1.89082436505833e-005	0.152501613930762	4.16822199884527e-006
-0.000149193061201327	8.4751583564792	-1.75077377508606e-005	-2.30561180166581	1.84913900919086e-005
-6.25218923501307e-006	0.2466146413244	2.36344444950941e-006	-0.0616585716369791	-5.21019770242371e-007
1.65770008245877e-005	-3.14110890141617	1.94530378266084e-006	0.807098250717748	-2.05459891168536e-006
6.94693821538494e-007	-0.0725972113392069	-2.62603852826079e-007	0.0181499126266486	5.78911492373 09e-008
-1.65770010614426e-006	0.853745459577171	-1.94530379946075e-007	-0.215708746586005	2.05459891116538e-007
-6.94693725120 74e-008	0.0167113135267355	2.62604055968912e-008	-0.00417789630639559	0
1.50700009573278e-007	-0.180903038087624	1.7684579989636e-008	0.0454389698640949	-1.86781719198552e-008
0	-0.00315020690298228	0	0.000787558584011059	0
-1.25583341313006e-008	0.0313762469276777	0	-0.00786223955581066	0
0	0.000502095586648373	0	-0.000125524529722719	0
0	-0.00460980667741425	0	0.00115386970135746	0

Columns 11 to 15:

9.33589105854401	-0.551949800946645	-15.7322461488647	0.427713894765701	16.8145326859293
-0.00693035802515222	0.00506100815382739	-0.00112142767108671	-0.000702659891076912	-0.000167296097416895
-15.6600606864701	0.654625498511605	20.396012180323 1	-0.426936393383302	-19.4642972118399
-0.00185737969 1267	-0.00704848778211518	0.00264608851254123	0.000689303301936734	7.523673125411 35e-007
67.3161691430014	-0.327361991274669	-32.5169459521587	0.213467708965332	13.640569730742
-0.0643854310925364	0.00242705532096998	0.00888429849453795	-0.000348078227699967	-0.00149440270795 69
-149.138581607583	0.10910880956753	37.333914731774	-0.0711560186171742	-8.5396895540057
-0.00913900587651299	-0.000759736536931944	0.00209073543174053	0.000116988179986877	-0.000214095152676008
90.8566301742243	-0.0272780278318884	-19.120729860713	0.0177889962650304	3.60767644220172
0.0189854997048439	0.000199395526780 63	-0.00309127580812255	-2.9168807024592e-005	0.000417360488859745
36.5455857952106	0.00536593658873111	5.49234178827161	-0.00355779952904195	-0.975567454990905
-0.0402814612211818	-136.994590887416	0.00674049972237155	5.83557877206116e-006	-0.000959741766603951
5.54134360997185	-0.000902220631308242	-93.2958970309 73	0.000593781513730144	0.19524942006003
0.0486252905999184	6.617776086669 97e-006	-0.00811730712135 98	10.56044054854 56	0.00115786855539761
-1.37469877026119	0.000129849797718626	0.261969211919318	-8.476286792808 7e-005	4.82501109797625
-0.0304933152035784	-9.45370942011222e-007	0.005083387141894	1.38938774404906e-007	-0.000726029694988081
0.494390810571122	-1.62368497536744e-005	-0.0869983339927904	1.05886889936237e-005	0.013168915761 7727
0.0123307320679562	1.18171835197324e-007	-0.0020552857211724	-1.73673438548548e-008	0.000293588858761906
-0.165526768976465	1.80409441686064e-006	0.02814878439444	-1.17652099929383e-006	-0.00411125253440251
-0.00362986056695304	-1.31302027292401e-008	0.00060499708755 5206	0	-8.642525159411 57e-005
0.0435967261681837	-1.80409441686956e-007	-0.00732667570335328	1.17652099929373e-007	0.001056515018852
0.0008355565763368	0	-0.000139263210213186	0	1.98944208651619e-005
-0.00913349500209986	1.64008583351749e-008	0.00152810663422261	-1.06956454481249e-008	-0.000219280672135375
-0.000157103451491 14	0	2.62519528003687e-005	0	-3.75024631307414e-006
0.00157664639906957	0	-0.000263287156168965	0	3.770181656933 66e-005
2.51047793324186e-005	0	-4.18415099075729e-006	0	5.977328412480 63e-007
-0.000231129270837 08	0	3.8562488750293e-005	0	-5.516451548721 05e-006

Columns 16 to 20:

-0.2222094511447 24	-11.3040211382614	0.0830447373043051	4.70738329184658	-0.02345892582140 95
0.000113407423614515	-2.0136008463366 5e-005	-1.2504209773433e-005	-2.32364959472085e-006	1.5756265407966e-006
0.222213724146891	12.2416321007652	-0.0830447195059407	-4.81864784264442	0.023458925879584
-0.000113239197353571	4.77541750979882e-005	1.25046915977331e-005	1.49103347629472e-008	-1.57563815931238e-006
-0.111106865008175	-6.90532831586776	0.041522359738222	2.50100588911038	-0.0117294629398454
5.67444695325624e-005	0.000159063176991631	-6.25218923501307e-006	-2.0752532839629e-005	7.8781225467772 3e-007
0.0370356208862275	2.896648406791 44	-0.0138407865833904	-0.901619019025112	0.00390982097993291
-1.89082436505833e-005	3.737182555320 67e-005	2.08408892704611e-006	-2.97327437233816e-006	-2.62603852826079e-007
-0.00925890528113129	-0.9312473990661	0.003460196645536	0.248972999166907	-0.0009774552449844 79
4.726933766000 33e-006	-5.5200073607743 4e-005	-5.21019770242371e-007	5.79668264567 66e-006	6.565101600959 79e-008
0.0018517810542316	0.222419479260 98	-0.0006920393291177 65	-0.0539461222298853	0.000195491048996853
-9.453709420111 22e-007	0.000120656056870698	1.04204075126046e-007	-1.33297465922044e-005	-1.31302027292401e-008
-0.000308630175741054	-0.0418533183341795	0.000115339888186103	0.009548426031933 07	-3.25818414994763e-005
1.575624543775 02e-007	-0.000144847823273105	-1.73673438548548e-008	1.607979221052 91e-005	0
4.408480119233 54e-005	0.007942860466505 29	-1.64771268837311e-005	-0.001586558337 81406	4.654548785639 46e-006
-0.360294524150491	9.077409447881 35e-005	0	-1.008376825251 24e-005	0
-5.510959973483 08e-006	-0.137871731069719	2.059665736243 17e-006	0.000308693839691575	-5.818185982040 32e-007
0	-3.670153844565 72e-005	0.008902792818 47445	4.077625854668 8e-006	0
6.123614597984e-007	0.000552227997 29435	-2.288502060158 59e-007	0.002675474530 98115	6.464641945659 74e-008
0	1.080351942062 87e-005	0	-1.200350688237 71e-006	-0.000171033097982842
-6.123614597 98401e-008	-0.000136001915 319818	2.288489844962 64e-008	1.611272868487 95e-005	0
0	-2.486843039521 17e-006	0	2.763114009050 27e-007	0
0	2.777668464305 56e-005	0	-3.178248321236 51e-006	0
0	4.687848714351 54e-007	0	-5.208675434825 19e-008	0
0	-4.743912687648 4e-006	0	5.348494207232 19e-007	0
0	-7.471698197780 87e-008	0	0	0
0	6.919971890340 52e-007	0	-7.749193696158 07e-008	0

Columns 21 to 25:

-1.25760187671844	0.00525553286135813	0.256620885127632	-0.000970761019097413	-0.0421489653691322
-2.237357884496 69e-007	-1.3893876036009e-007	-2.1124088381731e-008	1.432385738370 06e-008	0
1.276535497531	-0.00525553286120508	-0.258312253746842	0.000970761019097744	0.042356946774 3819
5.306253672028 65e-007	1.389387379692 29e-007	0	-1.432385712921 71e-008	0
-0.651244543588894	0.002627766430 60238	0.130329530300952	-0.000485380509548872	-0.021309054830 5529
1.767384545333 054e-006	-6.946937251207 4e-008	-1.886593261002 95e-007	0	1.338927705414 19e-008
0.225111283257521	-0.000875922143534174	-0.04417421834479 26	0.000161793503 82957	0.007174607314 7516
4.152439010968 56e-007	2.315645886921 13e-008	-2.702976152336 04e-008	0	0
-0.0589337769632832	0.000218980533883 54	0.011286138978518	-4.044837579573 93e-005	-0.001816462074 51877
-6.133341037213 2e-007	0	5.269711514712 03e-008	0	0
0.012259642707 5981	-4.379610717670 8e-005	-0.002300634445 62171	8.089675159147 87e-006	0.000367412767 704016
1.340622854976 3e-006	0	-1.211795144712 25e-007	0	1.015623374983 08e-008
-0.002108255950 31493	7.299351196118 e-006	0.000389450654 161396	-1.348279193191 31e-006	-6.181739594195 53e-005
-1.609420258580 46e-006	0	1.461799291866 66e-007	0	-1.219257771651 85e-008
0.000324690046 412627	-1.042764456588 29e-006	-5.779340574517 35e-005	1.926113133130 45e-007	9.021973861502 75e-006
1.008608559921 78e-006	0	-9.167062047738 52e-008	0	0
-5.177319267798 44e-005	1.303455570735 36e-007	8.244437859537 5e-006	-2.407641416413 06e-008	-1.214097067400 88e-006
-4.077947859467 81e-007	0	3.706930034872 62e-008	0	0
9.466657721702 69e-006	-1.448283967483 73e-008	-1.254144141143 87e-006	0	1.632145176935 77e-007
1.200390954700 29e-007	0	-1.091227924168 13e-008	0	0
-4.451076496222 58e-005	0	2.072777255226 13e-007	0	-2.315661424425 77e-008
-2.763158941089 97e-008	2.529094444985 74e-006	0	0	0
3.393366317686 15e-007	0	4.831749096884 6e-007	0	0
0	0	0	-2.954264504783 74e-008	0
-5.528682798422 72e-008	0	0	0	0
0	0	0	0	0
0	0	0	0	0

Columns 26 to 27:

0.0001522128194863 59	0.00584938740998558
0	0
-0.0001522128194863 58	-0.00586458761984144
0	0
7.61064097431792e-005	0.00294199467851022
0	0
-2.53688032477264e-005	-0.000986077407387028
0	0
6.3422008119316e-006	0.000248255967647146
0	0
-1.26844016238632e-006	-4.99657588143301e-005
0	0
2.11406693731053e-007	8.37221515908867e-006
0	0
-3.02009562472933e-008	-1.21072619654472e-006
0	0
0	1.57989004384032e-007
0	0
0	-1.97336223679219e-008
0	0
0	0
0	0
0	0
0	0
0	0
0	0
0	0